SPEED CONTROL OF HIGH PERFORMANCE PERMANENT MAGNET MOTORS

ASHRAFUL HOQUE

SPEED CONTROL OF HIGH PERFORMANCE PERMANENT MAGNET MOTORS

by

©Ashraful Hoque

A thesis submitted in partial fulfillment
of the requirements for the degree of
Doctor of Philosophy

Faculty of Engineering and Applied Science
Memorial University of Newfoundland

St. John's Newfoundland Canada

August 1996

Abstract

This thesis presents a novel technique of speed control for permanent magnet (PM) motors. Robust and precise speed control is of critical importance in the high performance drive applications. Unavoidable system disturbances, such as parameter variations, effects of sudden load impact and other system noises are resolved by developing on-line self tuning artificial neural network control structures for both PM dc and PM brushless synchronous motor drives. The newly devised artificial neural network controllers are capable of overcoming the limitations of model dependent conventional fixed gain and existing adaptive speed controllers.

Utilizing the concepts of inverse motor dynamics and non-linear load characteristics, artificial neural network based controllers are designed on the basis of feed-forward neural networks. The transient and dynamic behaviors of the proposed drive systems are improved by incorporating a unique feature of adaptive learning rate which aids the on-line robust speed control over a wide operating range. The stability of the proposed systems has been ensured by a combination of off-line and on-line trainings of the artificial neural networks.

As an integral part of this work, efforts have been directed at the real-time implementation of the artificial neural network based PM motor drive systems using a digital signal processor (DSP) controller board-DS1102. A new circuit topology

has been developed in order to lessen the computation burden of the DSP controller board for the implementation of the PM brushless synchronous motor drive system. A series of tests has been carried out with both PM dc and PM synchronous motors in order to evaluate the performances of the artificial neural network based drive systems. The laboratory test results validate the feasibility of the artificial neural network as an adaptive controller in the high performance drives.

Acknowledgments

I would like to express my sincerest gratitude and appreciation to my supervisor Professor M. Azizur Rahman for his guidance, advice and encouragement throughout my program. My sincerest thanks to Canadian International Development Agency (CIDA) for sponsoring the MUN/CIDA/BIT project which provided me the opportunity to pursue my graduate study at Memorial. I would also like to acknowledge the assistance from Dr. J.E. Quaicoe and Dr. B. Jeyasurya, the members of my supervisory committee for their useful comments and suggestions.

I would like to extend my appreciation to the School of Graduate Studies, all faculty and staff members especially the C-CAE staff members and also all fellow graduate students. I sincerely acknowledge the assistance received from laboratory technologists Mr. Richard Newman, Mr. Don Guy, Mr. Dennis Johnson and Mr. Tom Pike.

Finally I express my sincere appreciation to my wife Farhana, our daughter Noba as well as other family members and friends without whose support and encouragement it would not have been possible to complete this work. I would like to dedicate my thesis to my parents.

Contents

List of Figures

List of Tables

Chapter 1

Introduction

1.1 Electric Motor Drives

Electric machines, with their efficient capabilities of converting mechanical energy to electrical, play an important role in the development of modern technology. From the small household appliances to vast industrial plants, electric motors have been playing their crucial roles for many years. Direct current (dc), induction and synchronous are the three basic electric machines that serve industrial needs. With the day to day technological advancement, the application demand of the electric motors increases in a versatile manner. Recent developments in magnetic materials, semiconductor and microprocessor technologies have led to a revolutionary advancement on the design and control of electric machines. As a result of intensive research, new machines, such as brushless dc machines, switched reluctance machines, permanent magnet (PM) synchronous machines have come into the picture of modern technology [1].

Application areas of variable speed and high performance motor drive (HPD) have been primarily dominated by relatively expensive dc motors for the last few decades because they are easy to control due to the decoupled nature of the field and armature

magnetomotive forces (MMF). Moreover, they can be controlled by simple controlling devices, such as ac-dc or dc-dc converters. However, certain limitations are associated with dc motors, such as the lack of robustness and overload capability, narrow range of speed operations, and frequent maintenance requirement due to brush-gear and commutators. Nevertheless, permanent magnet (PM) dc motors draw wide attention, due to their compact size and rugged structure, in their use in modern drive applications. The main advantage of PM dc motors over conventional wire-wound excited dc motors is that the former does not need extra power supply for the field excitation, rather, excitation is achieved by high energy permanent magnet materials. Recently introduced modern power electronic devices, like buck/boost dc-dc converters, provide an excellent opportunity of using PM dc motors in the four quadrant operation. Newly developed light weight power amplifiers are also being used in critical applications, such as guided manipulations and robotics, together with PM dc motors where accuracy, weight and size are of paramount importance.

However, the shortcomings of dc motors have encouraged researchers to find alternative means of using them in high performance variable speed operations where reliability and maintenance free operations are of prime concern. Considerable attention has been directed towards the development of ac motor drives, such as induction, wire-wound synchronous or PM brushless motor drives in the areas of variable speed operation.

AC motors are usually found suitable for constant speed operations. But recent development of power electronics and very large scale integrated (VLSI) circuits, and the efficient use of microprocessors have made the use of ac motors in modern variable speed drive systems possible. Applications of vector control techniques, in particular, offer an excellent opportunity of using ac motors in modern variable speed drive

systems [2].

Among the ac motors used in drive technology, the induction motors, particularly, the squirrel cage type are considered as the workhorse in the industry because of their ruggedness, reliability, efficiency and low cost. But there are some limitations associated with the induction motors which discourage their use in high performance variable speed drive applications. One of the drawbacks of induction motors is that they always operate at a lagging power factor because of the fact that their rotor field excitations are supplied from the stator side. Moreover, due to I^2R slip power losses, the drive system is not as efficient as expected. Additional power losses and torque pulsation due to higher harmonics originating from the power converters are also considered to be major problems in the inverter-fed induction motor drives. Since induction motors always run at lower speeds than the synchronous speed, the control of these motors is rather complex. The real-time implementation of the induction motor drive requires sophisticated modeling and estimation of machine parameters with somewhat complex control circuitry.

The synchronous motor is offering a serious challenge to the induction motor in the variable speed application domain. The main advantage of synchronous motors over induction motors is their intrinsic ability to eliminate rotor I^2R slip power loss and to supply the reactive current. However, the wire-wound excited synchronous motors ha. ·me inherent disadvantages, such as the requirement of extra power supply, slip rings and brush-gears at the rotor to provide field excitation.

With the advent of high energy permanent magnets like samarium cobalt, neodymium-boron-iron, etc., the drive technology has entered into a new era of brushless PM motor drives. From the operational point of view, brushless PM motors are synchronous motors. The main advantageous feature associated with these kinds of

motors is that the magnetization is provided from a permanent magnet rotor. With brushless PM motors, it is possible to achieve motor performances that can surpass the conventional dc, induction, wire-wound excited synchronous motors. With respect to power density, torque to inertia ratio and efficiency, brushless PM motors are superior to the conventional ac motors. Hence, depending on the application, there are many instances where brushless PM motors are preferable. The basic classification of brushless PM motors is shown in Figs. 1.1(a) and (b). Figure 1.1 (a) show the classification of the brushless synchronous motor according to the insertion of conduction cage winding for starting the motor. If the rotor is provided with cage winding, it is known as the cage type. The other type is known as the cageless because the cage winding can be dispensed with for this case. The cage type brushless PM motors are capable of starting with rated supply voltage and frequency, because the rotor cage winding provides the starting torque. Also an inverter can be used to run a cage type brushless PM motor with variable voltage and frequency in open loop. The cageless brushless PM motors are usually driven with the help of an inverter. To maintain the synchronism, proper control strategy is applied. Depending upon the controlling topology, the brushless PM synchronous motor can be classified into two categories as shown in Fig. 1.1 (b); (i) the rectangular wave fed synchronous motors which are also known as brushless PM dc motor and (ii) the sinusoidal wave fed synchronous motors which are also known as brushless PM synchronous motors. In the former category, a discrete position feedback signal is used every 60 electrical degrees. The induced back emf is trapezoidal in shape. Consequently, the current is required to be held constant for at least 120° in order to generate a ripple-free torque. Since the motor emf is ideally sinusoidal in the latter category, it uses continuous rotor position feedback to force the sinusoidal-shaped current into the motor in order to produce

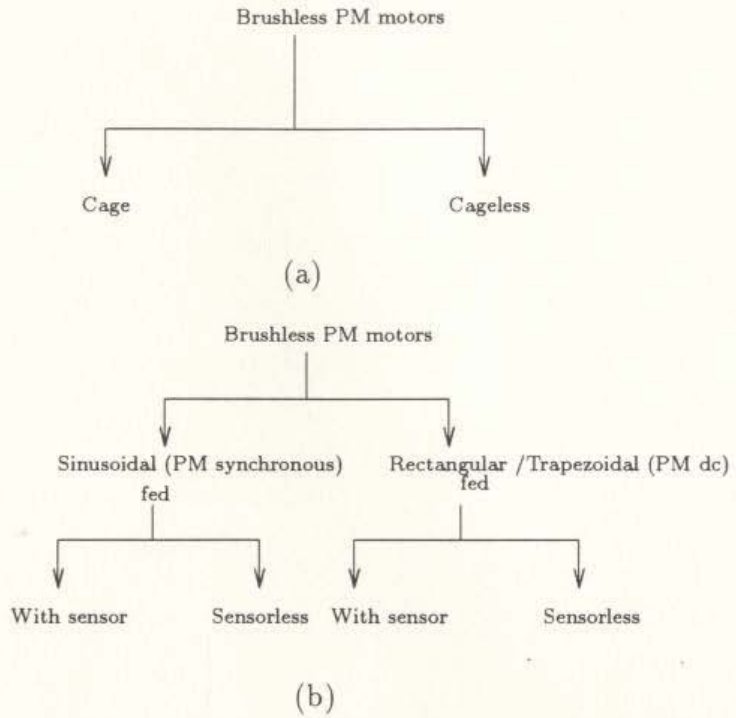

Figure 1.1: Classification of brushless PM motor drives; (a) based on cage winding; (b) based on control methods

constant and smooth torque. Generally, the pulse width modulation (PWM) control strategy is adopted by using a hysteresis or a ramp current controller for the brushless PM synchronous motor drives.

The brushless PM synchronous or brushless PM dc motor can further be categorized as: (i) with sensor and (ii) sensorless; brushless PM motors with sensors use mechanical sensors, such as Hall-effects sensors, absolute or incremental encoders and resolvers. Sensorless brushless PM motors use some form of rotor position detection scheme, such as observers or computation techniques using stator quantities. It is noteworthy that difficulty exists in implementing the sensorless schemes in brushless

PM synchronous motors because they require almost continuous position information. Thus considerable efforts are being made by a number of researchers to overcome this difficulty.

The brushless PM motor may also be classified in three types [3]: the first is the surface mounted type where the magnets are placed on the surface of the rotor; the second is the interior magnet type in which the magnets are buried either radially or circumferentially inside the rotor core; the third is the inset type where the magnets are inset within the rotor core.

1.2 Review of Brushless PM Motor Drive Systems

Brushless PM motors are now essential in the modern drive technology. Moderate to high performance drive systems are being devised using various kinds of controllers. These controllers include conventional fixed gain types, such as proportional-integral (PI), proportional-integral-derivative (PID) or pseudo-derivative-feedback (PDF); adaptive controllers, such as model reference adaptive controller (MRAC), sliding mode controller (SMC), variable structure controller (VSC), self tuning regulator (STR); modern controllers, such as artificial neural network, fuzzy logic or neuro-fuzzy controllers. A review of the literature of brushless PM motor drives with various types of controllers is given in the following sections.

1.2.1 Brushless PM motor motor drives with PI or PID controllers

Researchers continue their efforts on the development of a highly efficient drive system with the brushless PM dc motors [4]-[19]. An electronically commutated polyphase

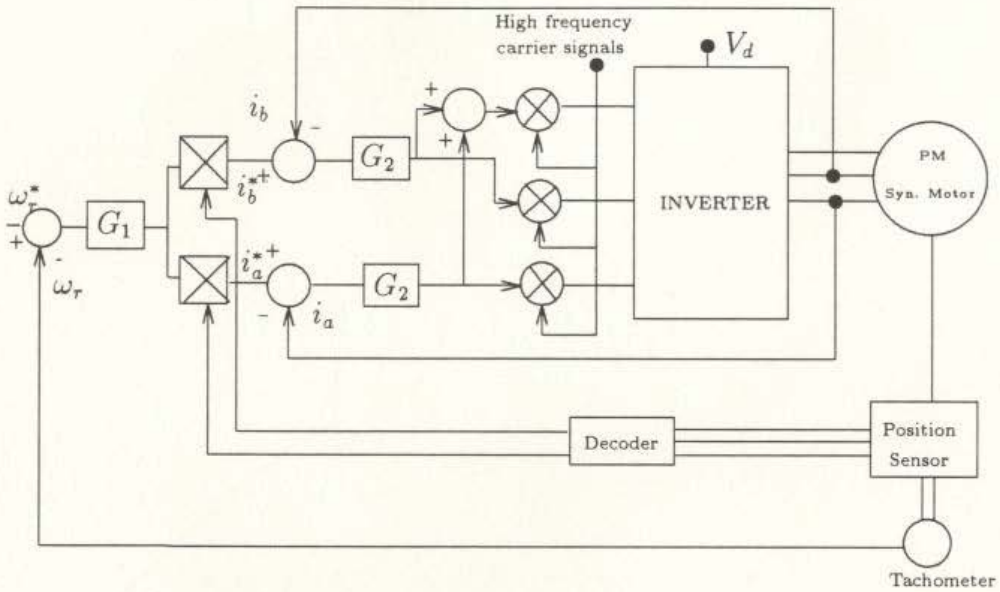

Figure 1.2: Control scheme of a brushless PM dc motor

synchronous motor with surface mounted permanent magnet is known as the brushless PM dc motor. Fig. 1.2 shows a control scheme for a brushless PM dc drive. Since the induced phase voltages of the machine are trapezoidal in shape, it can be shown that a six-step line current in phase with the induced voltage will maintain a constant torque. A Hall-effect or optical encoder properly aligned on the shaft with respect to the poles generates three phase 180° square pulses, which are shaped to six-step waves by the decoder. The speed loop generates the current command signals. The current control loops generate the voltage command, which is pulse width modulated

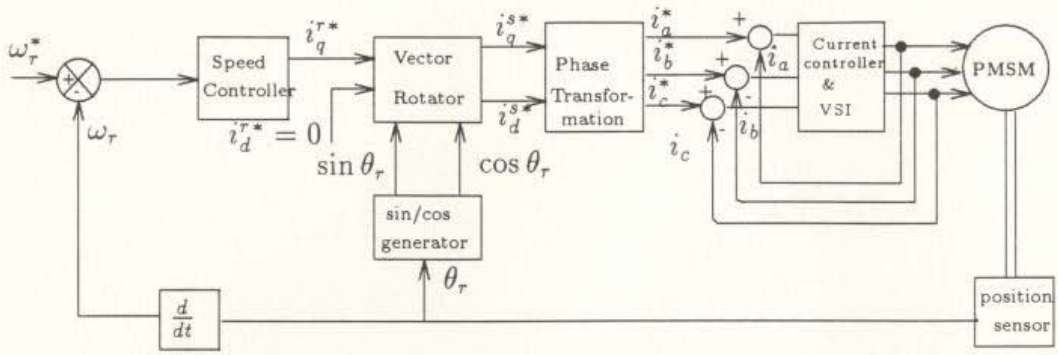

Figure 1.3: Vector control scheme of a brushless PM synchronous motor

(PWM) by a high frequency carrier wave.

Because of the simplicity of the machine, the position sensor in the control electronics makes the brushless PM dc drive popular in industrial motion control systems. However, the drive has a pulsating torque problem due to the mismatch of current switching instants and the machine back emf [20], [21]. Hence, attention is being focused on the vector control of sinusoidally fed brushless PM synchronous motors.

In the drive system comprising brushless PM synchronous motor, the inverter can synthesize sine wave line current. Consequently, the pulsating torque is greatly reduced. The effect of armature reaction in a surface mounted PM motor being negligible, the stator current phasor can be positioned orthogonal to the magnet flux with the help of a position sensor or using any sensorless algorithm. This is essentially done by vector control techniques which provide maximum available torque. It is analogous to the case of a decoupled separately excited dc motor. Fig. 1.3 shows a closed-loop speed control scheme using such a vector control technique. Since the permanent magnet rotor provides the air-gap flux, the stator does not supply any reactive current.

Many researchers continue their efforts on the development of a highly efficient PM synchronous motor drive [22]-[38]. Major points of the works on brushless PM synchronous motors [22]-[38] are briefly summarized below.

Gumaste and Slemon [22] have proposed a vector control strategy of the PM synchronous motor in which position feedback control is achieved by sensing the rotor position angle using a sensor. The analysis is performed for the constant torque and constant power modes. In order to obtain a stable operation, it is suggested to remove the damper winding if the drive system is operated by a voltage source inverter. Lessmeier *et al.* [23] have compared the performance of synchronous motors and induction motors incorporating microprocessors. They have proposed the vector control strategy of ac motors in a synchronously rotating frame. Quadrature axis (q-axis) current has been identified as a control parameter up to the base speed and after that an additional negative direct axis (d-axis) current is suggested to overcome the limitation of the maximum terminal voltage of the inverter. Mechanical sensors have been used to detect the rotor position in this scheme. A PM synchronous motor drive system with regenerative braking features has been presented by Murty [24]. A four quadrant operation with faster response characteristics is obtained in this work. The proposed technique demonstrates a PWM operation and regenerative braking action using the same inverter circuits. Analytical expressions are derived and experimental results are presented for both the open loop and closed loop cases. The speed error is fed to a PI controller used in the closed loop control scheme which sets the current limit of the PWM circuit. Change of logic signals at the forward/reverse input of the EPROM automatically puts the motor first into the regenerative braking till the zero speed is attained, and then accelerates in the reverse direction and brings the motor to the same reference speed in the opposite direction. Meshat and Person [25] have

proposed a design philosophy for a microprocessor-based inverter for vector control of the currents in the brushless PM synchronous motor. The optimum torque control in which d-axis current is forced to zero is applied in this scheme. Re-shaping the phase current is done for any speed in order to obtain the ripple-free torque. Since the generated current in each winding lags the command current, the phase angle advancing method is used to overcome the problem. Using the torque controlling technique, an adjustable speed control strategy for an interior permanent magnet (IPM) synchronous motor drive has been proposed by Jahns *et al.* [26]. In this work, the basis of torque control in an IPM motor is achieved by the orientation of the stator phase excitation with respect to the rotor at all times. The proposed closed loop regulation of the motor phase currents provides a means of achieving instantaneous torque control with IPM synchronous motor.

The performances of the drive systems discussed above are excellent from the point of view of output torque. However, since the gain constants of the PI controllers are fixed in those schemes, a wide range of variable speed operation is not possible. Moreover, parameter variations or extreme load excursions might make the drive system unstable.

Kume and Iwane [27] have presented a vector control technique of a 24 pole synchronous motor with a constant gain PI controller. This scheme successfully operates the motor at low speeds. The performance of the drive system is adversely affected by the non-linearity of the load due to the fixed gain PI controller. The authors have suggested an adaptive speed controller to overcome the problem. Pillay and Krishnan [28] have offered a detailed model involving analysis and simulation of a drive system for a vector controlled PM synchronous motor using a state-space model. The drive system is designed for a fixed speed of 1750 rpm. A PID type speed

controller has been used in this work. Moreover, the performance of the drive has not been demonstrated over a wide range of speeds. Furthermore, the performance of the drive system is parameter sensitive because of the use of a PID controller. The same authors [29] have presented another paper which deals with the design of speed controllers for a high-performance PM synchronous motor drive. The authors used the linear model of the PM synchronous motor to design the speed controller which is pseudo type. A complete control system with the PM motor is simulated for a wide range of speed operations. It is well known that with a linear model, it is very difficult to predict accurately the performance of the machine in real time, particularly at low speeds. Bose [30] proposed a high performance inverter-fed IPM synchronous motor drive system in which a closed loop torque control is implemented with a feedback torque estimation. The control strategy takes into account the effects of saturation, non-linearity and temperature variations. The drive system is designed to work in the constant torque region as well as in the constant power region where the flux weakening method is used. The performance of the drive system has not been investigated for variable speeds. Pillay *et al.* [31] have proposed a digital signal processor (DSP) based hysteresis current control scheme which is implemented using TMS 320E17/C17 and TMS 320E15/C15 processors. For the relatively slower speed control loop, a PI controller is used to obtain the peak value of the current command. Experimental results have illustrated the effectiveness of the current controller. The speed responses at various operating conditions are not provided in this work. Moreover, using look-up table for generating the reference currents might not be suitable under wide range of operating conditions. Morimoto *et al.* [32] have proposed a high performance servo drive system of a salient pole PM synchronous motor using the vector control technique. Demagnetization and magnetic saturation are taken into

account in this work. The PI type speed controller is used to obtain the peak value of the reference current. Using a look-up table and this peak value, the derived optimum phase angle of the current is chosen to obtain the maximum torque without making the d-axis current zero. The experimental results show that the proposed drive system is more efficient than the conventional one where the d-axis reference current is set to zero. The same authors [33] have proposed another vector control scheme of a PM synchronous motor using three types of current phase control approaches: (a) $i_d = 0$, (b) $cos\phi = 1$ and (c) constant flux-linkage control method. The speed controller used in this scheme is again a PI type. A look-up table is used to obtain the reference currents for the control scheme. In this work, it is argued that high torque is achievable without the problem of demagnetization for the $i_d = 0$ phase control method, but the inverter capacity needs to be increased for a salient pole machine. The $cos\phi = 1$ method gives less torque per unit current and this results in non-linear torque characteristics. However, this method may be used for constant speed drive since the inverter capacity need not be very large. The constant flux linkage control approach is suitable for an IPM synchronous motor because it provides almost linear torque characteristics and the required inverter capacity is small. Although magnetic saturation or demagnetizing effects are minimized in this work by the phase control technique, the problem of the adverse effects of the non-linearity and unpredictable load excursions remains still to be solved.

Most of the works discussed so far on the PM synchronous motor drive are based on the vector control technique of a speed range up to the base value. Researchers [34]-[38] are also working on the PM synchronous motor drive which can operate above the base speed. Generally the field weakening technique is applied for extending the speed range of the PM motors.

Bose and Szczesny [34] have worked on a microprocessor based control of an interior type PM synchronous motor. This drive system includes a constant torque region with low speed operation and field weakening constant power region at high speeds. The drive system is designed with one outer torque control loop for specific applications like electric vehicle propulsion. General application is not possible with such a drive drive since the position and speed control loops are absent. Considering the saturation of a current regulator, Jahns [35] has proposed a vector control strategy of the flux weakening operation for the IPM synchronous motor drive system over an extended speed range. In this flux weakening method, direct axis rotor current is obtained from the available phase currents of the motor and the d-axis reference current. The error is passed through a PI controller. Morimoto *et al.* [36] have proposed a control scheme using a flux-weakening approach to run the PM synchronous motor above the base speed. Closed loop control for direct axis stator current in the rotor reference frame is used to oppose the main flux produced by the PM rotor. The effects of parameter changes are studied. Bilewski *et al.* [37] have investigated a control strategy of the PM synchronous motor above the base speed using the field weakening technique. A flux observer based strategy is proposed to maintain synchronism. An IPM machine is suggested for this kind of operation. The system has been realized in real time. However, there is a limitation on the operating range of the drive. Morimoto *et al.* [38] have proposed a field weakening technique for the PM synchronous motor by considering the effect of magnetic saturation. A compensating technique based on the calculated value of L_q from the detected q-axis current is used in this control strategy. The d-axis current command is generated with the calculated L_q to nullify the effect of saturation.

In these works on the field weakening technique, the effects of parameter variations

due to noise, temperature, etc. are not considered. Moreover, the parameter L_q in the brushless PM synchronous motor depends on the load applied to the drive system. This effect is also not taken into account. Therefore, the drive systems may suffer from the problem of instability unless some adaptive scheme is incorporated.

The conventional PI and PID controllers have been used in the brushless PM synchronous motor drive. However, these controllers are sensitive to parameter variations and load disturbances. The performance varies with operating conditions, and it is difficult to tune the controller gain both on-line and off-line. Increased productivity and improved product quality demand fast response and a parameter-insensitive robust drive system. The conventional linear control technique can no longer satisfy the stringent requirements placed on high-performance drive applications. Therefore, there has been recent interest in applying modern control theories to drive systems. The availability of relatively inexpensive and powerful digital signal processors has stimulated increased interest in applying adaptive controllers to electric motor drive systems.

1.2.2 Brushless PM motor drives with adaptive controllers

In recent years, researchers have been focusing their attention on the application of brushless PM motors in high-performance drive systems, such as robotics, machine-tools, aero-space actuations and auto-motives with adaptive controllers which use precise control techniques to achieve fast transient response, parameter insensitivity and high adaptability to non-linear load variations.

In a model reference adaptive control (MRAC) technique, the response is forced to track the output of a reference model irrespective of the drive parameter variations. An MRAC system with a PI controller is based on an on-line search strategy.

The parameters of the PI controller can be adapted to compensate for the system parameter variations so that the system tracks the reference model. The controller parameters are varied by trial and error so that the error between actual and desired responses remains bounded within a hysteresis band. The reference model is determined on the basis of worst-case parameters of the drive system so that the control loop can physically track the reference model. Choy *et al.* [39] have proposed a vector control position servo of the brushless PM synchronous motor using the MRAC. The inner loop is the PI controller and the outer loop is the MRAC. This generates discontinuous control inputs which cause chattering. But this chattering problem is compensated by the steady-state error gain component of the PI controller.

Researchers [40]-[43] have reported the application of sliding mode control (SMC) or variable structure control (VSC) in synchronous motor drive systems. In the SMC, the drive is forced to follow a predefined trajectory in the phase plane irrespective of drive parameter variations. This is achieved by a set of switching control schemes. Namuduri and Sen [40] have proposed an adaptive controller based sliding mode approach for the vector control operation of a synchronous motor. The drive system comprises a phase controlled chopper and a GTO inverter to provide the torque component current. The complete scheme is proposed for a position servo drive. Control equations are derived for the SMC in order to obtain parameter and load torque disturbance insensitivity. Consoli and Antonio [41] have presented the simulation of a vector scheme of an IPM synchronous motor over the base speed employing the field weakening technique and sliding mode regulator for the torque control. Sliding mode strategy is developed mathematically taking into account the effect of constant acceleration, constant speed and constant deceleration. The chattering problem is reduced by considering the changing band-width. Using PM synchronous motor in brushless

dc motor operation, an adaptive control scheme has been proposed by Chung *et al.* [42]. This scheme uses an improved variable structure control (VSC) approach integrated with a sliding mode observer to overcome the problems of the conventional VSC, such as reaching problem, chattering and steady-state error due to the finite switching. Ghribi and Le-Huy [43] have proposed a scheme of variable speed PM synchronous motor drive which comprises two controllers: the first is the speed controller inserted in the outer-loop; and the second is the current controller which is inserted in the inner loop. The speed controller for this scheme has the characteristics of the reference model and optimum speed controller. The current controller is the predictive type which is used to obtain the improved robustness against any change in the system parameter.

There are some other types of adaptive controller drives reported which are based on self-tuning adaptive control techniques [44], [45]. In these methods, the controller parameters are tuned to adapt to the drive parameter variations. The identification block tracks the changes in system parameters. The information is used to update the controller parameters through the controller adaptation to guarantee a desired closed-loop performance. Sepe and Lang [44] have proposed an adaptive speed controller for the PM synchronous motor drive system which is very similar to the self-tuning regulator. It estimates the mechanical parameters of the motor. The estimation is based on the fact that the proposed algorithm redesigns the gain of the controller in real time. The inner loop of the drive system consists of the motor, inverter, current, speed controller and state-filter. The slower outer loop consists of the parameter estimator and the control algorithm for the controller. In an adaptive control scheme, Farhood and Ghandkly [45] have developed an optimized discrete self-tuning regulator by using generalized control structure. The authors have tuned the regulator parameters

by minimizing a steady-state quadratic criterion. One advantage of this algorithm is that by specifying only the order or structure. the existing fixed parameter or the fixed stru[illegible]ontroller can be tuned.

A serious drawback of the adaptive controllers is the computational burden required for the real time parameter identification. The other problem is the sensitivity of the system to numerical precision; and the observation noise which tends to grow undesirably as the number of the system state variables increase. In addition, most of the adaptive controllers have the problems of reaching, chattering and steady state errors due to the finite switching.

1.2.3 Brushless PM motor drives with artificial intelligence controllers

The control of systems with unknown and/or nonlinear dynamics, such as the brushless synchronous motor drive, presents real challenges. Over the last two decades, considerable efforts have been made in developing self-optimizing and adaptive controllers for systems with unknown parameters and nonlinearities. The basic idea was normally to estimate the parameters of a linearized model of the system and to use the model for updating the parameters of the controller. Recent solutions for linear time invariant systems with unknown parameter variations involve the feedback linearization technique in combination with other results of the adaptive nonlinear control theory. But one of the main focusing points of this research was to deal with linear variations of unknown parameters to known nonlinearities.

Neural Networks on the other hand do not need any information about the system nonlinearities. Currently significant efforts are being made on the use of artificial intelligence in motor control technology [13]-[15], [46]-[62]. Artificial intelligence in-

volves programming a computer so that it can mimic human thinking. Exploiting the inherent non-linear input and output mapping property of the artificial neural networks (ANNs), some controllers are being designed and implemented in dc motor drive systems with the aim of achieving the characteristics of adaptive controllers, [50]-[53]. Since human thinking is often qualitative, involving ideas, such as "large", "small" or "medium", fuzzy logic and fuzzy set theories have also been developed for computers to qualify and objectively evaluate the subjective ambiguity of human thinking. These days some work on the dc motor control is also being carried out using the fuzzy control approach [54], [55].

Although some research [56]-[61] has already been carried out using ANN techniques on the control of induction motors, researchers have just started focusing their attention on the use of neural network [13]-[15] or fuzzy logic [62] in brushless PM motor drive systems.

El-Sharkawi and El-Sayed [13] have proposed a neural network based control of the brushless dc motor. In this work, a multi-layer ANN controller is implemented incorporating a model reference adaptive controller. The inputs of the ANN are the estimated speed from the reference model and three consecutive samples of actual speeds. A back-propagation algorithm is used to train the network. This work is based on the off-line trained ANN structure. Due to the absence of the provision of on-line tuning of weights and biases, the speed control is not very precise and thus not very useful for different conditions particularly in cases of load changes, disturbances and parameter variations. In the work of a brushless dc servo motor drive by Inoue *et al.* [14], a fuzzy interferencer is used with a PI controller to tune the gain of the controller to overcome the disturbances from load inertia, mechanical vibration and time delays inside the control. The membership functions are generated from the

actual speed, reference speed and from the output of a reference filter. The servo drive is implemented using DSP-ADSP2101. Incorporation of additional reference generator, observer and fuzzy interferencer with two PI controllers makes the system complex from the computational point of view. Since fuzzy logics used in this work are developed by experience and trial and error, the design procedure of the complete system becomes somewhat time-consuming and cumbersome. In spite of the above facts, experimental results confirm the optimum response after several auto-tuning calculations even after the occurrence of an unstable state. Recently Shigou *et al.* [15] have proposed an off-line trained ANN based digital control of a brushless dc servo motor drive system with an analog speed controller in order to obtain better servo performances. Rather than looking into the precise speed control approach, this work focuses on the training issue of the ANN to be used in the servo system. Kovacic *et al.* [62] have proposed an adaptive control approach on the model reference based control of the brushless PM synchronous motor. The adaptation process is performed by a fuzzy logic adaptation mechanism. In the control system, system output consists of reference input, feedback output and fuzzy adapted output. The inputs of the fuzzy adapter are the error between the MRAC controller's output and the system output and the change in error between the previous and current samples. In this work, the developed control algorithm is based on a linearized model of the brushless PM synchronous motor. The simulation results verify the effectiveness of the developed algorithm for parameter variations of this linearized system. The algorithm may not be suitable for non-linear load characteristics. Moreover, the reference model used in this work is motor parameter dependent. Therefore, unavailability of the accurate value of the motor parameters may lead to an unstable operation of the system for unknown system behaviors.

From the above discussion it can be concluded that there exists a modern trend of research activities on the applications of ANN and fuzzy logic in ac motor drive systems. Although some research has been carried out on the brushless PM dc motor control using neural network [13], [15], a systematic research on the vector control of a brushless PM synchronous motor using an ANN remains unexplored. Research associated with these kinds of drives demands special attention due to the fact that synchronization and low speed operation of the interior type brushless PM synchronous motor is considered a major problem [16]. Therefore, a successful application of the artificial neural network in the vector control of an interior-type brushless PM synchronous motor is a challenge.

1.3 Problem Identification and Purpose of the Work

After brief examinations, it is fair to say that the brushless PM synchronous motor is one of the most efficient motors in ac drive technology.

Faster response, quicker recovery of speed from any disturbances and insensitivity to parameter variations are some of the main criteria of high performance drive systems used in robotics, rolling mills, machine tools, etc.. PM dc motors, with the feature of the armature voltage control, play an important role in these high performance drive applications. Equivalent performance characteristics of a separately excited dc motor can be obtained from the brushless PM synchronous motor if the closed loop vector control scheme is employed. The brushless PM synchronous motor drive system involving the vector control scheme not only decouples the torque and flux which provides faster response but also makes the control task easy. The speed

controller used in the brushless PM synchronous motor drive system plays an important role in meeting the other criteria of the high performance motor drive. It should enable the drive to follow any reference speed taking into account the effects of load impact, saturation, system disturbances and parameter variations. As discussed in the literature review, conventional controllers, such as proportional-integral (PI) or proportional-integral-derivative (PID) have been widely used in both dc and ac motor controls. But these types of controllers are difficult to design if an accurate system model is not available. Moreover, unknown load dynamics and other factors, such as noise, temperature and saturation affect the performance of these controllers for a wide range of speed operations. Existing adaptive controllers, such as the model reference adaptive controller (MRAC), sliding mode controller (SMC), variable structure controller (VSC) and self tuning regulator (STR) are involved in a system with large number of unknown parameters. In addition, these types of controllers are usually based on system model parameters. Hence, unavailability of the accurate system model often leads to a cumbersome design approach for these controllers.

Now-a-days, increasing interest has been seen on the use of artificial neural networks in system modeling and control applications. In high performance drive (HPD) applications using PM motors, the ANN can play a key role in system identification and speed control. Therefore, in this study an effort is directed at developing a practical and easy to implement PM motor drive system incorporating an artificial neural network based speed controller.

The main feature of this study is the efficient integration of the ANN with the vector control scheme of a brushless PM synchronous motor which provides highest torque sensitivity. However, before proceeding with the complex control of ac motors with the artificial neural network, an attempt is made to implement a high perfor-

mance PM dc motor drive system with the ANN. A unique feature of on-line weights and biases updating is also proposed for both PM dc and ac synchronous motor drives. This updating feature not only makes the drive system insensitive to parameter variations but also provides excellent tracking characteristics to the reference inputs.

In this study, systematic mathematical formulations are derived based on the inverse dynamics of the motor models for the accurate design of the ANN structures. These guarantee the exact system identification and precise speed control of PM motors. Experimental verification of the ANN controller based drive systems for both PM dc and brushless PM synchronous motors have also been carried out through hardware implementation.

The outline of the remaining chapters of this thesis is as follows:

The current controller is considered to be one of the main parts of any vector control scheme of ac drives. The performances of the proposed hysteresis current controller for the drive system have been studied in chapter 2. As part of the investigation, a vector control scheme of the brushless PM synchronous motor has been designed and experimentally implemented by integrating a conventional pseudo-type speed controller with the hysteresis current controller. The evaluated performances of the brushless PM synchronous motor drive system have been presented in this chapter.

Artificial neural networks proposed for this work are the feed-forward neural network (FFNN) and recurrent network types. General structures of ANNs with activation functions are described briefly in chapter 3. The training algorithm proposed for the ANN is based on the modified back-propagation approach. An outline of the training algorithm used for both the initial set of weights and biases and on-line

updating is also presented in this chapter.

The vector control scheme of a brushless PM synchronous motor offers equivalent control characteristics of a separately excited dc motor. Hence, before advancing with the proposed ANN based brushless PM synchronous motor, an implementation of the ANN controller is carried out on a laboratory PM dc motor drive. Details of design and implementation of the proposed ANN controller for the PM dc motor have been presented in chapter 4. The validity of the ANN controller on PM dc motor encourages us to carry on research on the design and implementation of the proposed ANN based scheme for the brushless PM synchronous motor.

Chapter 5 of the thesis contains the design of an innovative ANN structure used for the vector control of the brushless PM synchronous motor. Before laboratory implementation, the complete scheme has been successfully simulated to predict the performances of the proposed drive system. The simulation performances of the ANN based brushless PM synchronous motors are also presented in this chapter.

The ANN based brushless PM synchronous motor drive system has been successfully implemented in the laboratory using a digital signal controller board DS-1102. The detailed software and hardware implementations of the proposed scheme have been presented in chapter 6. The experimental results presented in this chapter not only verify the theoretical results presented in chapter 5 but also establish the ANN as an efficient control tool for a robust and high performance brushless PM synchronous motor drive.

The summary and conclusions of this thesis are highlighted in chapter 7, together with suggestions for further study in this area.

Chapter 2

Vector Control of Brushless PM Synchronous Motor Drive

A separately excited dc motor offers a highly desirable control characteristic because its armature and field currents are decoupled and hence can be controlled independently. Equivalent characteristics of a separately excited dc motor can be obtained from a brushless PM synchronous motor if the vector control technique is employed [63], [64]. The underlying principle of vector control is to eliminate the coupling between the torque and the magnetomotive force (MMF) by separating the direct and quadrature (d,q) axis currents which can be achieved by expressing the machine equations in the synchronously rotating rotor reference frame i.e. in the form of Park's model [65]. Thus starting with a brief introduction of Park's machine model, the concept of the vector control technique used in the high performance interior-type brushless PM synchronous motor drive is presented in this chapter. Since current and speed controllers are some of the main components in the vector controlled PM brushless synchronous motor drives, the detailed analysis and design procedures of a pseudo-type speed controller and a hysteresis current controller are also presented in

this chapter. The performances of both speed and current controllers are evaluated through simulations and experiments.

2.1 Brushless PM Synchronous Motor Equations

The brushless PM synchronous motor is the same as the field-excited synchronous motor from the analytical view point. The only exception is that the wire-wound dc rotor field excitation is replaced by permanent magnets, which provide constant flux linkage λ_M. The flux linkage in the three stator phase windings due to the permanent magnet rotor is given in the matrix form as [65]

$$[\lambda_F] = \begin{bmatrix} \lambda_{af} \\ \lambda_{bf} \\ \lambda_{cf} \end{bmatrix} = \begin{bmatrix} \lambda_M \sin\theta_r \\ \lambda_M \sin\left(\theta_r - \frac{2\pi}{3}\right) \\ \lambda_M \sin\left(\theta_r + \frac{2\pi}{3}\right) \end{bmatrix}. \tag{2.1}$$

The three phase flux linkage equations are defined as

$$\lambda_a = L_{aa} i_a + M_{ab} i_b + M_{ac} i_c + \lambda_M \sin\theta_r, \tag{2.2}$$

$$\lambda_b = M_{ba} i_a + L_{bb} i_b + M_{bc} i_c + \lambda_M \sin\left(\theta_r - \frac{2\pi}{3}\right), \tag{2.3}$$

$$\lambda_c = M_{ca} i_a + M_{cb} i_b + L_{cc} i_c + \lambda_M \sin\left(\theta_r + \frac{2\pi}{3}\right), \tag{2.4}$$

where L_{aa}, L_{bb}, L_{cc} are the self inductances and M_{ab}, M_{bc}, M_{ca} are the mutual inductances, respectively.

Now, the voltage equations for the three phase brushless PM synchronous machine can be written as

$$v_a = r_a i_a + \frac{d\lambda_a}{dt}, \tag{2.5}$$

$$v_b = r_b i_b + \frac{d\lambda_b}{dt}, \tag{2.6}$$

$$v_c = r_c i_c + \frac{d\lambda_c}{dt}, \tag{2.7}$$

or in the matrix form as

$$\begin{bmatrix} v_a \\ v_b \\ v_c \end{bmatrix} = \begin{bmatrix} r_a & 0 & 0 \\ 0 & r_b & 0 \\ 0 & 0 & r_c \end{bmatrix} \begin{bmatrix} i_a \\ i_b \\ i_c \end{bmatrix} + p \begin{bmatrix} \lambda_a \\ \lambda_b \\ \lambda_c \end{bmatrix}. \tag{2.8}$$

Equation (2.8) may be written in compact form as

$$[v_{abc}] = [r_{abc}][i_{abc}] + p[\lambda_{abc}], \tag{2.9}$$

where p is the operator defined as $p = \frac{d}{dt}$. In these voltage equations, the flux linkage component contains inductances which are functions of the rotor position θ_r, and the coefficients of the differential voltage equations are time varying except when the speed of the machine is zero. This makes the analysis complex, unless all the equations are transformed to the synchronously rotating rotor frame where the machine inductances will no longer be dependent on the rotor position.

2.1.1 Brushless PM synchronous motor dynamic equations

Park's equations in machine variables can be obtained by transforming the equations of the stationary axis to a synchronously rotating rotor reference frame axis [65]. The coefficient matrix can be written for the transformation to the rotating rotor reference frame as

$$[C] = \frac{2}{3} \begin{bmatrix} \cos\theta_r & \cos(\theta_r - \frac{2\pi}{3}) & \cos(\theta_r + \frac{2\pi}{3}) \\ \sin\theta_r & \sin(\theta_r - \frac{2\pi}{3}) & \sin(\theta_r + \frac{2\pi}{3}) \\ \frac{1}{2} & \frac{1}{2} & \frac{1}{2} \end{bmatrix}, \tag{2.10}$$

where θ_r is the rotor position angle defined as

$$\theta_r = \int_0^t \omega_r(\eta)\, d\eta + \theta_r(0). \tag{2.11}$$

In equation (2.11), ω_r is the mechanical speed expressed in radian/second.

The inverse of the matrix equation (2.10) can be found as

$$[C]^{-1} = \begin{bmatrix} \cos\theta_r & \sin\theta_r & 1 \\ \cos(\theta_r - \frac{2\pi}{3}) & \sin(\theta_r - \frac{2\pi}{3}) & 1 \\ \cos(\theta_r + \frac{2\pi}{3}) & \sin(\theta_r + \frac{2\pi}{3}) & 1 \end{bmatrix}. \tag{2.12}$$

The voltage equations in a stationary reference frame can be transformed to the orthogonal components of a rotating rotor reference frame as

$$[v^r_{qd0}] = [C][v_{abc}], \tag{2.13}$$

where the superscript r denotes quantities in the rotating rotor reference frame.

After some manipulations of equations (2.9) and (2.10), the voltage equation (2.13) can be written as

$$[v^r_{qdo}] = [r_{abc}][i^r_{qdo}] + P\omega_r[\lambda^r_{dq}] + p[\lambda^r_{qd0}], \tag{2.14}$$

where P is the number of pole pairs. Equation (2.14) can be written in the matrix form as

$$\begin{bmatrix} v^r_q \\ v^r_d \\ v^r_0 \end{bmatrix} = \begin{bmatrix} r_a & 0 & 0 \\ 0 & r_b & 0 \\ 0 & 0 & r_c \end{bmatrix} \begin{bmatrix} i^r_q \\ i^r_d \\ i^r_0 \end{bmatrix} + P\omega_r \begin{bmatrix} \lambda^r_d \\ -\lambda^r_q \\ 0 \end{bmatrix} + p \begin{bmatrix} \lambda^r_q \\ \lambda^r_d \\ \lambda^r_0 \end{bmatrix}. \tag{2.15}$$

If it is assumed that the stator phase resistances are equal, i.e.

$$r_a = r_b = r_c = R, \tag{2.16}$$

equation (2.15) can be written as

$$v^r_q = Ri^r_q + P\omega_r\lambda^r_d + p\lambda^r_q, \tag{2.17}$$

$$v^r_d = Ri^r_d - P\omega_r\lambda^r_q + p\lambda^r_d, \tag{2.18}$$

$$v^r_o = Ri^r_0 + p\lambda^r_0, \tag{2.19}$$

where λ_d^r, λ_q^r and λ_0^r can be determined from the following matrix as

$$\begin{bmatrix} \lambda_q^r \\ \lambda_d^r \\ \lambda_0^r \end{bmatrix} = \begin{bmatrix} L_q & 0 & 0 \\ 0 & L_d & 0 \\ 0 & 0 & L_l \end{bmatrix} \begin{bmatrix} i_q^r \\ i_d^r \\ i_0^r \end{bmatrix} + \lambda_M \begin{bmatrix} 0 \\ 1 \\ 0 \end{bmatrix}, \tag{2.20}$$

and

$$L_q = L_l + L_{mq} \tag{2.21}$$

$$L_d = L_l + L_{md} \tag{2.22}$$

L_d and L_q are the d-axis and q-axis inductances, respectively; L_{md} and L_{mq} are the d-axis and q-axis magnetizing inductances, respectively and L_l is the leakage inductance. It should be noted that for the interior-type brushless PM synchronous motor L_q is larger than L_d.

From equation (2.20), flux linkages can be expressed as

$$\lambda_q^r = L_q i_q^r \tag{2.23}$$

$$\lambda_d^r = L_d i_d^r + \lambda_M \tag{2.24}$$

$$\lambda_0^r = L_l i_0^r \tag{2.25}$$

Substituting equations (2.23) and (2.24) into equations (2.17) and (2.18), respectively and assuming a balanced three phase system (i.e ignoring the zero sequence terms), the following expressions are obtained.

$$v_q^r = (R + pL_q) i_q^r + P\omega_r L_d i_d^r + P\omega_r \lambda_M \tag{2.26}$$

$$v_d^r = (R + pL_d) i_d^r - P\omega_r L_q i_q^r \tag{2.27}$$

Using equations (2.26) and (2.27), the permanent magnet synchronous motor can be represented in the d- and q- axes by the equivalent circuit diagram shown in Fig. 2.1 [66]. The interior-type brushless PM motor parameters are given in Appendix A.

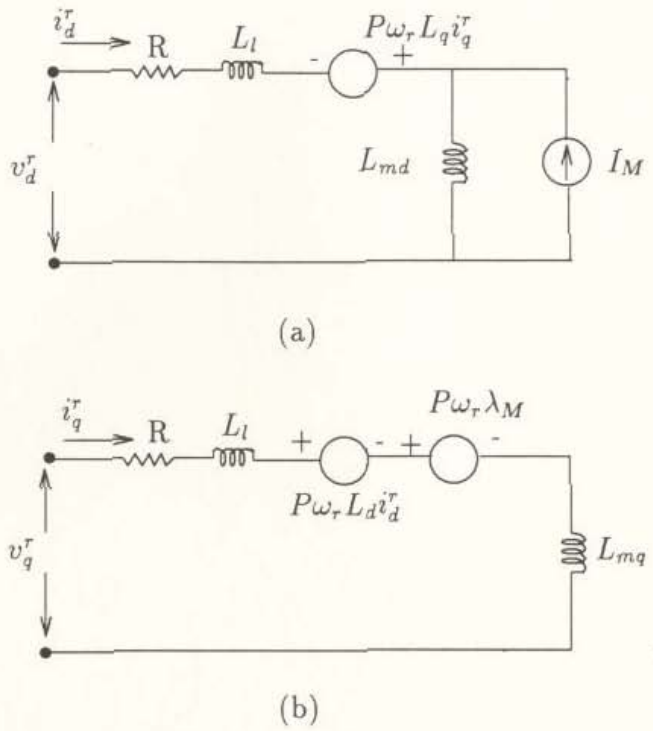

Figure 2.1: Model of the brushless permanent magnet synchronous motor: (a) d-axis (b) q-axis

The developed electric torque can be expressed as

$$T_e = \frac{3P}{2}[\lambda_M i_q^r + (L_d - Lq) i_d^r i_q^r]. \tag{2.28}$$

The first term of equation (2.28) represents the torque component due to permanent magnet excitation, while the second term is the reluctance torque component. The motor dynamic state can be represented by the following equation

$$T_e = Jp\omega_r + B\omega_r + T_L, \tag{2.29}$$

where T_L is the load torque, B is the damping coefficient and J is the rotor inertia.

2.2 Vector Control of the Brushless PM Synchronous Motor

The coupling between the flux and the torque component currents in the ac motor has been pointed out as one of the main reasons for the sluggish response of a closed loop control. The vector control technique has been accepted as one of the most effective methods for decoupling the q-axis and d-axis components of stator currents in the synchronously rotating rotor reference frame. As is well known in the Park's machine model, the sinusoidal quantities appear as constant values in the steady-state condition. This phenomenon offers an excellent opportunity for controlling a brushless PM synchronous motor. In the rotor reference frame, the stator current phasor has two components: the q-axis component of the stator current phasor known as the torque producing current component and the d-axis component known as the magnetizing current component, which is responsible for affecting the total air-gap flux linkage. As can be seen from equation (2.28), the generated motor torque is not only a function of q-axis current but also the product of q- and d-axis currents in the rotor reference frame. By keeping the magnetizing current component (i_d^r) at a constant value, the motor torque can be forced to vary linearly with the q-axis current. This concept of control is similar to the control of a separately excited dc motor. However, for an interior type brushless PM synchronous motor, an optimally efficient operation is achieved by controlling the stator current to ensure that the stator current phasor contains only a q-axis component when expressed in the rotor reference frame. In other words, the d-axis current in the rotor reference frame is forced to zero in order to achieve maximum torque per ampere, resulting the orientation of all the flux linkage in the d-axis. With this concept of control strategy, the second term of the

torque equation (2.28) is reduced to zero. Thus the torque equation (2.28) reduces to

$$T_e = \frac{3}{2} P \lambda_M i_q^r \tag{2.30}$$

Hence a constant torque can be obtained by maintaining constant q-axis current since the developed torque depends only on the q-axis current. With this control strategy, the machine model becomes linear as can be described by the following equations:

$$p i_q^r = \frac{1}{L_q}(v_q^r - R i_q^r - P \lambda_M \omega_r), \tag{2.31}$$

$$p \omega_r = \frac{1}{J}[T_e - T_L - B \omega_r]. \tag{2.32}$$

Equations (2.31) and (2.32) are obtained from equations (2.26) and (2.29). The developed torque T_e in the equation (2.30) is proportional to the q-axis current.

$$T_e = K_T i_q^r \tag{2.33}$$

where $K_T = (3P\lambda_M)/2$. Equation (2.33) resembles the torque expression of a separately excited dc motor, where i_q^r corresponds to the armature current of a dc machine and K_T corresponds to the constant flux linkage.

2.3 Implementation Strategy for the Vector Control Scheme for the Brushless PM Synchronous Motor

The practical configuration of a vector controlled brushless PM synchronous motor drive is shown in Fig. 2.2. The basic configuration of the drive system consists of a permanent magnet synchronous motor (PMSM) fed by a current controlled voltage source inverter (VSI). The three phase current commands are synchronized to the

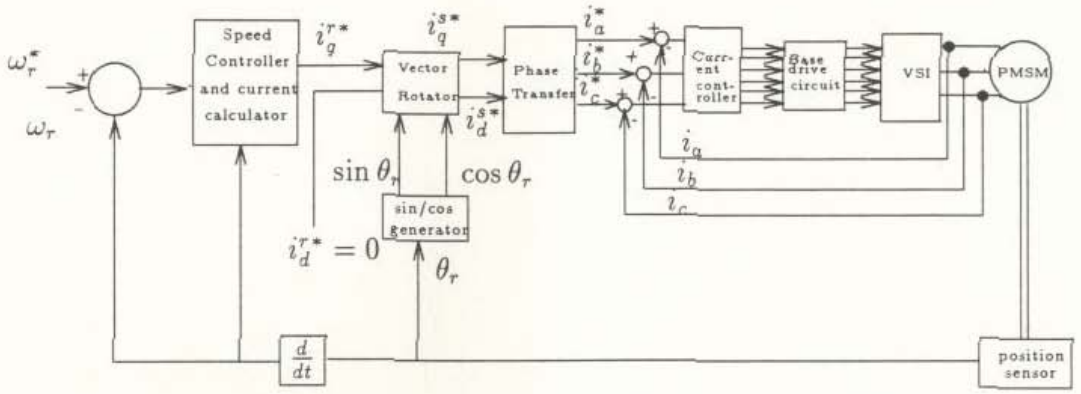

Figure 2.2: Block diagram for a vector-controlled PMSM drive

rotor position angle provided by an optical incremental encoder mounted on the motor shaft. The magnitudes and frequencies of the three phase current commands are determined from the vector control in d, q-axis rotor reference frame. Based on the control strategy discussed in section 2.2, the reference speed ω_r^* is compared with the actual speed. The resulting speed error is forwarded to the speed controller which generates a reference torque T_e^*, which is processed through a torque current calculator to produce the q-axis reference current i_q^{r*}. With this reference current and measured rotor position angle, the three phase reference currents are computed using the inverse Park's transformation. These reference currents and the actual three phase stator currents are processed through the current controller to generate the inverter switching control signals.

2.3.1 Design of a pseudo derivative feedback (PDF) type speed controller

For a relatively less expensive and moderate performance brushless PM synchronous motor drive, conventional speed controllers such as PI, PID or PDF types can be

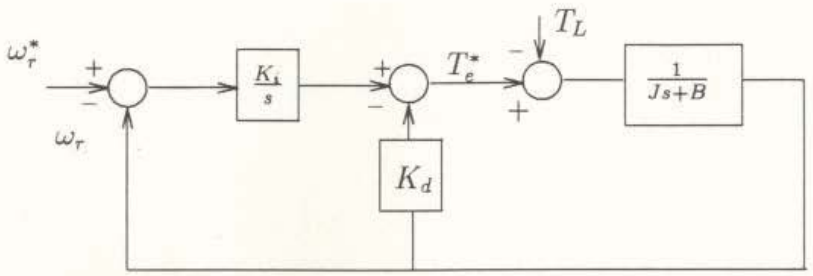

Figure 2.3: The simplified speed control block diagram of PMSM drive

used. A speed controller of PDF type without the forward differentiation as shown in Fig. 2.3 is designed and incorporated in the drive system [67]. The K_d and K_i shown in Fig. 2.3 are the differential and integral constants. In the PDF controller, the derivative (in the forward path of the PI or PID controller) is avoided by placing the integral part in the forward path of the speed error, and the speed feedback is subtracted from the output of the integral part. The transfer function of the control system with the speed controller constants can be expressed in the Laplace domain as

$$\omega_r(s) = \begin{bmatrix} \frac{1}{Js^2+(B+K_d)s+K_i} & -\frac{s}{Js^2+(B+K_d)s+K_i} \end{bmatrix} \begin{bmatrix} \omega_r^*(s) \\ T_L(s) \end{bmatrix}, \tag{2.34}$$

where J is the inertia constant of the permanent magnet rotor, B is the damping constant, T_L is the load torque, ω_r is the actual speed and ω_r^* is the reference speed. Therefore the characteristic equation of the simplified control system is given by

$$Js^2 + (K_d + B)s + K_i = 0 \tag{2.35}$$

With the design motor data of $J = 0.003\ kg.m^2$ and $B = 0.00008$ (N-m)/rad/sec as given in Appendix A, the damping factor ζ and the natural frequency ω_n can be

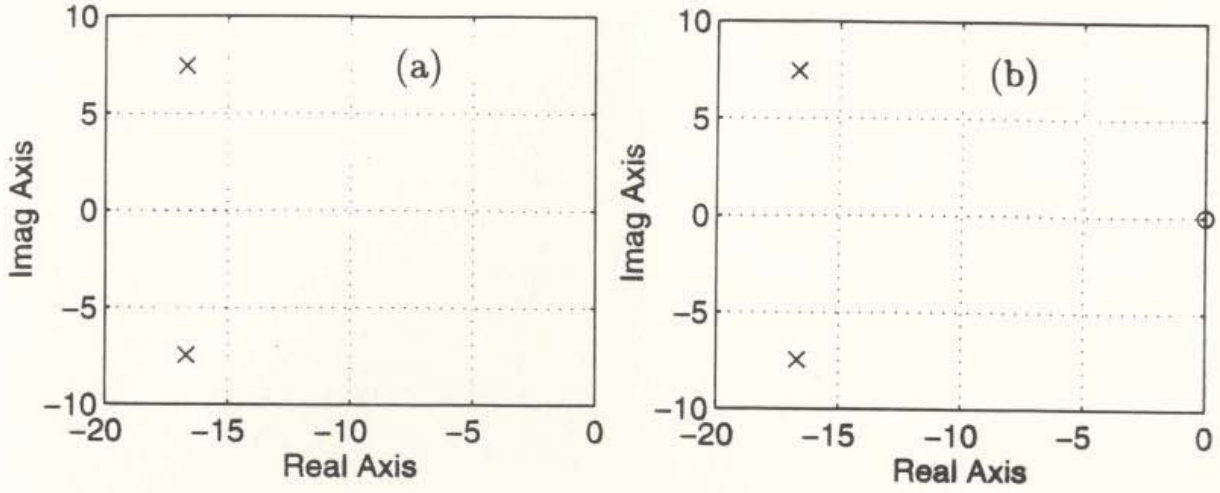

Figure 2.4: Pole-zero plots (a) input: ω_r^*, output: ω_r (b) input: T_L, output: ω_r

determined as

$$\zeta = \frac{K_d + B}{2\sqrt{JK_i}} \tag{2.36}$$

$$\omega_n = \sqrt{\frac{K_i}{J}} \tag{2.37}$$

The Routh's criteria of the characteristic equations reveal that the system is stable for the values of $K_d > 0.0022$. For a critically damped system, the value of ζ is chosen as 0.913. Hence, the values of K_d and K_i can be designed with the above criteria. For the design purpose, the value of K_d is chosen as 0.1. Therefore, the value of K_i is 1.001. The pole-zero plot of the above transfer functions are shown in Figs. 2.4(a) and (b). It is evident from Figs. 2.4(a) and (b) that the system is stable, since all the poles are in the second and third quadrants of the pole-zero plots. The small signal behaviors of the control system have been predicted through unit step responses of the two inputs ω_r^* and T_L individually. The corresponding results are shown in Figs. 2.5(a) and (b), respectively.

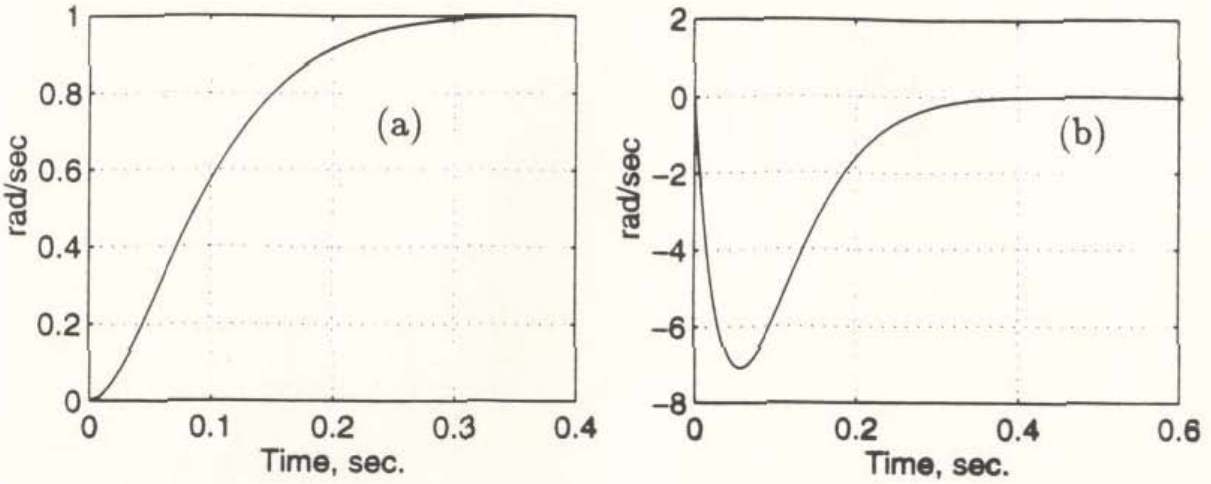

Figure 2.5: Small signal behavior of the simplified control system: (a) $\Delta\omega_r$ due to unit step change of ω_r^* (b) $\Delta\omega_r$ due to unit step change of T_L;

2.3.2 Current control scheme for the voltage source inverter

The function of the current controller is to force the load current to follow the reference current as closely as possible. Before implementing the current controller for a three phase voltage source inverter (VSI) in the brushless PM synchronous motor drive, its operation has been studied by considering a circuit consisting of resistance (R) and inductance (L) as shown in Fig. 2.6.

In this diagram, a balanced three phase R-L load is connected to the three phase transistor inverter. The neutral point of the load can be connected to the mid point of two equal capacitors connected across the dc supply. The measured currents are compared with the reference currents and the error signals are utilized by the current controller to generate the drive pulses, which activate the inverter power switches in such a manner that reduces the current error. In Fig. 2.6. N_A, N_B and N_C represent the three logic variables of the three legs of the inverter. The inverter conduction state is represented by these logics. The logic state 1 means transistor T_1 is conducting

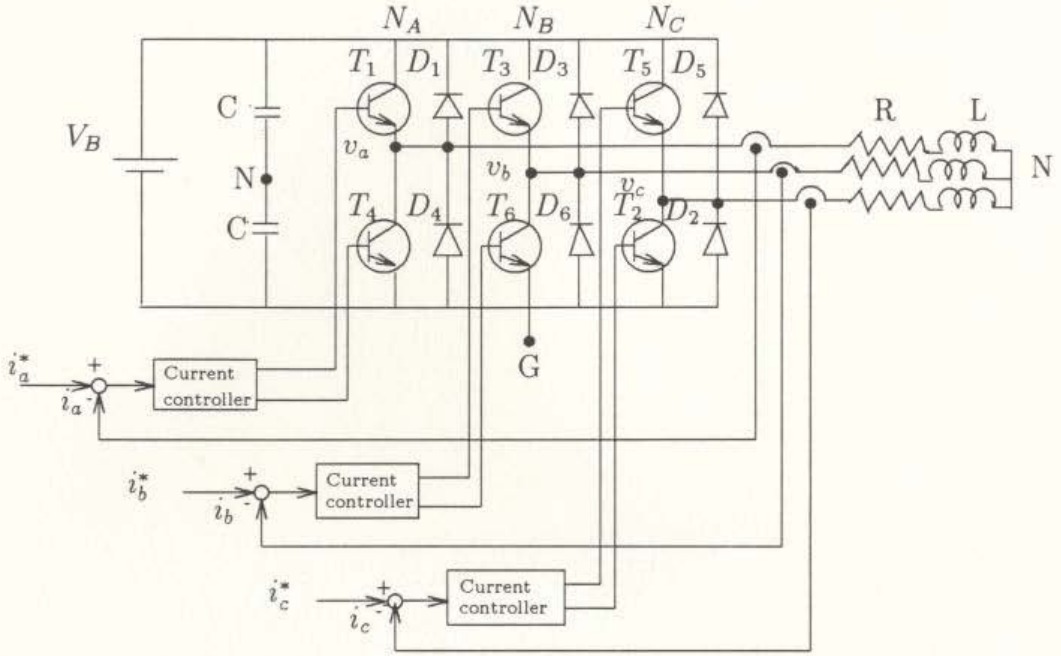

Figure 2.6: Current controlled voltage source inverter with R-L load

and the logic state 0 corresponds to the conduction of the transistor T_4.

Before analyzing any specific current controllers, the concept of voltage and current space phasors is utilized to simplify the representation of a set of three phase voltages and currents. The inverter output voltage phasor is defined as [68]

$$\bar{v} = \frac{2}{3}[v_a + av_b + a^2 v_c], \tag{2.38}$$

where $a = e^{j2\pi/3}$ and v_a, v_b, v_c are the three phase voltages. Following the same concept as applied to the voltage phasor, the current phasor can be defined as

$$\bar{i} = \frac{2}{3}[i_a + ai_b + a^2 i_c]. \tag{2.39}$$

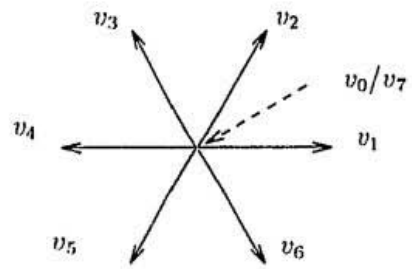

(a)

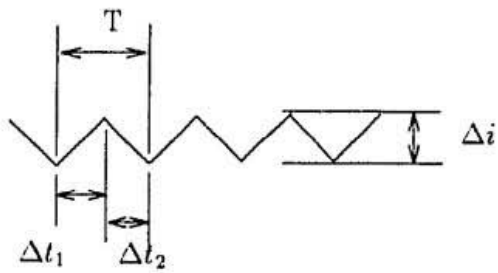

(b)

Figure 2.7: (a) Inverter voltage phasor (b) Switching current waveform

If the logic variables are expressed as

$$[v_{abcG}] = \begin{bmatrix} N_A \\ N_B \\ N_C \end{bmatrix} V_B, \tag{2.40}$$

then the phase voltages can be expressed in terms of the bus voltage and logic variables, giving

$$[v_{abcN}] = \frac{1}{3} \begin{bmatrix} 2 & -1 & -1 \\ -1 & 2 & -1 \\ -1 & -1 & 2 \end{bmatrix} [v_{abcG}] \tag{2.41}$$

Table 2.1: Logic operation of VSI under current control

state, L	T_1	T_4	T_3	T_6	T_5	T_2	operation mode	voltage phasor
0	0	1	0	1	0	1	freewheeling	v_0
1	1	0	0	1	0	1	active	v_1
2	0	1	1	0	0	1	active	v_2
3	1	0	1	0	0	1	active	v_3
4	0	1	0	1	1	0	active	v_4
5	1	0	0	1	1	0	active	v_5
6	0	1	1	0	1	0	active	v_6
7	1	0	1	0	1	0	freewheeling	v_7

There are eight switching combinations for the six switches of the inverter. With these combinations, the voltage phasors can be expressed as [69]

$$\bar{v_L} = \begin{cases} \frac{2}{3} V_B e^{(L-1)\pi/3} & \text{for L=1,2 ..., 6} \\ 0 & \text{for L=0,7} \end{cases} \tag{2.42}$$

The logic operation of the VSI under current control is summarized in Table 2.1.

Figure 2.7 shows the voltage phasors corresponding to the six active states. Each vector has the amplitude of $2V_B/3$ except vectors v_0 and v_7 which correspond to the free-wheeling states and the amplitudes of which are equal to zero.

2.3.3 Hysteresis current controller

The hysteresis current controller is used for the proposed drive. The reason for choosing this particular kind of current controller is that it offers an excellent dynamic performance which is one of the main concerns of high performance drives. In addition, this type of controller is very simple to implement in real time. The switching frequency of a hysteresis current controller depends on several factors. To determine

these factors, let one phase of the R-L load be described by the following equation

$$\frac{di}{dt} = \frac{v}{L} - \frac{R}{L}i \tag{2.43}$$

An idealized PWM inverter is switched from $+V_B$ to $-V_B$ and generates a switching current waveform as shown in Fig. 2.7 (b), where Δi is the peak-to-peak current ripple, T is the cycle period, Δt_1 and Δt_2 are the times at which the inverter output voltage is switched between $+V_B$ to $-V_B$, respectively. The Δt is the time in which the line current increases by Δi. This time can be determined from equation (2.43) as

$$\Delta t = \frac{L\Delta i}{v - Ri} \tag{2.44}$$

Thus the switching frequency can be determined as

$$f = \frac{1}{\Delta t} \tag{2.45}$$

The switching frequency is affected by several factors, such as the load inductance, the dc bus voltage, the magnitude of the load current as well as its ripple content. The fundamental line to neutral voltage varies periodically.

A simplified diagram of a typical three phase hysteresis current controller is shown in Fig. 2.8. The purpose of the current controller is to control the load current by forcing it to follow a reference current which offers a unity power factor operation. For example, the reference current can be expressed as

$$i_{ref} = I_m sin(\omega t) \tag{2.46}$$

An upper band reference and a lower band reference current can be defined by adding or subtracting a band limit H with the reference current, giving

$$i_{up} = i_{ref} + H \tag{2.47}$$

$$i_{lo} = i_{ref} - H \tag{2.48}$$

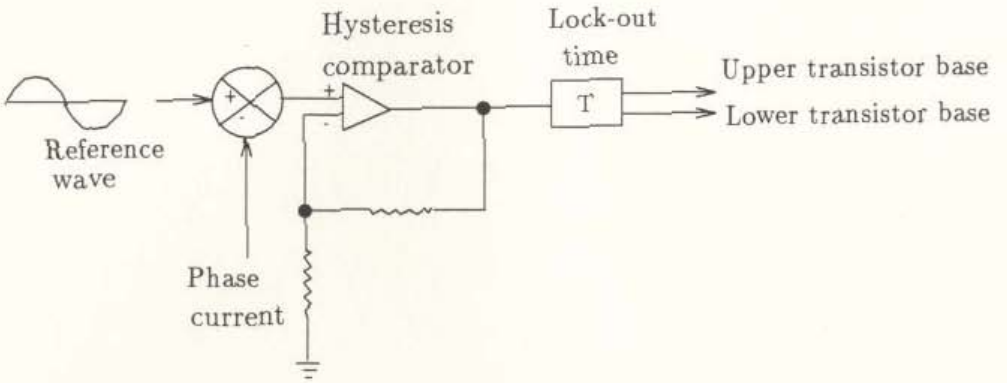

(a)

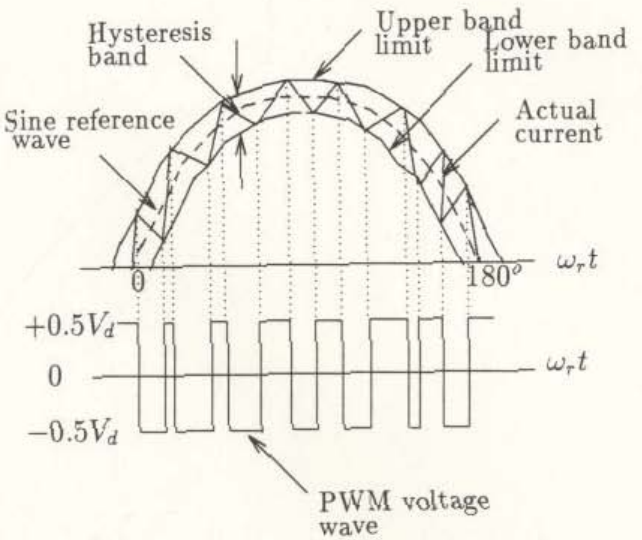

(b)

Figure 2.8: (a) Hysteresis current controller scheme (b) Waveform of a typical hysteresis current controller

Referring to Fig. 2.8(b), if $i_a > i_{up}$, then switching logic $N_A = 0$, i.e. the inverter output voltage switches to negative in order to reduce the line current. Similarly, if $i_a < i_{lo}$, then $N_A = 1$. At this instant the inverter output voltage switches to positive in order to increase the line current.

2.3.4 Simulation and experimental results of the hysteresis current controller with R-L Load

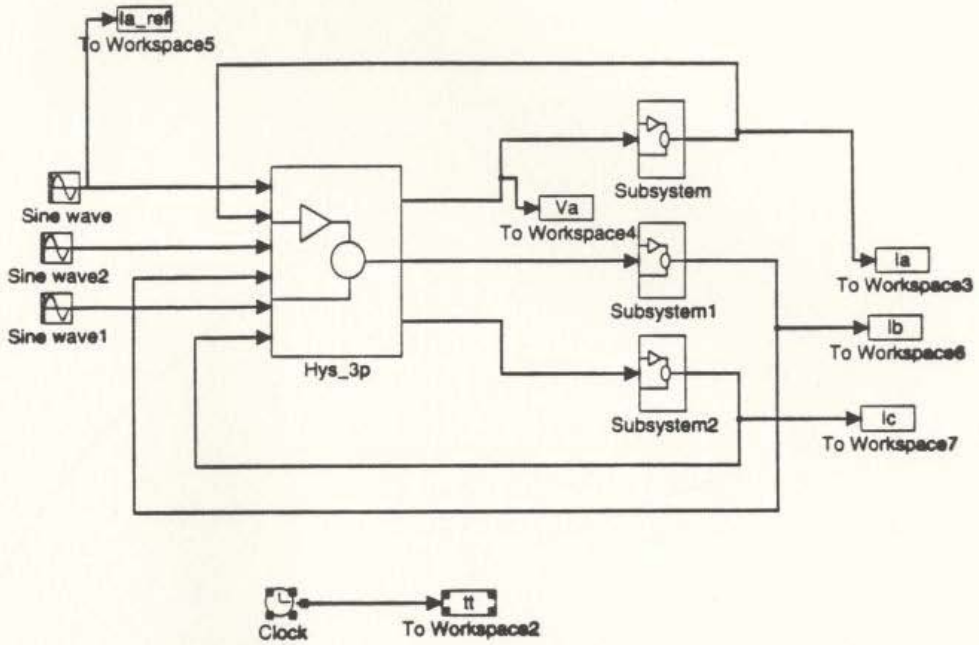

Figure 2.9: SIMULINK block diagram for hysteresis current controlled VSI

The simulation of the three phase hysteresis current controller with an R-L load was carried out using the SIMULINK software [70]. The schematic of the block diagram using SIMULINK is shown in Fig. 2.9. Laboratory experiments have been carried out to evaluate the performances of the hysteresis current controller with the R-L

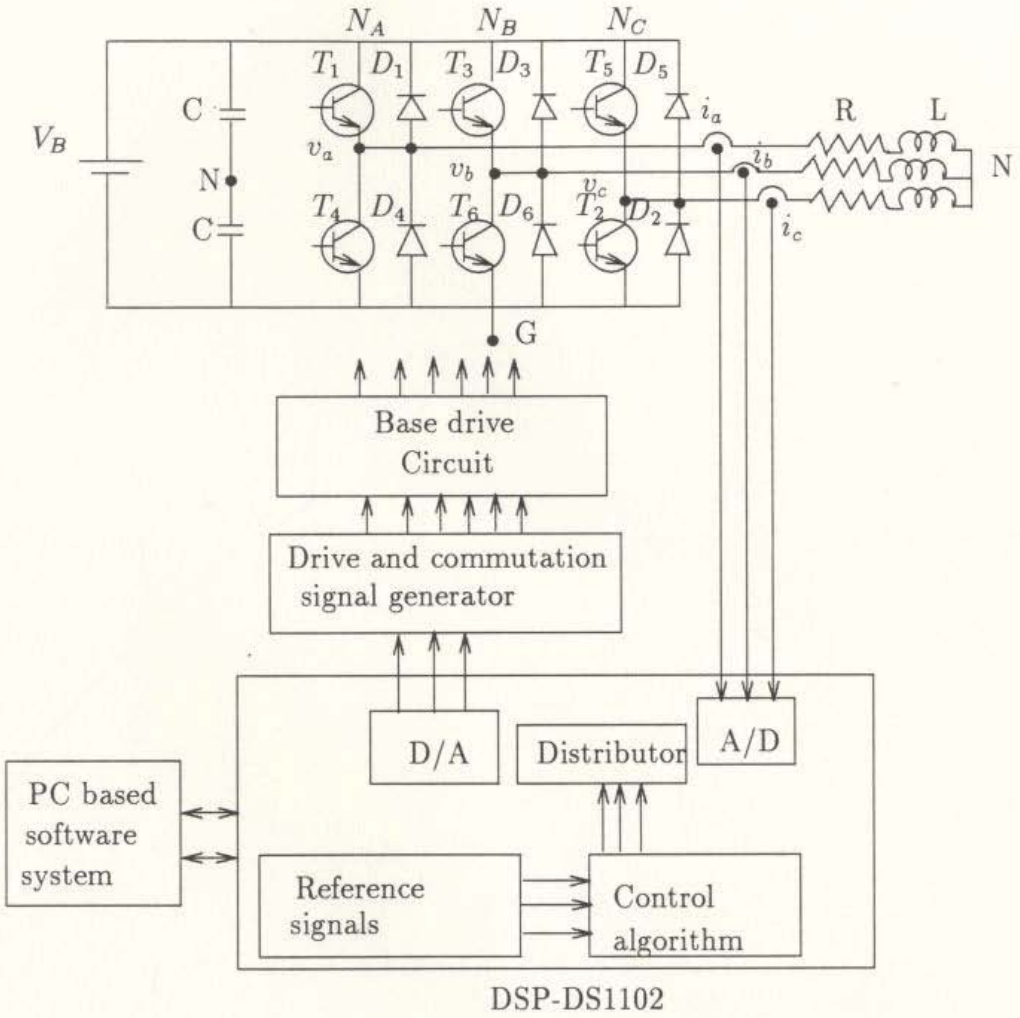

Figure 2.10: Schematic diagram of the digital current controlled VSI

load using DSP controller board DS-1102. The circuit configuration of the three phase voltage source inverter and the digital current controller using DSP is shown in Fig. 2.10. The actual load currents are captured by Hall-effect transducers and fed to the A/D port of the DSP board. The controller samples the phase currents and compares them with the reference currents. Upon this comparison, the switching logics corresponding to the three phases of the inverter are fed to the D/A port. The six switching signals have been derived using interface circuit as shown in Appendix C. The DSP board is completely controlled by a software developed system using a personal computer. The flow chart of the real-time implementation of the hysteresis current controller with R-L load is shown in Fig. 2.11. The details of the three phase PWM signals generation as shaded in the Fig. 2.11 are shown in the flow chart of Fig. 2.12.

Figures 2.13-2.18 show the simulation and experimental current responses of the hysteresis current controlled VSI. All results have been obtained with a reference current peak of 1 amp and hysteresis band limit of 0.1 amp. Figure. 2.13 (a) shows the simulation current responses of phase 'a' and phase 'b' for the reference current frequency of 60 Hz. Fig. 2.13 (b) shows the corresponding experimental current responses. Fig. 2.14(a) shows the simulation current responses of phase 'a' and phase 'c' and Fig. 2.14(b) shows their experimental results of the same frequency. It is observed from Figs. 2.13 and 2.14 that the load currents are within the prescribed band and they have maintained the proper phase difference. Figures 2.15(a) and 2.16(a) show the simulation current responses of phases 'a', 'b' and phases 'a', 'c', respectively for a reference frequency of 30 Hz. Figures 2.15(b) and 2.16(b) show the corresponding experimental responses. The lower frequency of the reference current provides lower inductive reactance. Since the magnitudes of the dc bus voltage and

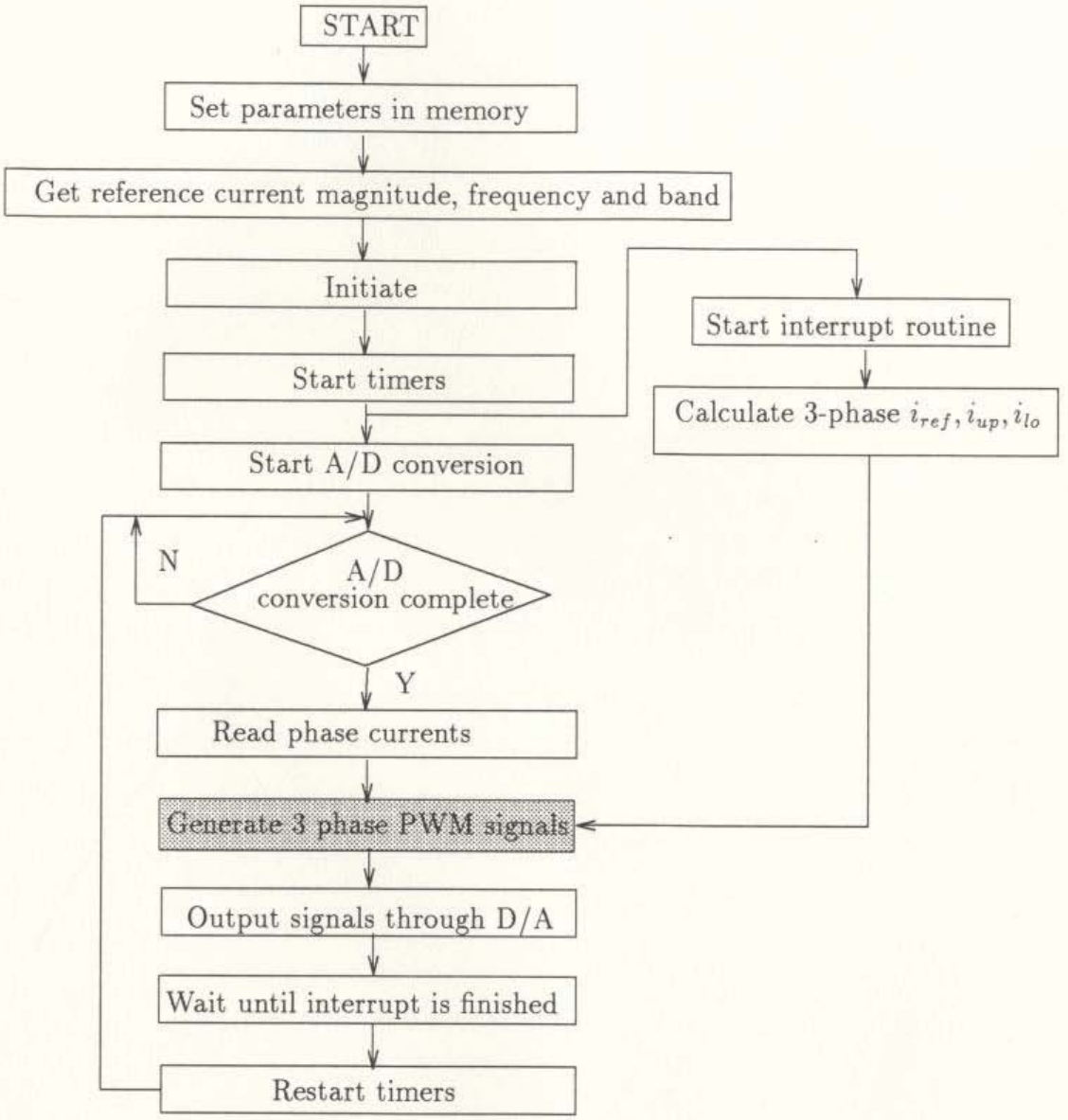

Figure 2.11: Flow chart of the real-time implementation of the hysteresis current controller with R-L load

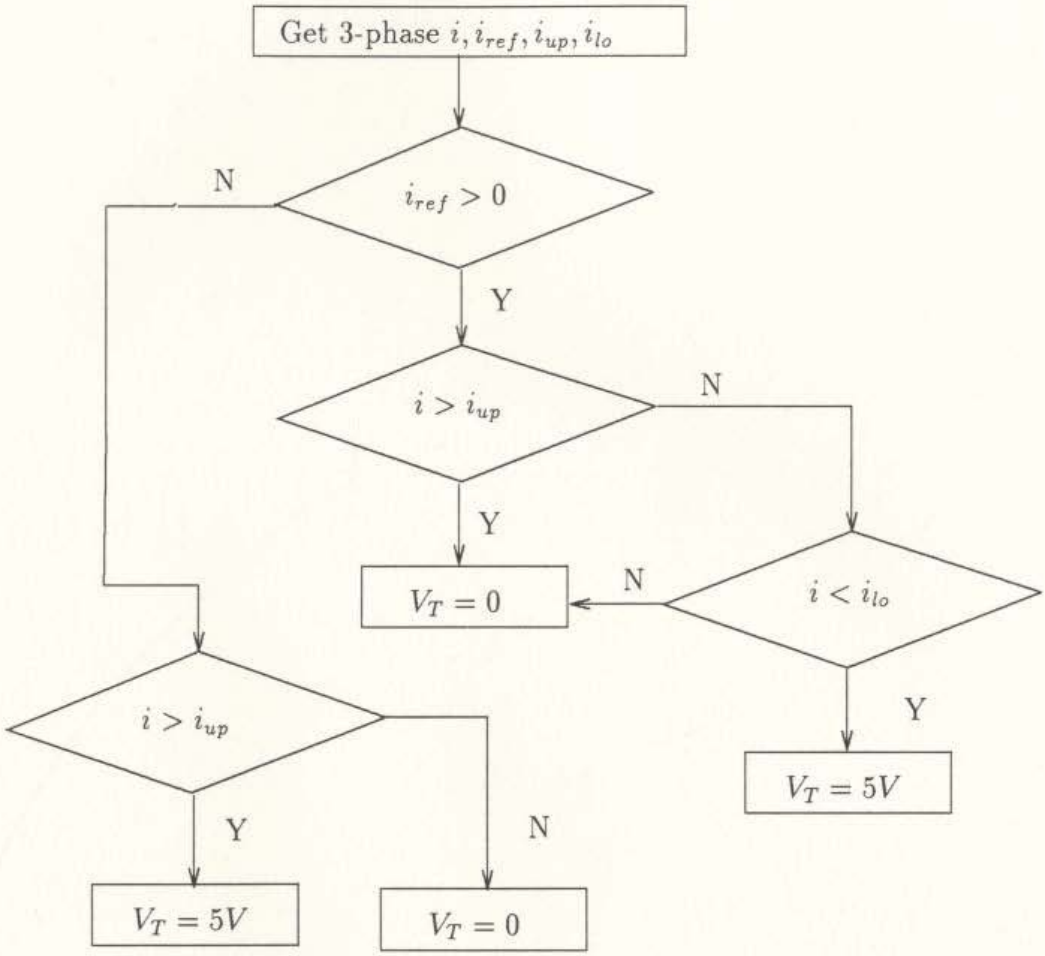

Figure 2.12: Flow chart of three phase PWM signals genaration

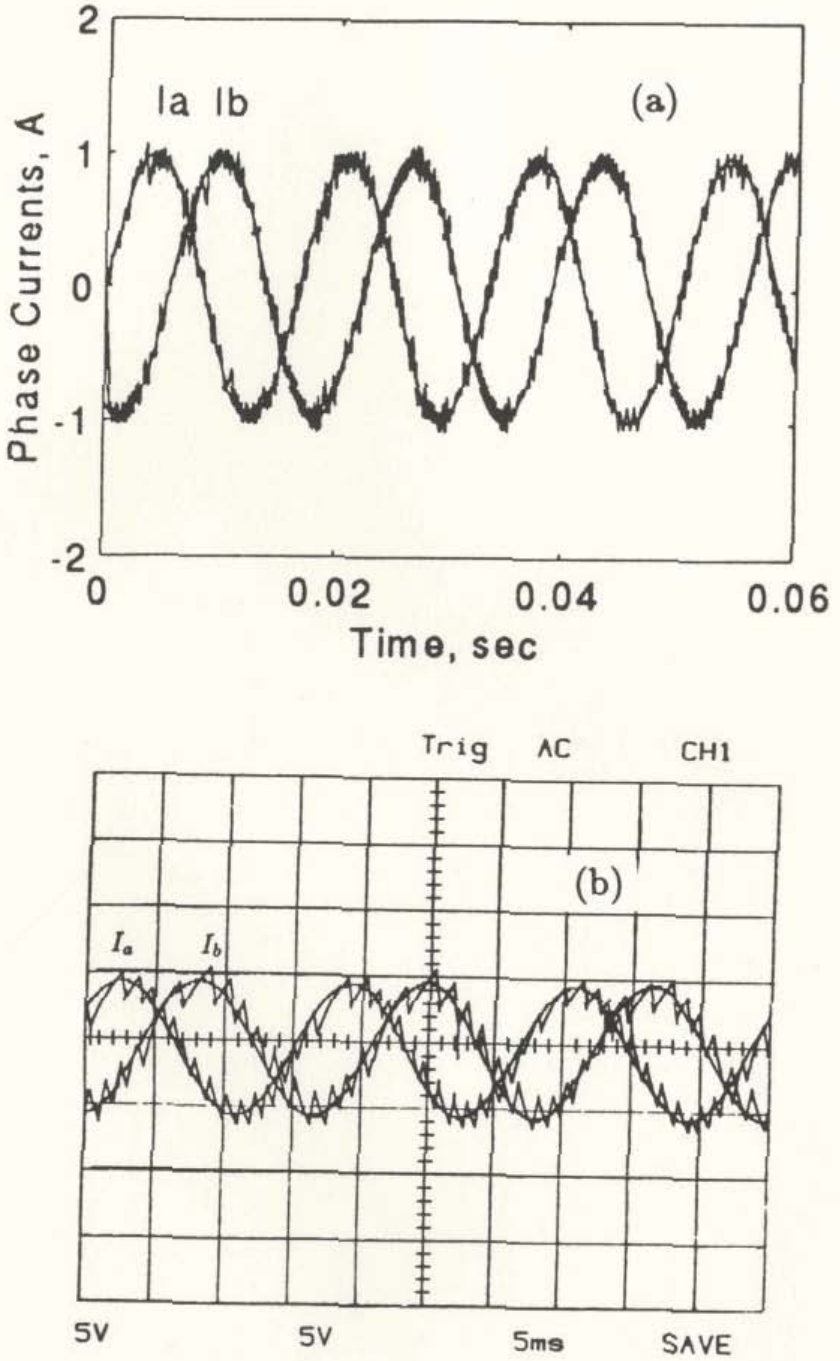

Figure 2.13: Current responses of the hysteresis current controller at the reference frequency 60 Hz: (a) Simulation responses for phase 'a' and phase 'b' (b) Corresponding experimental responses; Y-scale: 1 A/div.

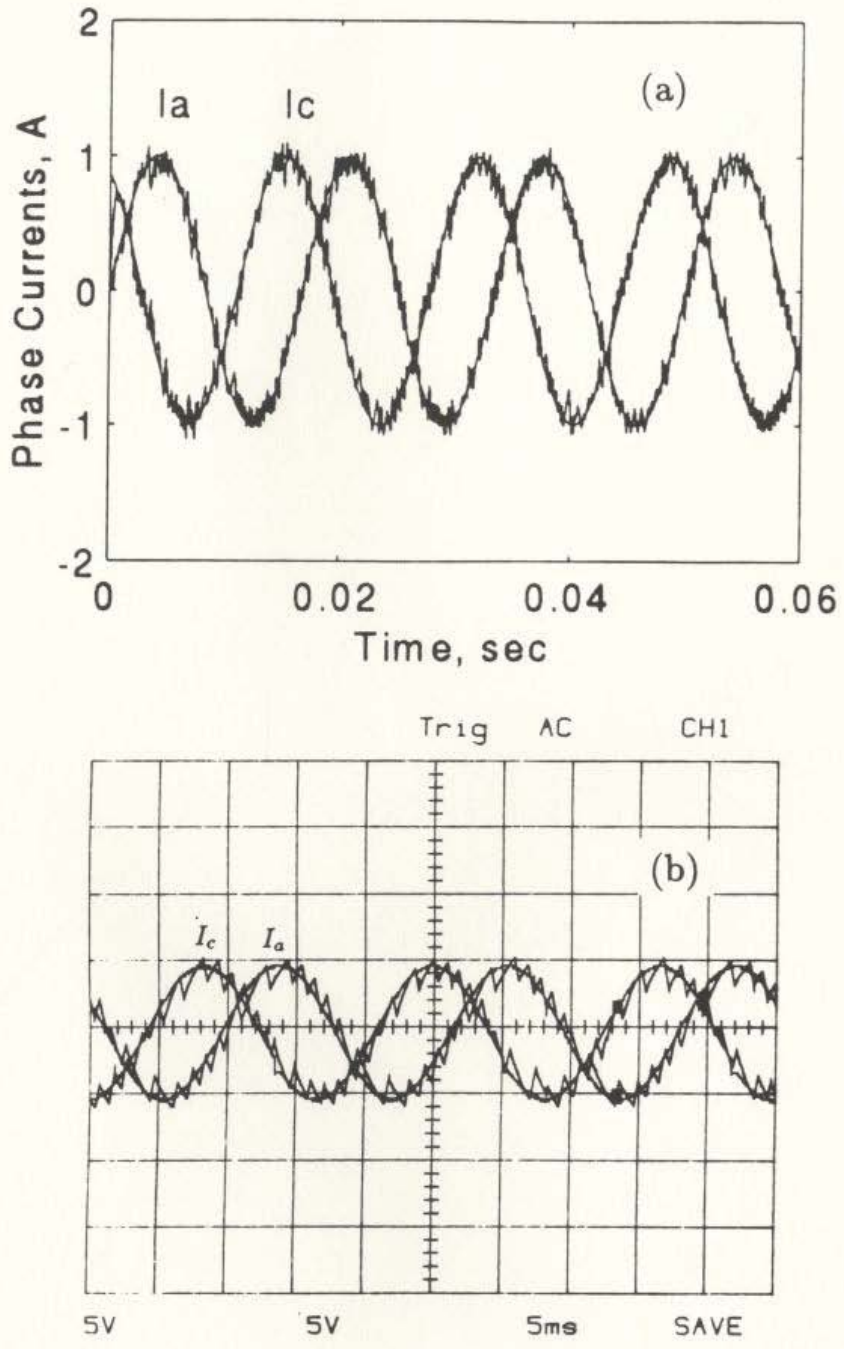

Figure 2.14: Current responses of the hysteresis current controller at the reference frequency 60 Hz: (a) Simulation responses for phase 'a' and phase 'c' (b) Corresponding experimental responses; Y-scale: 1 A/div.

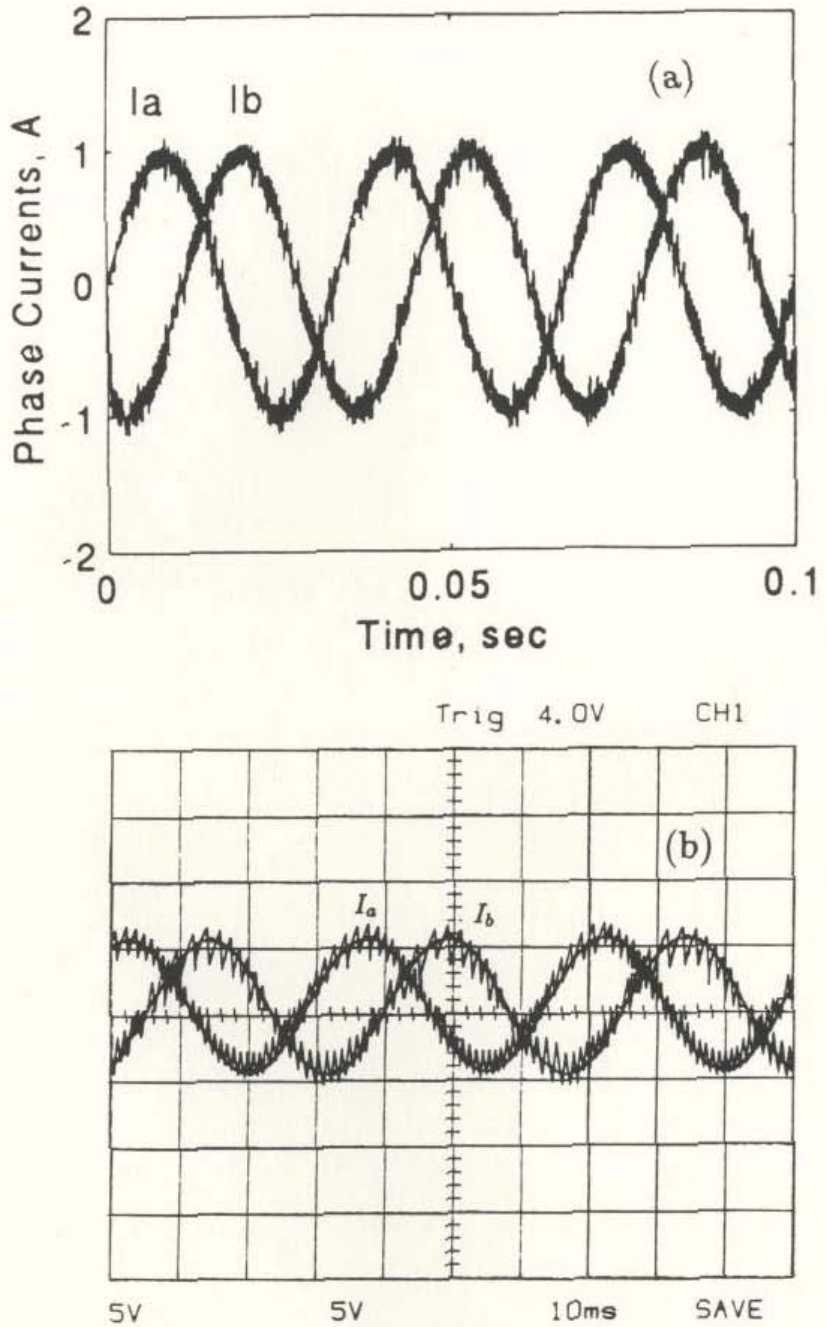

Figure 2.15: Current responses of the hysteresis current controller at the reference frequency 30 Hz: (a) Simulation responses for phase 'a' and phase 'b' (b) Corresponding experimental responses; Y-scale: 1 A/div.

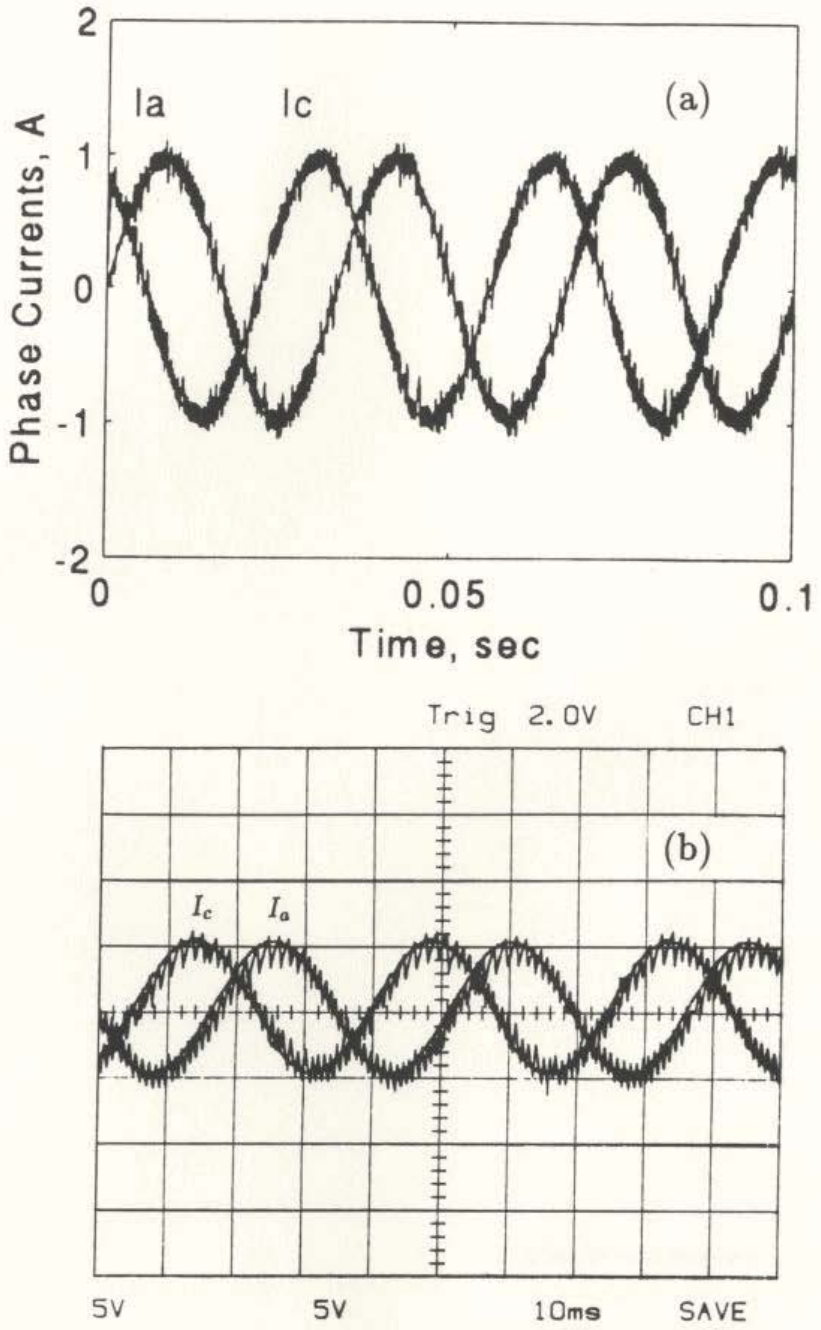

Figure 2.16: Current responses of the hysteresis current controller at the reference frequency 30 Hz: (a) Simulation responses for phase 'a' and phase 'c' (b) Corresponding experimental responses; Y-scale: 1 A/div.

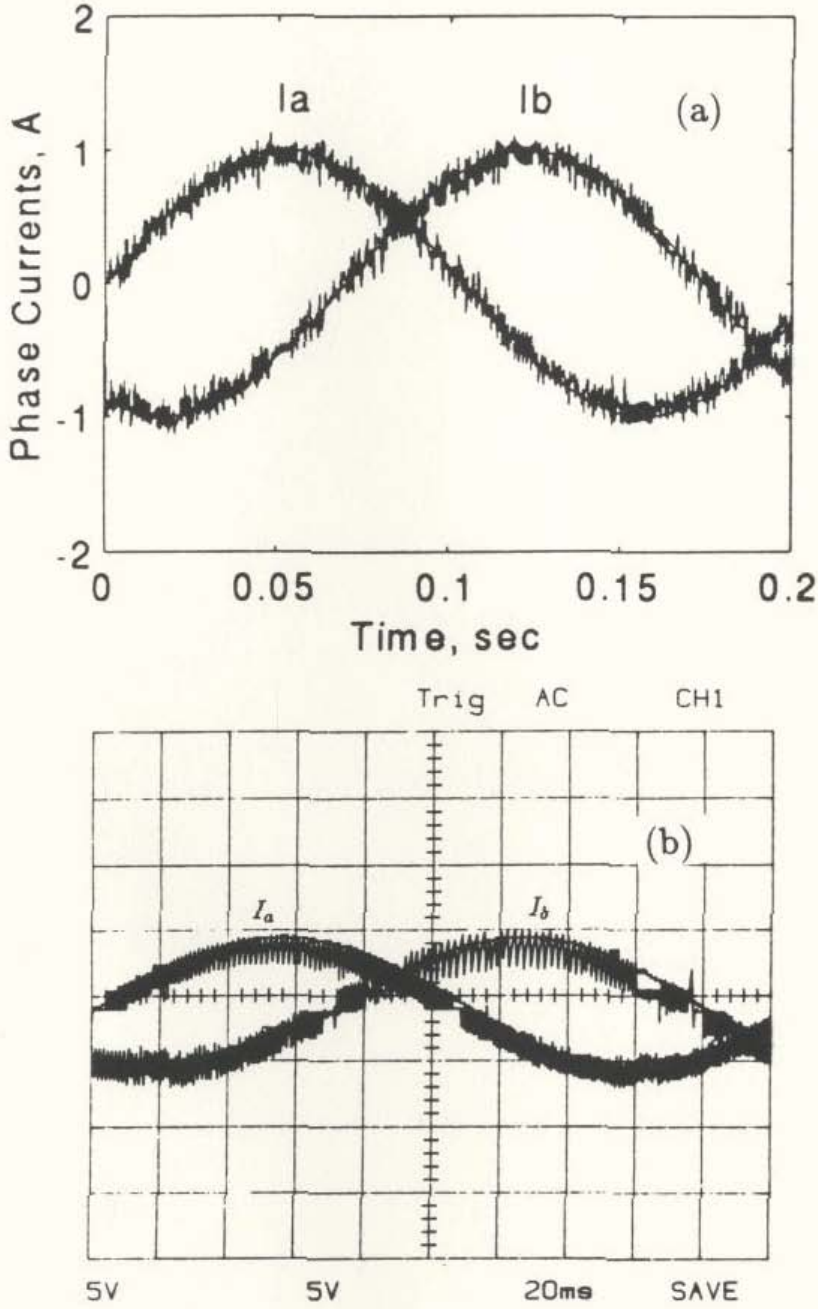

Figure 2.17: Current responses of the hysteresis current controller at the reference frequency 5 Hz: (a) Simulation responses for phase 'a' and phase 'b' (b) Corresponding experimental responses; Y-scale: 1 A/div.

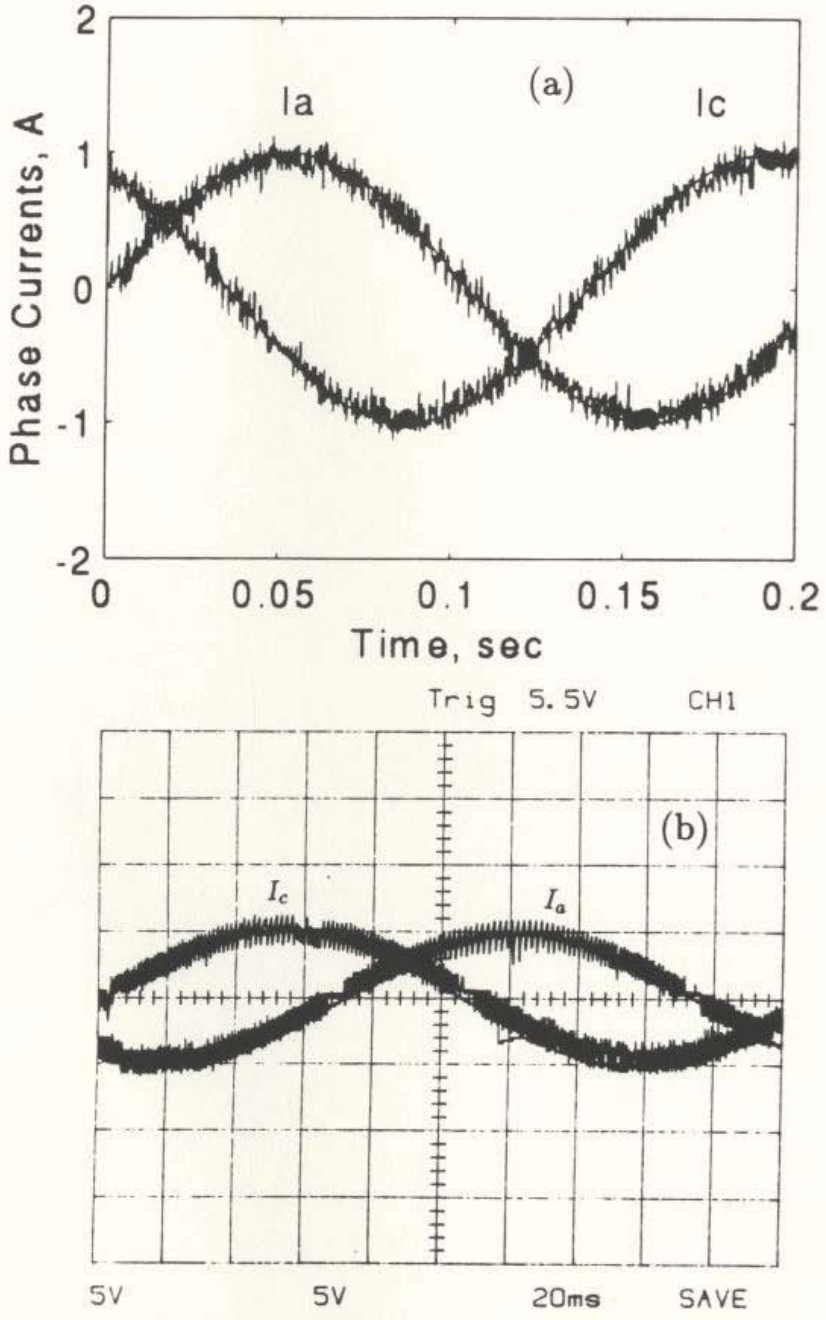

Figure 2.18: Current responses of the hysteresis current controller at the reference frequency 5 Hz: (a) Simulation responses for phase 'a' and phase 'c ' (b) Corresponding experimental responses; Y-scale: 1 A/div.

the reference current are kept constant, the switching frequency of the VSI increases in order to decrease the output voltage. Even though the switching frequency increases, the load currents follow the reference current within the specified band. Experiments have also been carried out to evaluate the performance of the proposed controller for a low reference frequency, such as 5 Hz. Figures 2.17 (a) and 2.18(a) show simulation responses and Fig. 2.17(b) and Fig. 2.18(b) show the corresponding experimental results of phases 'a', 'b' and phases 'a', 'c', respectively. Although the switching frequency increases tremendously for this case, the current controlled VSI does an excellent job of forcing the load current to follow the reference currents. These current responses at the very low frequency ensure successful operation of the hysteresis current controller at low speeds for the brushless PM synchronous motor drive.

2.4 Computer Simulation of the Conventional (PDF type) Speed Controller Based Brushless PM Synchronous Motor Drive

Now-a-days, it is a common practice to evaluate the system performances through computer simulation before the real-time implementation. Therefore, a computer simulation of the brushless PM synchronous motor drive system consisting of a conventional non-adaptive PDF type speed controller has been carried out. The schematic block diagram of the complete system is shown in Fig. 2.2. The inverter transistors are modeled as ideal controlled switches with instantaneous turn-on and turn-off. The switches in each inverter leg have complementary switching states.

There exist many softwares which are specifically developed to simulate the dynamics of the system, namely, electromagnetic transient program (EMTP), simulation

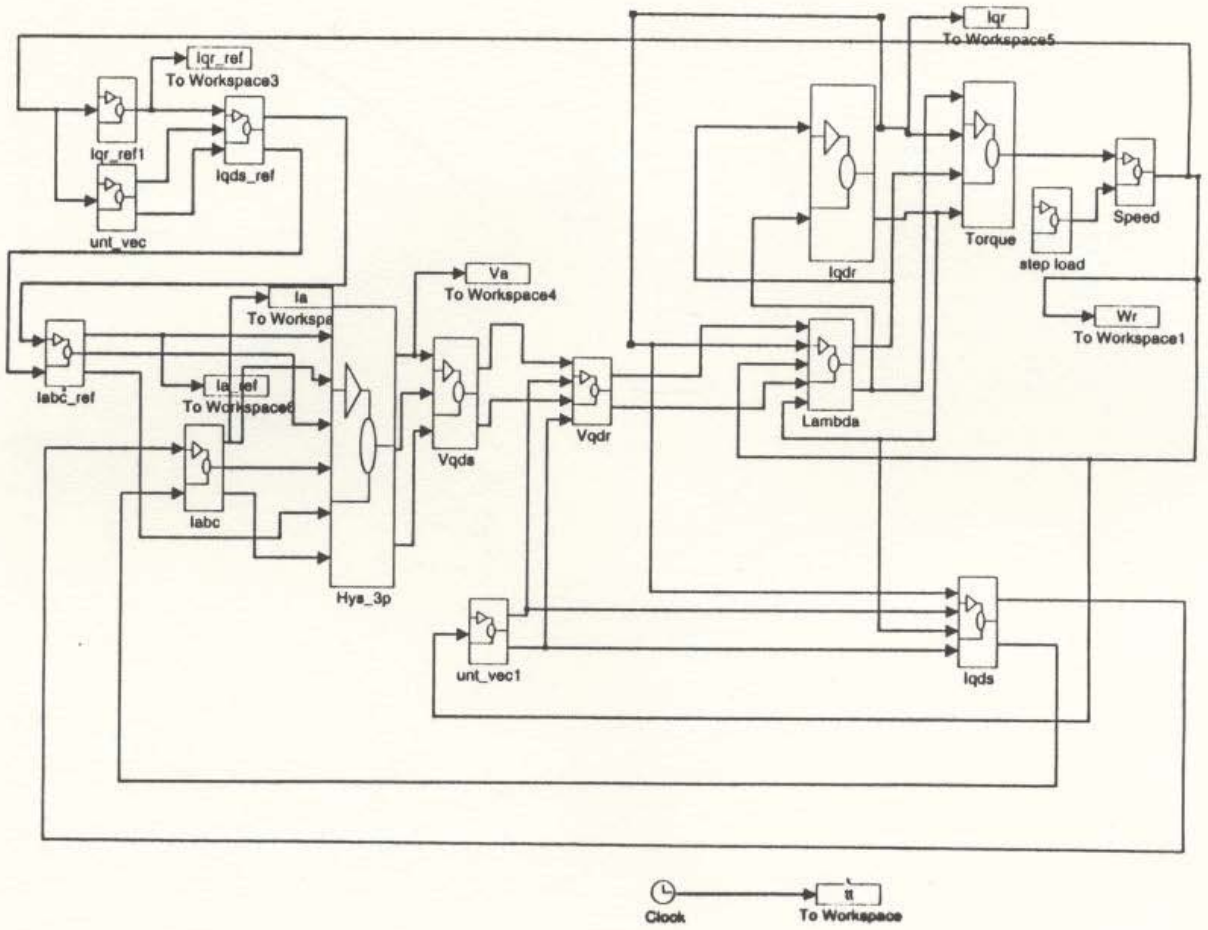

Figure 2.19: SIMULINK brushless PM synchronous motor drive system model with the PDF type speed controller

of nonlinear systems (SIMNON) and SIMULINK [70]. The SIMULINK software has been successfully used in this research. The simulation carried out in this work enables the investigation of both the transient and the steady state operation of the system. Simulation inputs include all the drive circuit parameters along with the reference speed ω_r^*. The simulation outputs consist of the instantaneous current and speed. The SIMULINK software uses metaphors of a block diagram to represent a dynamic system. In order to obtain an accurate and efficient simulation result with SIMULINK, the equations describing the system are required to be arranged in the form of block diagrams. The approach used to obtain the simulation results of the drive system is outlined below.

- The structure of the brushless PM synchronous motor is constructed in the form of block diagrams as shown in Fig. 2.19.
- SIMULINK subsystems of the various components of the drive system are constructed and used in Fig. 2.19. These subsystems are are shown in Appendix D.
- The real-time switching model is used to represent the inverter.
- The built-in Runge-Kutta algorithm is used to obtain the system performances.

2.5 Real-time Implementation of the Conventional Speed Controller Based Brushless PM Synchronous Motor Drive

Experiments have been performed to evaluate the performance of the speed controller

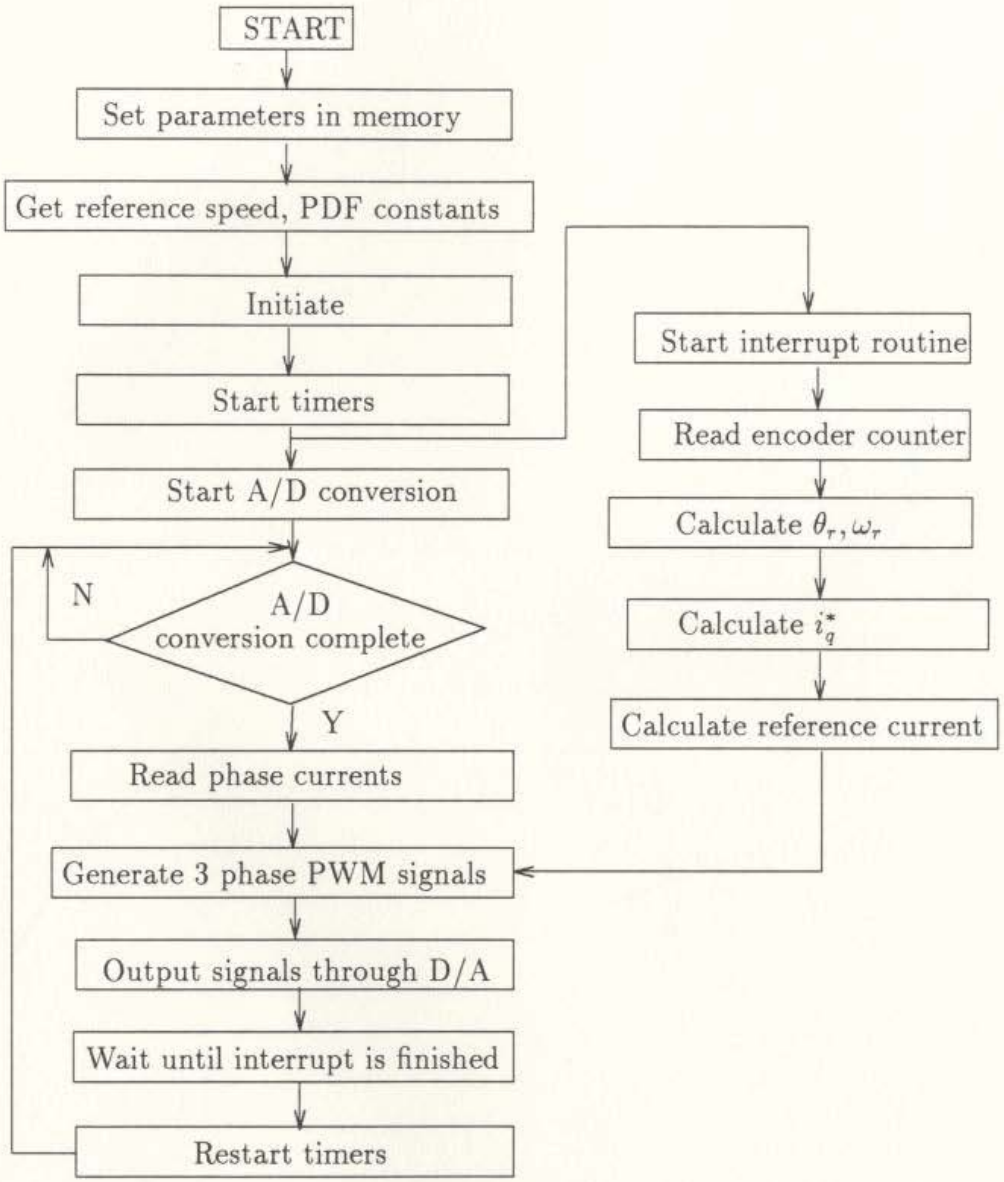

Figure 2.20: Flow chart of the software used for the real-time implementation of the PDF based brushless PM synchronous motor drive

used in the brushless PM synchronous motor drive in real time using the DSP controller board. The state-space model of the speed controller is implemented through the software. The flow chart of the real-time implementation of the PDF type speed controller with the developed hysteresis current controller for the brushless PM synchronous motor drive is shown in Fig. 2.20. Hall-effect current transducers are used to measure the actual line currents, and these are fed to the A/D port of the controller board. The rotor position is measured by an optical incremental encoder installed at the motor shaft. The encoder generates the necessary pulses according to the position information, and are fed to the built-in encoder port of the controller board. A 32 bit counter counts the pulses and is read by a calling function in the software. The motor speed is deduced from the rotor position angle by backward difference interpolation. The peak value of the reference current is determined by the discrete equations of the speed controller and the error between the actual and reference speeds. The three phase reference currents are then computed using the fedback rotor position information. The measured actual currents and the reference currents are used in the hysteresis current controller which provides the necessary switching signals for the voltage source inverter. The complete control algorithms are implemented in software using a high level program written in C. The program is compiled using Texas Instrument C code generator and then down loaded to the DSP controller.

2.6 Results and Discussions

Figures 2.21-2.28 illustrate the simulation and experimental results of the conventional PDF type speed controller based brushless PM synchronous motor drive. All experimental speed responses documented in this work are the oscilloscopic recordings

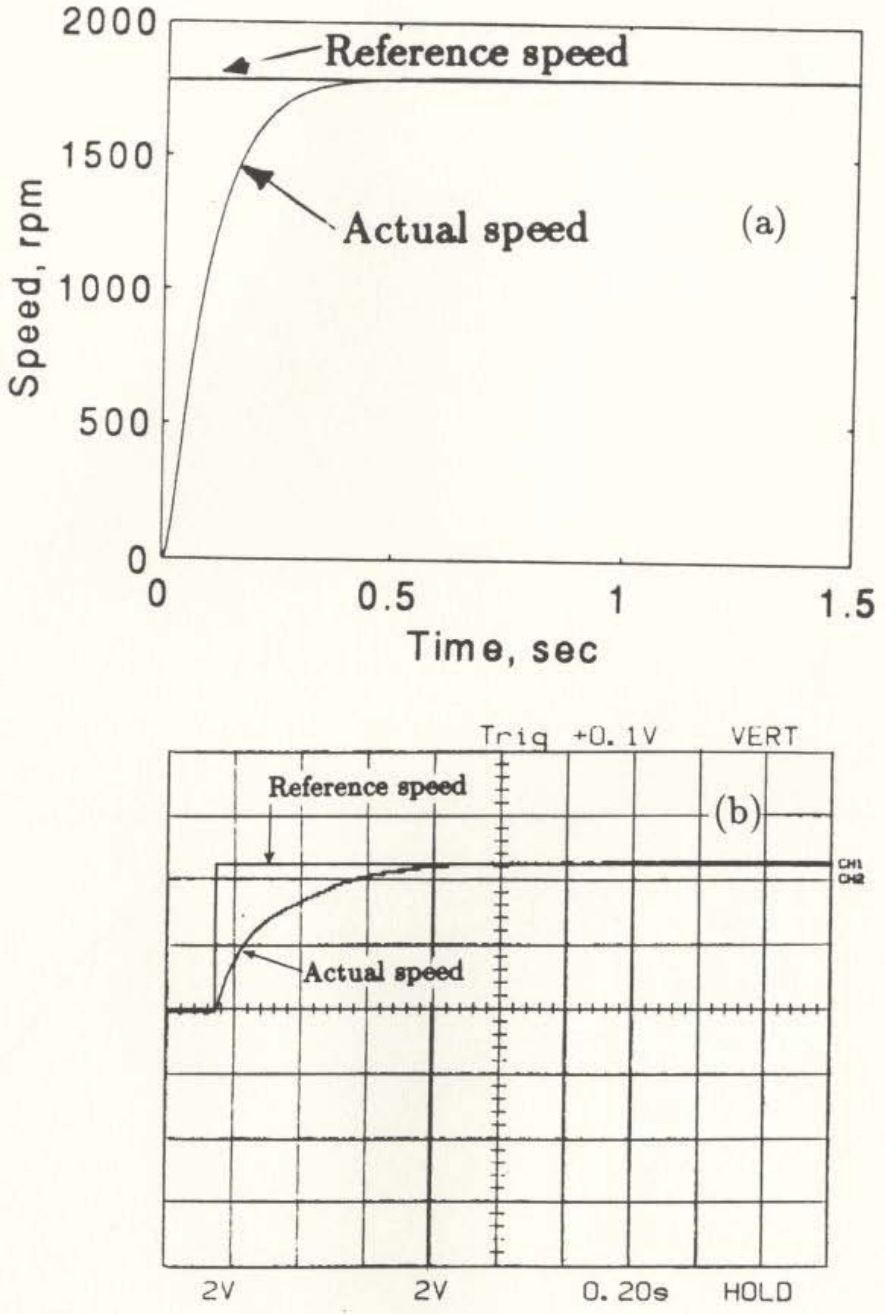

Figure 2.21: Results of the PDF type speed controller based brushless PM synchronous motor drive (a) Simulation speed response at no load with $\omega_r^* = 1800$ rpm (b) Corresponding experimental speed response; Y-scale: 750 rpm/div.

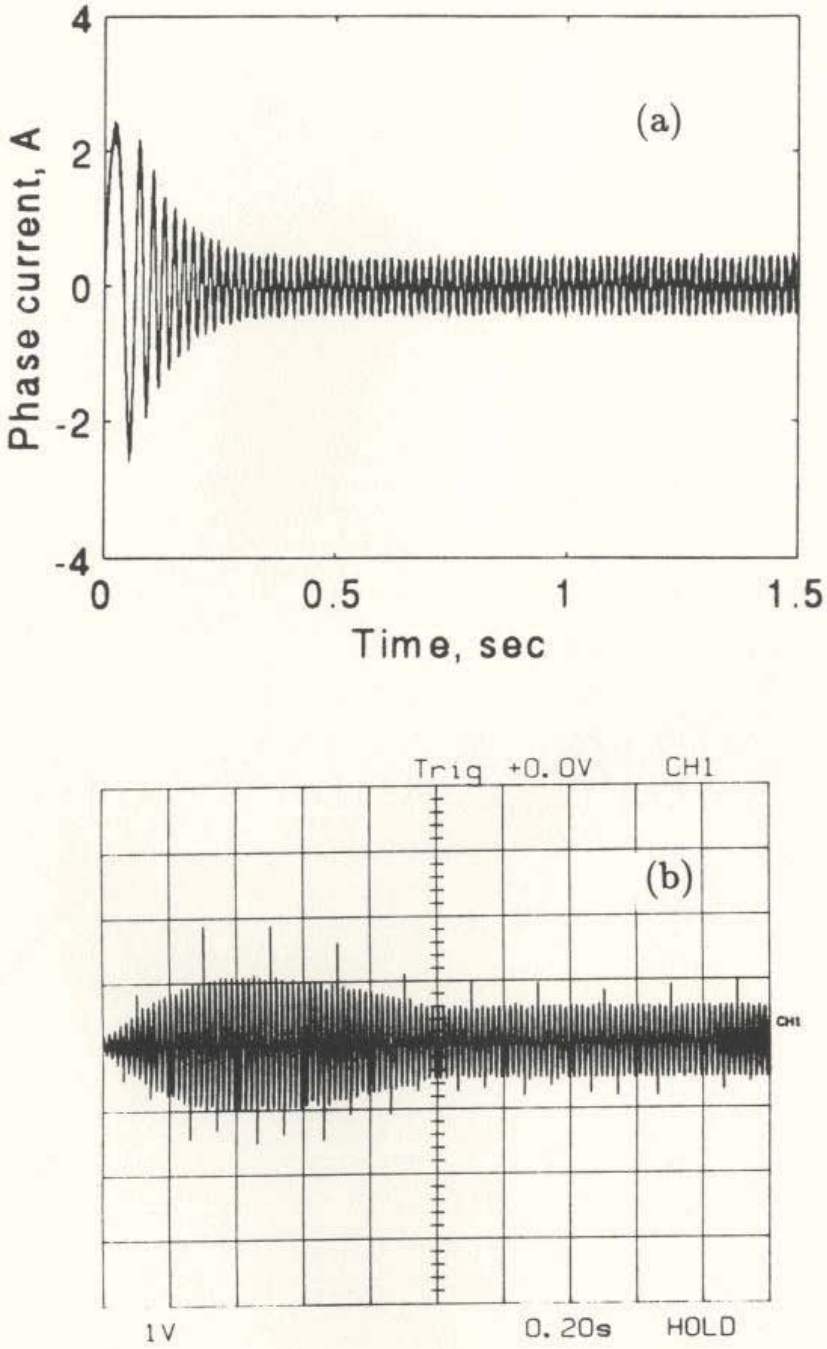

Figure 2.22: Results of the PDF type speed controller based brushless PM synchronous motor drive (a) Simulation current response at no load with $\omega_r^* = 1800$ rpm (b) Corresponding experimental current response; Y-scale: 1 A/div.

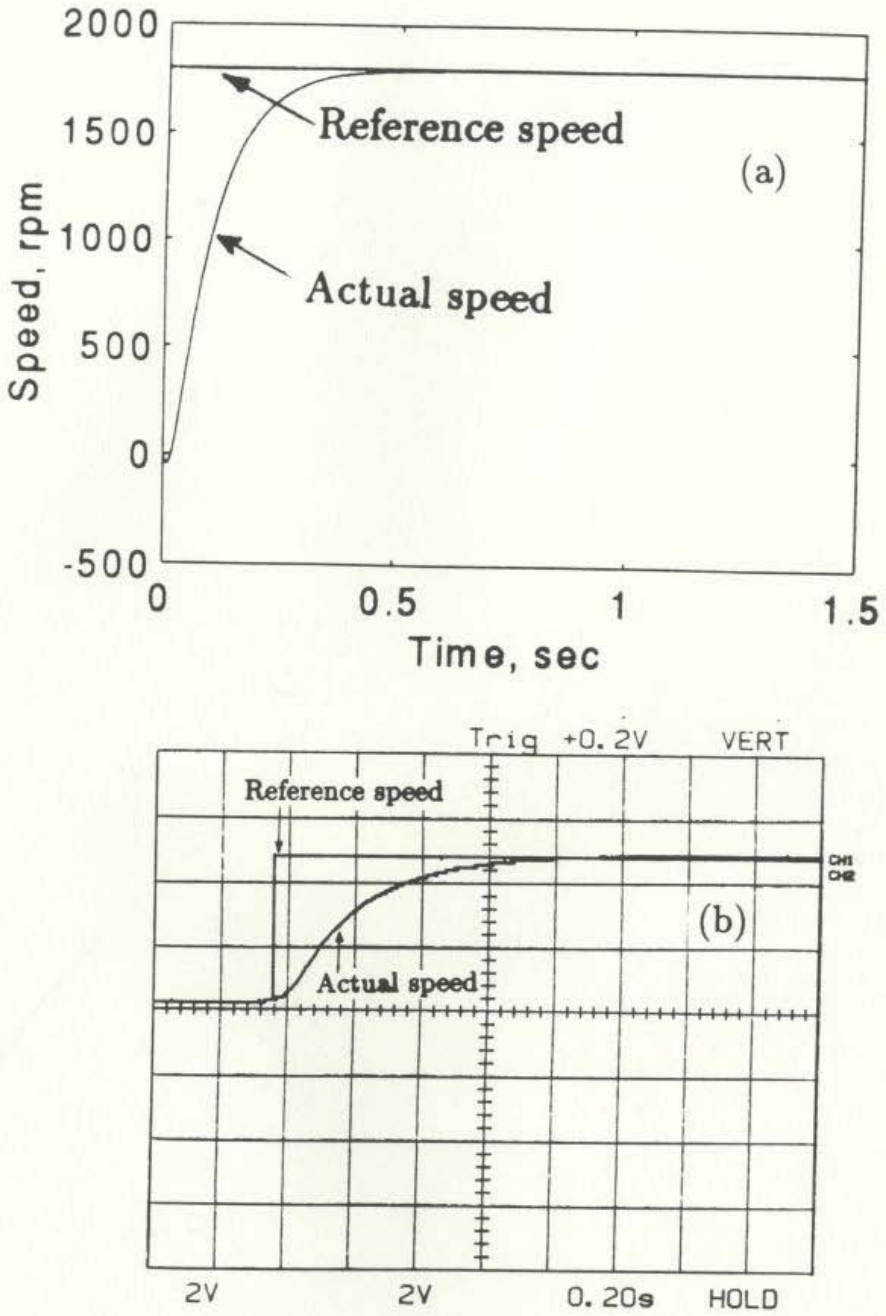

Figure 2.23: Results of the PDF type speed controller based brushless PM synchronous motor drive (a) Simulation speed response at rated load with $\omega_r^* = 1800$ rpm (b) Corresponding experimental speed response; Y-scale: 750 rpm/div.

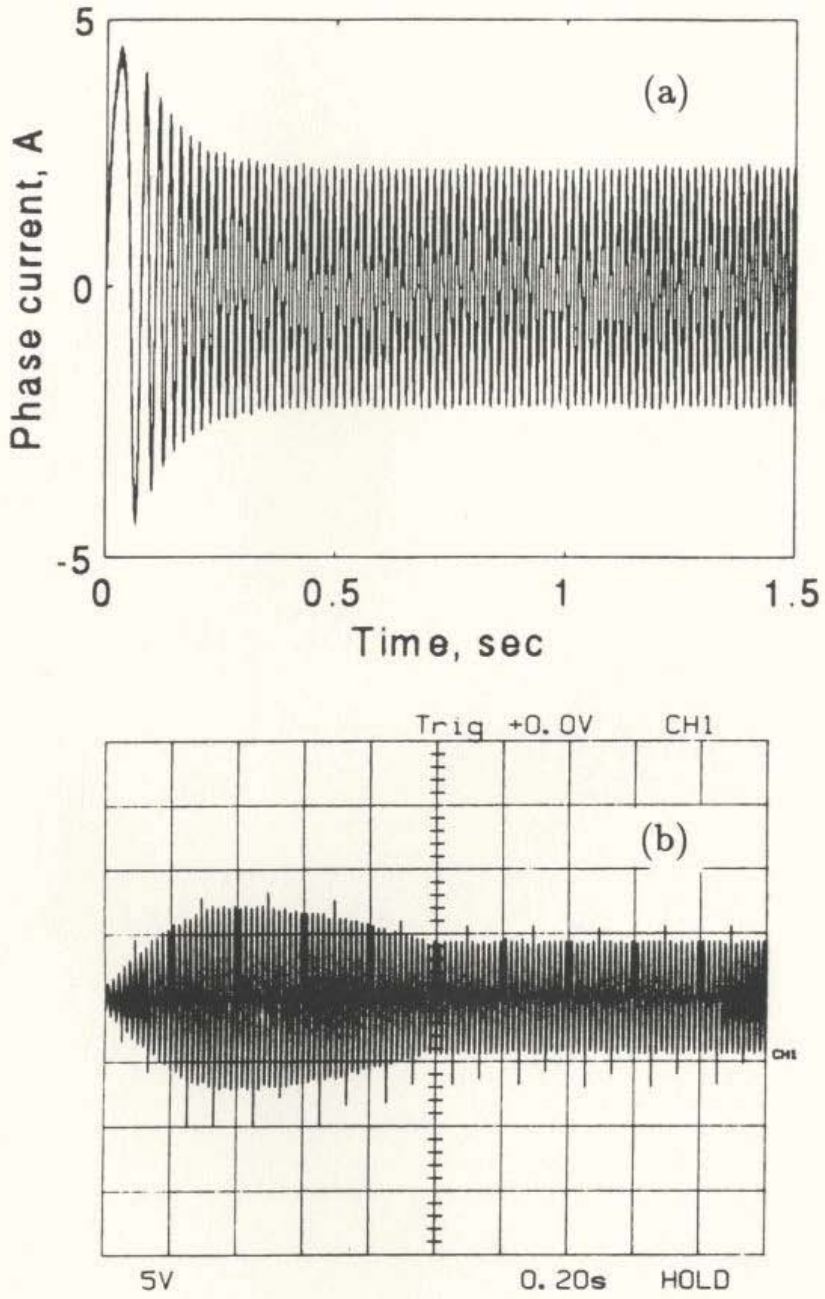

Figure 2.24: Results of the PDF type speed controller based brushless PM synchronous motor drive (a) Simulation current response at rated load with $\omega_r^* = 1800$ rpm (b) Corresponding experimental current response; Y-scale: 5 A/div.

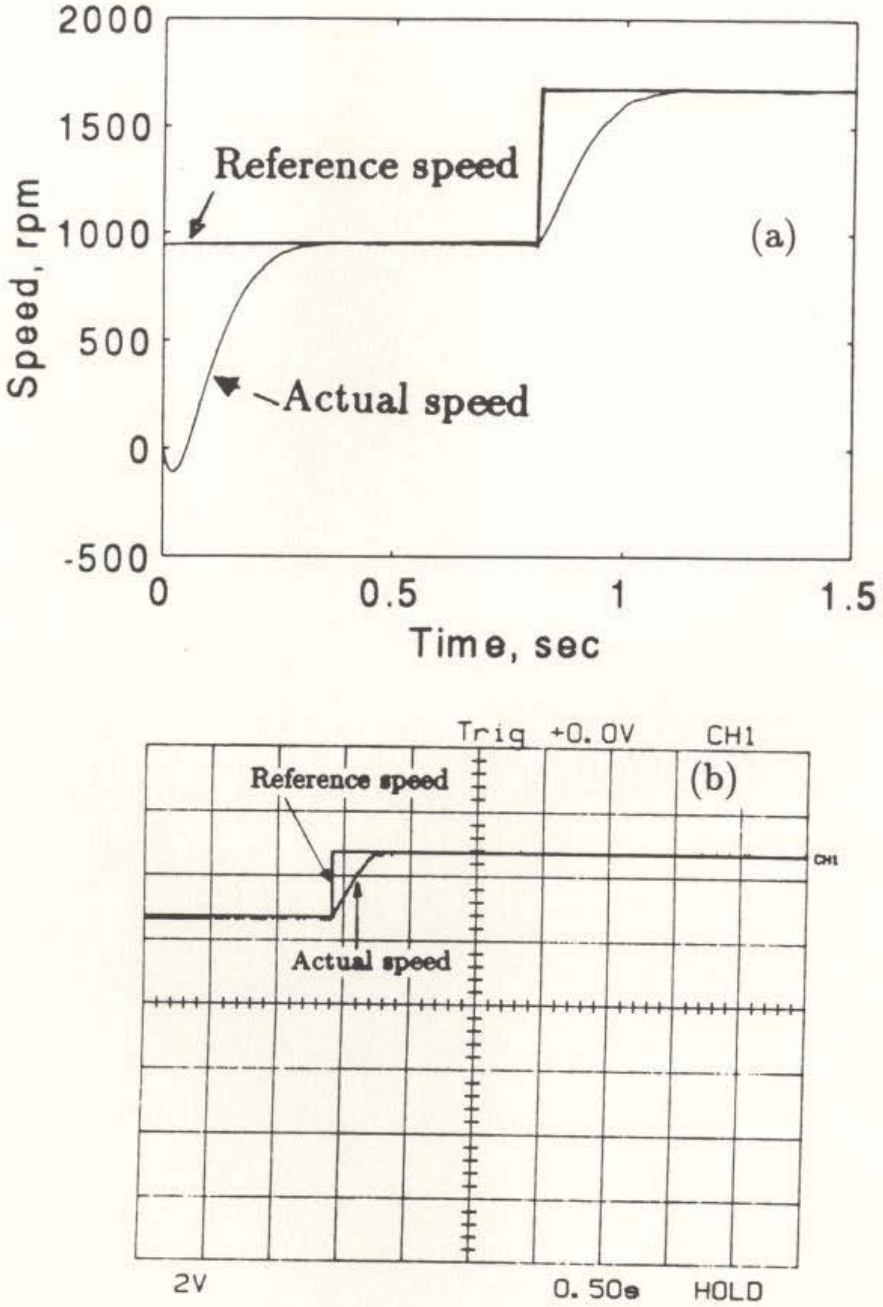

Figure 2.25: Results of the PDF type speed controller based brushless PM synchronous motor drive (a) Simulation speed response at rated load with step change in speed (b) Corresponding experimental speed response; Y-scale: 750 rpm/div.

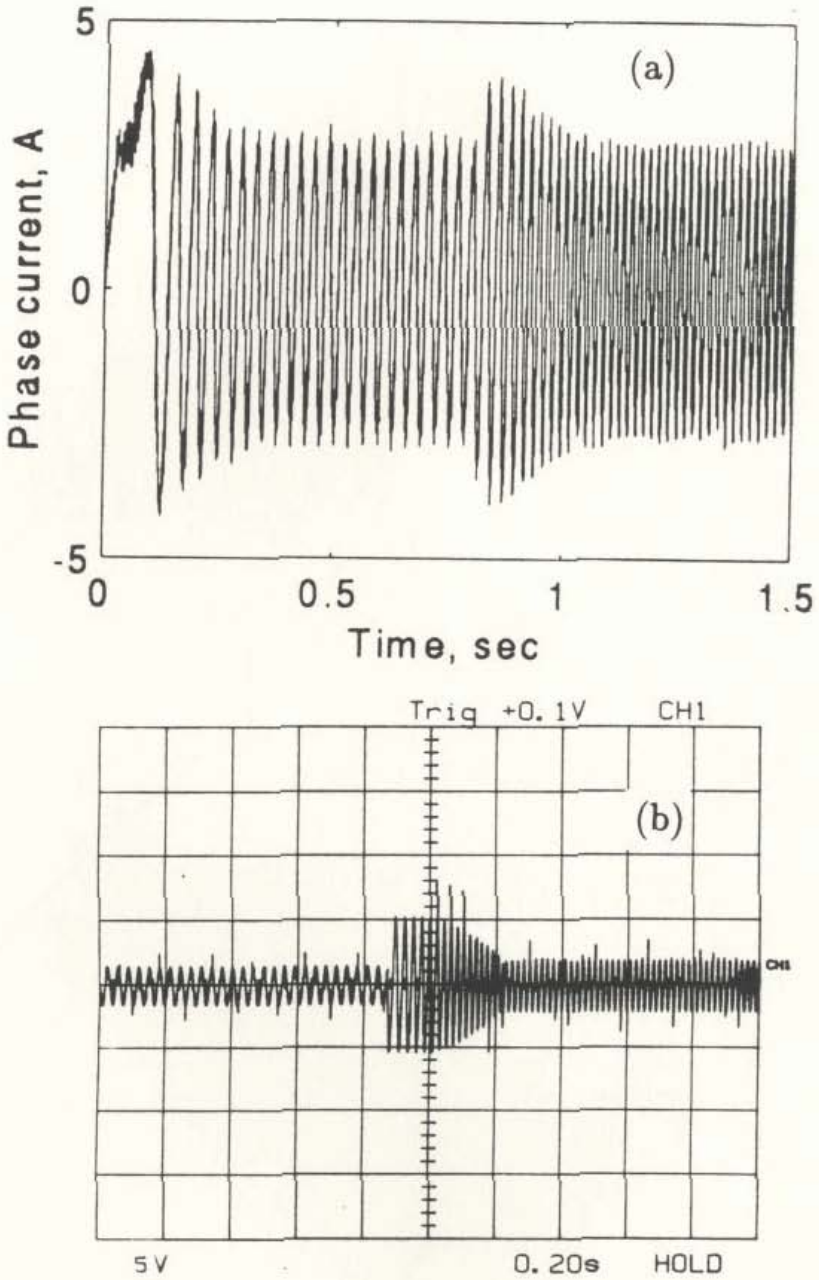

Figure 2.26: Results of the PDF type speed controller based brushless PM synchronous motor drive (a) Simulation current response at rated load with step change in speed (b) Corresponding experimental current response; Y-scale: 5 A/div.

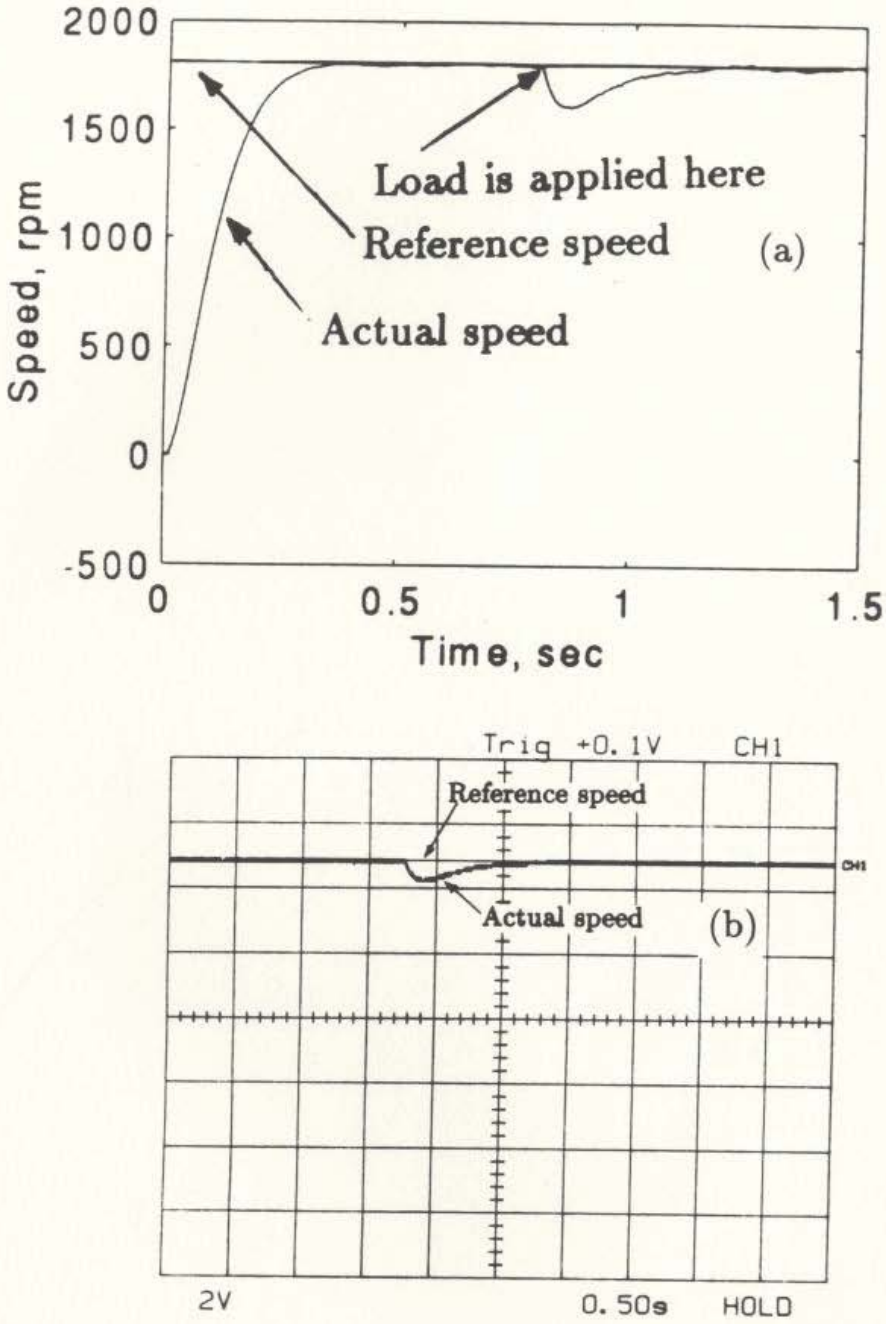

Figure 2.27: Results of the PDF type speed controller based brushless PM synchronous motor drive (a) Simulation speed response at rated speed with step change in load (b) Corresponding experimental speed response; Y-scale: 750 rpm/div.

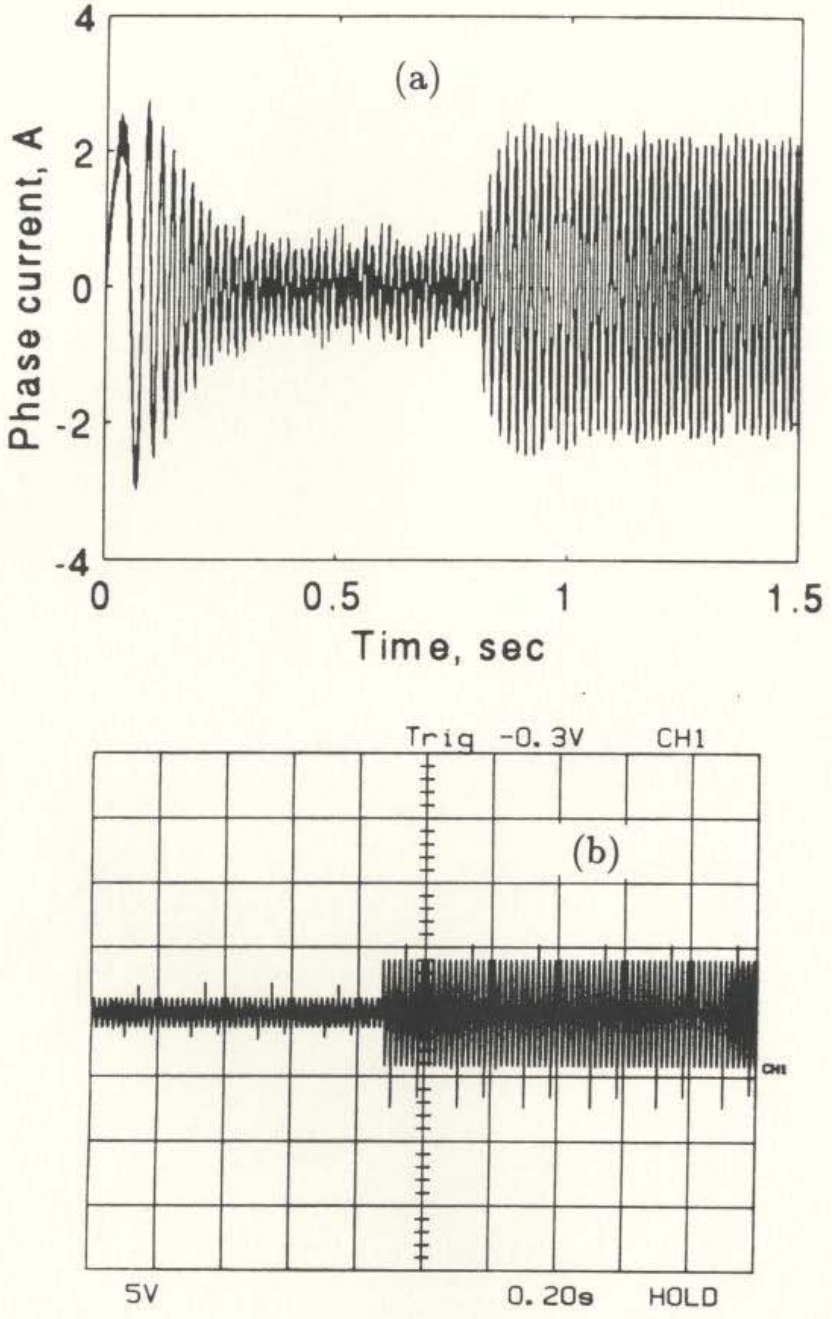

Figure 2.28: Results of the PDF type speed controller based brushless PM synchronous motor drive (a) Simulation current response at rated speed with step change in load (b) Corresponding experimental current response; Y-scale: 5 A/div.

obtained from the tacho-generator. The y-axis of the experimental speed responses represents the voltage corresponding to the speed in rpm and x-axis represents time in second.

Figures 2.21(a) and (b) show the simulation and experimental speed responses with reference speed 1800 rpm at no load condition. The designed speed controller has provided under-damped speed responses of the drive system. It is seen from Fig. 2.21 that the drive can follow the reference speed quite accurately. The experimental speed response in Fig. 2.21(b) shows the reference speed as 1650 rpm. However, the actual reference speed applied was 1800 rpm. The discrepancy of 150 rpm is due to the shifting down of the ground reference level of the oscilloscope by one small division when the speed signals were applied. Figures 2.22 (a) and (b) show the simulation and experimental current responses under no load condition at the rated reference speed. Figures 2.23(a) and (b) show the simulation and experimental speed responses under the full load condition at the reference speed of 1800 rpm. It is again evident from Fig. 2.23 that the actual speed trajectory of the PDF type speed controller based drive system follows the reference speed without over-shootings or speed oscillations at the rated conditions. Figures 2.24 (a) and (b) show the corresponding current responses of the drive system at full load. Performances have also been evaluated for the step change in speed and loading conditions. Figures 2.25(a) and (b) show the simulation and experimental speed responses with the step change in speed. Figures 2.26(a) and (b) show the corresponding current responses of the drive system for this condition. Simulation and experimental speed responses upon a sudden load impact are shown in Figs. 2.27(a) and (b). The simulation speed response of Fig. 2.25(a) shows the transient response as well as the dynamic response at the instant of change in reference speed. However, Fig. 2.25 (b) represents the experimental

speed response with dynamic step change in reference speed at the steady-state condition. Figures 2.28(a) and (b) show the corresponding current responses of the drive system for change in reference speed . Simulation and experimental speed responses upon sudden load impact are shown in Figs. 2.27(a) and (b), respectively. Figure 2.27(a) shows the simulated transient as well as the dynamic speed responses of the drive system, whereas Fig. 2.27(b) depicts the experimental dynamic speed response with the sudden load impact at the steady-state condition. Figure 2.28 (a) and (b) show the corresponding current responses. It is apparent that there is a considerable amount of speed drop on the application of sudden load which is not acceptable for high performance drive systems. Attempts have also been made to obtain speed responses with low reference speed and parameter variations such as change in inertia and/or adding additional resistance in the stator circuits, but the fixed gain speed controller fails to track the reference speed satisfactorily for these conditions unless the parameters are readjusted.

The envelopes of the current responses as shown in Figs. 2.22, 2.24, 2.26 and 2.28 represent the q-axis reference currents. From these figures it is clear that the conventional PDF-type speed controller based brushless PM synchronous motor drive system is capable of providing the required q-axis currents for specific operating conditions. The transient as well as the steady-state values of the phase currents are within the prescribed limit of 10 ampere.

Certain observable differences are found between the simulation and experimental current responses of the PDF type brushless PM synchronous motor drive system. These are due to the fact that a ramp rather than a step dc voltage has been applied in the experiment to the inverter to ensure its safe operation. In Figs. 2.26 and 2.28, experimental currents are recorded after they reach the steady-state values in order

to depict the dynamic responses at step change in reference speed and step change in load. However, the simulation current responses for these conditions contain transient as well as dynamic responses.

2.7 Concluding Remarks

From the evaluated system performances, it can be concluded that the conventional speed controller like the PDF type is not suitable either for wide range of speed operations or system parameter variations. Moreover, other factors such as saturation, disturbances, temperature may affect the performance of the drive with the conventional controller. Hence an adaptive controller is required which can tackle the above control system problems. As reviewed in the literature, since the ANN has been considered as one of the promising techniques to solve the above mentioned control system problems, the speed control of the ANN based brushless PM synchronous motor drive needs to be explored.

Chapter 3

Artificial Neural Network Based High Performance Motor Drives

The term "Artificial Neural Network (ANN)" is well recognized as the application of artificial intelligence. ANNs try to imitate the biological brain structure through mathematical models by acquiring knowledge through learning and storing that information using inter-neuron connection strengths known as synaptic weights. Thus in every ANN, there are some simple nonlinear elements known as neurons. These neurons are interconnected and the strengths of the interconnections are denoted by parameters called weights. Depending on the task to be performed, the weights are adjusted either via some prescribed off-line training, which remain fixed during operation, or via an on-line training algorithm that are continuously updated according to the operating conditions by minimizing some objective functions. When a desired error goal is achieved through learning, the best values of the actual strength of interconnections are stored. The interconnections and their strength provide the memory which is necessary in a learning process.

Feed forward and other types of neural networks are used to obtain a controller

having the on-line adaptive properties for the brushless PM synchronous motor drive. This chapter highlights the capabilities and advantage of artificial neural networks. The general structures with activation functions of the ANN are discussed. The training algorithm used in this work is the back-propagation. The basic concept of the back-propagation is also outlined with the weights and bias updating algorithm. Finally, the feasibility of using the ANN for the interior-type brushless PM synchronous motor drive is discussed.

3.1 Capabilities and Advantages of Neural Networks

ANNs have the capabilities of learning and self-organization. They also have the capabilities of performing massive parallel processing which is in contrast to the Von Neumann digital computers in which the instructions are executed sequentially. ANNs can also provide, in principle, significant fault tolerance, since damage to a few links need not significantly impair the over-all performance [71].

ANNs can simplify modeling complexity, often discontinuous nonlinearities, by providing basic components needed to model many forms of harsh nonlinearities. In addition, ANNs can learn changes in parameters of systems with discontinuous nonlinearities as well as continuous linearities with relatively simple estimation techniques if the ANN is structured to closely mimic the physical process. It has been observed that ANNs prove very effective at learning and compensating for discontinuous nonlinearities such as dead time and saturation, which dominate many drives and motion control problems [72].

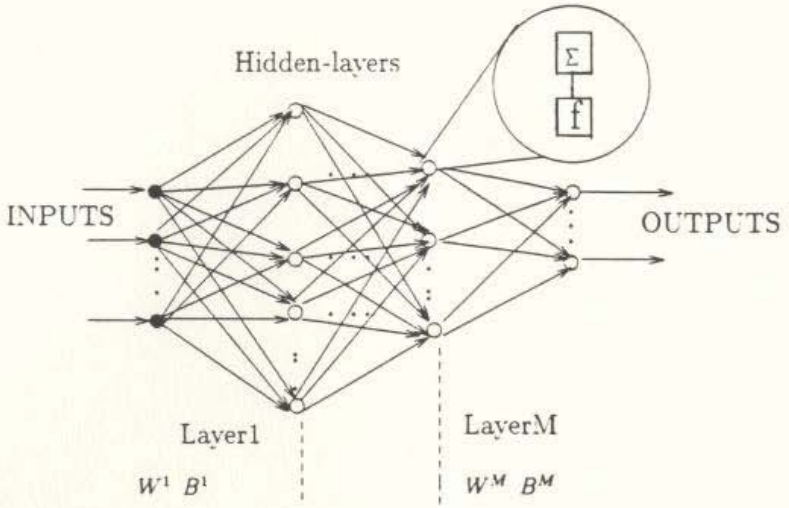

Figure 3.1: A feed forward neural network

3.2 Descriptions of Mostly Used ANNs in Drive Technology

Two classes of ANNs which have received considerable attention in the area of ANN based motor drives are:

1. Multi-layer Feed Forward Neural Network (FFNN).

2. Recurrent Networks.

The artificial neural network of Fig. 3.1 is referred to as a feed forward neural network. When at least one feedback from the output is added in the FFNN, the ANN is known as a recurrent neural network. A general view of a recurrent neural network is shown in Fig. 3.2. The recurrent networks have been used in associative memories as well as for the solution of optimization problems [72]. Since the proposed work is mainly based on the feed forward neural network, this type of ANN is discussed briefly in the following section.

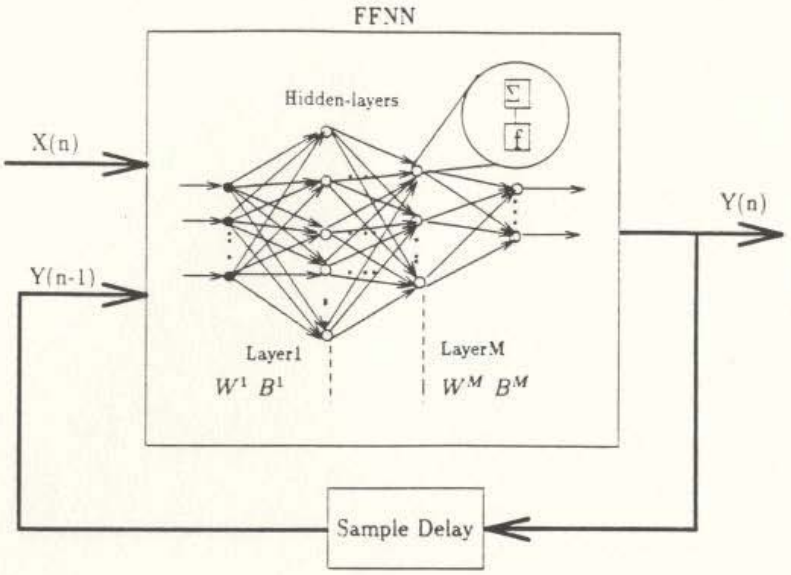

Figure 3.2: A recurrent neural network

3.2.1 Feed forward neural networks

Multi-layer feed forward neural networks have proved extremely successful in pattern recognition, image processing and speech recognition [73]-[75]. These networks with back-propagation training algorithm are receiving wide attention in control application [46], [72]. Model uncertainty is one of the major problems faced by control engineers. For a highly non-linear, composite and complex drive system, it is not possible to represent adequately the system characteristics such as non-linearity, time delay, saturation and time varying parameters. Classical control design uses a constant gain controller such as PI or PID which stabilizes a class of linear system over a small range of system parameters, while adaptive control adjusts the control characteristics to stabilize a system with unknown parameters in the robust control design. But implementation of the system in real time with conventional adaptive controller sometimes becomes very difficult because these involve complex computations with large number of unknown parameters. FFNNs have enough potential to solve the

control problems, because that have the capability to learn system characteristics through a non-linear mapping.

3.3 General Description of an ANN

The blank circles shown in Figs. 3.1 and 3.2 are known as the neurons of the network. These are the information processing units which are fundamental to the operation of a neural network. An artificial neural network consists of an input layer, at least one hidden layer and an output layer. The introduction of the hidden layer is to intervene between the external input and the network output. The source nodes in the input layer of the network supply respective elements of the input vectors which constitute the input signals of the second layer of the network. The output of this layer serves as the inputs to the third layer of the network and so on. The set of the output signals of the neurons in the output or the final layer of the network constitutes the overall response of the network. Fig. 3.3 shows the model of a neuron. There are three basic elements of the neuron model, namely, a set of connecting links, an adder for summing the input signals and the activation function.

In general, the *kth* neuron can be represented mathematically by the equations

$$S_k = \sum_{j=1}^{N} W_{kj} I_j, \tag{3.1}$$

$$O_k = f(S_k + B_k), \tag{3.2}$$

where $I_1, I_2, ..., I_N$ are the input signals ; $W_{k1}, W_{k2}, ..., W_{kN}$ are the synaptic weights of the neuron k; S_k is the linear combined output; B_k is the bias; $f(.)$ is the activation or transfer function: and O_k is the output signal of the neuron.

The activation or transfer function denoted by $f(.)$, defines the output of the neuron

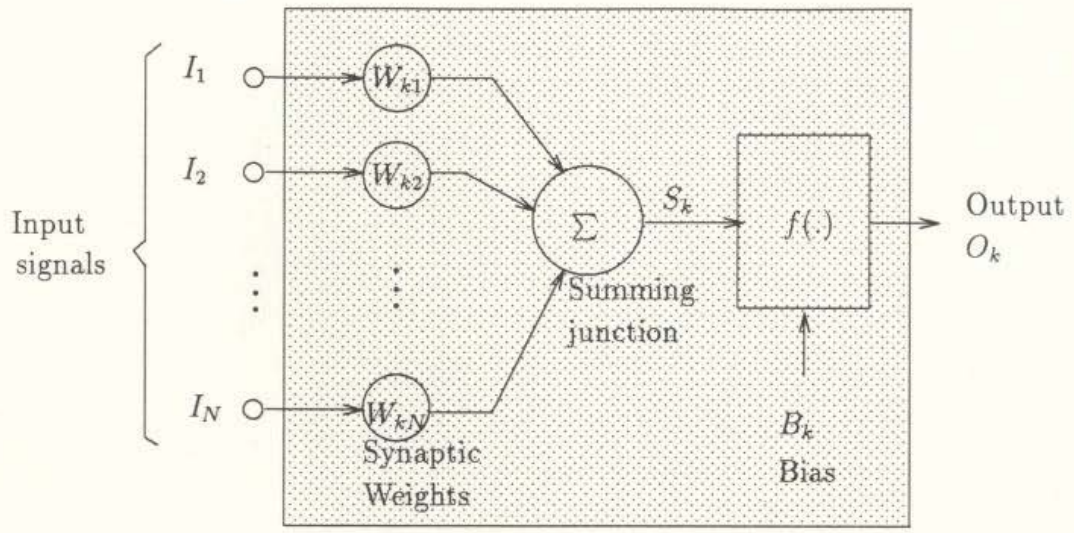

Figure 3.3: A neuron model

in terms of the activity level at its input. The following are the typical activation functions used in the ANN.

Binary Threshold

$$f_{T+}(v) = 1, v > 0 \tag{3.3}$$

Binary Linear Saturation

$$f_{L+}(v) = min\{max\left(\frac{v+1}{2}, 0\right), 1\} \tag{3.4}$$

Binary Sigmoid or Tan-sigmoid

$$f_{S+}(v) = (1 + e^{-v})^{-1} \tag{3.5}$$

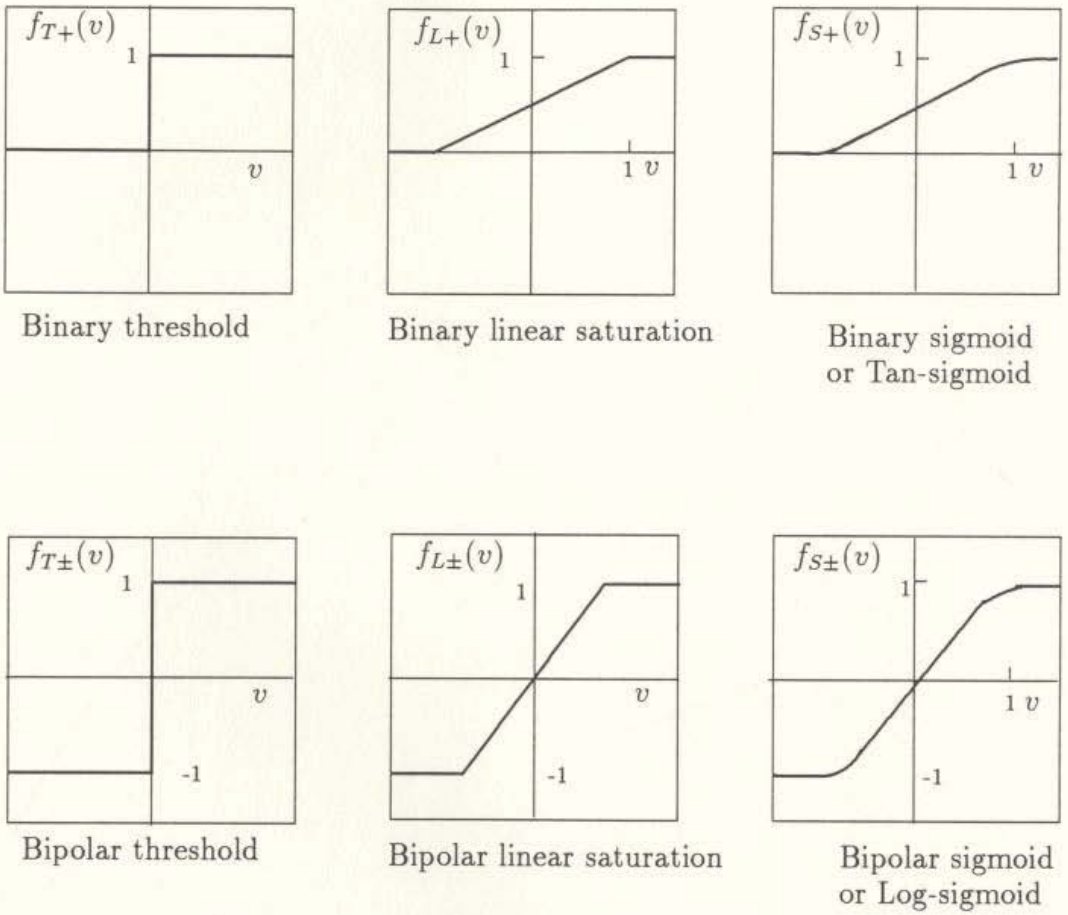

Figure 3.4: Graphical representation of activation functions

Bipolar Threshold

$$f_{T\pm}(v) = sgn(v) \tag{3.6}$$

Bipolar Linear Saturation

$$f_L\pm(v) = min\{max(v, -1), 1\} \tag{3.7}$$

Bipolar Sigmoid or Log-sigmoid

$$f_{S\pm}(v) = \frac{1 - e^{-v}}{1 + e^{-v}} \tag{3.8}$$

The above activation functions are shown graphically in Fig.3.4.

3.3.1 Back-propagation algorithm for the ANN

An ANN can approximate virtually any useful function to any desired level of accuracy if it has enough number of neurons and if it has the proper weights and biases. Unfortunately, without any pre-imposed structure, determining the correct number of neurons and interconnecting weights is considered as one of the major problems. However, weight optimization can be performed through the least square gradient descent training procedure known as the back-propagation training [71]. Basically the back-propagation consists of two passes through the different layers of the network; one is the forward pass and the other is known as the backward pass.

Network training

Consider a vector set of P pairs $(x_1, y_1), (x_2, y_2), ..., (x_p, y_p)$, where the non-linear functional relationship between x and y is given as

$$y = \phi(x), \tag{3.9}$$

where $x \in R^N, y \in R^M$. The objective is to train the network so that it learns an approximation

$$O = y' = \phi'(x). \tag{3.10}$$

It is to be noted here that learning in an ANN means finding an appropriate set of weights and biases. Because there exists a non-linear as well as multi dimensional mapping between inputs and outputs, the steepest descent gradient is used in this algorithm [71].

A vector $x_p = (x_{p1}, x_{p2}, ..., x_{pN})^t$ is applied to the input layer of the network. The net input to the jth hidden unit is given by

$$S_j^h = \sum_{i=1}^{N} W_{ji}^h x_i + B_j^h. \tag{3.11}$$

where W_{ji}^h is the weight on the connection from the ith input unit to jth neuron at the hidden layer and B_j^h is the bias. The superscript h refers to the quantities at the hidden layer. The output of the jth neuron at the hidden layer can be written as

$$O_j^h = f_j^h(S_j^h). \tag{3.12}$$

For the kth neuron, the equations of the output nodes can be expressed as

$$S_k^o = \sum_{j=1}^{L} W_{kj}^o O_j^h + B_k^o, \tag{3.13}$$

$$O_k^o = f_k^o(S_k^o), \tag{3.14}$$

where W_{kj}^o is the weight on the connection from the jth neuron at the hidden layer to the kth neuron at the output layer. The superscript o refers to the output layer quantities.

Weight updating:

As mentioned above, the weights and biases need to be updated unless a desired error goal is achieved. The error function is given by

$$e_k = (T_k - O_k^o). \tag{3.15}$$

where T_k is the target and O_k^o is the actual output from the kth unit. The error to be minimized is governed by the delta rule which works with sum-squared error for all output units, and is expressed as [71]

$$E = \frac{1}{2}\sum_{k=1}^{M} e_k^2 \tag{3.16}$$

$$= \frac{1}{2}\sum_{k}^{M}(T_k - O_k^o)^2, \tag{3.17}$$

where M is the number of outputs.

Output-layer weight updating:

A correction or change in weight ΔW_{kj}^0 on the kth neuron at the output layer is proportional to the instantaneous negative gradient $\delta E/\delta W_{kj}^0$. Using the chain rule, the negative gradient can be written as

$$\frac{\delta E}{\delta W_{kj}^O} = -(T_k - O_k^o) \times \frac{\delta O_k^0}{\delta S_k^o} \times \frac{\delta S_k^o}{\delta W_{kj}^O}. \tag{3.18}$$

The use of the negative sign in equation (3.18) accounts for gradient descent in weight space. Differentiating both sides of equation (3.14), it can be written as

$$\frac{\delta O_k^0}{\delta S_k^o} = f_k^{o\prime}(S_k^o). \tag{3.19}$$

Next, differentiating equation (3.13) with respect to W_{kj} gives

$$\frac{\delta S_k^o}{\delta W_{kj}^o} = O_j^h. \tag{3.20}$$

Hence, substituting equations (3.19) and (3.20) into equation (3.18) gives

$$\frac{\delta E}{\delta W_{kj}^o} = -(T_k - O_k^o) f_k^{o\prime}(S_k^o) O_j^h \tag{3.21}$$

Now, the change in weight can be written as

$$\Delta W_{kj}^{0} \propto -\delta E/\delta W_{kj}^{0} \tag{3.22}$$

$$= -\eta \delta E/\delta W_{kj}^{0}, \tag{3.23}$$

where η is a constant that determines the rate of learning. It is also known as the learning rate parameter of the back-propagation algorithm. Substituting equation (3.21) into equation (3.23) gives

$$\Delta W_{kj}^{0} = \eta (T_k - O_k^o) f_k^{o\prime}(S_k^o) O_j^h \tag{3.24}$$

$$= \eta \delta_k^o O_j^h, \tag{3.25}$$

where $\delta_k^o = (T_k - O_k^o) f_k^{o\prime}(S_k^o)$ is known as the local gradient. Hence the weight on the kth neuron at the output layer is updated as

$$W_{kj}^{0}(n+1) = \Delta W_{kj}^{0}(n) + W_{kj}^{0}(n). \tag{3.26}$$

Hidden layer weight updating:

The gradient of the mean-squared error for the hidden layer weight on the jth neuron is given by

$$\frac{\delta E}{\delta W_{ji}^{h}} = \frac{1}{2} \sum_k \frac{\delta (T_k - O_k^o)^2}{\delta W_{ji}^{h}} \tag{3.27}$$

$$= -\sum_k (T_k - O_k^o) \times \frac{\delta O_k^o}{\delta S_k^o} \times \frac{\delta S_k^o}{\delta O_j^h} \times \frac{\delta O_j^h}{\delta S_j^h} \times \frac{\delta S_j^h}{\delta W_{ji}^{h}}. \tag{3.28}$$

Differentiating equations (3.11) to (3.14) with respect to the proper factors yield the corresponding equations:

$$\frac{\delta O_k^o}{\delta S_k^o} = f_k^{o\prime}(S_k^o), \tag{3.29}$$

$$\frac{\delta S_k^o}{\delta O_j^h} = W_{kj}^{0}, \tag{3.30}$$

$$\frac{\delta O_j^h}{\delta S_j^h} = f_j^{h'}(S_j^h). \tag{3.31}$$

$$\frac{\delta S_j^h}{\delta W_{ji}^h} = x_i. \tag{3.32}$$

Substituting equations (3.29) to (3.32) into equation (3.28), gives

$$\frac{\delta E}{\delta W_{ji}^h} = -\sum_k (T_k - O_k^o) f_k^{o'}(S_k^o) W_{kj}^0 f_j^{h'}(S_j^h) x_i. \tag{3.33}$$

Hence again applying the delta rule, the change in weight in the hidden layer on the jth neuron can be written as:

$$\Delta W_{ji}^h = -\eta \frac{\delta E}{\delta W_{ji}^h} \tag{3.34}$$

$$= \eta f_j^{h'}(S_j^h) x_i \sum_k (T_k - O_k^o) f_k^{o'}(S_k^o) W_{kj}^0 \tag{3.35}$$

$$= \eta f_j^{h'}(S_j^h) x_i \sum_k \delta_k^o W_{kj}^0 \tag{3.36}$$

$$= \eta \delta^h x_i, \tag{3.37}$$

where

$$\delta^h = f_j^{h'}(S_j^h) \sum_k \delta_k^o W_{kj}^0. \tag{3.38}$$

Therefore, the updated weight at the hidden layer on the jth neuron at the $(n+1)th$ instant is

$$W_{ji}^h(n+1) = \Delta W_{ji}^h(n) + W_{ji}^h(n) \tag{3.39}$$

Based on the above equations, a procedure for training the ANN using the back-propagation algorithm is as follows.

1. Apply the input vector $x_p=(x_{p1}, x_{p2}, ..., x_{pN})^t$ to the input units.

2. Calculate the net-input values to the hidden layer unit using equation (3.11).

3. Calculate the outputs from the hidden layer using equation (3.12).

4. Move to the output layer. Calculate the net-input values to each unit using equation (3.13).

5. Calculate the outputs using equation (3.14).

6. Calculate the error terms from equations (3.15) to (3.17).

7. Update weights on the output layer using equations (3.24) to (3.26).

8. Update weights on the hidden layer using equations (3.37) to (3.39).

9. Calculate the error term $E = \frac{1}{2}\sum_{k=1}^{M} \delta_{pk}^2$. When the error is acceptably small, stop training.

Two classes of training approaches draw wide attention in the applications of ANN: off-line and on-line techniques. Off-line approaches are characterized by distinct learning and application phases. The ANN is trained on a fixed data set first and is then integrated into a control structure after the training is finished. Image processing is a particular example for the off-line approach.

In contrast to this, with on-line techniques data generation and operation of the control structure occur simultaneously. This structure is capable of immediately reacting to time-variant parameters in the control systems. This is why on-line approaches are so attractive and demanding. The main drawback of this approach is the impossibility of proving stability for the overall system. Because the gradient descent typically occurs on an extremely complex and high dimensional nonlinear er-

ror surface, there are instances of instability during the on-line learning phase. This problem can be resolved by combining the off-line and on-line learnings.

3.4 ANN for an Interior-type Brushless PM Synchronous Motor Drive

In an interior-type brushless PM synchronous motor, permanent magnets are buried within the rotor structure resulting in smooth rotor surface and reduced air gap. This provides an opportunity of using this kind of motor in high speed operation with better dynamic performance. In addition to the magnet component of the motor torque, some reluctance torque is also present in the interior-type PM machine as noted in equation (2.28). Since L_q is larger than L_d for the interior-type PM machine, the reluctance torque provides some advantages both on its application and cost. However, the operation of the interior-type brushless PM synchronous motor is strongly affected by the rotor saliency and by armature reaction effects [76]. Therefore, the optimal speed control of this type of motor demands special attention. Particularly, saturation of the iron portions around the magnets produces a distortion of the total air-gap flux and affects the behavior of the machine at different operating conditions. Thus, an intelligent control of an interior-type PM brushless synchronous motor is a necessity in high performance drive applications.

The following convenient features can be obtained using the ANN in high performance drive applications involving the interior-type brushless PM synchronous motor:

System knowledge

ANN can be used in an interior-type PM brushless synchronous motor drive system without prior knowledge of the exact system modeling and accurate values of the system parameters.

Tuning complexity

The degree of parameter variation in the PM synchronous motor drive systems differs according to the configuration of the drive systems. Parameters may change because of the operating conditions, such as the increase of resistance with the temperature, and change in inertia due to mechanical load. The ANN is an excellent tool for parameter adaptation particularly if used with an on-line learning technique for a brushless PM synchronous motor drive. Certainly, on-line training for motor drives is a hard task especially for high performance drives, but the ANN can be very effective in several situations such as changes in inertia or the application of a sudden load.

Control efficacy

The use of the ANN in the brushless PM synchronous motor drive can offer a convenient way of control especially when on-line self-tuning ANN is applied.

Cost

As the element that mostly affects the drive system choice in the majority of applications where other issues such as weight, size and reliability are not relevant, the cost of using ANN could be one of the main concerns, since high speed digital signal processors are needed for the on-line computation. But when compared with other

existing adaptive controllers for high performance drive applications which need sophisticated and expensive control hardware, the use of the ANN in the brushless PM synchronous motors may be cost competitive.

3.5 Concluding Remarks

The main objective of using the ANN in the vector controlled interior-type brushless PM synchronous motors is to achieve robust speed control under on-line parameter variations. Since the equations of the PM synchronous motor in d-q axis rotor reference frame are similar to those of a separately excited dc motor, it is worthwhile to evaluate the performances of an ANN for the speed control of a PM dc motor. This provides a test bench for the ANN based PM motor control. As an integral part of this investigation, the speed control of a PM dc motor using the ANN has been successfully developed and implemented in the laboratory. Details of the ANN based PM dc motor drive system are presented in the next chapter.

Chapter 4

Artificial Neural Network Based PM DC Motor Drive

This chapter presents an on-line self-tuning artificial neural network (ANN) controller based speed control scheme of a permanent magnet direct current (PM dc) motor. Instead of using the fixed weights and biases of the ANN, an on-line training algorithm with adaptive learning rate is introduced for precise speed control. The complete system is implemented in the real-time using the digital signal processor controller board on a laboratory PM dc motor. The stability over a wide speed range is obtained using an ANN structure with a local feedback provision. An experimental ANN controller using the FFNN structure and back-propagation training algorithm with one feedback loop is proposed. The performances of the proposed scheme are evaluated under different operating conditions in order to validate its efficacy. The experimental results show that the ANN controller based speed control scheme of a permanent magnet dc motor is robust, accurate and insensitive to parameter variations and load disturbances.

4.1 Brief Description of the PM DC Motor Drive

Although relatively expensive, dc motors are still widely used in high performance drive (HPD) applications because they are reliable and very easy to control due to the decoupled nature of the field and armature magnetomotive forces (MMFs). Among the commonly used two types of dc motors, namely separately excited and PM dc motors, the latter has the advantage that it does not require any extra dc supply for the field as the permanent magnet itself acts as the source of the flux. Thus the PM dc motor is compact in size, robust and efficient. The complete PM dc motor drive model is comprised of the following components:

1. Speed controller
2. Control circuit
3. Power amplifier
4. Permanent magnet dc motor

The block diagram of the dc drive is shown in Fig. 4.1. The speed of the PM dc motor can be controlled only by changing the input voltage as there is no provision for controlling the flux. A dc-dc converter is usually used to provide the necessary voltage to run the motor. Now-a-days an efficient power amplifier is being used to drive small electric motors. An input control voltage, which is the output of a speed controller, is applied to the low voltage input port of the power amplifier. Depending on the amplitude of the control voltage, the output voltage can be linearly controlled using high voltage at the high voltage port of the amplifier [77].

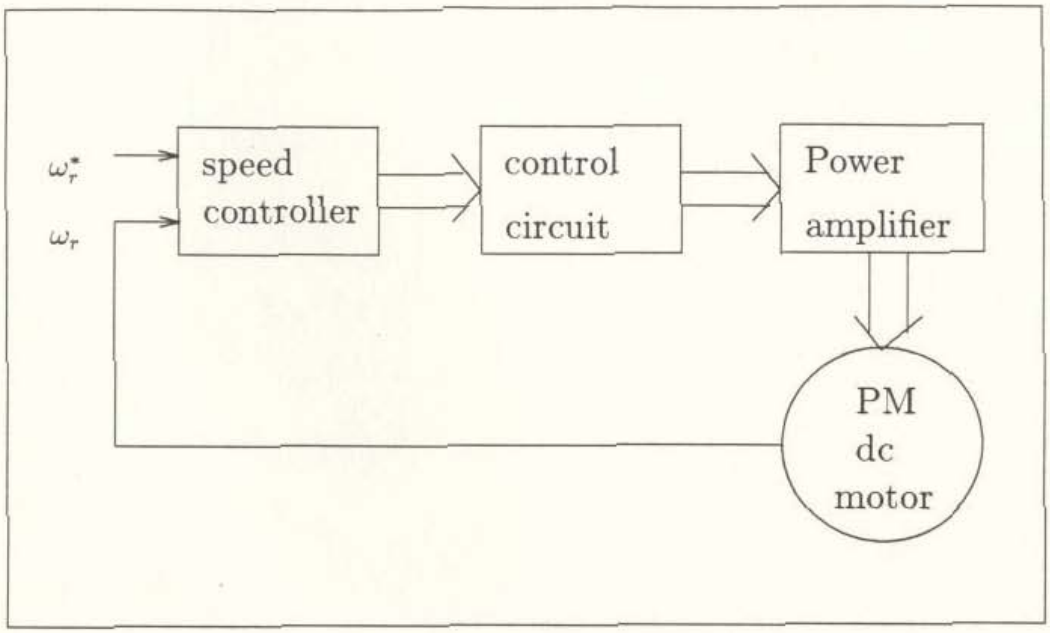

Figure 4.1: The PM dc motor drive model

4.2 DC Motor Drive System Dynamics

In spite of the fact that it is not mandatory to obtain a motor model if the ANN is used in the motor control system, it may be worth doing so from the analysis point of view in order to establish the foundation of the ANN structure.

The dynamics of the PM dc motor drive system can be described by the following equations [1]

$$v(t) = R_a i(t) + L_a \frac{di(t)}{dt} + e_b(t) \tag{4.1}$$

$$e_b(t) = K_e \omega_r(t) \tag{4.2}$$

$$T(t) = K_t i(t) \tag{4.3}$$

$$T(t) = J_m \frac{d\omega_r(t)}{dt} + B_m \omega_r(t) + T_l(t) + T_f \tag{4.4}$$

where $v(t)$, $e_b(t)$ and $i(t)$ are the time varying PM dc motor terminal voltage, back-emf and armature current, respectively; $\omega_r(t)$ is the motor speed; R_a and L_a are the armature resistance and inductance, respectively; K_e and K_t are the motor back-emf and torque constants, respectively; $T(t)$, $T_l(t)$ and T_f are the developed torque, load torque and frictional torque, respectively; J_m and B_m are the inertia and viscous constants, respectively. The relation between the load torque and speed can be described by the following equation [50]

$$T_l(t) = v\omega_r{}^2(t)[sign\{\omega_r(t)\}] \tag{4.5}$$

where v is a constant used to model a non-linear load. Although the load torque expressed by equation (4.5) is assumed to be a fan or propeller type for the modeling purpose, in real life it is uncertain and usually has unknown non-linear mechanical characteristics.

In order to make the control task easier, the PM dc motor drive system can be expressed as a single input single output system by combining equations (4.1) to (4.4), giving

$$L_aJ_m\frac{d^2\omega_r(t)}{dt^2} + (R_aJ_m + L_aB_m)\frac{d\omega_r(t)}{dt} + (R_aB_m + K_eK_t)\omega_r(t) + L_a\frac{dT_l(t)}{dt} + R_a\{T_l(t) + T_f\} - K_tv(t) = 0 \tag{4.6}$$

The discrete time model can be derived by substituting equation (4.5) into equation (4.6) and then replacing the continuous quantities by the finite difference equations, giving

$$\omega_r(n+1) = K_1\omega_r(n) + K_2\omega_r(n-1) + K_3[sign\{\omega_r(n)\}]\omega_r^2(n) + K_4[sign\{\omega_r(n)\}]\omega_r^2(n-1) + K_5v(n) + K_6 \tag{4.7}$$

where K_1, K_2, K_3, K_4, K_5 and K_6 are constants and can be expressed in terms of the motor parameters. If T_s is taken as the sampling period, the constants are given by

$$K_1 = \frac{2L_aJ_m + T_s(R_aJ_m + L_aB_m) - T_s^2(R_aB_m + K_eK_t)}{L_aJ_m + T_s(R_aJ_m + L_aB_m)} \tag{4.8}$$

$$K_2 = -\frac{L_aJ_m}{L_aJ_m + T_s(R_aJ_m + L_aB_m)} \tag{4.9}$$

$$K_3 = -\frac{T_s(vL_a + R_aT_s)}{L_aJ_m + T_s(R_aJ_m + L_aB_m)} \tag{4.10}$$

$$K_4 = \frac{T_sv}{L_aJ_m + T_s(R_aJ_m + L_aB_m)} \tag{4.11}$$

$$K_5 = \frac{K_tT_s^2}{L_aJ_m + T_s(R_aJ_m + L_aB_m)} \tag{4.12}$$

$$K_6 = -\frac{T_fR_aT_s^2}{L_aJ_m + T_s(R_aJ_m + L_aB_m)} \tag{4.13}$$

The PM dc motor parameters are given in Appendix B. Equation (4.7) can further be modified to obtain the inverse dynamic model of the drive system as

$$v_c(n) = f[\omega_r(n+1), \omega_r(n), \omega_r(n-1)] \tag{4.14}$$

where $v_c(n)$ is the control voltage of a power converter and is linearly proportional to the terminal voltage $v(n)$. The right hand side of equation (4.14) is a non-linear function of the speed ω_r and is given by

$$f[\omega_r(n+1), \omega_r(n), \omega_r(n-1)] = [\omega_r(n+1) - K_1\omega_r(n) - K_2\omega_r(n-1) - K_3[sign\{\omega_r(n)\}]\omega_r^2(n) - K_4[sign\{\omega_r(n)\}]\omega_r^2(n-1) - K_6]/K_5 \tag{4.15}$$

The purpose of using the ANN is to map the non-linear relationship between the control voltage $v_c(n)$ and the speed $\omega_r(n)$ of the dc motor according to equation (4.14). Equation (4.14) reveals the structure of the ANN for the speed control of the PM dc motor drive.

4.3 ANN Structure for the PM DC Motor Drive

The most important task of designing an ANN is to determine the inputs and output(s). The inverse dynamics of the PM dc motor drive as described in equation (4.14) basically dictates the inputs and output of the ANN used in the drive system under consideration. The inputs to the ANN are the left-hand side of equation (4.15): $\omega_r(n+1), \omega_r(n)$ and $\omega_r(n-1)$, i.e. the three consecutive values of speed. The corresponding output target is the control voltage $v_c(n)$. The number of hidden layers and number of neurons in the hidden layer are chosen by trial and error, keeping in mind that the smaller the numbers are, the better it is in terms of both memory and time requirement to implement the ANN in the motor control. For the present work, a structure of one hidden layer having three neurons gives satisfactory results. The ANN structure without a local feedback provision for the PM dc motor drive is shown in Fig. 4.2. The activation or transfer functions used in the hidden and output layers are log-sigmoid and tan-sigmoid, respectively. Once this basic design of the ANN structure is done, the next step is to determine the weights and biases of the ANN through the training to achieve the specific target with the given inputs. The back-propagation training algorithm is used for this purpose. Depending on the applications, the training of the ANN could be off-line or on-line. If the weights and biases of the ANN are determined through the off line training only, then an intensive training has to be performed considering almost all operating conditions of the drive system which is almost impossible for the control of a PM dc motor. As for example in reference [50], the load is modeled by equation (4.5) which is not always correct in all practical situations. Hence, the need for on-line weights and biases updating arises. However, the on-line training task could be eased and the system can be made

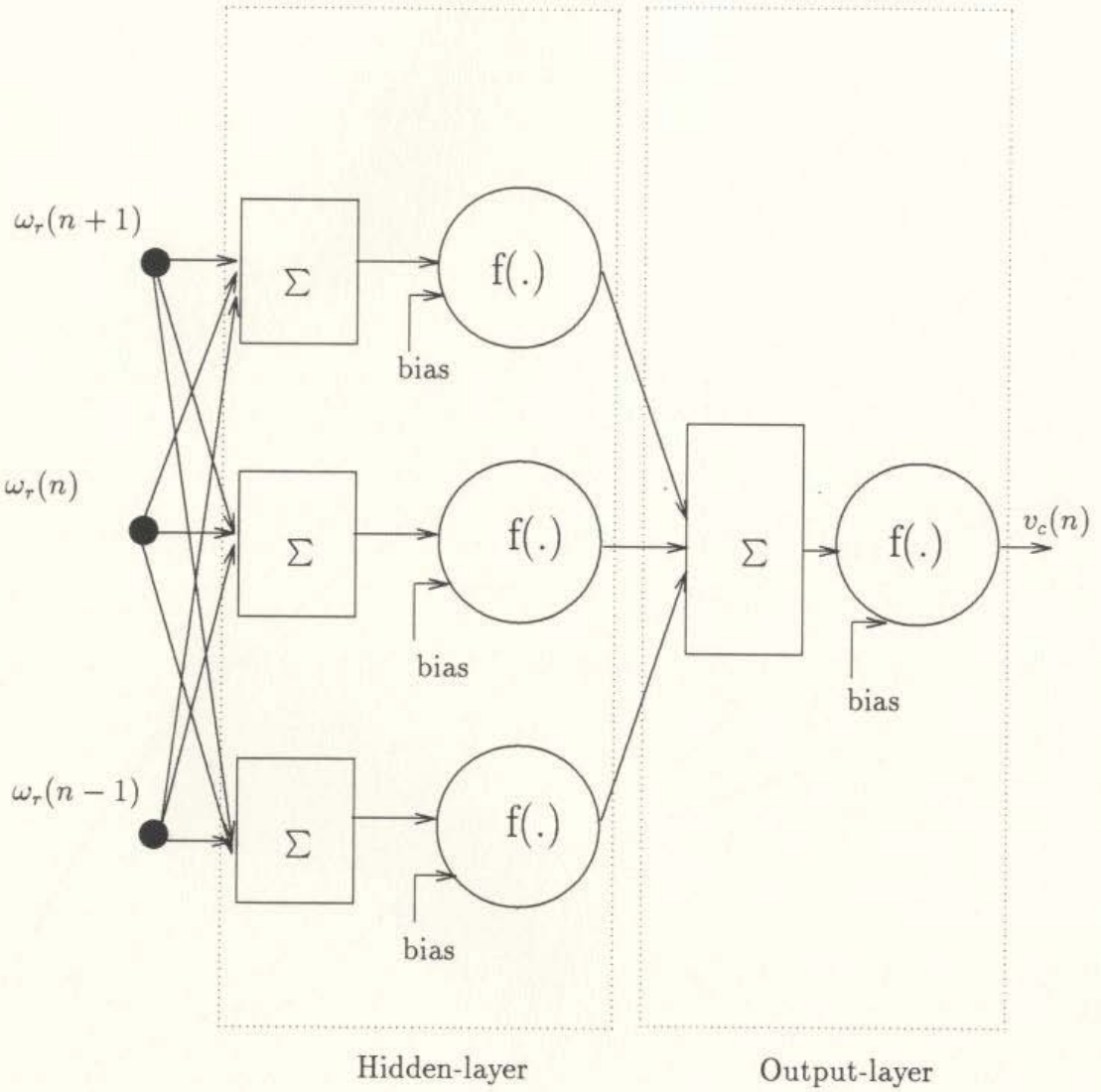

Figure 4.2: ANN structure without local feedback for the PM dc motor drive

more stable if an initial set of weights and biases is generated a priori through the off-line training. A combination of off-line and on-line trainings has been used for the present work. The initial weights and biases are obtained through the off-line training. These are updated only when an error limit between the actual output and the target of the ANN exceeds a preset value.

4.3.1 Off-line training for the initial set of weights and biases

Data for the off-line training can be obtained either by simulation or by experiment depending on the availability of the motor parameters. If the motor parameters are not available, the motor can be run on open loop and input voltages and output speeds can be recorded under different operating conditions to generate the training data for the ANN. If the motor parameters are available, equation (4.15) can be used to generate randomly the input patterns of $[\omega_r(n+1), \omega_r(n), \omega_r(n-1)]$. The corresponding target can be generated by using these speed values and K_1, K_2, K_3, K_4, K_5 and K_6 in the right hand side of equation (4.15). For the present work, off-line training data were obtained by simulation using SIMULINK [70] in an open-loop PM dc motor control scheme by considering the load as described by equation (4.5). The simulation is carried out at random voltages in order to obtain various speeds according to the specified voltages. At first, the simulation data for speed and voltage were down sampled by 20 times, and finally two sets of data with 501 samples were obtained. A window length of three $[\omega_r(n+1), \omega_r(n), \omega_r(n-1)]$ was slided over the entire speed samples and an input matrix of size 3×501 was formed. The output vector of size 1×501, contains the terminal voltage data. The off-line training of the ANN is performed with these training data using the back-propagation algorithm of

Table 4.1: Initial weights and biases of the ANN for PM dc drive

	NW1	
-0.5024	-0.1020	-0.9748
0.0	0.7319	0.72233
-0.9286	0.3966	-0.3794
	NW2	
-0.3598	-2.6174	-5.1035
	NB1	
-0.0815	1.259	1.2582
	NB2	
	6.0734	

the MATLAB Neural Network tool-box [78]. The initial set of weights and biases obtained through the off-line training is given in Table 4.1.

4.4 Real-time Adaptive Speed Control through On-line Tuning of the ANN

The principal objective of the control system is to generate the proper terminal voltage for the dc motor so that the motor can track a reference speed $\omega_{ref}(n)$. In the real-time, a control voltage $v_c(n)$ is generated by the ANN which is fed to a power amplifier circuit. The output of the power amplifier is applied to the terminal of the motor. The complete control scheme is illustrated in Fig. 4.3. The reference speed trajectory is selected using a second order reference model that makes the system asymptotically

stable [50]. The reference model can be described by the following equation

$$\omega_r^*(n+1) = a_1\omega_r^*(n) + a_2\omega_r^*(n-1) + r(n) \tag{4.16}$$

where a_1 and a_2 are constants chosen for a specific reference trajectory which ensure that the poles and zeros of the reference model are within the unit circle; $r(n)$ is the bounded input to the reference model. The value of $r(n)$ can be calculated before hand using equation (4.16) for a desired reference speed $\omega_r^*(n)$. If the tracking error is assumed to be small, and since the selected reference model is asymptotically stable, the rotor speed at the (n+1)th sample can be predicted from equation (4.16) as [50]

$$\hat{\omega}_r(n+1) = a_1\omega_r(n) + a_2\omega_r(n-1) + r(n) \tag{4.17}$$

Hence with one sample of predicted speed and two samples of actual speed, an input sequence $[\hat{\omega}_r(n+1), \omega_r(n) + \omega_r(n-1)]$ is formed and used as the input to the ANN as shown in Fig. 4.3. With the initial weights and biases and this sequence of input, the predicted output of the ANN, $\hat{v}_c(n)$ is computed. Using actual speed samples $[\omega_r(n+1), \omega_r(n), \omega_r(n-1)]$ as an input sequence, another output $v_c(n)$ is also computed and compared with $\hat{v}_c(n)$. The resulting error of $\hat{v}_c(n) - v_c(n)$ is used to update the previous set of weights and biases using the back-propagation algorithm. It is worth mentioning here that the two ANNs shown in Fig. 4.3 have the same set of weights and biases with two different sets of inputs and outputs.

The weights and biases are updated at each instant using the improved back-propagation algorithm as illustrated in chapter 3. The minimized error function is given by

$$E(n) = \frac{1}{2}e^2(n), \tag{4.18}$$

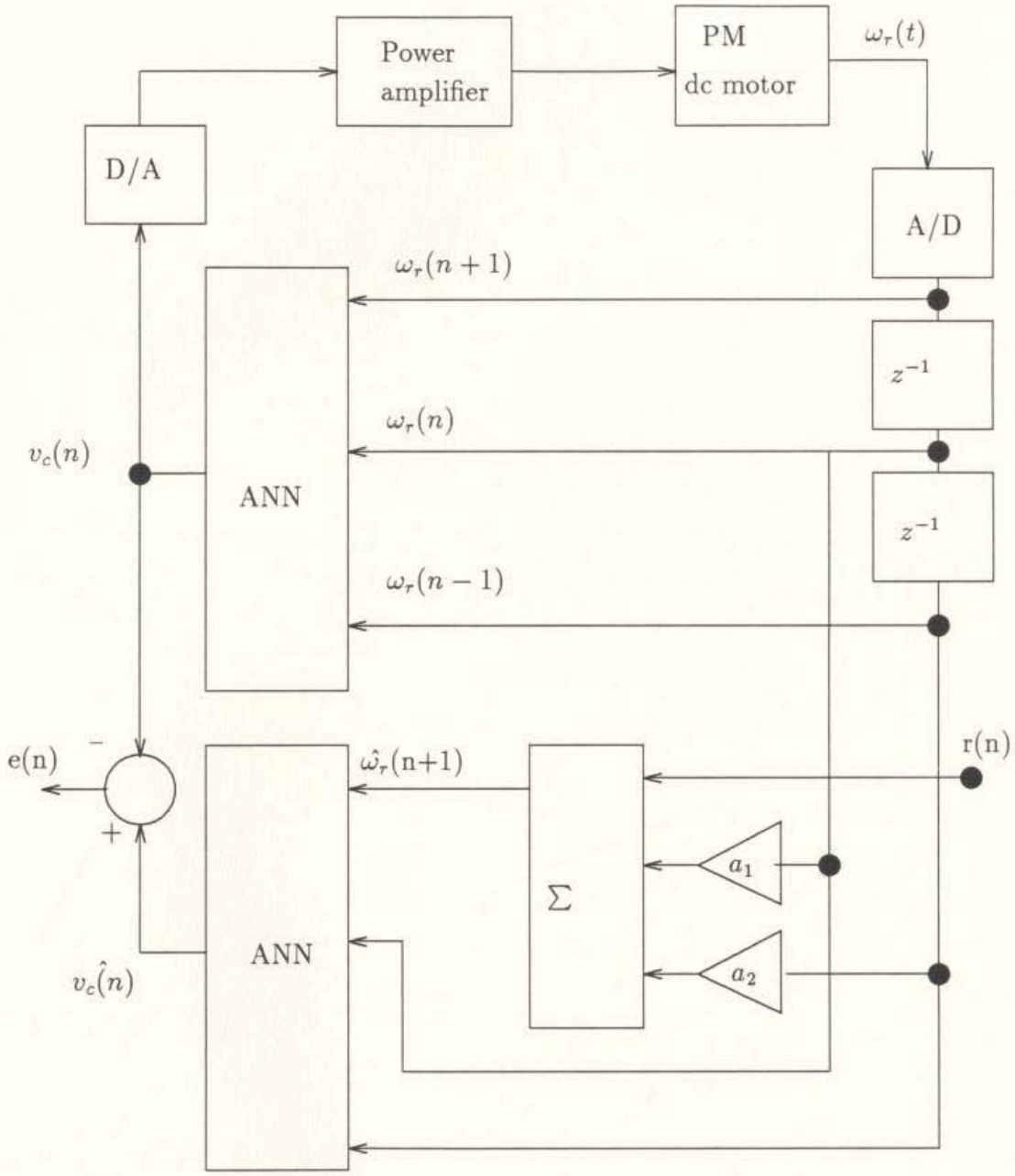

Figure 4.3: Block diagram of ANN controller based PM dc motor drive

where

$$e(n) = error = \hat{v}_c(n) - v_c(n). \tag{4.19}$$

(a) Output layer weights and biases update:

Weights and biases of the output layer are updated as:

$$W^o_{jk}(n+1) = W^o_{jk}(n) + \eta \delta^o_k(n) O^h_j(n), \tag{4.20}$$

$$B^o_k(n+1) = B^o_k(n) + \eta \delta^o_k(n), \tag{4.21}$$

where η is the learning rate and $\delta^o_k(n)$ is the local gradient at the output layer and is expressed as

$$\delta^o_k(n) = e(n) \frac{\delta e(n)}{\delta O^o_k(n)} S^o_k(n)(1 - S^o_k(n)) O^h_j(n). \tag{4.22}$$

(b) Hidden layer weights and biases update:

The updated weight at the hidden layer can be written as:

$$W^h_{ij}(n+1) = W^h_{ij}(n) + \eta \delta^h_j(n) I_i(n), \tag{4.23}$$

$$B^h_j(n+1) = B^h_j(n) + \eta \delta^h_j(n), \tag{4.24}$$

where the local gradient at the hidden layer is expressed as

$$\delta^h_j(n) = \delta^o_k(n) W^o_{jk}(n)[1 - S^h_j(n)]^2. \tag{4.25}$$

In the real-time implementation, the error is calculated at each instant and when it goes beyond a predetermined level, weights and biases updating procedure is enabled. If the error is within the prescribed level, the previous set of weights and biases is kept intact to compute the control voltage.

4.4.1 Adaptive learning rate for on-line weights and biases updating

For high performance motor drive application, over-shootings and response times, etc., are some of the main concerns. It has been observed that the learning rate of the ANN is a key factor which affects over-shooting and response time. A faster learning rate gives over-shooting on the speed and slower learning rate makes the response time too slow. Therefore, for on-line updating of the ANN, a novel feature of adaptive learning rate is incorporated as shown in the flow chart of Fig. 4.4 [79].

4.4.2 Modified ANN structure with enhanced stability

In the present experiment, the proposed ANN structure is modified to include a local feedback loop as shown in Fig. 4.5. The modified configuration of the ANN provides greater stability on the performances of the motor controller [53], [80]. This structure works after initialization with the structure shown in Fig. 4.2. The switching of the structures is controlled by software.

4.4.3 Laboratory implementation

The ANN controller based PM dc motor drive system was implemented in the real-time using the PC based DSP controller board. The schematic diagram and the

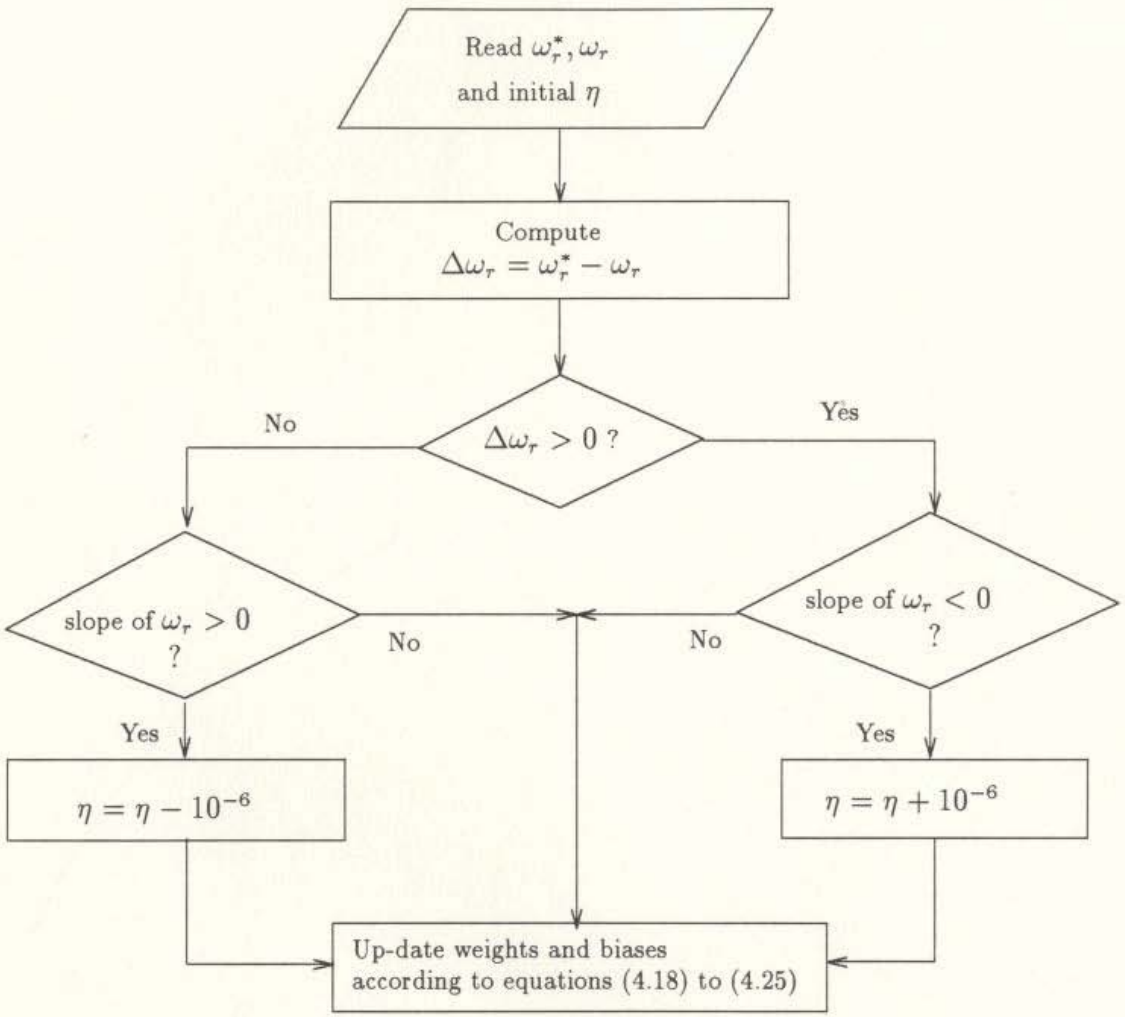

Figure 4.4: Real-time operational flow chart for weights and biases updating with adaptive learning rate

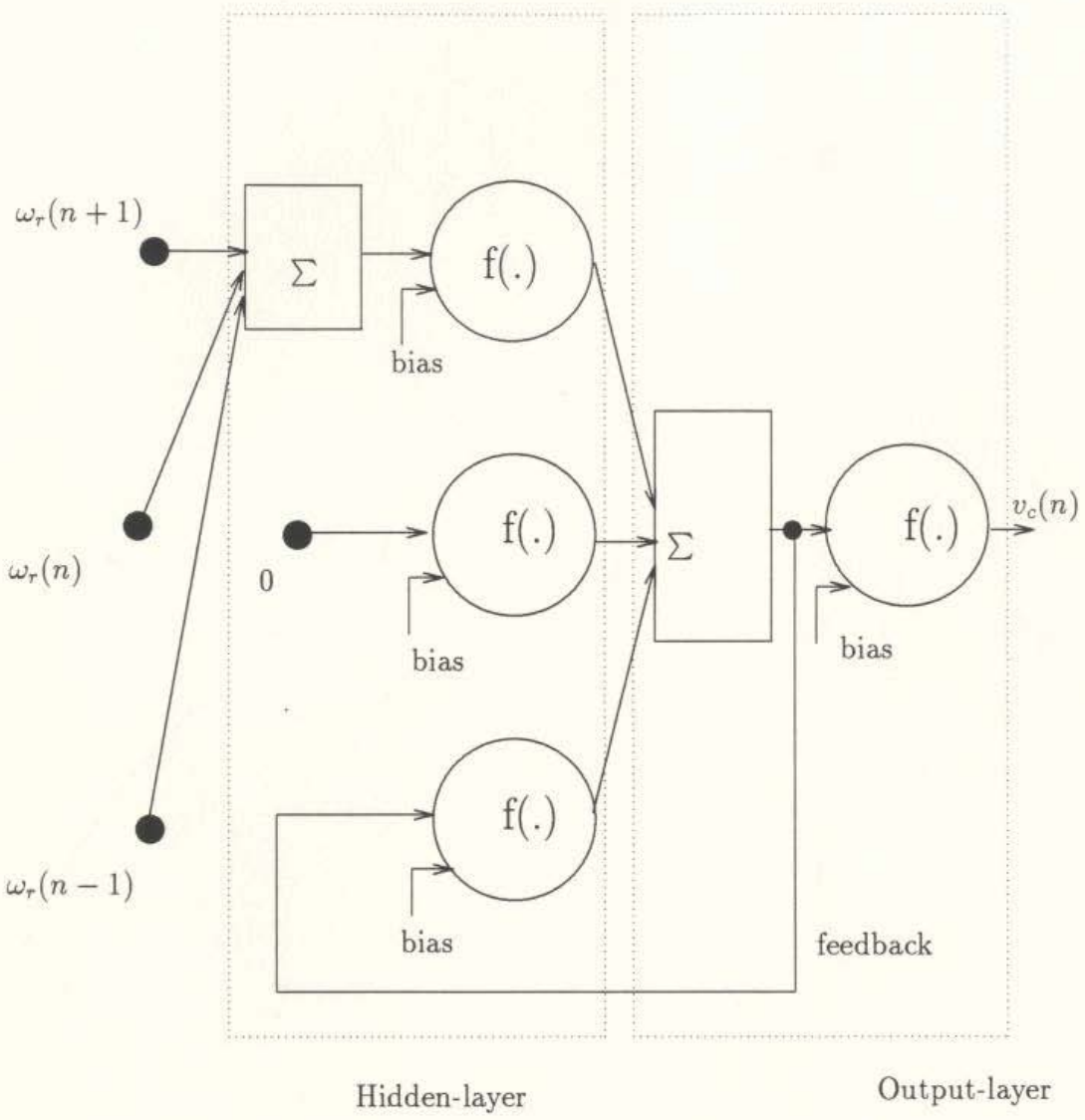

Figure 4.5: Modified ANN structure with feedback loop

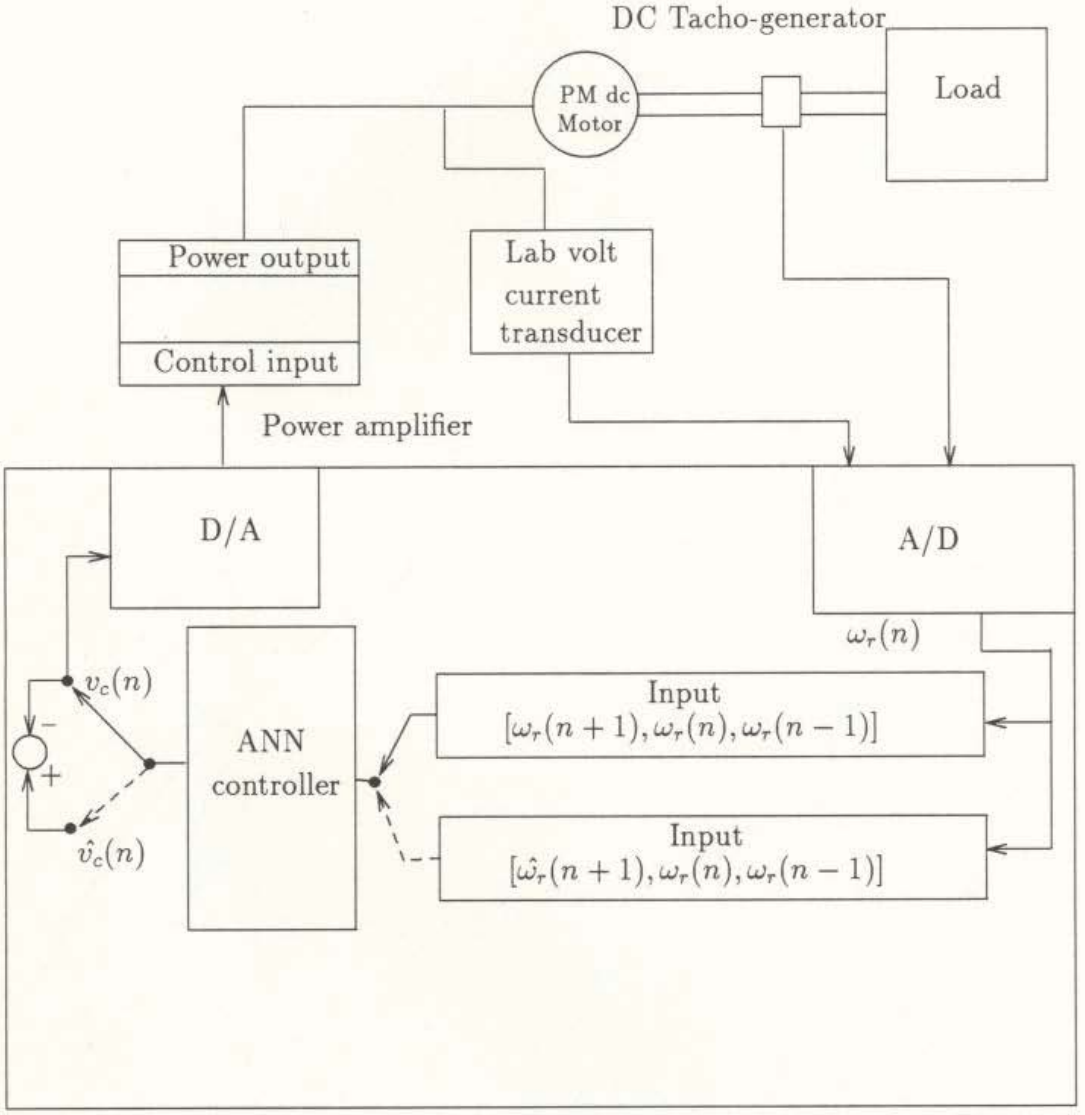

Figure 4.6: Schematic diagram of ANN controller based PM dc motor drive system

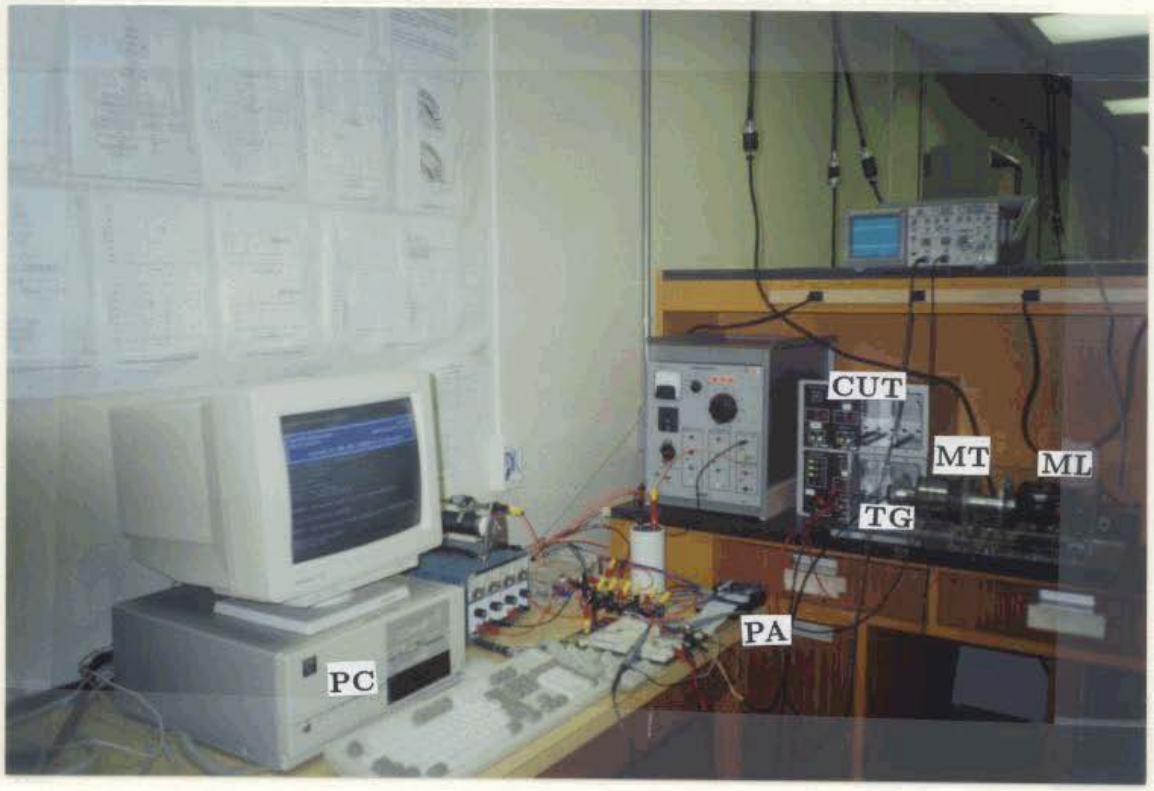

Figure 4.7: Experimental set-up of the PM dc motor drive

laboratory set-up of the drive systems are shown in Figs. 4.6. and 4.7, respectively. In Fig. 4.7, the test and loading motors are labeled 'MT' and 'ML', respectively. The DSP controller board DS-1102 is installed inside the computer labeled 'PC'. The labels 'PA' and 'CUT' represent the power amplifier and current transducer, respectively. The tacho-generator attached to the test motor is labeled 'TG'. The software program was written in C language in order to realize the ANN structure in the real-time. The weights and biases obtained from the off-line training were used to initialize the system. It is a common practice to use a current feedback to limit the motor current in the speed control of a motor drive system. In this work, the actual motor current is sensed by Lab-volt current transducer and compared with a preset peak value. If for any reason, the current exceeds the preset value, the control voltage is forced to remain at its previous sample to limit the current. A tacho-generator was used to acquire the speed. The speed signal is fed to the built-in A/D converter of the DSP board for processing. Through the D/A converter of the DSP controller board, the control voltage $v_c(t)$ was fed to the control port of the power amplifier. The high voltage port of the power amplifier provides the required terminal voltage $v(t)$ to the armature of the experimental PM dc motor.

For comparison purposes, a proportional-integral (PI) controller based PM dc motor drive system was also developed and experimentally implemented. The PI controller was designed for the critically damped response of the speed with the best estimation of the motor parameters.

4.5 Results and Discussions

In this work, several experiments were performed to evaluate the performances of both the PI controller and ANN controller based PM dc motor drives. The speed and current responses under various operating conditions such as change in reference speed, step change in load, and parameter variations were observed. Speed responses documented in this section are voltage signals obtained from a dc tacho-generator. These were recorded in a storage type oscilloscope Tektronix 2212. Currents were measured by a Lab volt current transducer and also recorded in the oscilloscope. Some sample results are presented in this section.

Tests were performed to obtain the speed responses for varying reference speed under no load and full load conditions. The updated weights and biases for the ANN controller for various operating conditions are given in Tables 4.2 to 4.6. Figures 4.8(a) and (b) show the speed and corresponding armature current responses of the PI controller based system under no-load condition. Figures 4.9(a) and (b) show the responses of the ANN controller based drive under identical operating conditions. Speed responses have also been obtained for varying reference speed under full load condition. Figures 4.10 and 4.11 illustrate the responses of PI controller and ANN controller based systems for this operating condition. From Figs. 4.8 to 4.11, it is observed that the performances of the ANN controller based system are better than those of the PI controller based system. The PI controller based drive system has the problem of over-shooting around 200 rpm when there is a change of reference speed for both the no load and full load conditions. On the other hand, the speed response of the ANN controller based system is more robust because of the on-line tuning of the weights and biases as well as the adaptive learning rate feature. It is

Table 4.2: Updated weights and biases with step change of load

	NW1	
0.4487	0.4502	-0.4291
-0.6962	0.3274	00.3235
-0.5655	0.6073	-0.1713
	NW2	
-0.3336	-2.580	-5.057
	NB1	
1.5080	0.2087	1.8029
	NB2	
	6.131	

Table 4.3: Updated weights and biases with $J_m \rightarrow 2J_m$ at no load

	NW1	
0.4801	0.3967	-0.4804
-0.7191	0.3665	0.3611
-0.5539	0.5865	-0.1910
	NW2	
-0.3322	-2.5815	-5.057
	NB1	
1.555	0.1742	1.8021
	NB2	
	6.132	

Table 4.4: Updated weights and biases with $J_m \rightarrow 2J_m$ at full load

	NW1	
0.5242	0.3219	-0.5549
-0.7510	0.4215	0.4159
-0.5379	0.5577	-0.2198
	NW2	
-0.3288	-2.5831	-5.054
	NB1	
1.6213	0.1263	1.8441
	NB2	
	6.1347	

Table 4.5: Updated weights and biases with $R_a \rightarrow 2R_a$ at no load

	NW1	
0.6258	0.4839	-0.3952
-0.8245	0.3039	0.2998
-0.4987	0.6196	-0.1587
	NW2	
-0.3150	-2.582	-5.040
	NB1	
1.773	0.0160	1.9029
	NB2	
	6.149	

Table 4.6: Updated weights and biases with $R_a \rightarrow 2R_a$ at full load

	NW1	
0.7169	0.3293	-0.5470
-0.8906	0.4172	0.4111
-0.4662	0.5597	-0.2175
	NW2	
-0.3095	-2.5875	-5.037
	NB1	
1.9104	-0.0830	1.9510
	NB2	
	6.1536	

possible to reduce the over-shooting of the PI controller by designing the drive system a little more under-damped but in that case, the drive system becomes too sluggish compared to the ANN controller based system.

Figures 4.12(a) and (b) show the speed and current responses of the PI controller based system for a step change of load. The motor was running at no load condition and after some time the rated load was applied suddenly. Figures. 4.13(a) and (b) show the responses of the ANN controller based system under this operating condition. The ANN adjusts its weights and biases on-line to this changing circumstance of sudden load impact and provides the appropriate control voltage so that the drive system responds according to the reference speed. It is again quite evident from Figs. 4.12 and 4.13 that the performances of the ANN controller based system are superior to those of the PI controller based system. As can be seen from Fig. 4.12(a) for the PI controller based system, the speed drops by about 600 rpm at the point of loading, whereas for the ANN controller based system, the effect of loading on speed is very

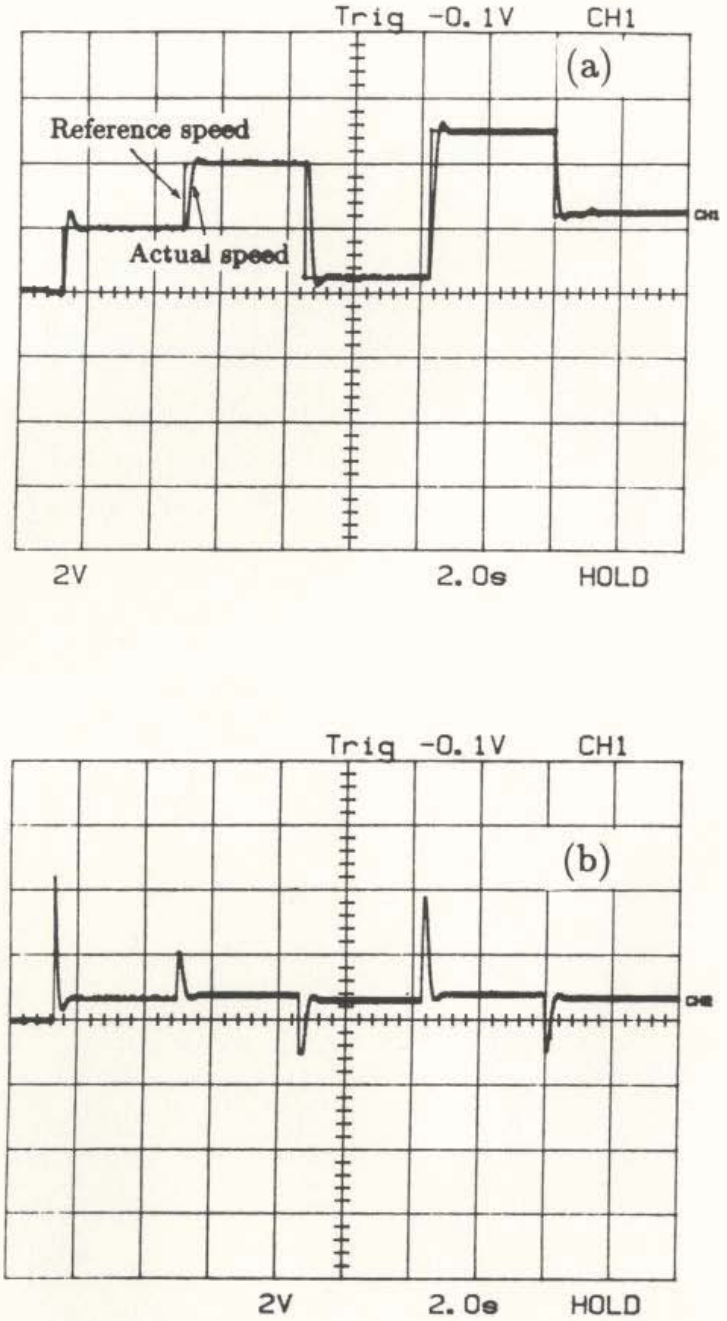

Figure 4.8: Experimental results of the PI controller based PM dc drive system with change in reference speed at no load; (a) speed; Y-scale: 2 krpm/div. (b) current; Y-scale: 2 A/div.

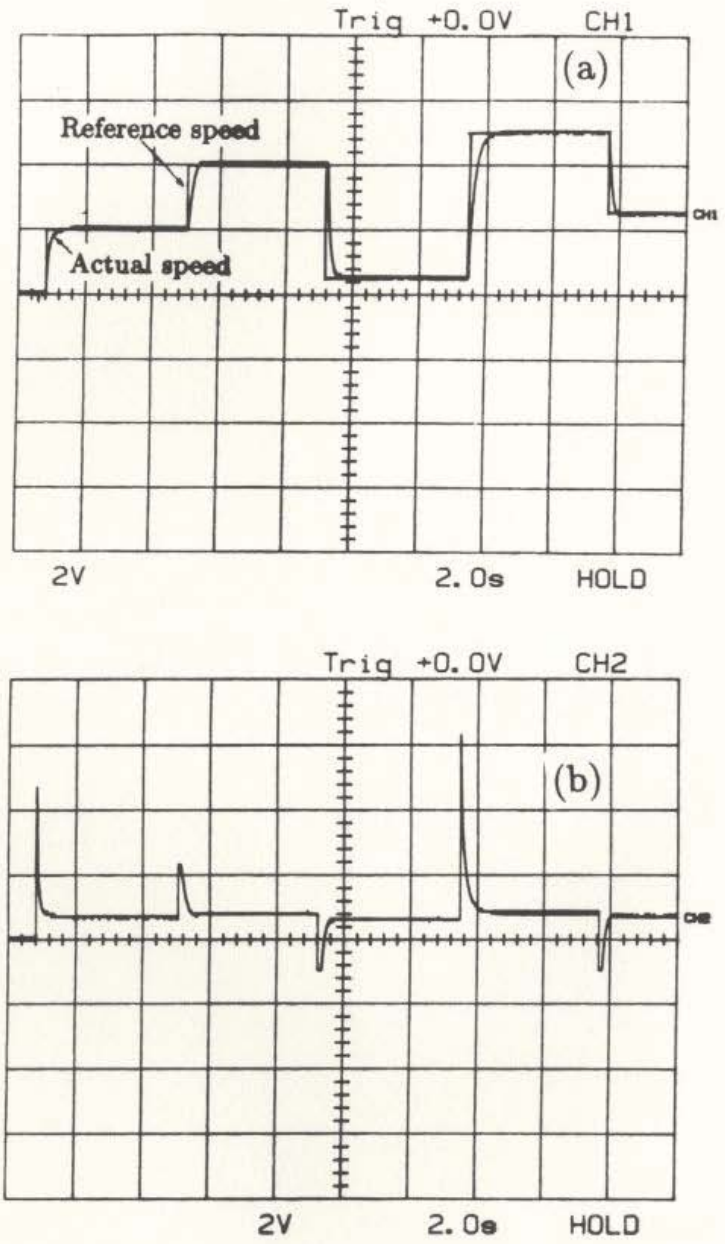

Figure 4.9: Experimental results of the ANN controller based PM dc drive system with change in reference speed at no load; (a) speed; Y-scale: 2 krpm/div. (b) current; Y-scale: 2 A/div.

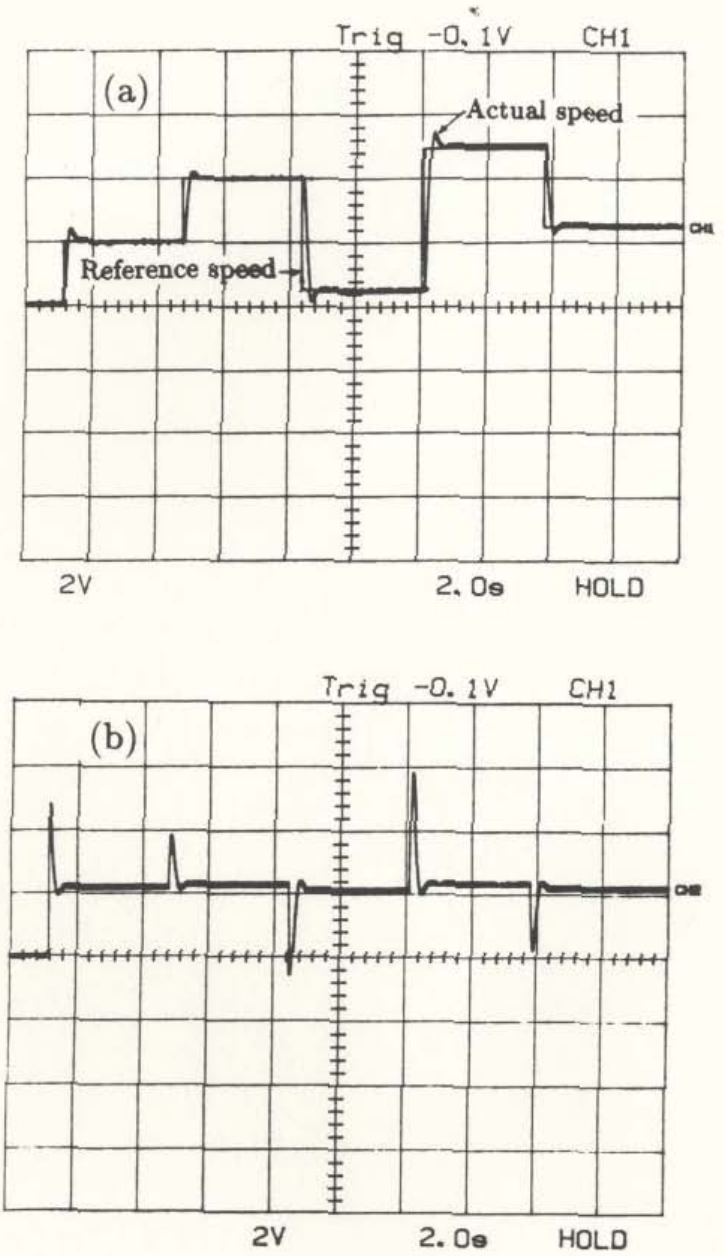

Figure 4.10: Experimental results of the PI controller based PM dc drive system with change in reference speed at full load; (a) speed; Y-scale: 2 krpm/div. (b) current; Y-scale: 2 A/div.

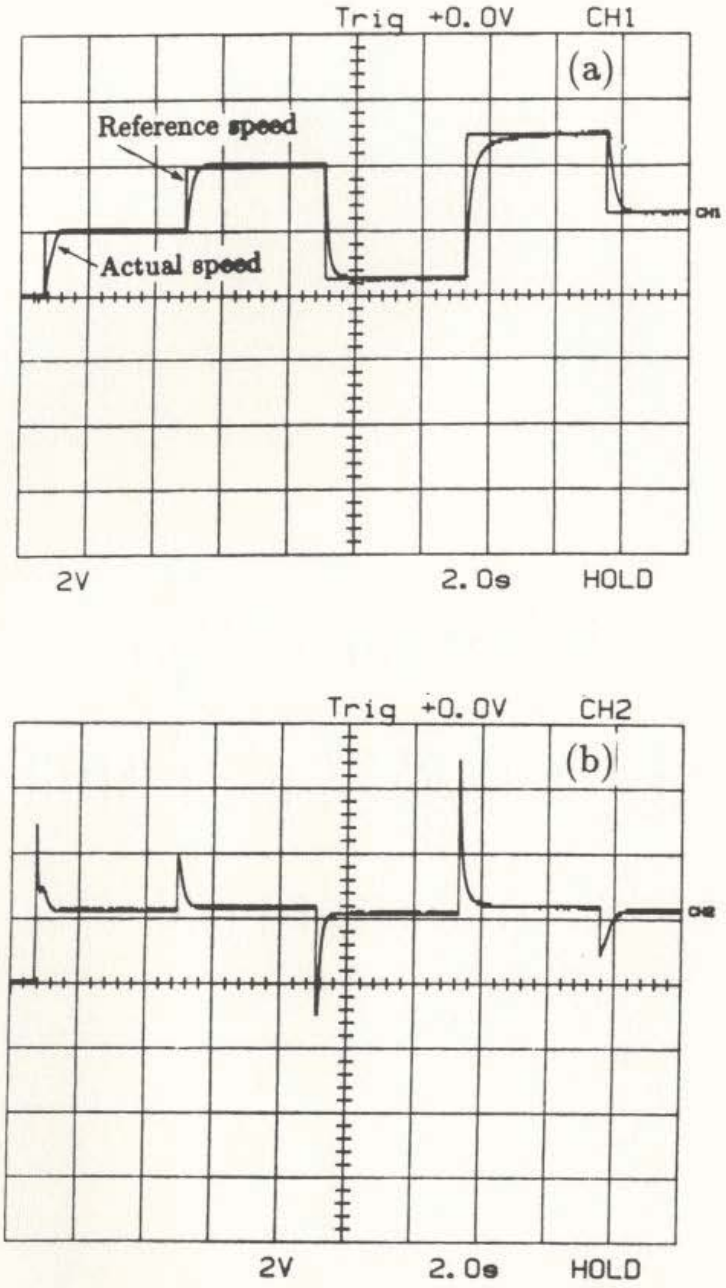

Figure 4.11: Experimental results of the ANN controller based PM dc drive system with change in reference speed at full load; (a) speed; Y-scale: 2 krpm/div. (b) current; Y-scale: 2 A/div.

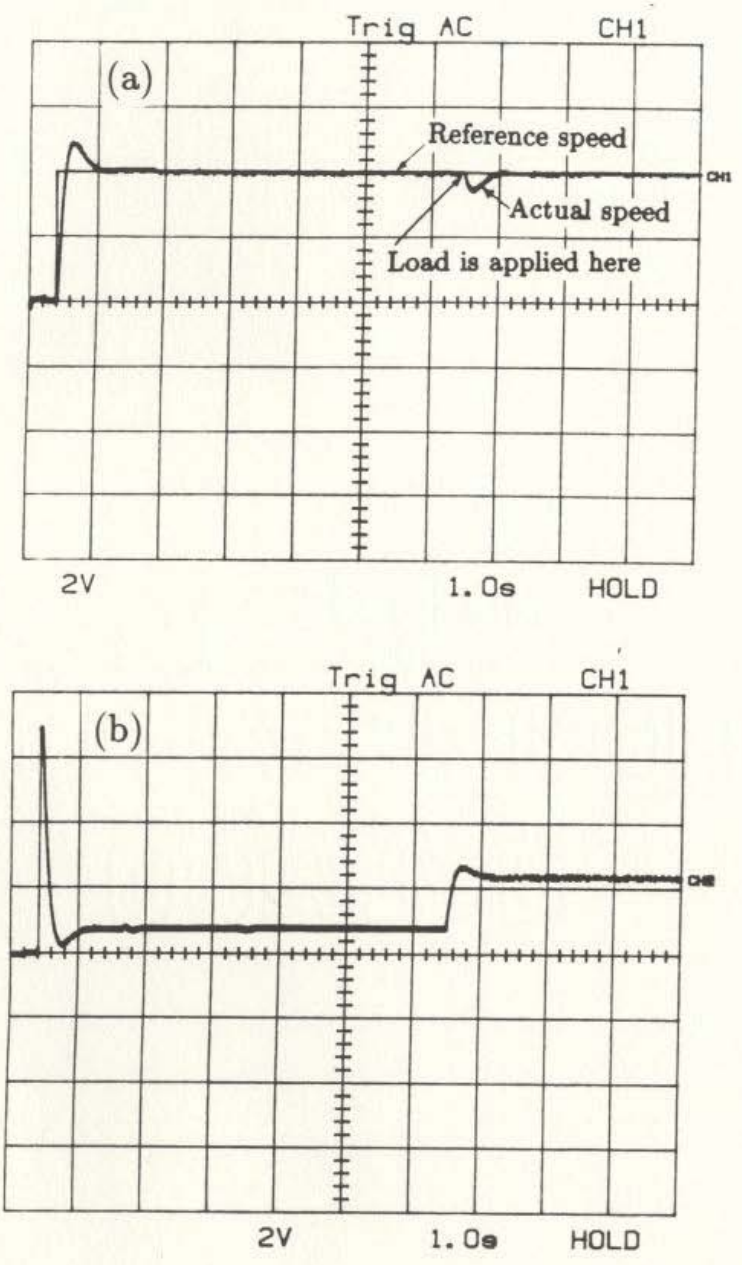

Figure 4.12: Experimental results of the PI controller based PM dc drive system with step change in load (a) speed; Y-scale: 2 krpm/div. (b) current; Y-scale: 2 A/div.

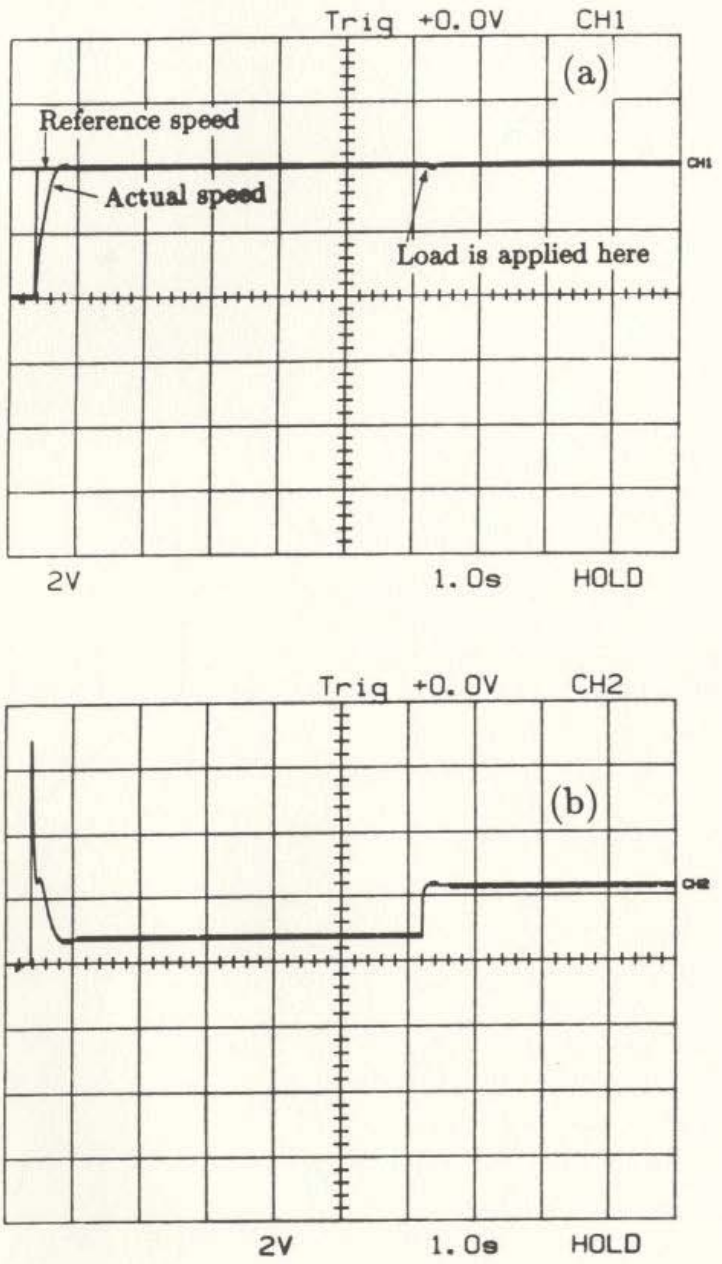

Figure 4.13: Experimental results of the ANN controller based PM dc drive system with step change in load; (a) speed; Y-scale: 2 krpm/div. (b) current; Y-scale: 2 A/div.

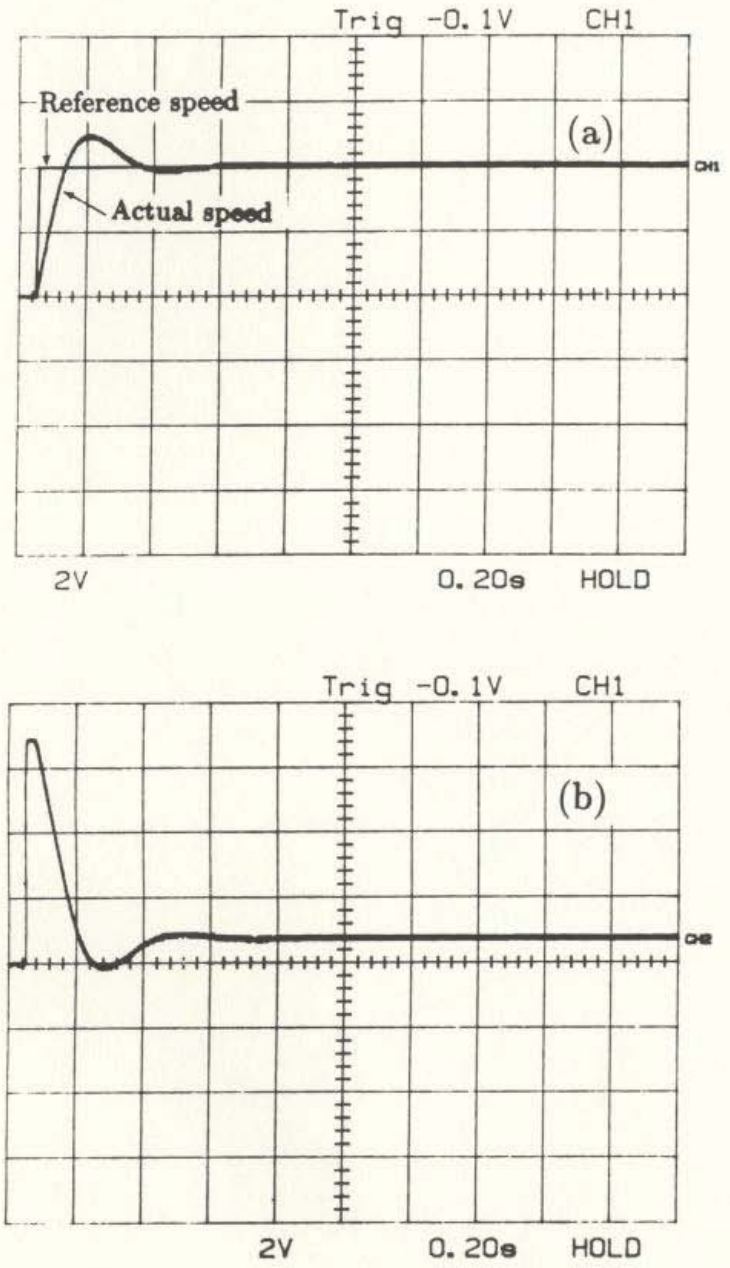

Figure 4.14: Experimental results of the PI controller based PM dc drive system with change in inertia $J_m \rightarrow 2J_m$ at no load; (a) speed; Y-scale: 2 krpm/div. (b) current; Y-scale: 2 A/div.

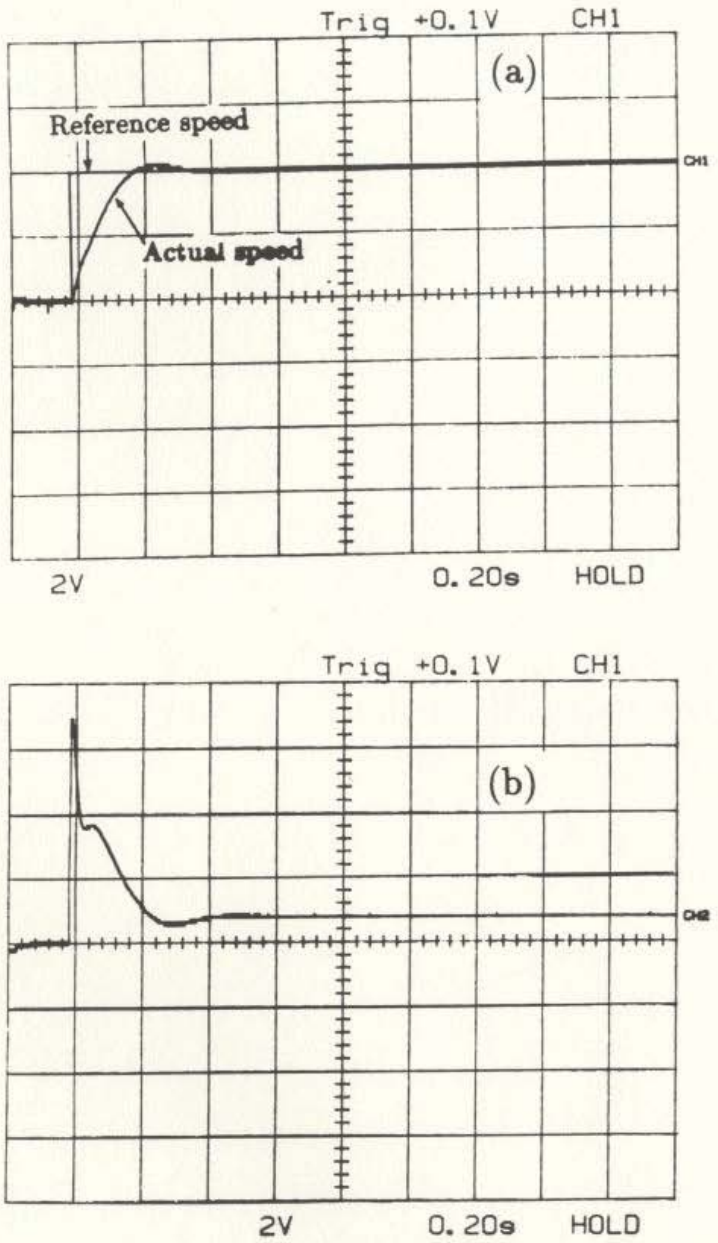

Figure 4.15: Experimental results of the ANN controller based PM dc drive system with change in inertia $J_m \rightarrow 2J_m$ at no load; (a) speed; Y-scale: 2 krpm/div. (b) current; Y-scale: 2 A/div.

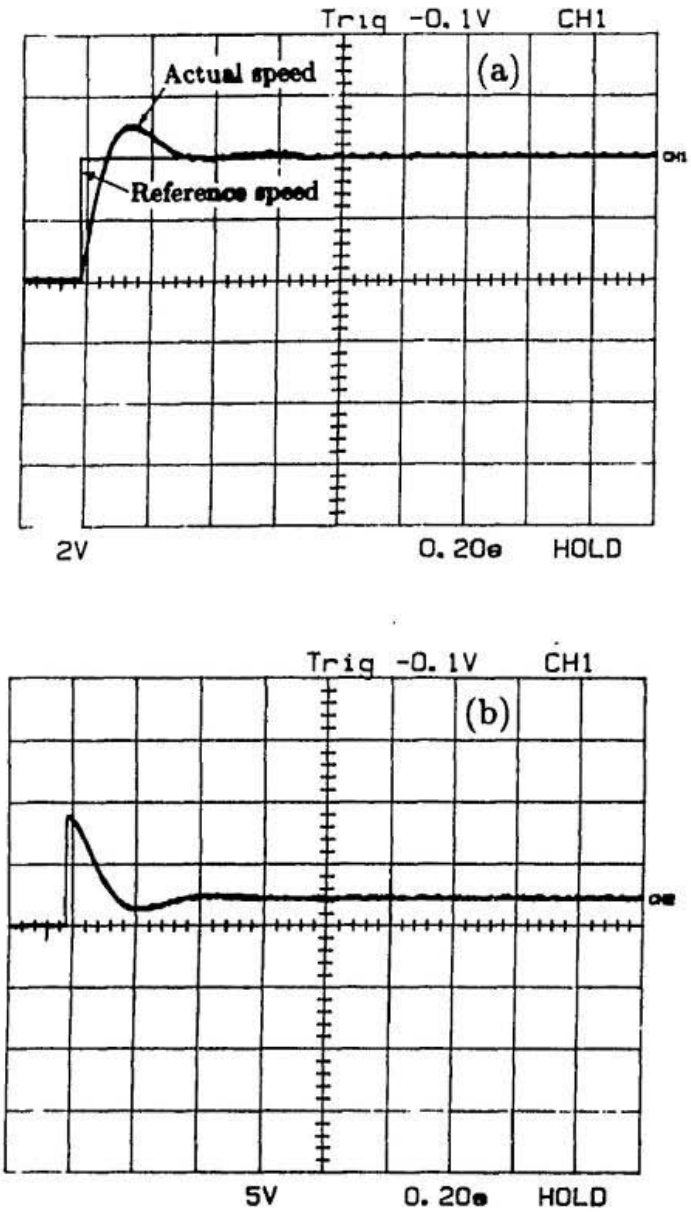

Figure 4.16: Experimental results of the PI controller based PM dc drive system with change in inertia $J_m \rightarrow 2J_m$ at full load; (a) speed; Y-scale: 2 krpm/div. (b) current; Y-scale: 5 A/div.

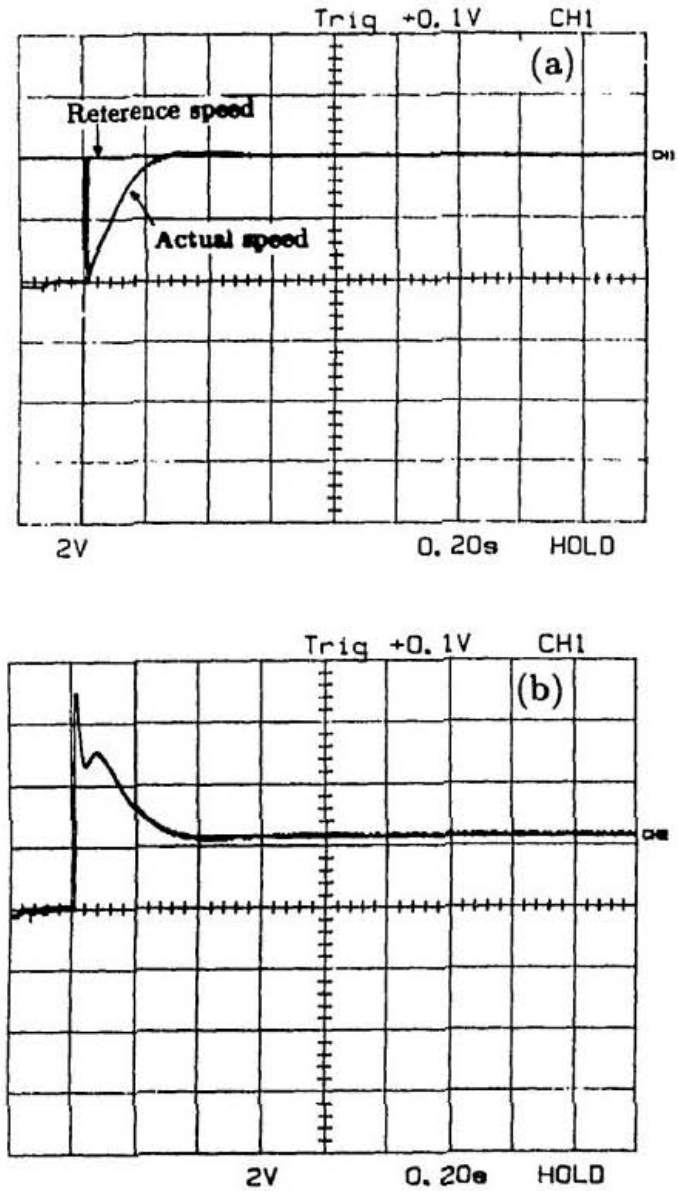

Figure 4.17: Experimental results of the ANN controller based PM dc drive system with change in inertia $J_m \rightarrow 2J_m$ at full load; (a) speed; Y-scale: 2 krpm/div. (b) current; Y-scale: 2 A/div.

insignificant as illustrated in Fig. 4.13(a).

The performances of the drive system are also evaluated experimentally with parameter variations for both the PI controller and ANN controller based systems. In this experiment, two parameters are changed under no-load and full load conditions: (i) the inertia of the motor is doubled by coupling it with another motor with higher inertia and (ii) an additional resistance is inserted in the armature circuit. Figures 4.14 to 4.21 illustrate the effects of changes in inertia and armature resistance on speeds and currents for the PI controller and ANN controller based drive systems, respectively. It should be noted that with the initial design, the PI controller based system becomes unstable under these parameter variations. Therefore, it is redesigned with new motor parameters ($J_m \rightarrow 2J_m, R_a \rightarrow 2R_a$). The results presented here are the performances of the newly designed PI controller based drive system. Figures 4.14 and 4.15 show the experimental speed and current responses for the PI controller and ANN controller based system, respectively, with no-load condition for the changes in inertia. Figures 4.16 and 4.17 show the speed and current responses at the rated load for both the PI controller and ANN controller based systems, respectively. It is well-known that armature resistance increases with temperature. Thus the system performances have been evaluated for both no-load and full load conditions for the PI controller and ANN controller based PM dc drive systems by inserting additional resistance in the armature circuit. Figures 4.18 to 4.21 demonstrate the experimental results for this change in armature resistance under no load and rated load conditions. It is clear from the experimental results of Figs. 4.14-4.21 that even with the newly designed constants, the performances of the PI controller is not as good as the performances of the ANN controller based system. For the PI controller based system, there is a considerable amount of over-shooting of the speed when the motor

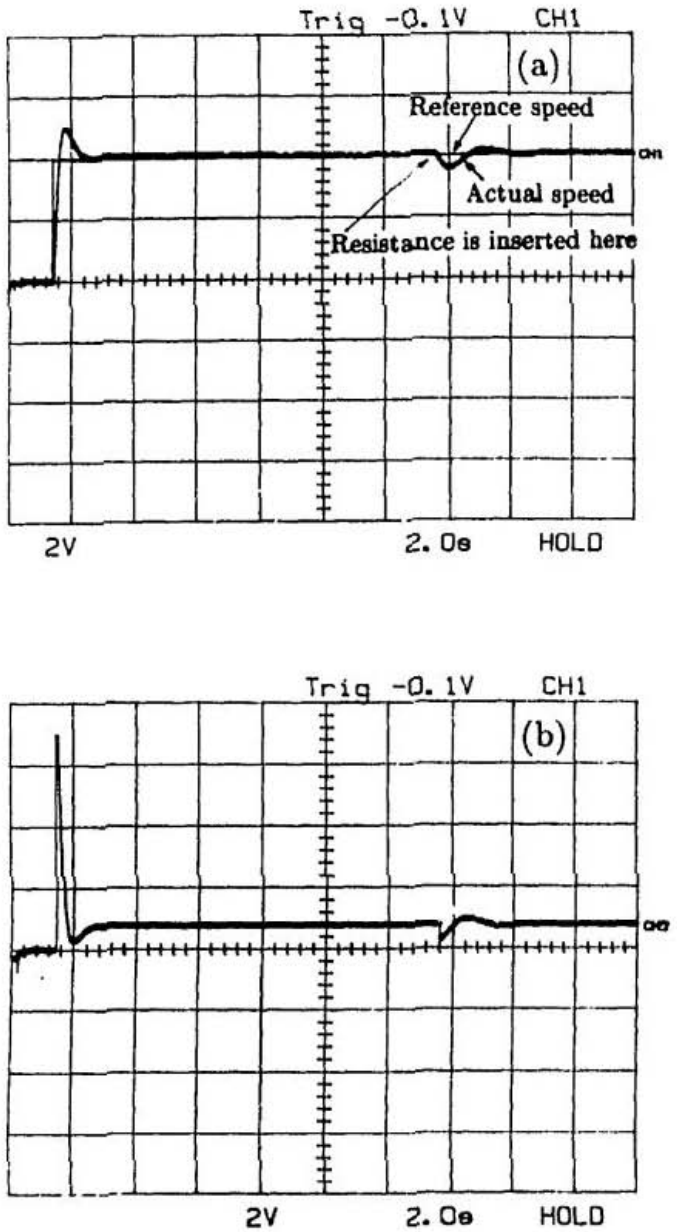

Figure 4.18: Experimental results of the PI controller based PM dc drive system with change in armature resistance $R_a \rightarrow 2R_a$ at no load; (a) speed; Y-scale: 2 krpm/div; (b) current; Y-scale: 2 A/div.

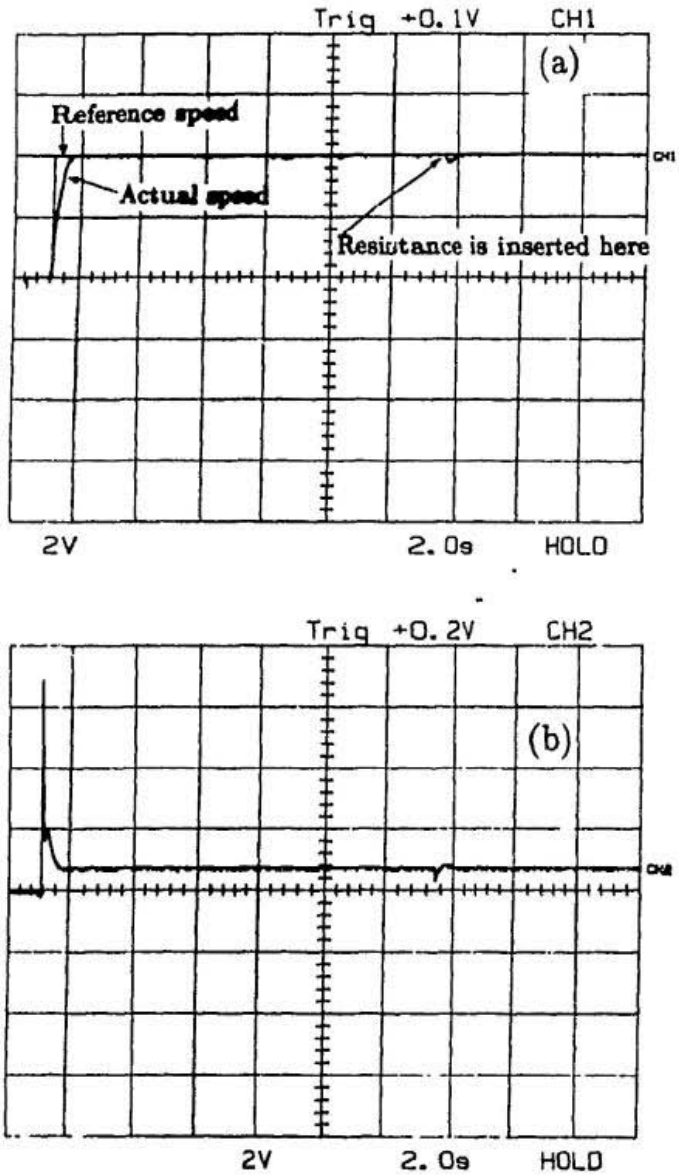

Figure 4.19: Experimental results of the ANN controller based PM dc drive system with change in armature resistance $R_a \rightarrow 2R_a$ at no load; (a) speed; Y-scale: 2 krpm/div; (b) current; Y-scale: 2 A/div.

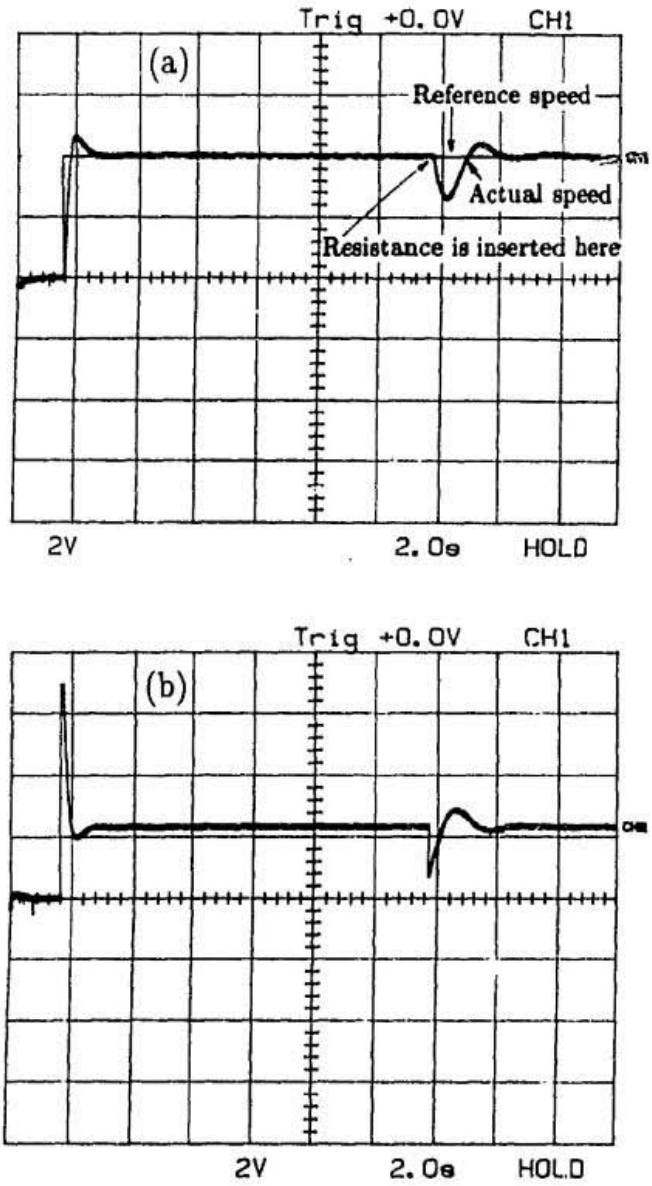

Figure 4.20: Experimental results of the PI controller based PM dc drive system with change in armature resistance $R_a \rightarrow 2R_a$ at full load; (a) speed; Y-scale: 2 krpm/div; (b) current; Y-scale: 2 A/div.

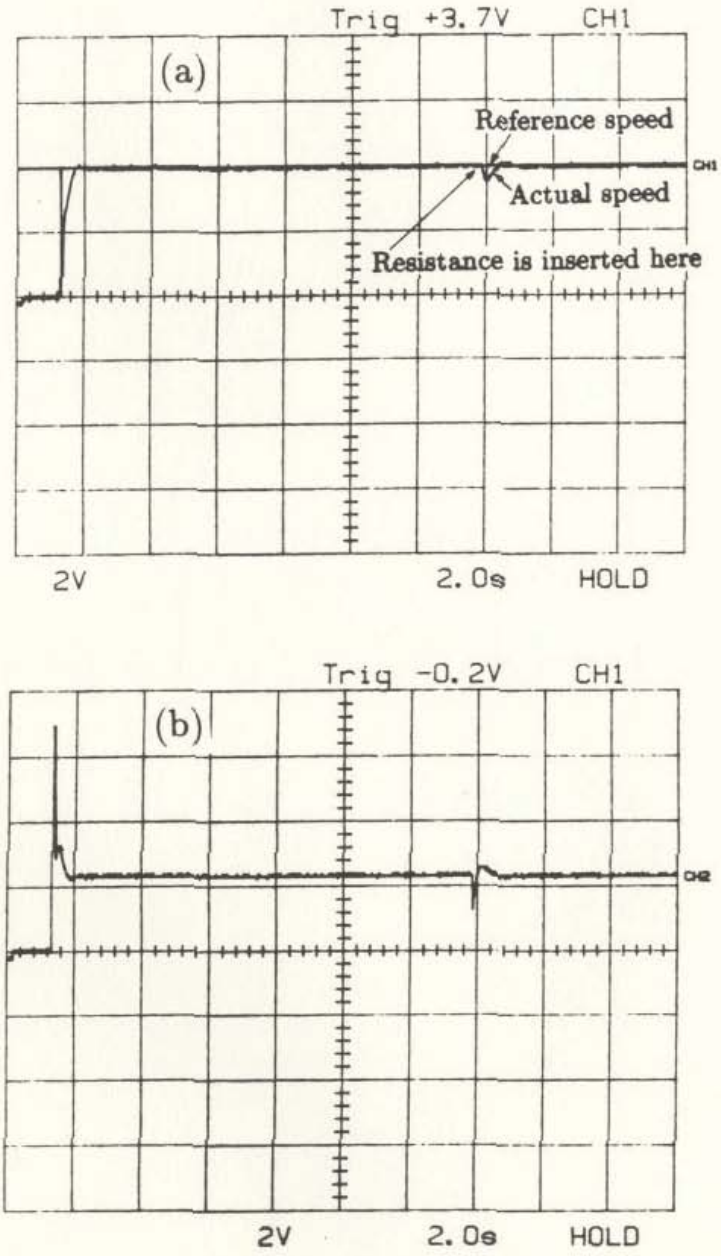

Figure 4.21: Experimental results of the ANN controller based PM dc drive system with change in armature resistance $R_a \rightarrow 2R_a$ at full load; (a) speed; Y-scale: 2 krpm/div; (b) current; Y-scale: 2 A/div.

starts with the changed inertia as shown in Figs. 4.14(a) and 4.16(a). However, the speed response of the ANN controller based system is critically damped with negligible over-shooting as shown in Figs. 4.15(a) and 4.17(a). Also when the armature resistance is changed, there is a significant drop of speed for the PI controller based system. This is illustrated in Figs. 4.18(a) and 4.20(a). The ANN again proves its superiority as can be seen from Figs. 4.19(a) and 4.21(a). There is very little speed drooping and also the recovery time is faster than that of the PI based system. As expected, due to the on-line weights and biases updating of the ANN with adaptive learning rates, the proposed system becomes very insensitive to parameter variations and thus tracks the reference speed quite accurately.

The transient currents in both cases of PI and ANN controllers for the PM dc motor are within the prescribed range as can be seen from Figs. 4.8 to 4.21. The power amplifier used in the experiment provided ripple free dc currents which ensure the smooth operation. The current responses clearly show the excellent dynamic performances of the drive due to changes in reference speed and loading condition as well as parameter variations.

4.6 Concluding Remarks

In this work, an on-line self-tuning ANN controller based speed control scheme is developed and experimentally implemented for a laboratory PM dc motor. A PI controller based drive system is also implemented in the laboratory. The performances of both the PI controller and ANN controller based drive systems for the PM dc motor are compared. The comparative results clearly show that the performances of the ANN controller based system are superior, particularly in cases of parameter varia-

tions and load disturbances. The use of the adaptive learning rate in the proposed system reduces the possibilities of over-shooting during transient conditions. The feedback provision in the modified ANN structure not only reduces computations in real-time but also enhances the stability of the system. The proposed ANN based speed control system of the PM dc motor is found to be robust, efficient and easy to implement. The successful use of ANN in the PM dc motor drive is considered as a foundation to extend it to the case of a brushless PM synchronous motor drive which is the subject of the next chapters.

Chapter 5

Artificial Neural Network Based Brushless PM Synchronous Motor Drive

Although the ANN based PM dc motor drive system offers excellent control features as discussed in chapter 4, certain inherent drawbacks limit the use of dc motors in high performance drive (HPD) applications. Recent developments in microelectronics, power converter devices and permanent magnet materials have provided an excellent opportunity for using ac motors in modern HPD systems. As discussed in the literature review, among the various types of ac motors, the brushless PM synchronous motor is one of the best choices which can be used in the modern drive applications. This chapter presents a novel approach of speed control for a brushless PM synchronous motor using an on-line self-tuning artificial neural network. Based on the motor dynamics and the non-linear load characteristics, an ANN speed controller is developed and integrated with the vector control scheme of the brushless PM synchronous motor drive [81]. The combined use of the off-line and on-line train-

ings of ANN offers a unique feature of the on-line system identification and a precise speed control of the high performance PM brushless synchronous motor drive. In order to predict the performances of the proposed drive system under various operating conditions, the drive system with the ANN is simulated. The simulation results are presented and discussed in this chapter.

5.1 Inverse Dynamics of the Brushless PM Synchronous Motors

As mentioned earlier, the use of the ANN in any system does not require a knowledge of the model of the system under study. The inputs and outputs of the ANN are arbitrarily chosen from the system variables. However, it is preferred to model the dynamics of the drive system so that inputs and outputs of the ANN can be selected in a more defined and systematic way [13]. This guarantees that the ANN will capture most of the system dynamics.

In this work, like the conventional approach of controlling the speed, the vector control technique is incorporated with the ANN in order to obtain the highest torque sensitivity of the brushless PM synchronous motor drive. The vector control strategy is formulated in the rotating reference frame in the same way as discussed in chapter 2. The mathematical model of a brushless PM synchronous motor is briefly summarized in the d-q synchronously rotating reference frame to formulate the structure of the ANN. The q, d-axis voltage equations are given as

$$v_q^r = Ri_q^r + p\lambda_q^r + P\omega_r\lambda_d^r \tag{5.1}$$

$$v_d^r = Ri_d^r + p\lambda_d^r - P\omega_r\lambda_q^r \tag{5.2}$$

and the developed electric torque is given by

$$T_e = \frac{3P}{2}[\lambda_M i_q^r + (L_d - L_q) i_d^r i_q^r]. \tag{5.3}$$

The motor dynamics with the load torque can be expressed as

$$T_e = Jp\omega_r + B\omega_r + T_L, \tag{5.4}$$

where T_L is the load torque, B is the damping co-efficient, and J is the rotor inertia. The load torque in equation (5.4) can have any non-linear unknown mechanical characteristics. The following equation can be used to model a non-linear load [51]

$$T_L = A_1\omega_r^2 + B_1\omega_r + C_1, \tag{5.5}$$

where A_1, B_1 and C_1 are constants. In order to obtain the maximum torque with minimum current, the control strategy of forcing the d-axis reference current to zero is used in the proposed ANN based brushless PM synchronous motor drive which renders the machine model simpler. The simplified machine model is given as

$$pi_q^r = \frac{1}{L_q}(v_q^r - Ri_q^r - K_b\omega_r), \tag{5.6}$$

$$p\omega_r = \frac{1}{J}[T_e - T_L - B\omega_r], \tag{5.7}$$

where $K_b = P\lambda_M$ and the developed torque T_e in equation (5.3) is proportional to the q-axis current and is given by

$$T_e = K_T i_q^r, \tag{5.8}$$

where $K_T = \frac{3P}{2}\lambda_M$. Although the machine model becomes simpler with the proposed control strategy, the load is still non-linear as described by the equation and unpredictable in real-time. Therefore an ANN is a good choice for this non-linear mapping

of the inputs and output(s). Moreover, difficulties due to parameter variations of the speed control of the HPD using an interior-type brushless PM synchronous motor are efficiently solved using the proposed adaptive ANN.

Now to make the control task easier, the brushless PM synchronous motor equations can be expressed as a single input single output system in continuous time domain by combining equations (5.5) to (5.8) to give

$$\begin{aligned} & L_q J \frac{d^2\omega_r(t)}{dt^2} + (RJ + L_q B + B_1 L_q)\frac{d\omega_r(t)}{dt} + \\ & (RB + K_b K_T + B_1 R)\omega_r(t) + A_1 L_q \frac{d\omega_r^2(t)}{dt} + \\ & A_1 R\omega_r^2(t) + C_1 R - K_T v_q^r(t) = 0. \end{aligned} \tag{5.9}$$

The discrete time model of the simplified brushless PM synchronous motor drive can be obtained by replacing all continuous quantities by their finite differences as

$$\begin{aligned} \omega_r(n+1) &= \alpha\omega_r(n) + \beta\omega_r(n-1) + \gamma\omega_r^2(n) + \\ & \quad \delta\omega_r^2(n-1) + \epsilon v_q^r(n) + \vartheta, \end{aligned} \tag{5.10}$$

where $\alpha, \beta, \gamma, \delta, \epsilon$ and ϑ are functions of the motor parameters as well as the sampling interval ΔT and are defined as

$$\begin{aligned} \alpha &= [2L_q J + \Delta T(RJ + L_q B + B_1 L_q) - \Delta T^2(RB + K_T K_b \\ & \quad + B_1 L_q)]/D, & (5.11) \\ \beta &= -L_q J/D, & (5.12) \\ \gamma &= -[\Delta T A_1(L_q + R\Delta T)]/D, & (5.13) \\ \delta &= [\Delta T A_1 L_q]/D, & (5.14) \\ \epsilon &= [K_T \Delta T^2]/D, & (5.15) \\ \vartheta &= -[C_1 R\Delta T^2]/D, & (5.16) \end{aligned}$$

where,

$$D = L_q J + \Delta T(RJ + L_q B + B_1 L_q). \tag{5.17}$$

Equation (5.10) is modified in order to obtain the inverse model of the drive system as

$$\begin{aligned} v_q^r(n) &= [\omega_r(n+1) - \alpha\omega_r(n) - \beta\omega_r(n-1) - \gamma\omega_r^2(n) \\ &\quad -\delta\omega_r^2(n-1) - \vartheta]/c. \end{aligned} \tag{5.18}$$

Now in discrete form, the q-axis current can be expressed in terms of $v_q^r(n)$ and $\omega_r(n)$ by replacing the continuous terms of equation (5.6) by their finite differences, giving

$$i_q^r(n) = A_2 i_q^r(n-1) + B_2 v_q^r(n) + C_2\omega_r(n), \tag{5.19}$$

where,

$$A_2 = 1 - \frac{R\Delta T}{L_q}, \tag{5.20}$$

$$B_2 = \frac{\Delta T}{L_q}, \tag{5.21}$$

$$C_2 = -\frac{\Delta T K_b}{L_q}. \tag{5.22}$$

Thus substituting the expression of $v_q^r(n)$ from equation (5.18) in equation (5.19), the expression for the q-axis current can further be modified as

$$\begin{aligned} i_q^r(n+1) &= A_2 i_q^r(n) + B_2[\omega_r(n+1) - \left(\alpha - \frac{cC_2}{B_2}\right)\omega_r(n) - \\ &\quad \beta\omega_r(n-1) - \gamma\omega_r^2(n) - \delta\omega_r^2(n-1) - \vartheta]/c, \end{aligned} \tag{5.23}$$

where $(n+1)$th sample is considered as the present sample. This form of the expression for the q-axis current is derived in order to include all parameters of the motor. This facilitates the training of the ANN with the provision of parameter variations. The

right hand side of equation (5.23) is a non-linear function of the speed $\omega_r(n)$. The purpose of using the ANN is to map the non-linear relationship between the q-axis current i_q^r and the speed ω_r according to equation (5.23). The structure of the ANN for the speed control of the brushless PM synchronous motor drive can be devised using equation (5.23).

5.2 ANN Structure for the Brushless PM Synchronous Motor Drive

One of the important aspects of applying an ANN to any particular problem is to formulate the inputs and output(s) of the ANN structure under study. The inverse dynamics of the brushless PM synchronous motor drive as described in equation (5.23) dictates the inputs and output of the ANN used in the control system. According to equation (5.23), the inputs of the proposed ANN are the speeds of the motor at the present and previous two sample intervals, in addition to the previous sample of the q-axis current. Therefore the input vector becomes $[\omega_r(n+1), \omega_r(n), \omega_r(n-1), i_q^r(n]$. The corresponding output target is the present sample of q-axis current $i_q^r(n+1)$. After the inputs and the output are formulated, the number of hidden layers is determined. Considerable research is being conducted to determine the optimum number of hidden layers and number of neurons in the hidden layer for a particular problem. So far the number of hidden layers and number of neurons in the hidden layer(s) are determined by trial and error. The facts considered in selecting these parameters are that the system should provide stable operation under the chosen operating conditions while keeping the numbers as small as possible to facilitate minimum computation time and memory requirement. For the present work, it has been observed that the structure of

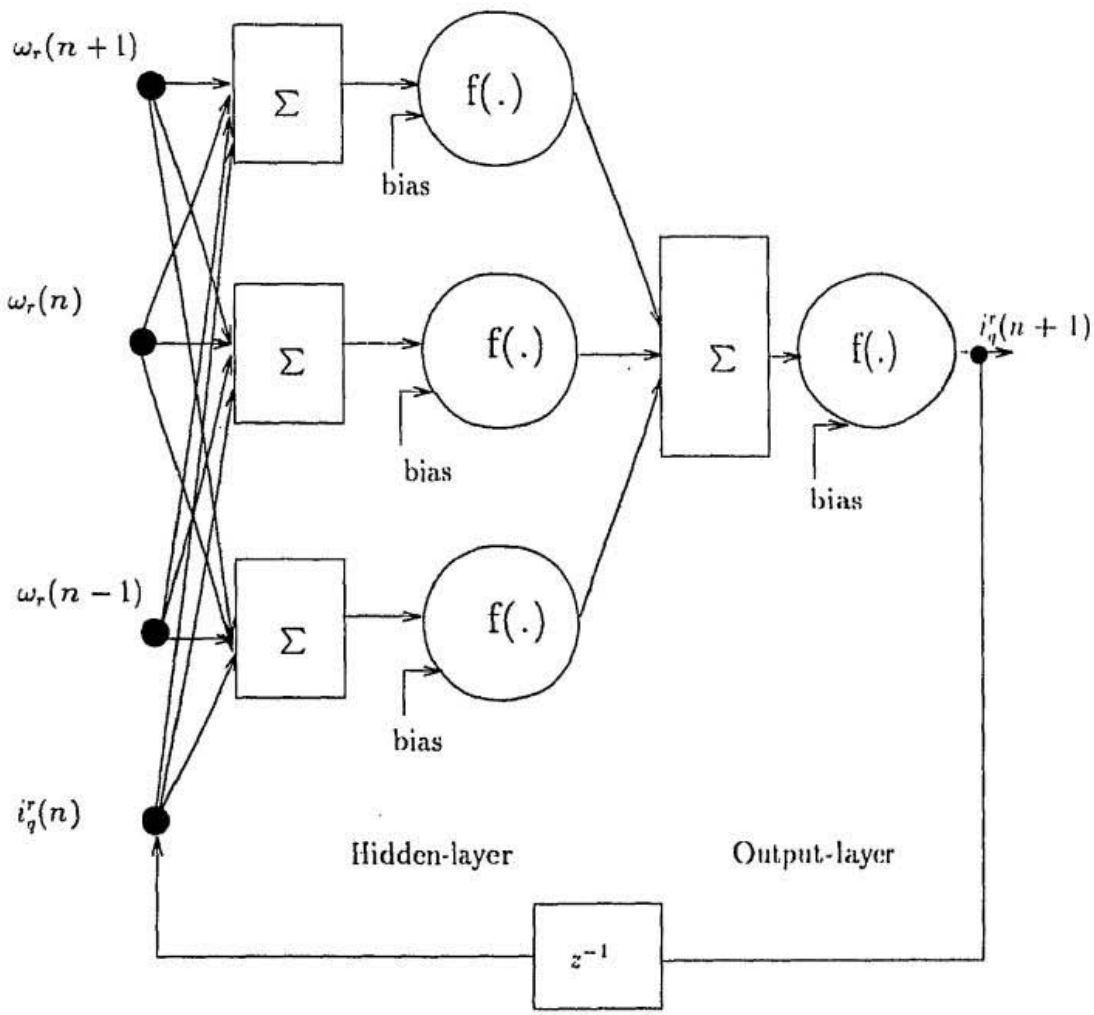

Figure 5.1: ANN structure for the brushless PM synchronous Motor

one hidden layer having three neurons gives satisfactory results. The ANN structure for the brushless PM synchronous motor drive is shown in Fig. 5.1. The log-sigmoid and tan-sigmoid type transfer functions are used in the hidden and output layers, respectively. Now it is necessary to determine the weights and biases of the ANN through training in order to achieve the specific target with the given inputs. The back-propagation training algorithm is used for this purpose, and is based on the principle of minimization of a cost function of the error between the outputs and the target of the ANN as described in chapter 3. There are a number of applications where the off-line training is sufficient to generate the weights and biases of the ANN, as for example, when system parameters are relatively constant. But in applications like HPD with interior-type brushless PM synchronous motors, where the parameters change with temperature and loading, an on-line weight updating feature is almost mandatory in order to obtain proper system performances. However, the on-line training task could be eased and the system can be further stabilized if an initial set of weights and biases is generated beforehand through off-line training. A combination of the off-line and on-line trainings has been used for the present work. The initial weights and biases are obtained through off-line training. In the case of on-line training, these are updated only when an error limit between the actual output and the target of the ANN exceeds a preset value.

5.3 Off-line Training for Initial Weights and Biases

In neural network applications, availability of training data is one of the main concerns. For the proposed work, off-line training data can either be generated by sim-

Table 5.1: Initial set of weights and biases for ANN used in brushless PM synchronous motor drive

	NW1	
-0.4266	0.2340	0.0410
0.4397	0.6552	0.5160
-0.7329	0.0680	-0.4717
	NW2	
-3.7272	-0.9813	-3.7907
	NB1	
-0.1266	0.5937	1.4648
	NB2	
	3.4837	

ulation or experiment. Generating training data by simulation is easier if the PM motor parameters are available, otherwise an experiment has to be performed, such as running the motor on open loop basis and recording input currents and output speeds at different operating conditions. Since the motor parameters are available, off-line training data have been generated using equation (5.23) for this work. The input quantities used for generating the data are $\omega_r(n+1), \omega_r(n), \omega_r(n-1), i_q^r(n)$. The corresponding target $i_q^r(n+1)$ can be generated by using this input vector and $\alpha, \beta, \gamma, \delta, \epsilon, \vartheta$ and A_2, B_2, C_2 in the right hand side of equation (5.23). The simulation is carried out at random q-axis currents in order to obtain various speeds according to the specified currents. At first, the simulated speed and current data are down sampled by 50 times and finally two sets of data with 800 samples are obtained. A

window length of four, containing $\omega_r(n+1), \omega_r(n), \omega_r(n-1), i_q^r(n)$, is slided over the entire speed and q-axis current samples giving an input matrix of size 4×800. The output vector of size 1×800, contains the q-axis current $i_q^r(n+1)$ data. The off-line training of the ANN is performed with these training data using the back-propagation algorithm of the MATLAB neural network tool-box [78]. The initial set of weights and biases obtained through the off-line training is given in Table 5.1.

5.4 Real-time ANN Based Brushless PM Synchronous Motor Drive

The main goal of the control system is to track the reference speed of the drive by providing an appropriate q-axis current i_q^r depending upon the operating conditions. In the real-time, the rotor position information and the output of the ANN which is considered now as q-axis reference current i_q^{r*} are used to generate the three phase reference currents i_a^*, i_b^* and i_c^*. This is accomplished by Park's axis transformation [65]. The three phase reference currents are compared with the actual motor currents in a hysteresis current controller which provides the necessary drive signals for the inverter. The complete control scheme is shown in Fig. 5.2.

The reference speed trajectory is selected using a second order reference model that makes the system asymptotically stable [13]. The reference model can be described by the following equation

$$\omega_r^*(n+1) = b_1\omega_r^*(n) + b_2\omega_r^*(n-1) + r(n) \tag{5.24}$$

The poles and zeros of the reference model are placed within the unit circle in order to ensure system stability. This is accomplished by properly selecting the constants

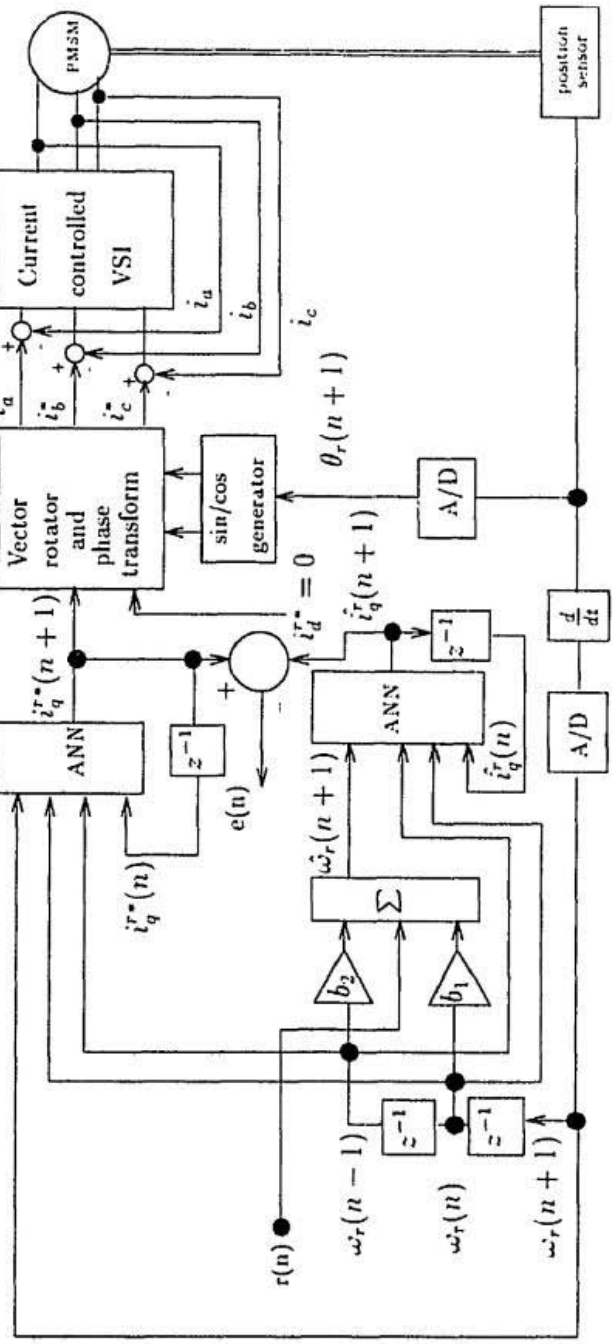

Figure 5.2: Block diagram of the proposed ANN based brushless PM synchronous motor drive

b_1 and b_2 for a specific reference trajectory. In equation (5.24), $r(n)$ is the bounded input to the reference model, the value of which can be calculated beforehand using equation (5.24) for a desired reference speed. The rotor speed at the $(n+1)th$ sample can be predicted from equation (5.24) by considering the fact that the tracking error is small and the selected reference model is asymptotically stable [13], giving

$$\hat{\omega}_r(n+1) = b_1\omega_r(n) + b_2\omega_r(n-1) + r(n) \tag{5.25}$$

Hence in addition to the previous sample of the predicted q-axis current, with one sample of predicted speed and two samples of actual speed, an input sequence of $\hat{\omega}_r(n+1), \omega_r(n), \omega_r(n-1), \hat{i}_q^r(n)$ is formed and used as the input to the ANN as shown in Fig. 5.2. With the initial weights and biases and this sequence of input, the predicted output of the ANN, $\hat{i}_q^r(n+1)$ is computed. Using actual speed samples and one delayed sample of q axis current another input sequence containing $\omega_r(n+1), \omega_r(n), \omega_r(n-1), i_q^{r*}(n)$ is also formed in order to generate the output $i_q^{r*}(n+1)$. This $i_q^{r*}(n+1)$ is compared with $\hat{i}_q^r(n+1)$ to compute the error which is used to update the previous set of weights and biases using the back-propagation algorithm. It is noted here that the two ANNs shown in Fig. 5.2 have the same set of weights and biases with two different sets of inputs and outputs.

The weights and biases are updated at each instant using improved back-propagation algorithm with similar types of weights and biases updating equations as described in chapter 4. The minimized error function is given by

$$E(n) = \frac{1}{2}e^2(n) \tag{5.26}$$

where $e(n) = error = \hat{i}_q^r(n+1) - i_q^{r*}(n+1)$

5.5 Simulation of the ANN Based PM Synchronous Motor Drive

The complete ANN based brushless drive system has been simulated by writing a program in MATLAB [82]. The initial set of weights and biases are down loaded first and then updated depending upon the operating conditions. The reference input r(n) has been generated a priori according to the desired reference speed. The inverter switching has also been incorporated in the simulation.

The proposed drive system has been simulated to predict the speed responses at the rated reference speed 1800 rpm and at low reference speeds, as for example at 239 rpm (8 Hz) under no load and at rated load conditions. The reference speed could not be decreased beyond this value because of the switching frequency limitation of the experimental voltage source inverter. Figures 5.3 to 5.6 depict the speed and current responses for these operating conditions. From Figs. 5.3 to 5.6, it is quite evident that the ANN based system is capable of operating at wide range of speeds under no load and full load conditions.

The proposed drive system has also been simulated with a step change in reference speed under no load and full load conditions. The simulated results are shown in Figs. 5.7 and 5.8. It is clear from these figures that the on-line adaptive properties of the ANN efficiently generate the q-axis reference currents for the current controller which eventually operate the proposed system according to the reference speeds.

Performance prediction with a sudden load impact has been carried out at the rated reference speed. A 2.5 N-m of load is suddenly applied to the running motor. Fig. 5.9 shows the speed and current responses for this operating condition. Unlike the conventional controller based system as shown in chapter 2, there is negligible

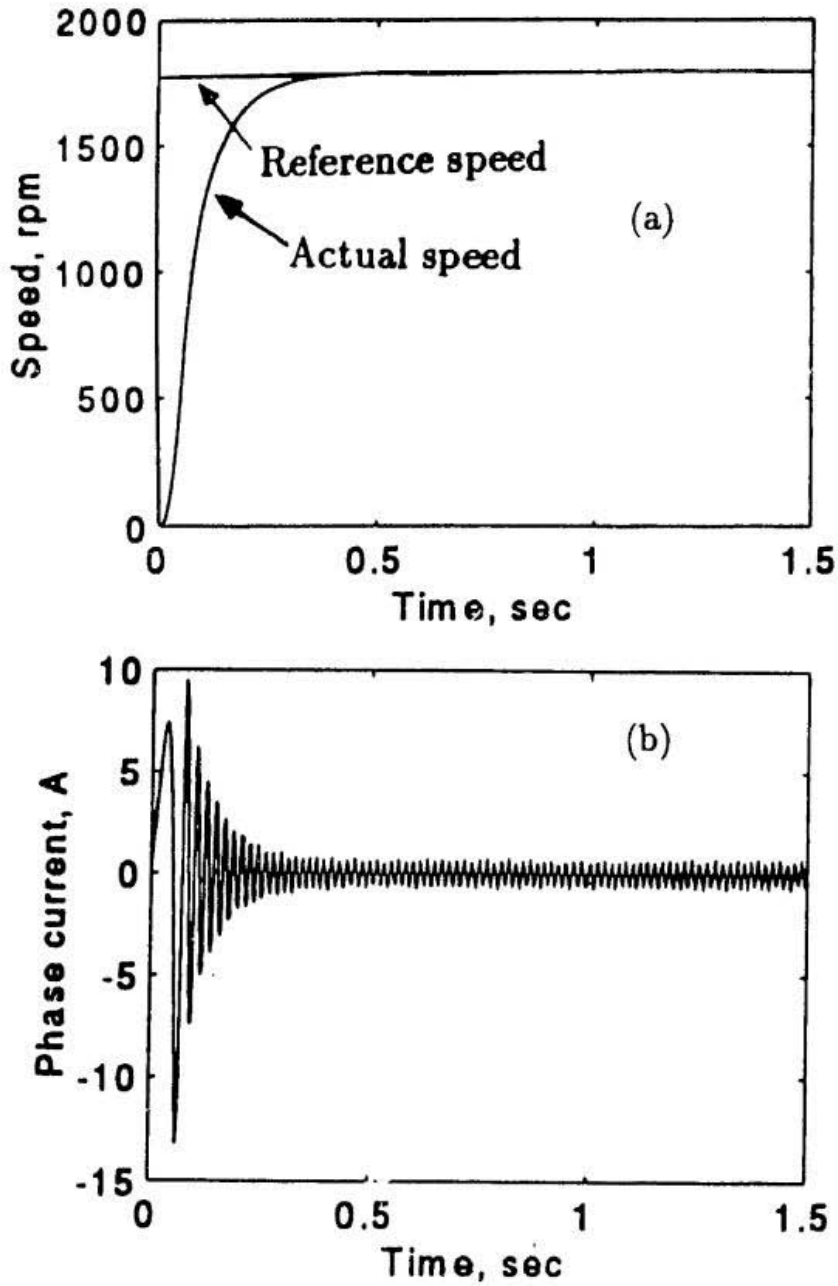

Figure 5.3: Simulation results of the ANN based brushless PM synchronous motor drive at no load with reference speed 1800 rpm; (a) speed response (b) current response

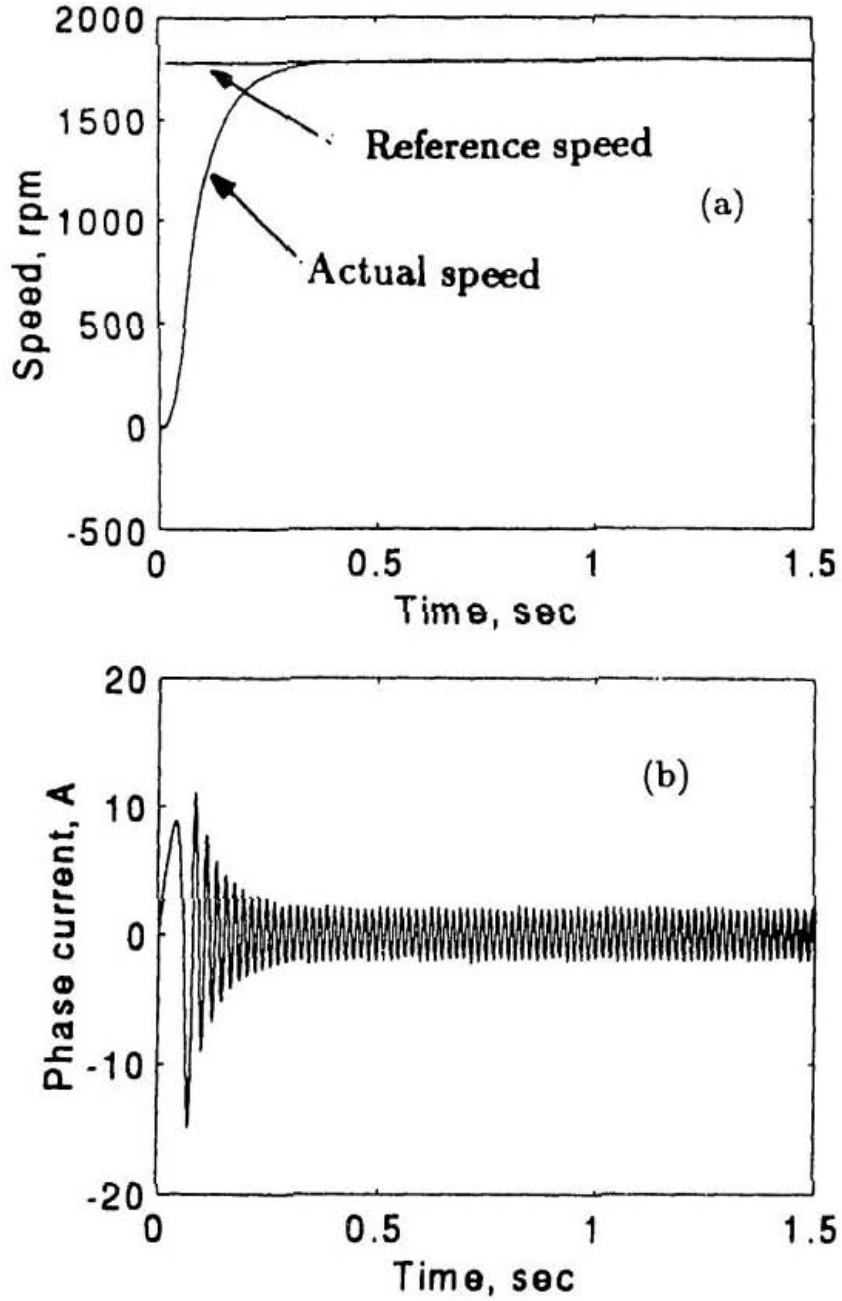

Figure 5.4: Simulation results of the ANN based brushless PM synchronous motor drive at rated load with reference speed 1800 rpm; (a) speed response (b) current response

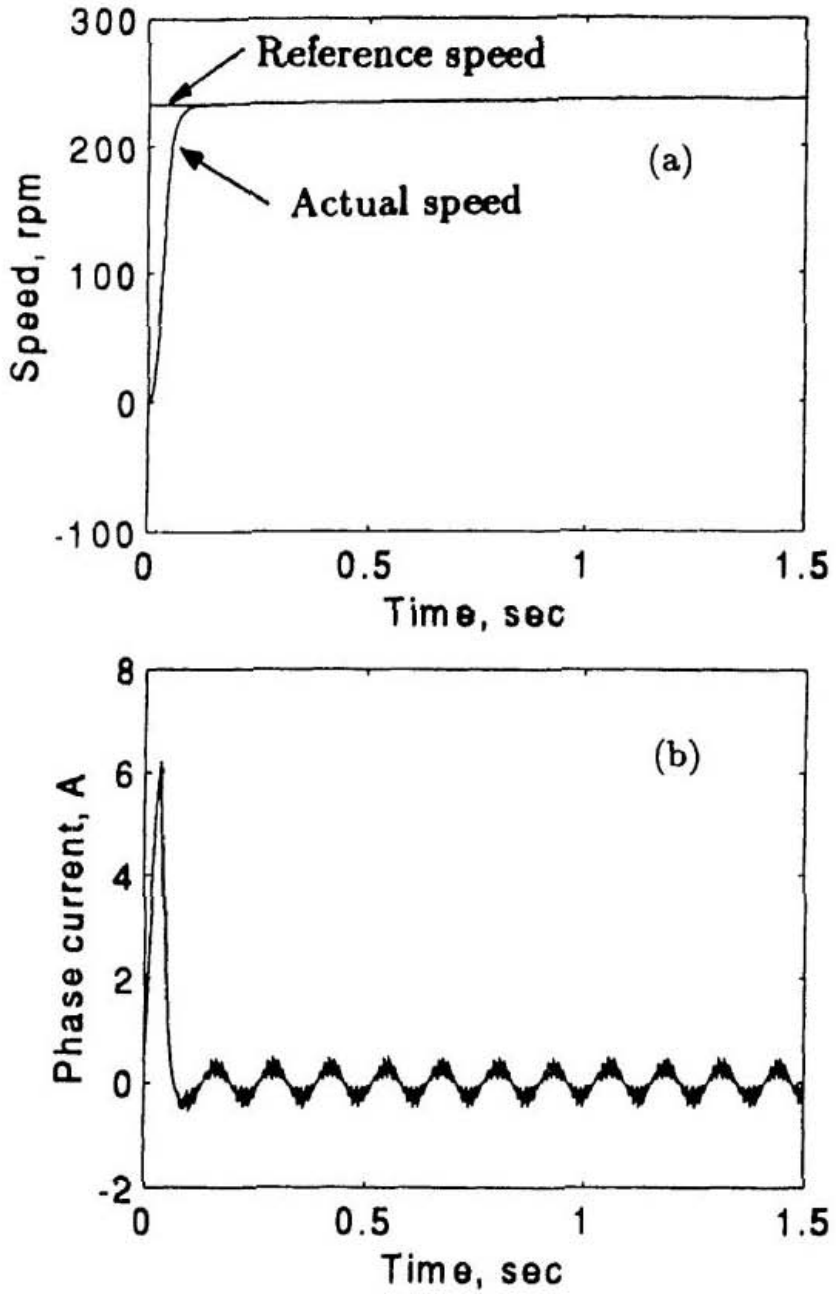

Figure 5.5: Simulation results of the ANN based brushless PM synchronous motor drive at no load with reference speed 239 rpm; (a) speed response (b) current response

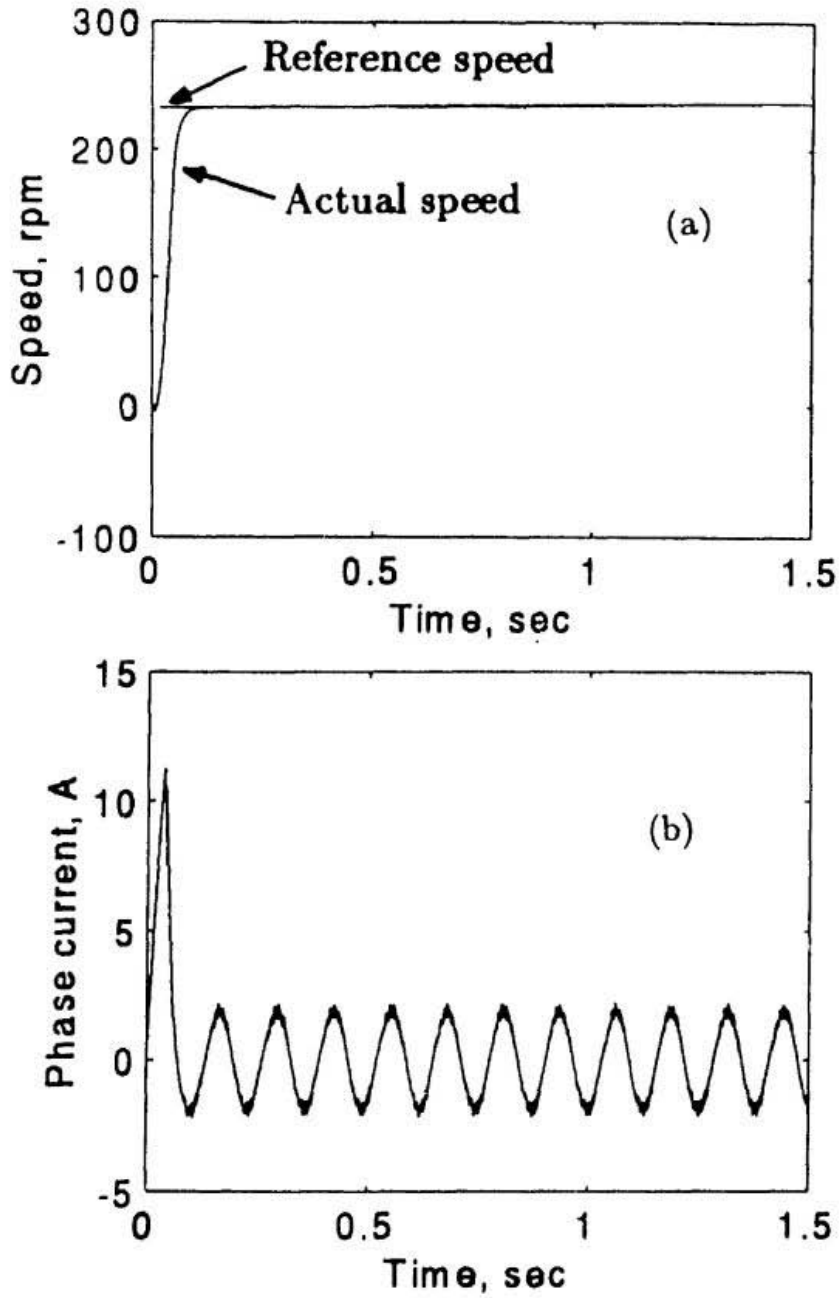

Figure 5.6: Simulation results of the ANN based brushless PM synchronous motor drive at rated load with reference speed 239 rpm; (a) speed response (b) current response

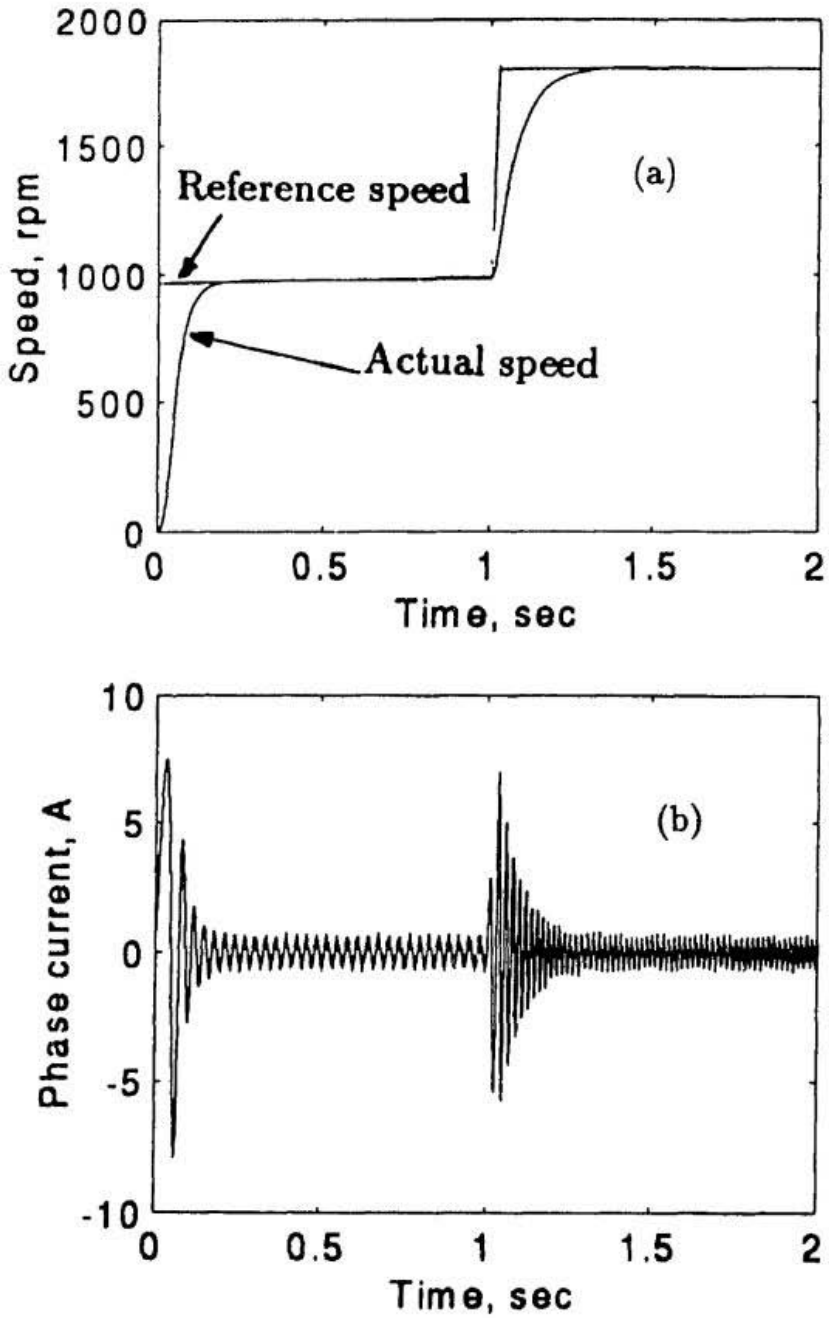

Figure 5.7: Simulation results of the ANN based brushless PM synchronous motor drive at no load with change in reference speed (a) speed response (b) current response

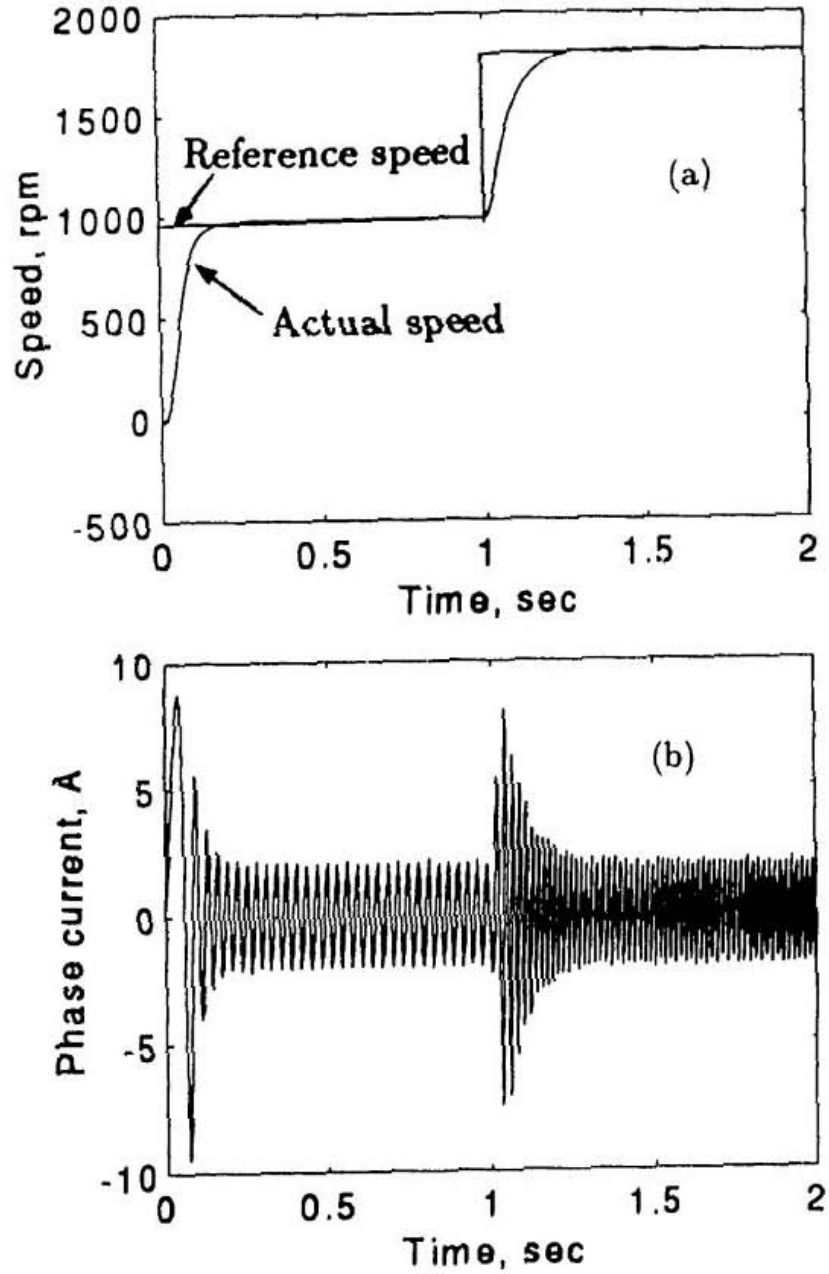

Figure 5.8: Simulation results of the ANN based brushless PM synchronous motor drive at rated load with change in reference speed (a) speed response (b) current response

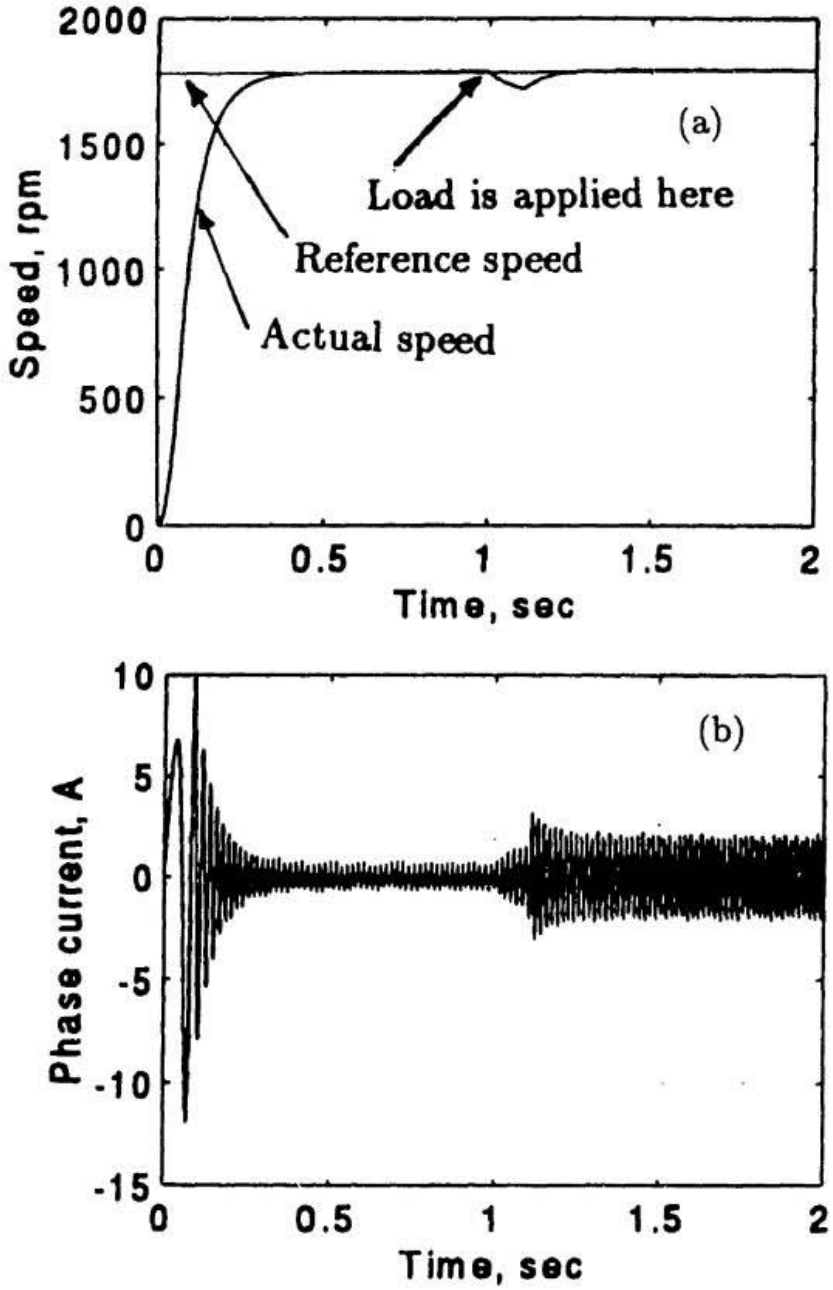

Figure 5.9: Simulation results of the ANN based brushless PM synchronous motor drive at rated speed with sudden load impact (a) speed response (b) current response

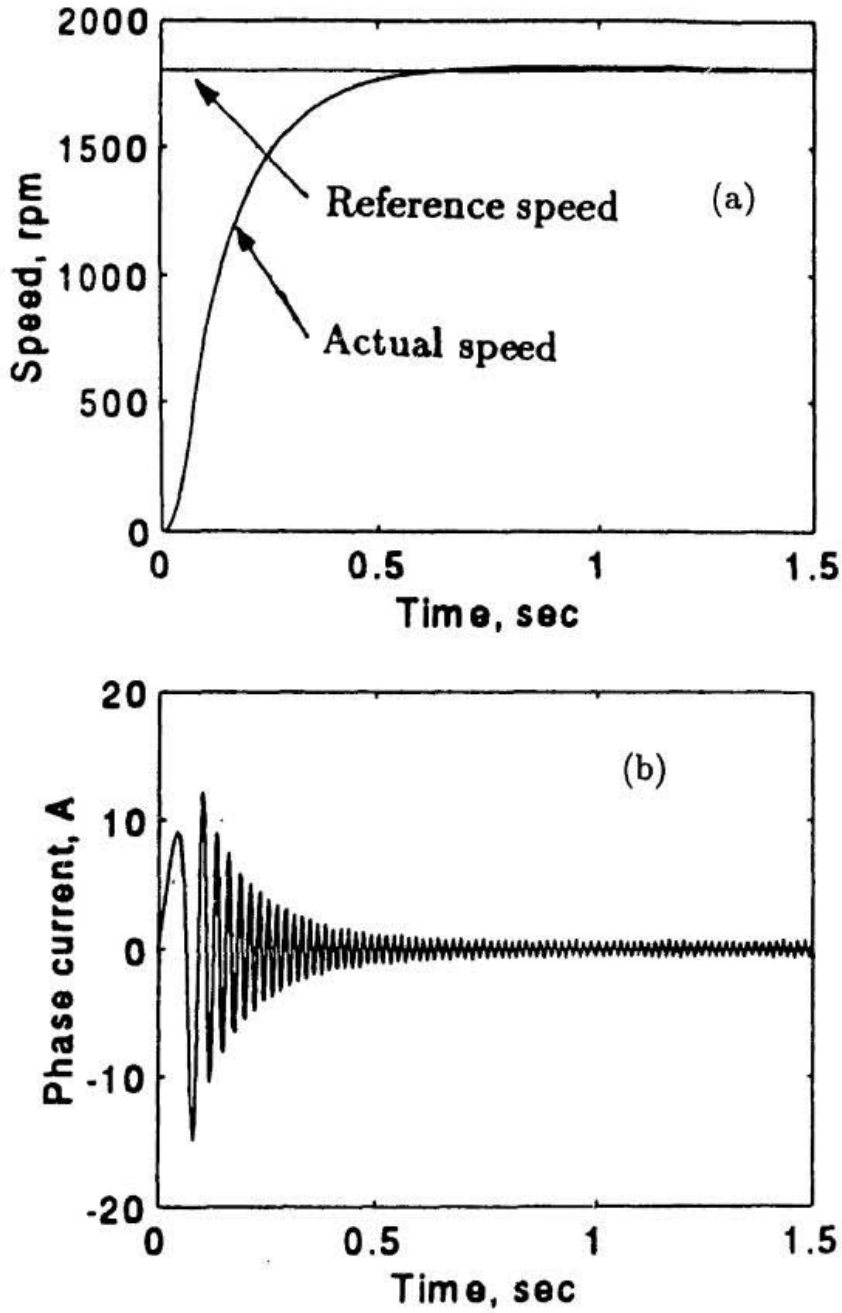

Figure 5.10: Simulation results of the ANN based brushless PM synchronous motor drive at no load with change in inertia $J \rightarrow 2J$ (a) speed response (b) current response

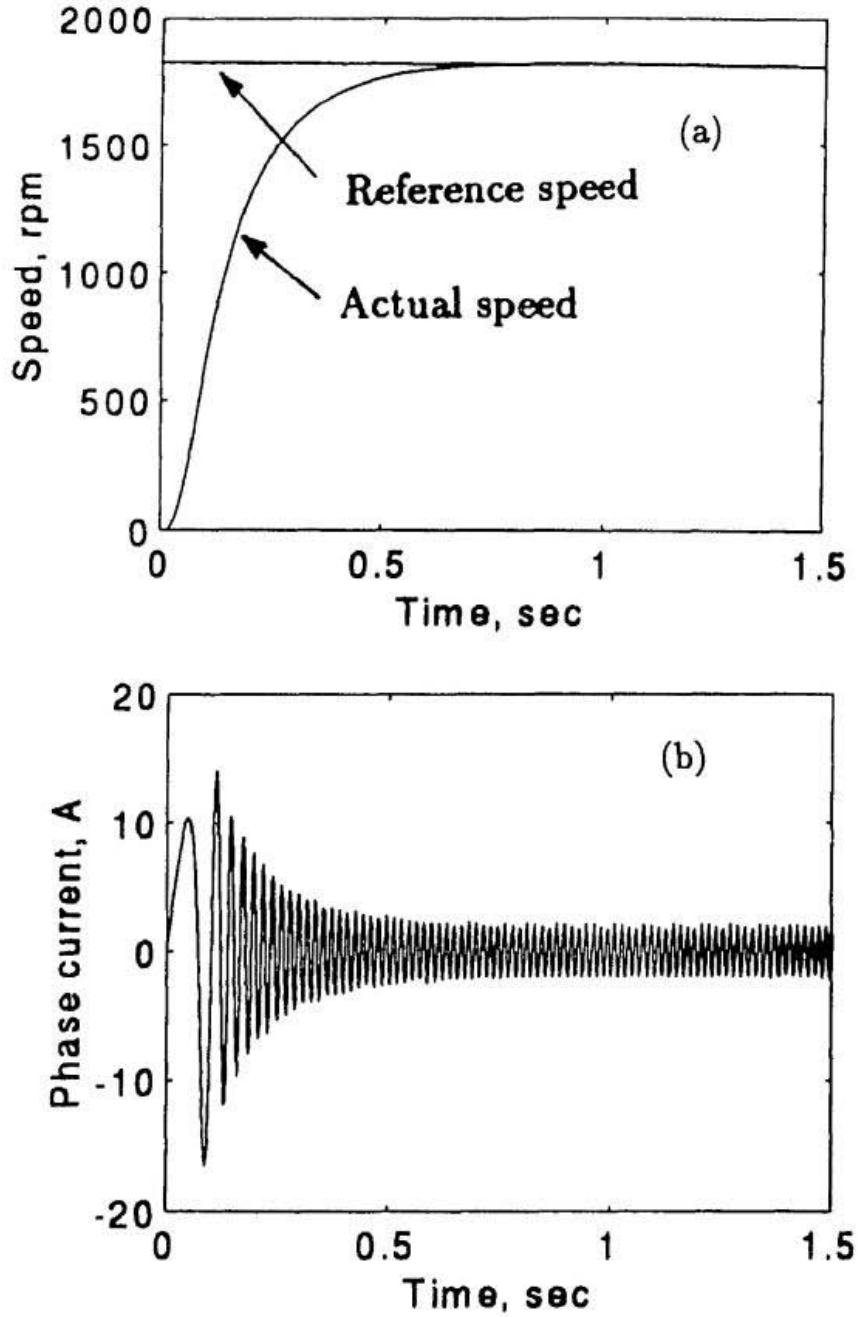

Figure 5.11: Simulation results of the ANN based brushless PM synchronous motor drive at rated load with change in inertia $J \rightarrow 2J$ (a) speed response (b) current response

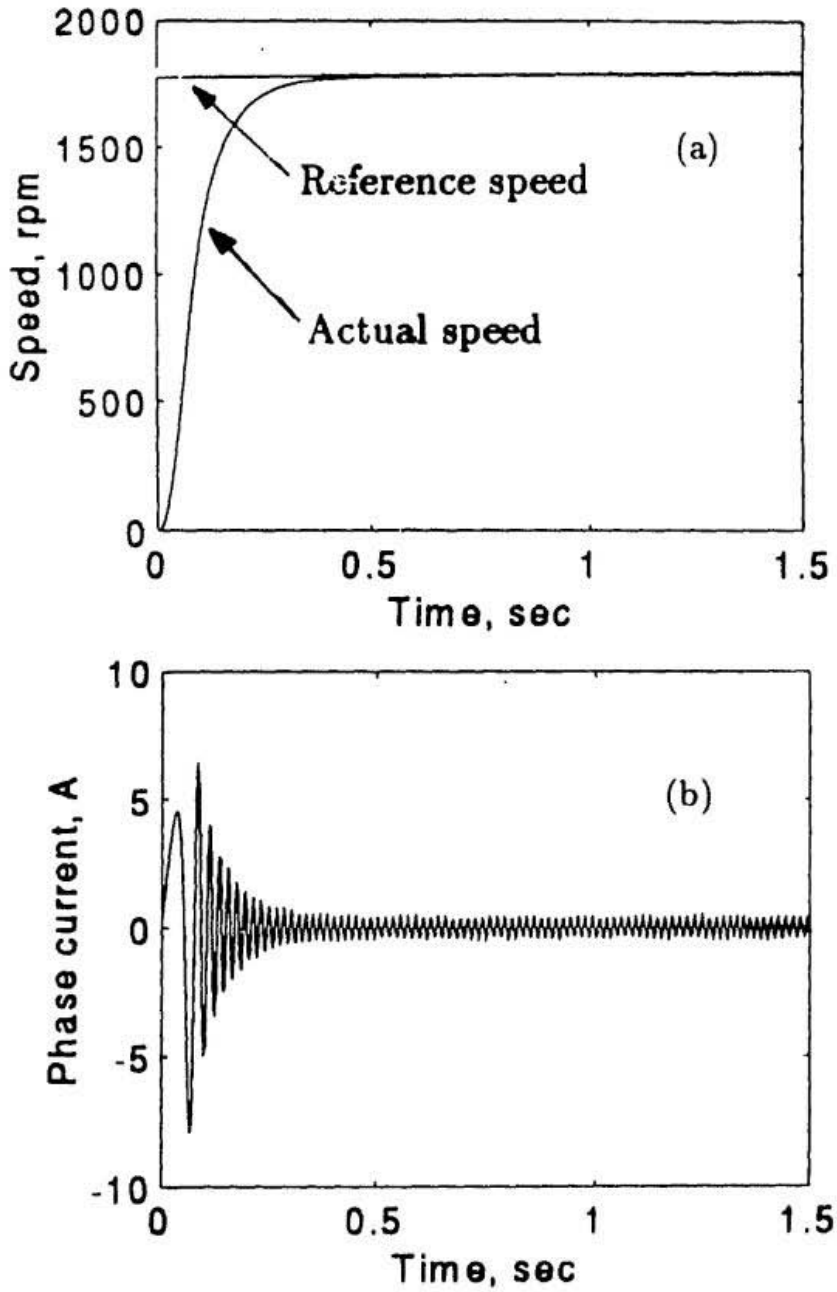

Figure 5.12: Simulation results of the ANN based brushless PM synchronous motor drive at no load with change in stator resistance $R \rightarrow 2R$ (a) speed response (b) current response

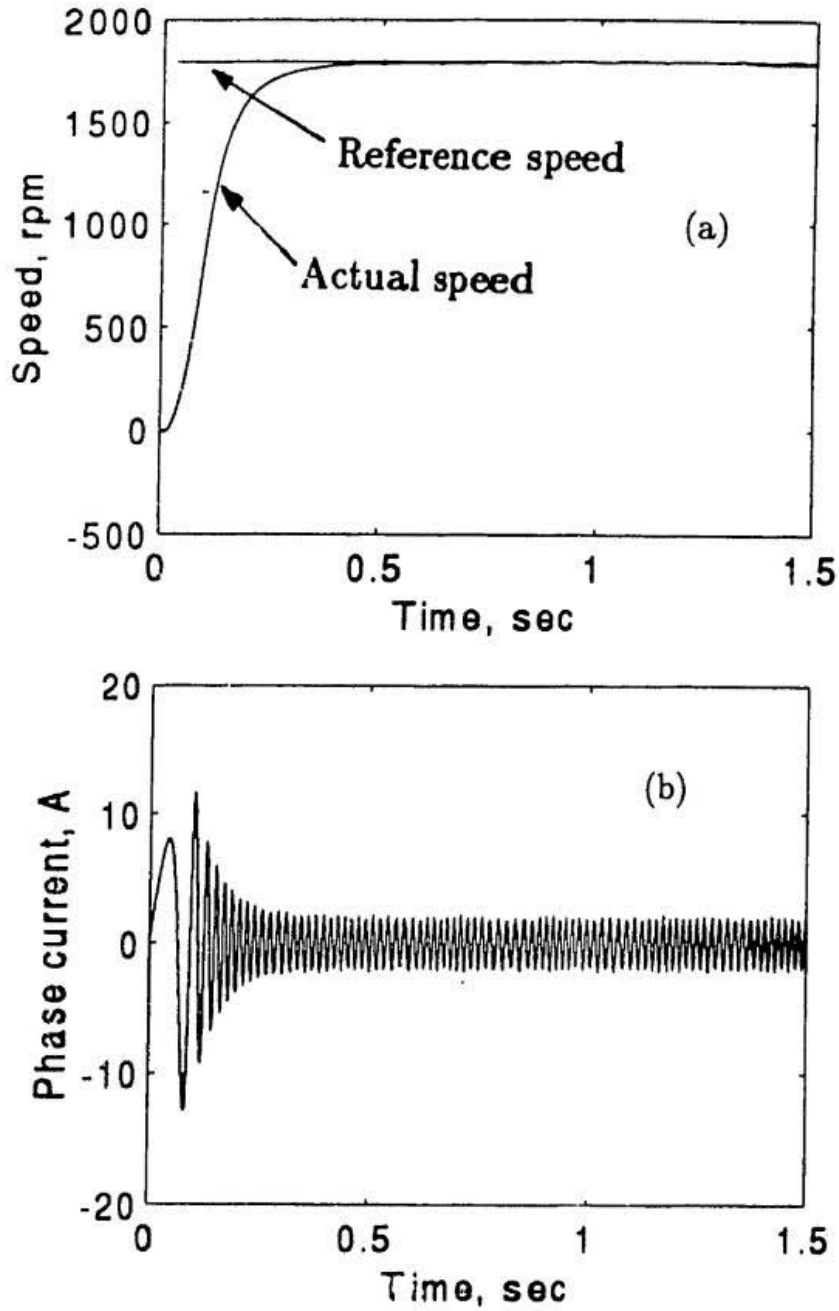

Figure 5.13: Simulation results of the ANN based brushless PM synchronous motor drive at rated load with change in $R \rightarrow 2R$ (a) speed response (b) current response

speed drooping due to load impact. The system performances have been improved due to adaptive properties of the ANN used in the proposed system. The weights and biases have been updated with this changing circumstance of load impact and the drive follows the reference speed quite accurately.

Simulation has also been carried out with parameter variations. As in the conventional speed controller based brushless PM synchronous motor drive, two parameters have been changed: (i) the inertia of the motor is doubled, and (ii) an additional resistance is inserted in the stator circuit. Simulations have been carried out with parameter variations under the rated load and the no load conditions. Figures 5.10 to 5.13 illustrate the effects of changes in inertia and stator resistance on speeds and currents for these conditions. From these figures, it is seen that although there is a negligible over-shooting in the case of change in inertia, the ANN based brushless PM synchronous motor drive system accurately follows reference speeds for both cases of parameter changes. The on-line weights and biases updating feature of the ANN makes the control scheme robust against these parameter variations.

The simulation current responses as shown in Figs. 5.3 to 5.13 show the transient as well as dynamic behaviors of the ANN based brushless PM synchronous motor drive system. The envelopes of the current responses are the q-axis reference currents which are outputs of the ANN controller at various operating conditions. The peak value of the transient currents never exceeds the prescribed limit of 10 ampere. From the simulation results of the current responses, it is evident that the transient and dynamic current responses of the proposed ANN based drive systems are satisfactory.

5.6 Concluding Remarks

In this chapter, the vector control scheme of a brushless PM synchronous motor drive is designed and simulated using an ANN based speed controller. In order to achieve adaptive control over a wide operating range of speeds, an on-line training method based on the back-propagation algorithm is introduced. This allows the ANN controller to adjust itself according to operational conditions. The uniqueness of this work is the provision of a substitute for the conventional fixed gain PI or PID controller. The ANN controller makes the brushless PM synchronous motor drive robust, efficient, and immune to the adverse effects of load changes, parameter variations and non-linearities of the load. The simulation results of the proposed scheme are very encouraging. A successful on-line laboratory implementation of the drive system using controller board DS-1102 will validate the efficacy of the proposed brushless PM synchronous motor drive with the ANN based controller.

Chapter 6

Laboratory Implementation of the ANN Based Brushless PM Synchronous Motor Drive System

The implementation of the ANN in real-time for a motor drive system is considered one of the challenging problems encountered by the control engineers. This is because of the fact that there are not many commercial functional integrated circuits (ICs) of the ANN available for the experimental work. Therefore, a combination of hardwares and softwares has been used in this work for the real-time implementation of the proposed ANN based brushless PM synchronous motor drive system. The DSP controller board DS-1102 has been used for the software implementation of the ANN algorithm. In addition, other conventional hardwares, such as pulse amplifier, voltage source inverter, and current transducers have been used to operate the drive system. This chapter presents a detailed laboratory implementation of the proposed ANN based brushless PM synchronous motor drive system, and documents the experimental results with pertinent discussions.

6.1 General Description of the Laboratory Setup

The laboratory setup used for the experiment is shown in Fig. 6.1. The test motor is labeled as 'M'. This motor is coupled to an induction generator labeled as 'L' which works as a load. The power generated in the loading induction machine is dissipated in a resistor bank labeled as 'R_L'. A tacho-generator is mounted on the induction machine for the purpose of tracing the speed response only. Motor currents are captured by the non-inductive type current transducers having good linear response over a range of 0 to 30 ampere current operations. These transducers are labeled as 'T'. The rotor position of the test motor is detected by an optical encoder labeled as 'E'. This encoder is mounted on the motor shaft. An interface circuit labeled as 'F' has been used between the control and the power circuit. The purpose of using the interface circuit is to generate the necessary commutating signals to make sure that transistors on the same leg of the inverter do not switch on at the same instant. Moreover, in this circuit, three phase drive signals from the DSP have been converted to six drive signals for the six transistors of the inverter. The six drive pulses are amplified through a pulse amplifier module labeled as 'A'. The power circuit of the brushless PM synchronous motor drive comprises a transistor inverter labeled as 'I' and rectifier labeled as 'R'. The inverter consists of three pairs of Darlington BJT transistors with six free-wheeling power diodes.

6.2 Hardware Implementation

As mentioned earlier, the control algorithm of the ANN based drive system has been implemented through the DS-1102 DSP controller board [83]. The main processor in this board is the Texas Instrument TMS320C31 floating point type. The board has

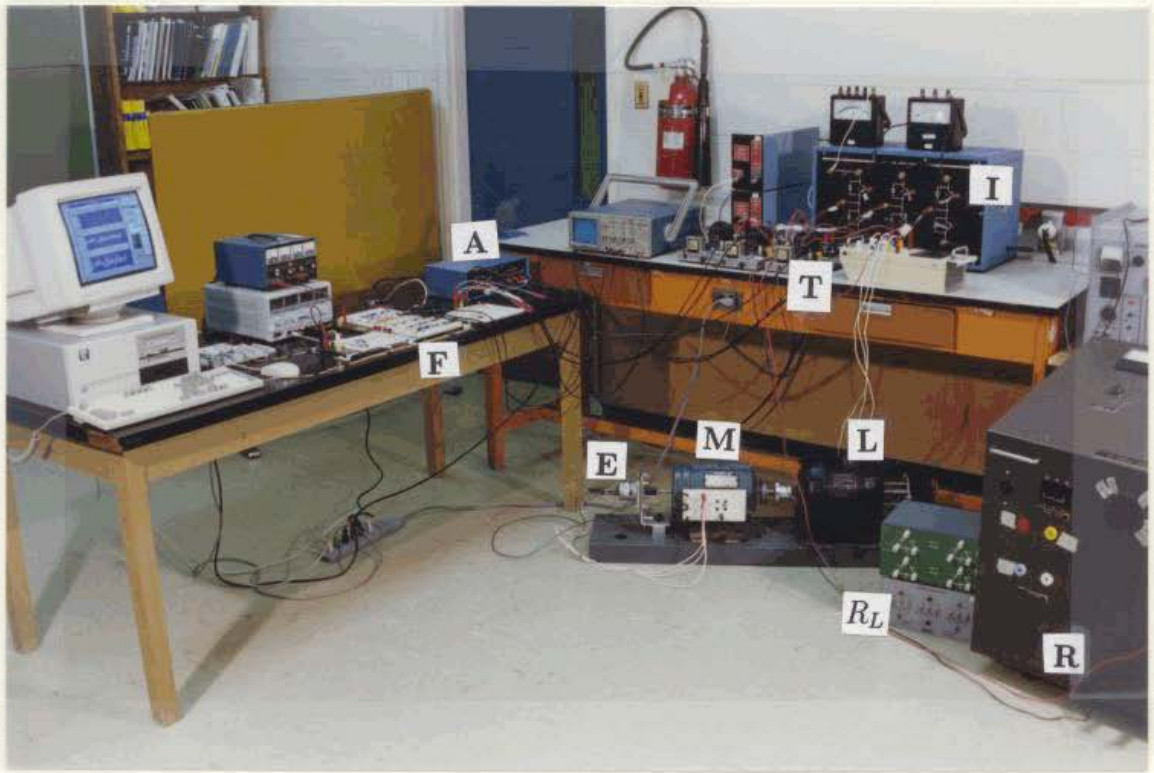

Figure 6.1: Experimental set-up of the brushless PM synchronous motor drive

been supplemented by a set of on-board peripherals used in digital control systems, namely, analog to digital (A/D), digital to analog (D/A) converters and incremental encoder interfaces. The board includes a DSP microcontroller based digital I/O subsystem which includes a fixed point Texas Instrument processor TMS320P14. This processor is used as a slave processor. The complete DS-1102 board is installed in a PC-AT with a capability of uninterrupted communication with the PC through a dual port memory provision. Therefore the PC monitor can be used to edit and down load the software.

The schematic diagram of the hardware implementation is shown in Fig. 6.2. Feedback signals to the controller board are the actual motor currents and the rotor position angle. The currents are measured by the Hall-effect transducers which provide excellent frequency responses down to the dc level. The currents are then buffered and fed to the A/D ports of the controller board. The motor shaft position is measured by an optical incremental encoder installed at the motor shaft. The encoder generates 4096 pulses per revolution of the rotor. The outputs of the encoder are connected to the incremental sensor interface board. By using a built-in four fold pulse multiplication, the encoder output pulses have been increased to 4x4096 pulses for greater accuracy. A 24 bit position counter is used to count the encoder pulses and is read by a calling function in the software. The counter is reset once per revolution by the index pulse generated from the encoder. The motor speed has been computed from the measured rotor position angle using numerical differentiation. The outputs of the controller board are three kinds of pulses for three phases of the inverter through three D/A channels of the board. The fourth channel of the D/A has been used to obtain the rotor position angle. An analog circuit has been designed to obtain the six pulses for the six transistors of the inverter from the four outputs of

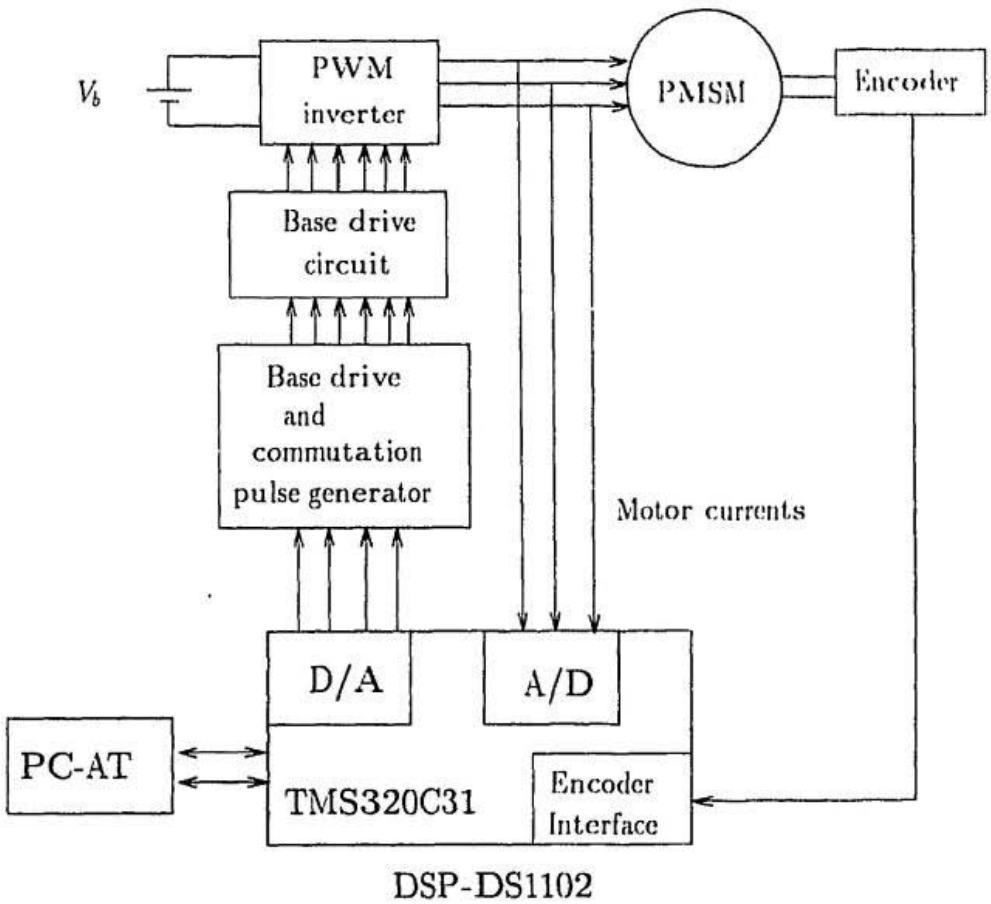

Figure 6.2: Schematic of the hardware implementation

the D/A of the DSP controller board. The commutating signals for the drive pulses have also been generated in this circuit. The details of this analog interface circuit have been shown in Appendix C. The six drive pulses have been amplified through a pulse amplifier and fed to the base drive circuit of the transistorized inverter. The control algorithm has been implemented via the controller board using C language programming. In addition to the control routine, the program comprises several I/O functions to access the peripherals of the DS-1102 board. The block diagram of the DSP controller board is shown Fig. 6.3.

6.3 Software for the Real Time Implementation of the ANN Based Brushless PM Synchronous Motor Drive

The control algorithm for the block diagram of the ANN based PM synchronous motor drive as shown in Fig. 5.2 has been implemented through a software by developing a program in ANSI C. After initializing the required variables, the initial set of weights and biases obtained from the off-line training of the proposed ANN structure is down loaded. With the fedback speed samples and a delayed sample of q-axis current, actual and estimated q-axis reference currents are computed using the back propagation algorithm. The error between the estimated and actual q-axis reference is used to update the previous set of weights and biases if the error exceeds a prescribed limit. Three phase reference currents are generated utilizing the actual q-axis reference current and the rotor position angle obtained through the encoder. Appropriate vector rotating and phase transformation techniques are utilized in this stage. Computed three phase reference currents are converted to upper hysteresis and

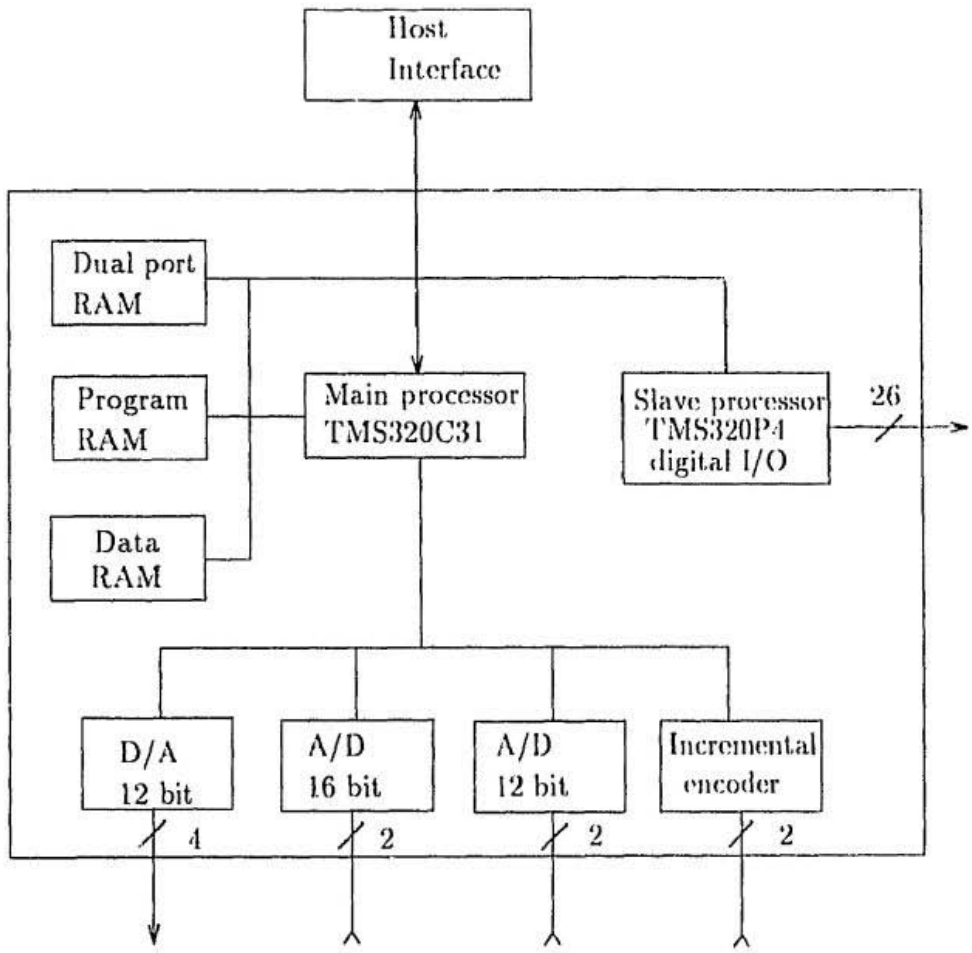

Figure 6.3: Block diagram of DS-1102 controller board

lower hysteresis by adding and subtracting a preselected band. Hysteresis currents are compared with actual motor currents and PWM signals are generated. These PWM signals are fed to the analog interface circuit through D/A ports of the controller board by calling the built-in functions. A provision of the adaptive learning rate is also incorporated to reduce any over- or under-shootings of the speed response during the dynamic and transient conditions. The technique of adaptive learning has been discussed in chapter 4. The flow chart of the software for implementing the real-time ANN based brushless PM synchronous motor drive is shown in Fig. 6.4.

The sampling frequency used for implementing the above algorithm in the DSP controller is 5 kHz. The C code for the above control algorithm is compiled and assembled by Texas Instrument C compiler. Once the object file of the C code is obtained, it is down loaded to the DSP by a loader program.

6.3.1 Peripheral initialization

Peripheral initialization is one of the major tasks in the software for perfect utilization of the DSP board. This controller board has been supplied with several macro functions to initialize and to access the on-board peripherals. As for example, the macro function called *init*() initializes the DAC subsystem of the DS-1102 for output. Also with this, the DS-1102 interrupt request bits are reset and the 16 bits ADCs are calibrated. The next peripheral to be initialized is the programmable timers. This is an essential feature for the real-time implementation because it requires a regular sampling rate. The functions *timer*0() and *timer*1() can be used to initialize the TMS320C31's on chip timers to generate timer interrupts at a predefined sampling rate [83]. On-board peripheral initialization is another important task which is accomplished by available I/O macro functions. Some of the functions are utilized to

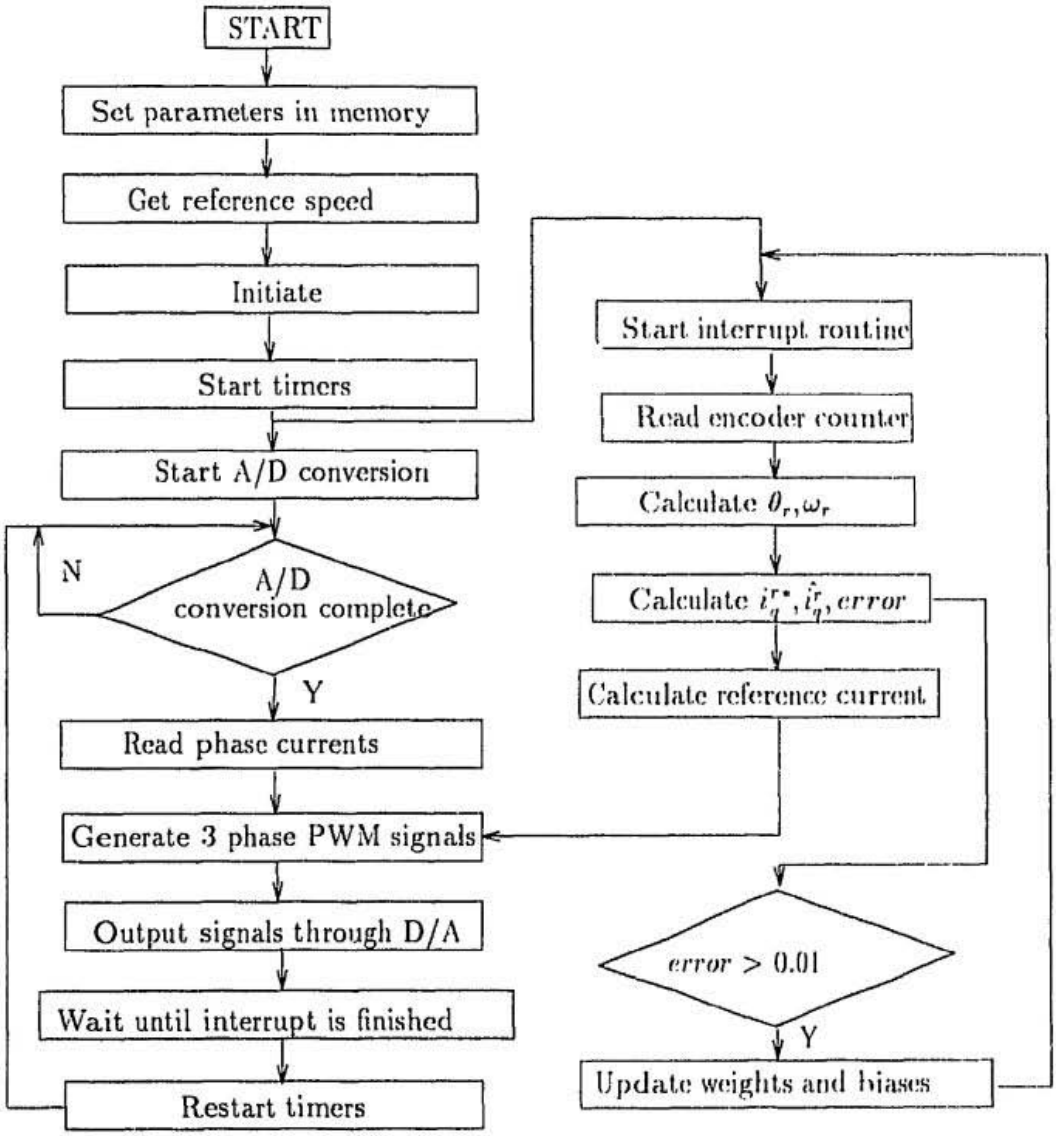

Figure 6.4: Flow chart of the software used for the real-time implementation of the ANN based brushless PM synchronous motor drive

start and read all four A/Ds, while others can be used to initialize the slave DSP's 16 bit I/O for digital inputs and outputs. However, in this work the slave processor has not been used since it takes additional time from the computation of the the ANN based algorithm, which is not acceptable. Therefore, the external analog circuit has been used to generate the six PWM drive signals from the three D/A's outputs.

6.3.2 Interrupt service routines

The current loop routine is driven by a software interrupt starting at every 200 μsec. In this interrupt, A/D conversions of the actual current measurements are initialized, rotor position angle is measured and the incremental encoder index line is detected to clear the counter. When the A/D conversions are finished, an interrupt service routine containing the main code for the current loop starts. The motor speed is calculated from the rotor position information every 0.2 msec. The incremental encoder interface on the DS-1102 board consists of a 24 bit counter and expands the input to 4x4096 pulses per revolution as mentioned earlier.

6.4 Experimental Results

A series of experimental tests have been carried out to verify the validity of the proposed ANN based vector control scheme for the interior-type brushless PM synchronous motor in real-time. Tests have been performed under no load and full load conditions at rated and low reference speeds. Verification of the simulation results have also been done for a step change in the reference speed under the no load and the rated load conditions. Effects of the sudden load impact on speed and current responses have also been experimentally observed. The essence of the ANN based

drive system is that the drive system must follow the reference speed adaptively under parameter variations. Some tests have been conducted to observe the speed and current responses with change in inertia and stator resistance under no load and full load conditions. The design data of the laboratory brushless PM synchronous motor are given in Appendix A. The experimental results are shown in Figs. 6.5 to 6.15. Figures 6.5(a) and (b) show the experimental speed and phase current responses of the ANN based PM brushless synchronous motor drive, respectively, under no load conditions for a reference speed of 1800 rpm. Figures 6.6(a) and (b) depict the speed and current responses under rated load condition for the reference speed of 1800 rpm. From these Figs. 6.5 and 6.6 it is observed that the proposed ANN based PM brushless synchronous motor drive is capable of running at the rated load and no load conditions by adjusting its weights and biases. Tests have also been performed to evaluate the performance of the proposed ANN based system at low reference speed, as for example at 239 rpm under no load and rated load conditions. The speed and phase current responses of the proposed system under these conditions are shown in Figs. 6.7 and 6.8, respectively. It is quite evident from Figs. 6.7 and 6.8 that ANN provides accurate reference currents in order to follow the low reference speed of 239 rpm under no load and full load conditions. It is worth mentioning that ANN has taken care of the effect of braking torque which is considered one of the major problems of running an interior-type PM brushless synchronous motor at low reference speeds. Figures 6.9 and 6.10 demonstrate the performance of the proposed ANN based PM brushless synchronous motor for a step change in reference speed under no load and rated load conditions. Figures 6.9(a) and 6.10(a) show the speed responses and Figs. 6.9(b) and 6.10(b) show the experimental current responses. The ANN in the proposed system provides the necessary reference current by adjusting its

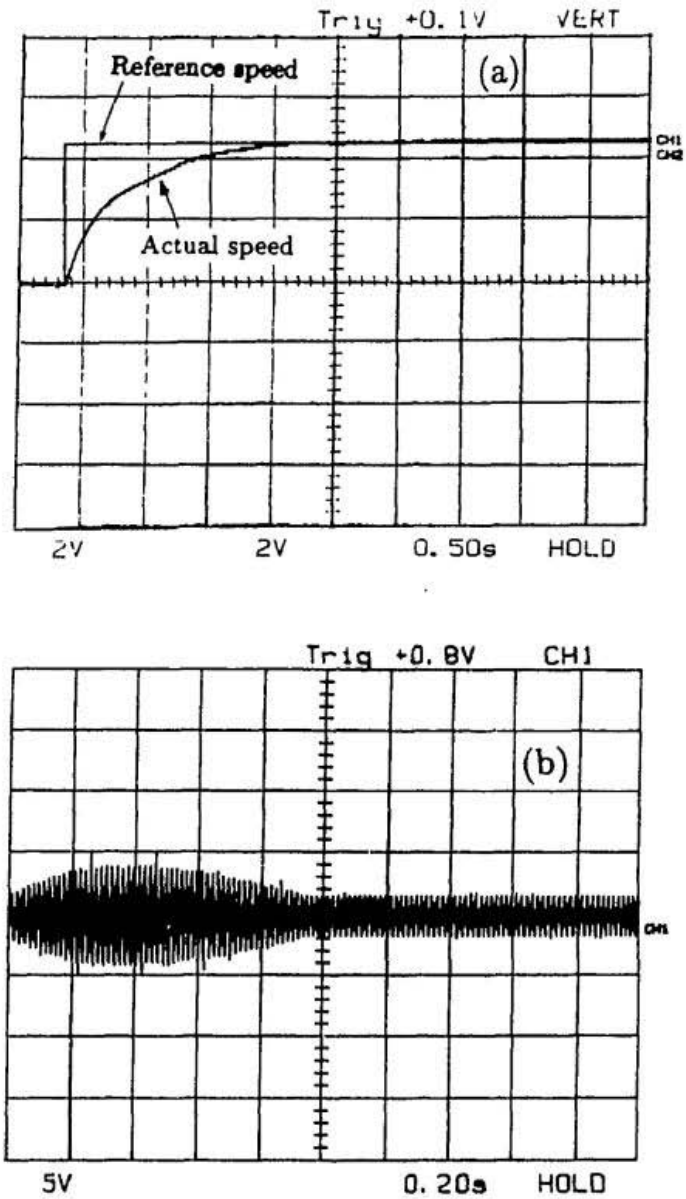

Figure 6.5: Experimental results of the ANN based brushless PM synchronous motor drive at no load with reference speed 1800 rpm; (a) speed response; Y-scale: 750 rpm/div. (b) current response; Y-scale: 5 A/div.

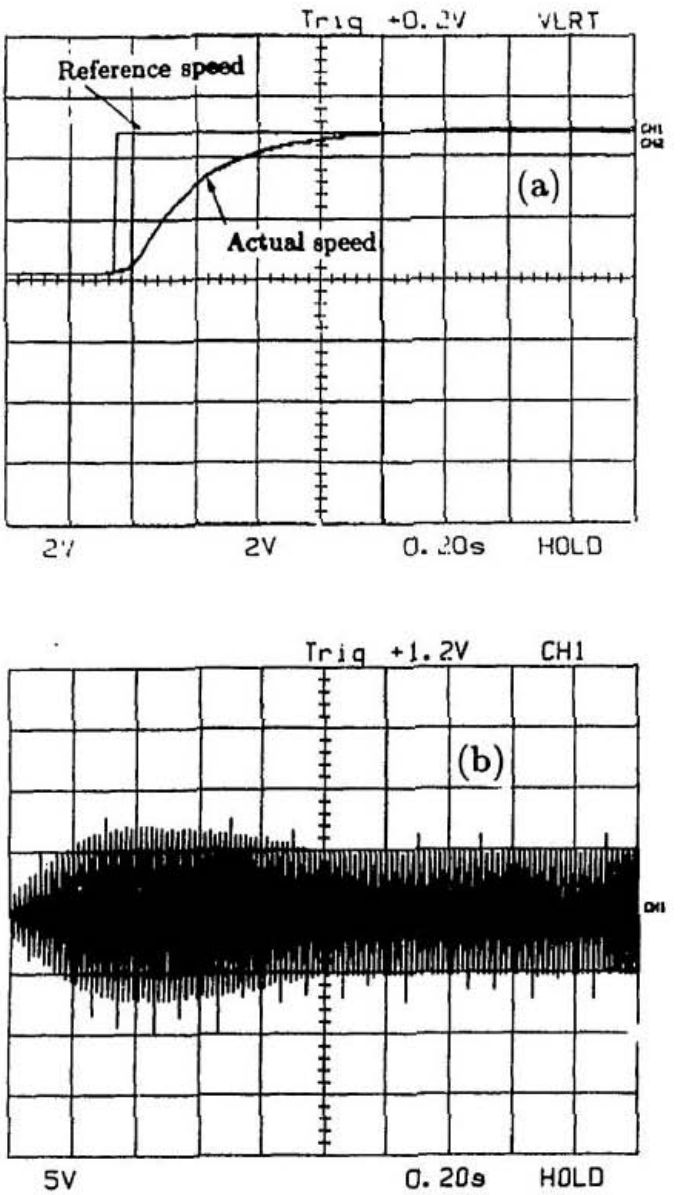

Figure 6.6: Experimental results of the ANN based brushless PM synchronous motor drive at rated load with reference speed 1800 rpm; (a) speed response; Y-scale: 750 rpm/div. (b) current response; Y-scale: 5 A/div.

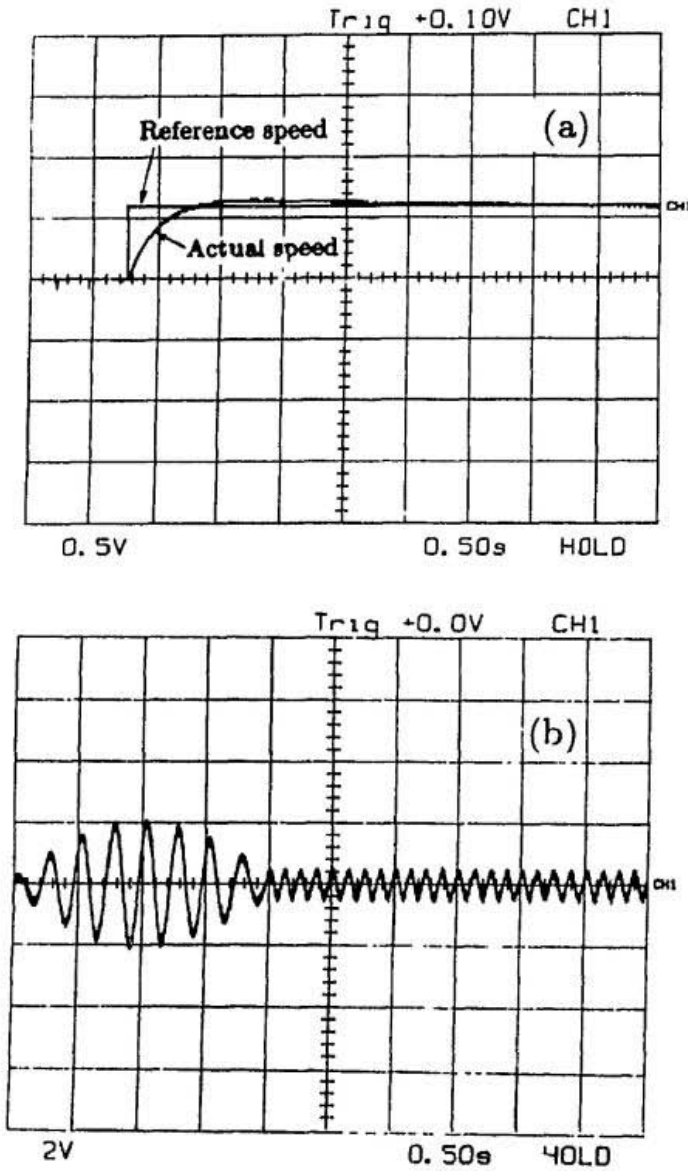

Figure 6.7: Experimental results of the ANN based brushless PM synchronous motor drive at no load with reference speed 239 rpm; (a) speed response; Y-scale: 187 rpm/div. (b) current response; Y-scale: 2 A/div.

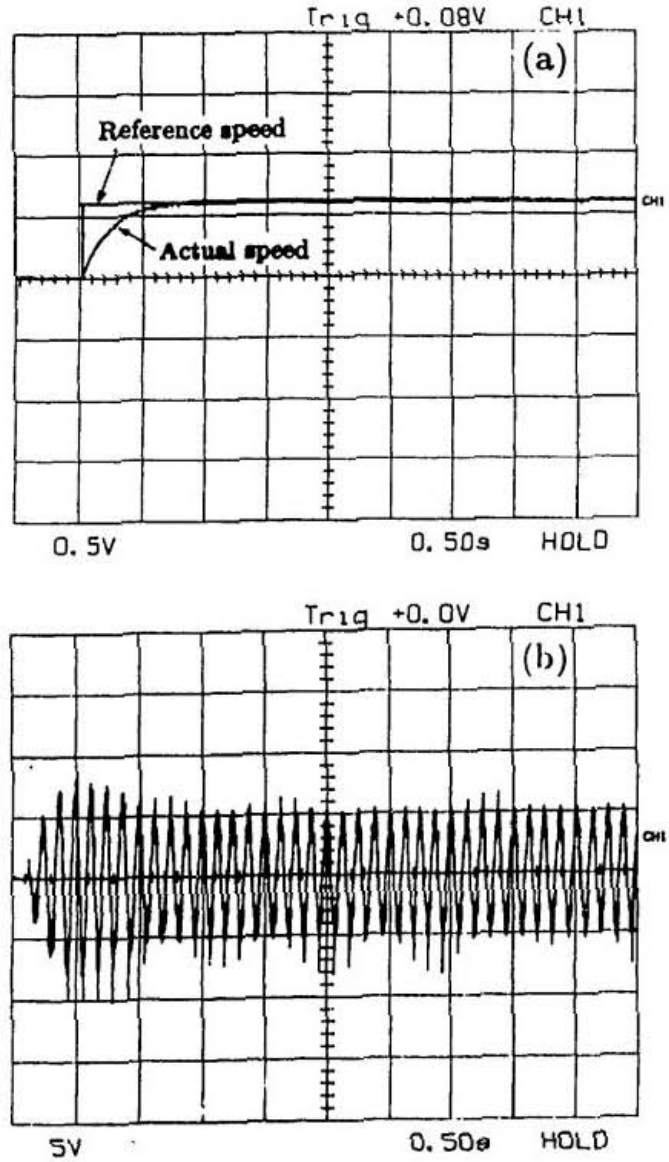

Figure 6.8: Experimental results of the ANN based brushless PM synchronous motor drive at rated load with reference speed 239 rpm; (a) speed response; Y-scale: 187 rpm/div. (b) current response; Y-scale: 5 A/div.

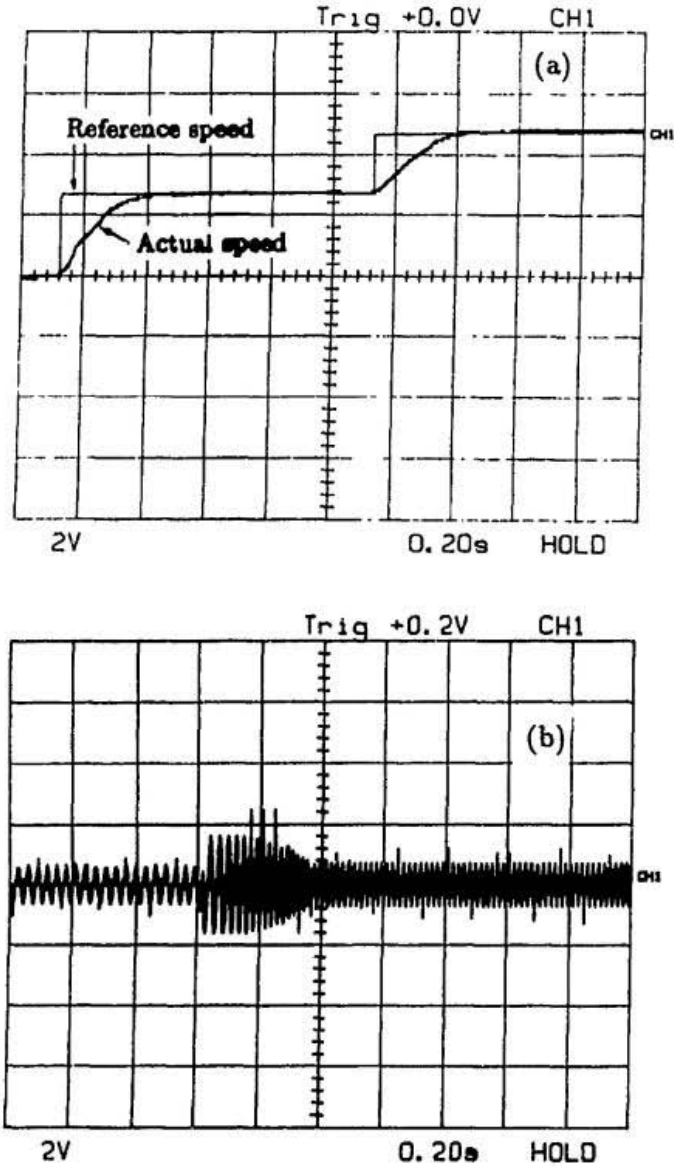

Figure 6.9: Experimental results of the ANN based brushless PM synchronous motor drive at no load with change in reference speed (a) speed response; Y-scale: 750 rpm/div. (b) current response; Y-scale: 2 A/div.

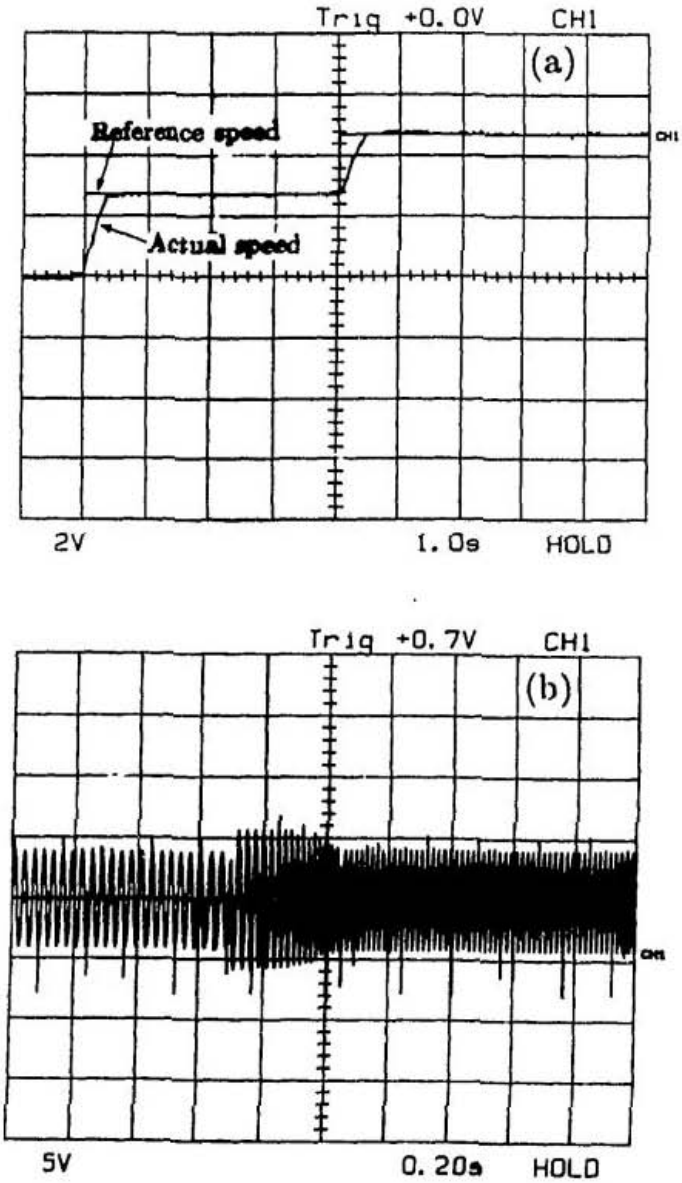

Figure 6.10: Experimental results of the ANN based brushless PM synchronous motor drive at rated load with change in reference speed (a) speed response; Y-scale: 750 rpm/div. (b) current response; Y-scale: 5 A/div.

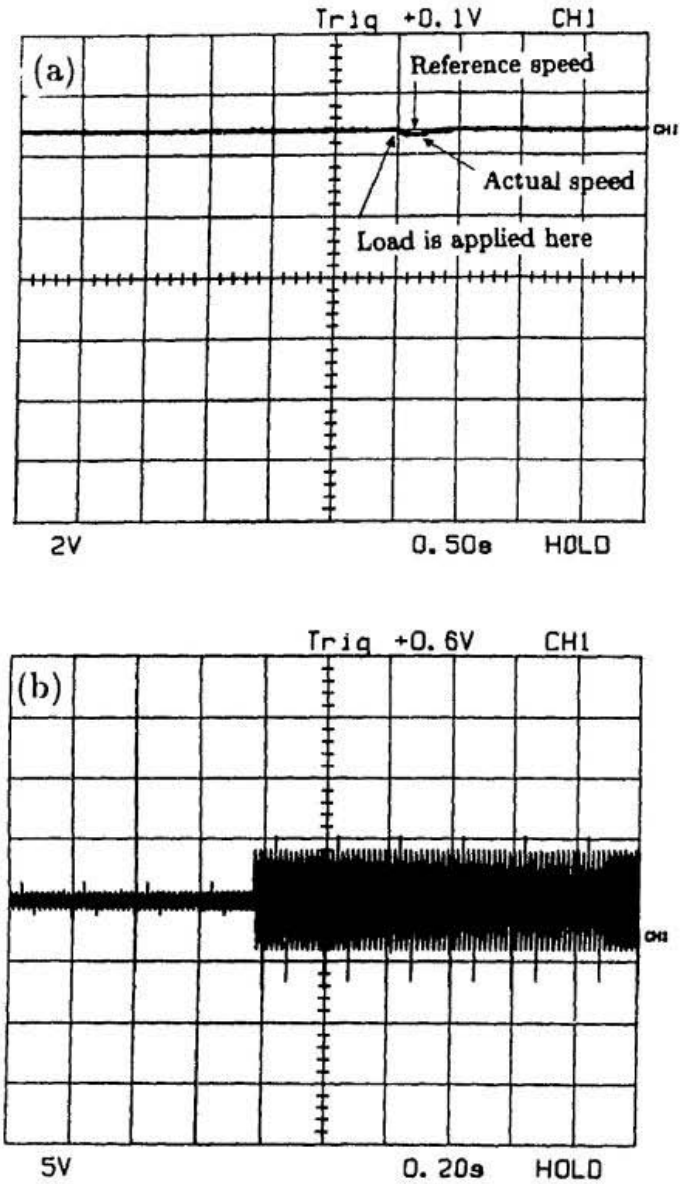

Figure 6.11: Experimental results of the ANN based brushless PM synchronous motor drive at rated speed with sudden load impact (a) speed response; Y-scale: 750 rpm/div. (b) current response; Y-scale: 5 A/div.

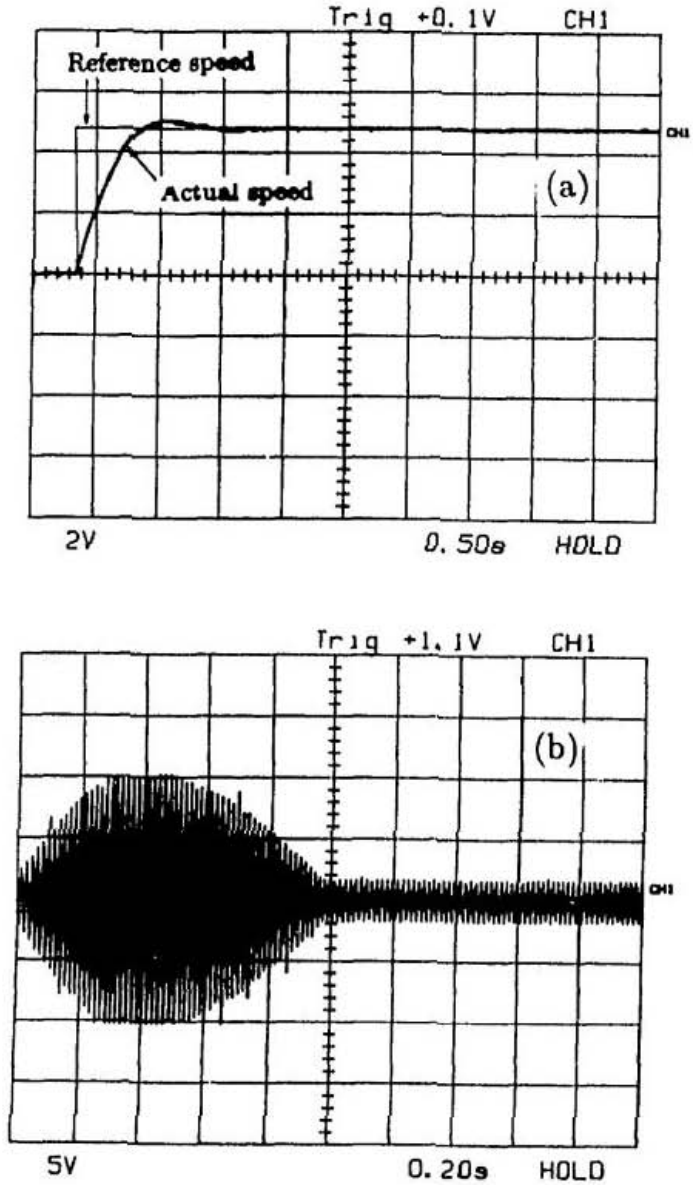

Figure 6.12: Experimental results of the ANN based brushless PM synchronous motor drive at no load with change in inertia $J \rightarrow 2J$ (a) speed response; Y-scale: 750 rpm/div. (b) current response; Y-scale: 5 A/div.

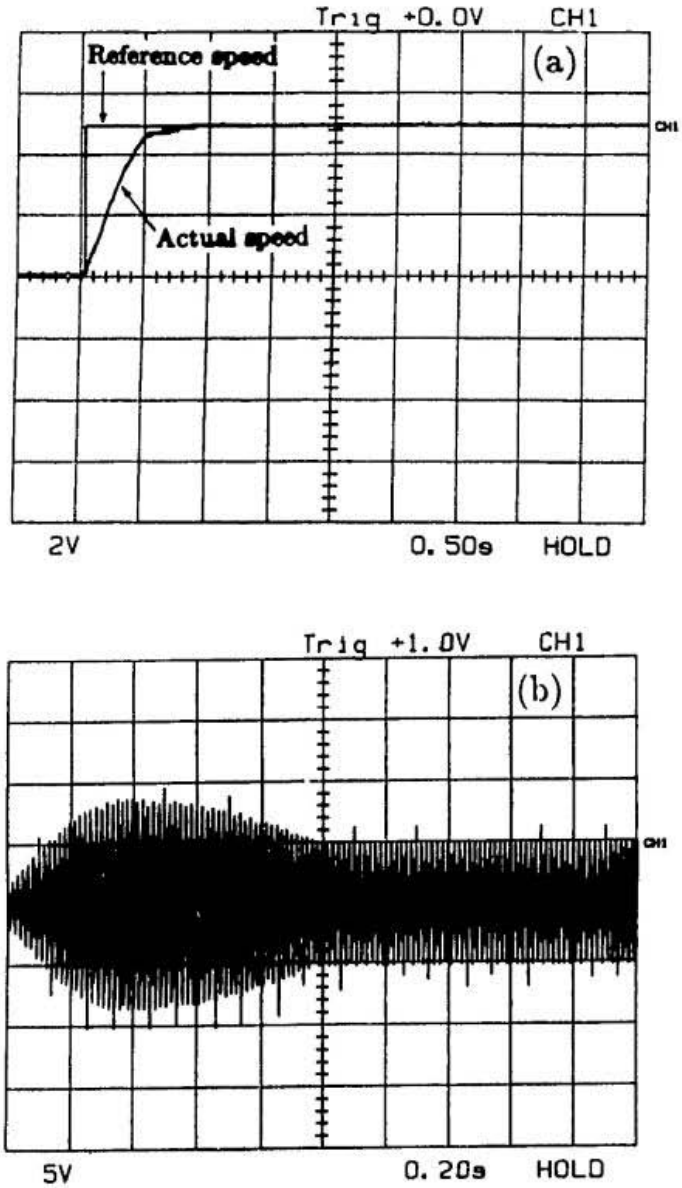

Figure 6.13: Experimental results of the ANN based brushless PM synchronous motor drive at rated load with change in inertia $J \rightarrow 2J$ (a) speed response; Y-scale: 750 rpm/div. (b) current response; Y-scale: 5 A/div.

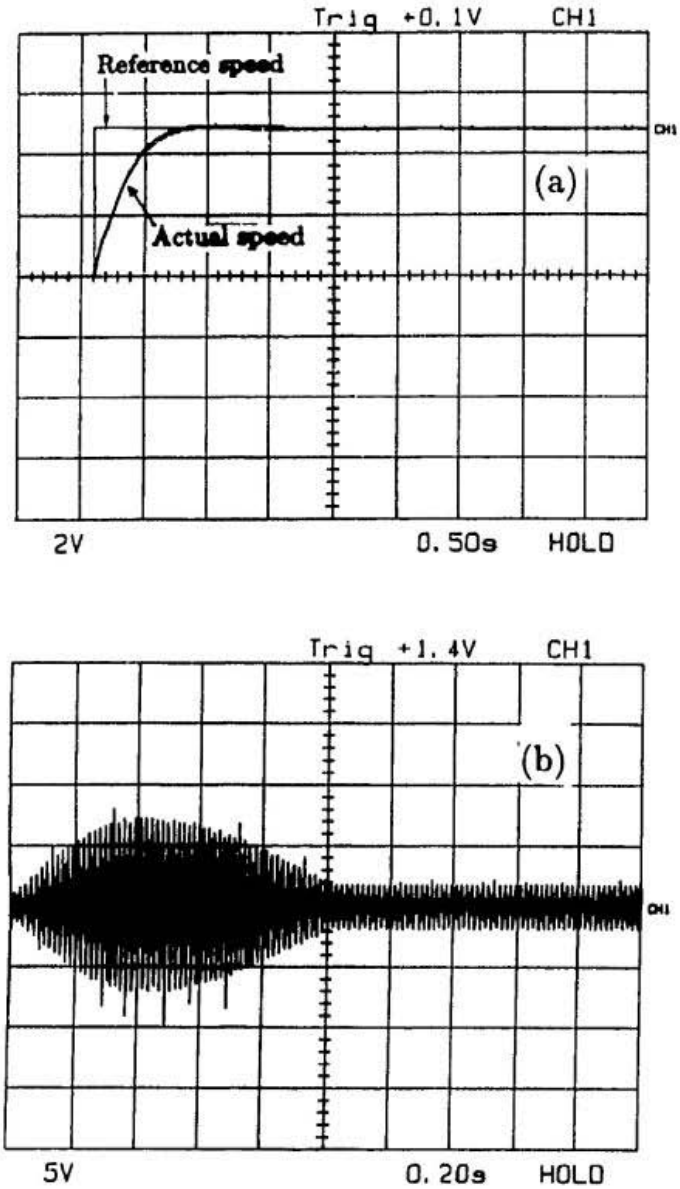

Figure 6.14: Experimental results of the ANN based brushless PM synchronous motor drive at no load with change in stator resistance $R \rightarrow 2R$ (a) speed response; Y-scale: 750 rpm/div. (b) current response; Y-scale: 5 A/div.

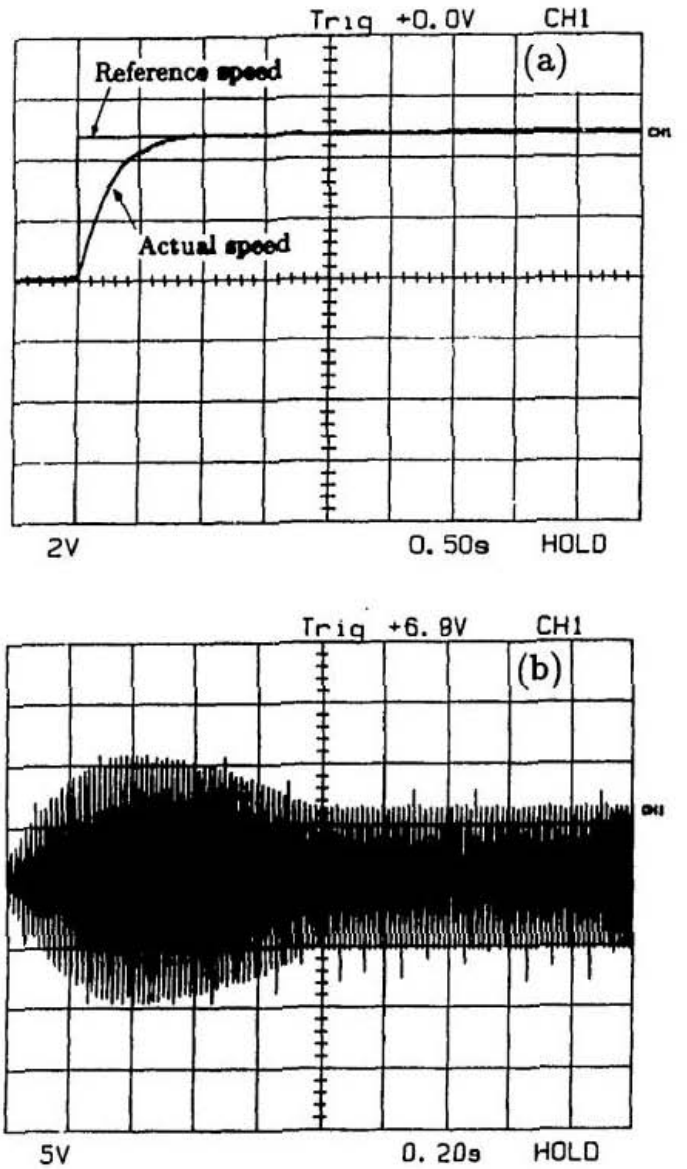

Figure 6.15: Experimental results of the ANN based brushless PM synchronous motor drive at rated load with change in $R \rightarrow 2R$ (a) speed response; Y-scale: 750 rpm/div. (b) current response; Y-scale: 5 A/div.

weights and biases for these dynamic changes in reference speed and the drive system accurately follows the reference speeds for both the cases of loading conditions. The step change in reference speed has been performed only for low to high speed. The step change in reference speed for high to low speed has been avoided because of the regeneration problem of the inverter. The dynamic performances of the proposed system due to the step change in load are shown in Fig. 6.11. Figure 6.11(a) show the experimental speed response and 6.11(b) show the current response for this step change in load. From Fig. 6.11 it is clear that the performance of ANN based system is better than that of the PDF based system as noted in Fig. 2.24. The effect of sudden load impact on speed is insignificant for the ANN based system because of the on-line weights and biases up-dating feature. The experimental evaluations of speeds and currents with parameter variations of the ANN based PM brushless synchronous motor drive are shown in Figs. 6.12 to 6.15. Figures 6.12 to 6.13 show the speed and current responses of the proposed system for change in inertia under no load and rated load conditions. The inertia of the motor has been doubled by coupling the PM synchronous motor with an induction motor of higher inertia. It is observed that the proposed drive system follow the reference speed with negligible over-shootings under no load conditions as shown in Fig. 6.12(a). For the case of rated load with double inertia as shown in Fig. 6.13(a), the drive system accurately follows the reference speed with no over-shooting. Experimental evaluations of effects of parameter variation for the case of change in stator resistance of the proposed ANN based drive system are shown in Figs. 6.14 to 6.15 under no load and rated load conditions. In both cases, the drive system is capable of following reference speeds without any over-shootings or under-shootings.

The rise time of the experimental speed responses of the proposed ANN based drive

system is little slow. This is due to the time consuming computations of the ANN algorithm for the weights and biases updating from their initial values. Incorporation of the magnetization characteristics of PM motors with the ANN may improve the overall response.

It is observed that in all cases of experimental results, the speed responses are critically damped. The adaptive learning rate of the ANN plays its vital role for doing so.

The envelopes of the experimental current responses as shown in Figs. 6.5 to 6.15 show the real-time ANN controller's output, i.e the q-axis reference currents. Depending upon the operating conditions, the real-time ANN provides accurate q-axis current for the successful operation of the PM synchronous motor drive system. The transient and dynamic responses of the drive system are accurately reflected in the current responses. The peak current in all cases are within 10 ampere which was selected as the prescribed limit.

It is noted here that the dc bus voltage of the inverter has been applied through a variac in all experiments. This is done to ensure the safe operation of the inverter's power transistors by considering the fact that direct switching of the dc voltage causes spikes of dc voltage for a significant amount of time duration which may be higher than the safe turn-on time of the power transistor. This arrangement of applying dc bus voltage affects the transient synchronizing time of the proposed drive system which are longer than those obtained from the simulation results.

6.5 Concluding Remarks

In all experimental results, it is seen that the proposed drive system is capable of following the reference speed quite accurately. There is no significant over-shooting in any of the cases. The drive can handle the step change of reference speed under various loading conditions. The speed drooping at the sudden impact of load is also within the acceptable range. The adaptive on-line weights and biases updating feature of the ANN provides the appropriate q-axis reference current so that the drive system does not have any difficulty following the reference trajectory even in case of parameter variations. Moreover, the proposed drive offers an excellent feature of wide range speed operations from very low to rated speed under no load and rated load conditions. As can be seen from the experimental results, the dynamic response time is within the range of 0.5 to 0.8 sec. This is acceptable for any kind of adaptive controller based ac motor drive systems.

The ANN based control scheme for the brushless PM synchronous motor drive has been successfully implemented and tested on a laboratory 1 hp interior-type PM synchronous motor. Experimental results validate the efficacy of the ANN as an adaptive controller for PM motor drives. The overall system performances are quite good in terms of dynamic, transient and steady-state responses.

Chapter 7

Summary and Conclusions

Fast response and quick recovery from load disturbances and insensitivity to parameter variations are some of the principal criteria in designing and implementing a high performance variable speed electric motor drive system. Review of relevant literature enables us to conclude that the brushless PM synchronous motor with a suitable speed controller has the potential to fulfill the required criteria of high performance variable speed motor drive applications.

Conventional constant gain controller based motor drive systems need accurate mathematical models to describe the system dynamics. Sophisticated system models incorporating unavoidable conditions such as saturation, disturbances, parameter drifts, and temperature variations are often unavailable in the real world. Thus the performances of the constant gain controller based drive systems are unpredictable under abnormal operating conditions. Furthermore, uncertainty and non-linearity from the motor mechanical load sometimes cause the drive system to become unstable in the absence of proper control. Hence an adaptive controller is essential in a high performance PM motor drive system. Existing adaptive controllers such as model reference adaptive controller, sliding mode controller and self-tuning regulator

are based on the system model parameters. Unavailability of the accurate system model data often makes it difficult and cumbersome to design and implement these types of adaptive controllers in real-time. Moreover, a large number of parameters are associated with these types of controllers which make them expensive.

In recent years, artificial neural networks (ANNs) has become a popular choice for the adaptive control of electric motors due to their inherent properties of generalization, parameter insensitivity, parallel processing and non-linear mapping between the inputs and outputs. Based on the multi-layer ANN structure, this work has introduced a novel adaptive speed control method for high performance PM motor drives. The objective of using the ANN based speed controller in the PM motor drives is to overcome the limitations of conventional controller based drive systems. In order to verify the feasibility of using ANN as a speed controller for high performance drive systems, an ANN based PM dc motor drive has been experimentally implemented in the real-time for a laboratory $\frac{1}{8}$ hp PM dc motor. From the results of the ANN based PM dc motor drive system, it is observed that the ANN speed controller can adaptively tackle the problems of parameter changes and load variations, and enables the drive system to follow the reference speed. These encouraging performances of ANN controller in the PM dc motor drive provided the motivation for us to extend its application to the case of a brushless PM synchronous motor drive.

In chapter 1, an extensive literature survey on variable speed ac motor drives has been carried out. A critical review of different types of electric motors with various control structures provides a clear picture of the problems associated with high performance variable speed motor drive systems. Problems involving the precise speed control of the PM motors have been identified and a solution using artificial neural network based control structure has been proposed.

In chapter 2, the control strategy of the proposed drive system has been derived. As an integral part of the control structure, the theoretical basis of the hysteresis current controller has been first investigated and then its performances have been experimentally verified in the laboratory. Finally, a complete drive brushless PM synchronous motor drive system based on the conventional pseudo-type speed controller has been successfully simulated and experimentally tested. This study provides a basis for further investigation of the variable speed high performance PM motor drive system with the modern speed controller.

In chapter 3, the concept of artificial neural network together with its applicability to the speed control of brushless PM synchronous motor is introduced. In recent years, the application of the ANN in motor control is becoming increasingly popular. It is, however, important to choose an appropriate structure and a training algorithm of the ANN for a particular problem. The multi-layer property of the ANN has proven to be most successful in the control of an electric motor. Multi-layer feed forward and other type of networks have been used in this work. The general structure with various functional elements of the ANN has been discussed, and details of the back propagation training algorithm have been presented.

Chapter 4 presents an ANN based PM dc motor drive system. Since the vector control of brushless PM synchronous motor offers similar control properties to a separately excited dc motor, as a test example an on-line adaptive ANN based PM dc motor drive has been successfully implemented and tested in the laboratory. Deriving the inverse dynamic model of the PM dc motor, a real-time ANN controller has been designed which has the provision of adaptive weights and bias updating feature together with an adaptive learning rate. A proportional-integral (PI) controller based PM dc motor drive has also been tested in the laboratory and the test results are

compared with those of the proposed adaptive controller based system.

Chapter 5 mainly concentrates on the derivation and design of the on-line self tuning ANN controller for the speed control of the brushless PM synchronous motor along with the simulation of the complete drive system. Performance prediction through simulations have been carried out for many cases, as for example, the study of speed and current responses at rated reference and low speed under no load and full load conditions. The effects of a step change of reference speed, a sudden load impact and parameter variations on the speed and current responses of the proposed system have also been investigated through simulations. The simulation results give an overview of the capability of the ANN used in the proposed system for the above operating conditions.

Chapter 6 provides the details of the implementation and experimental results of the on-line self tuning ANN based brushless PM synchronous motor drive system. Discussing the various elements of the experimental set up and DSP controller board DS-1102, the experimental results have been presented which verify the simulated performances of the proposed system as presented in chapter 5.

7.1 Major Contributions of the Thesis

The major contribution of the thesis are

- Mathematical formulation of a three phase hysteresis current controller has been developed and experimentally tested on a three phase R-L load before integrating with the proposed drive system.

- A novel non-adaptive pseudo-derivative feedback (PDF) type speed controller has been designed to investigate the performances of the conventional controller

based brushless PM synchronous motor.

- Performances of the PDF speed controller and the hysteresis current controller on the brushless PM motor have been evaluated by simulation as well as by experiment.

- The applicability of the artificial neural network in speed control of permanent magnet motors has been justified.

- A novel speed control technique using an on-line self-tuning artificial neural network has been experimentally implemented for a PM dc motor.

- An innovative method of on-line learning rate is integrated with the ANN based PM dc motor to reduce the overshoots during transient and dynamic changes.

- A modified ANN controller for the PM dc motor with feedback loop has been experimentally implemented with enhanced stability.

- A simple inverse dynamic model of the brushless PM motor has been derived for the first time for the artificial neural network based vector control scheme.

- An interface circuit system has been developed and used with the DSP controller board to drive the base drive circuits of the experimental voltage source inverter.

- The developed ANN based system has been successfully simulated and implemented in real-time at the power research laboratory of the Memorial University.

- The developed ANN based PM brushless synchronous motor drive system is capable of operating from low speeds to the rated speed under no load and rated load conditions.

- The developed ANN based PM brushless synchronous motor drive system exhibits excellent dynamic performances for the step change in reference speed and sudden load impact. The on-line weights and biases up-dating feature of the ANN makes the proposed PM brushless synchronous motor drive insensitive to parameter variations.

7.2 Conclusions

Some of the major conclusions of this study are

- Conventional speed controller based brushless PM synchronous motors are useful for medium performance drive systems, because this type of drive system is sensitive to parameter variations and not suitable for low speed operations.

- Artificial neural network controllers can be used for the speed control of PM motors which provide robust performances and are suitable for a wide range of speed operation.

- It is highly preferred to obtain an inverse dynamic model of the motor in order to design an appropriate ANN structure which guarantees to capture most of the system dynamics.

- A local feedback loop in the ANN should be used to ensure stable operation of a PM dc motor drive.

- Rather than using a fixed learning rate in the on-line weights and biases updating, an adaptive learning rate technique provides critically damped speed response for high performance PM motor drives.

- Initial set of weights and biases obtained from the off-line training is updated on-line which provides a unique feature of adaptive controller. This offers an efficient, robust and easy to implement high performance drive system.

7.3 Future Scope of Work

This study focuses on the use of different types of speed controllers for high performance motor drives Artificial neural networks with multi-layer feed forward and other structures have been used with the back-propagation training algorithm for this work. It has been observed that like other types of existing adaptive speed controllers, the response of the ANN based system is not very fast due to extensive computations. Therefore, other efficient and less time consuming on-line training algorithms should be devised to make the system work faster.

The ANN based brushless synchronous motor drive system has been developed for operation at constant torque region allowing the motor to be operated over a variable speed range up to the rated value. The field-weakening method should be incorporated with the proposed system for the speed operation above the base speed.

The overall system stability has not been studied from the control point of view, and more research has to be carried out in this regard.

Selection methods of quick estimation of the initial weights and biases should be explored.

The impact of feedback provision of the output to the hidden layers of the artificial neural networks on the over all stability of the drive system should be studied.

References

[1] G.R. Slemon, *Electric machines and drives*, Addison-Wesley Publishing Company, 1992.

[2] F. Blaschke,"The Principle of field orientation as applied to the new transvector closed-loop control system for rotating-field machines", *Simens Review*, 1972.

[3] M.A. Rahman, " Permanent magnet synchronous motors- a review of the state of design art", *Proceedings of International conference on Electrical Machines, Athens*, 1980, pp. 312-319.

[4] N.A. Demerdash and T.W. Nehl, "Dynamic modelling of brushless dc motors for aerospace actuation", *IEEE Trans. on Aerospace and Electronic Systems*, Vol. AES-16, No. 6, 1980, pp. 811-821.

[5] P.F. Muir and C.P. Neumann, "Pulse-width modulation control of brushless dc motors for robotic applications", *IEEE Trans. on Industrial Electronics*, Vol. IE-32, No. 3, 1985, pp. 222-229.

[6] P. Pillay and R. Krishnan, "Modelling, simulation and analysis of a permanent magnet brushless dc motor drive", *Proceedings of IEEE/IAS Meeting*, 1987, pp. 7-14.

[7] T.M. Jahns, "Torque production in permanent magnet synchronous motor drive with rectangular current excitation", *IEEE Trans. on Industry Applications*, Vol. IA-20, No. 4, 1984, pp. 803-813.

[8] P. Pillay, and R. Krishnan, "An investigation into the torque behaviour of brushless dc motor drive", *Proceedings of IEEE/IAS Meeting*, 1988, pp. 201-208.

[9] R. Becerra and M. Ehsani, "High speed torque control of brushless permanent magnet motors", *IEEE Trans. on Industrial Electronics*, Vol. 35, No. 3, 1988, pp. 402-406.

[10] W. Sakmann, "A brushless dc motor controlled by a microprocessor with examples for a 3 phase motor", *IEEE Trans. on Industrial Electronics*, Vol. 34, No. 3, 1987, pp. 339-344.

[11] N. Matsui and H. Ohashi, "DSP based adaptive control of a brushless dc motor", *IEEE Trans. on Industry Applications*, Vol. 28, No. 2, March/April, 1992, pp. 448-454.

[12] T. Takeshita and N. Matsui, "Sensorless brushless dc motor drive with EMF constant identifier", *Proceedings of IEEE/IECON*", 1994, pp. 14-19.

[13] M.A. El-Sharkawi and M.L. El-Sayed, "High performance drive of dc brushless motors using neural network", *IEEE Trans. on Energy Conversion*, Vol. 9, No. 2, 1994, pp. 311-316.

[14] K. Inoue, Y. Takakado and M. Nakaoka, "Auto-tuning technology for fuzzy algorithms based dc brushless servo systems", *Proceedings of PESC*, 1993, pp. 446-450.

[15] C. Shiguo, D.G. Holmes and W.A. Brown, "Digital control of a servo system using neural networks", *Proceedings of IEEE/IAS Meeting*, 1995, pp. 129-133.

[16] Slemon, G.R., "On the Design of High Performance Permanent Magnet Motors", *Proceedings of IEEE/IAS Meeting*, 1992, pp. 279-285.

[17] N. Matsui and T. Takeshita, "A novel starting method of sensorless salient pole brushless motor", *Proceedings of IEEE/IAS Meeting*, 1994, pp. 386-392.

[18] S. Kang and S. Sul, "Direct torque control of brushless DC motor with nonideal trapezoidal back emf", *IEEE Trans. on Power Electronics*, Vol. 10, No. 6, 1995, pp. 796-802.

[19] N. Matsui, "Sensorless PM brushless DC motor drives", *IEEE Trans. on Industrial Electronics*, Vol. 43, No. 2, 1996, pp. 256-267.

[20] T.M. Jahns and W.L. Soong, "Pulsating torque minimization techniques for permanent magnet ac motor drives-a review", *IEEE Trans. on Industrial Electronics*, Vol. 43, No. 4, 1996, pp. 321-330.

[21] T. Sebastian and V. Gongla, "Analysis of induced emf waveforms and torque ripple in a brushless permanent magnet machines", *IEEE Trans. on Industry Applications*, Vol. 32, No. 1, 1996, pp. 195-200.

[22] A.V. Gumaste and G.R. Slemon, "Steady-state analysis of a permanent magnet synchronous motor drive with voltage source inverter", *Proceedings of IEEE/IAS Meeting*, 1981, pp. 143-151.

[23] R. Lessmeier, W. Schumacher and W. Leonhard, "Microprocessor controlled ac servo drives with synchronous or induction motors: which is preferable?", *IEEE Trans. on Industry Applications*, Vol. 22, No. 5, 1986, pp. 812-819.

[24] B.V. Murty, "Fast response reversible brushless dc drive with regenerative braking", *Proceedings of IEEE/IAS Meeting*, 1984, pp. 445-450.

[25] S. Meshkat and E.K. Persson, "Optimum current control brushless servo amplifier using microprocessor", *Proceedings of IEEE/IAS Meeting*, 1984, pp. 451-457.

[26] T.M. Jahns, G.B. Kliman and T.W. Neumann, "Interior permanent magnet synchronous motors for adjustable speed drives", *Proceedings of IEEE/IAS Meeting*, 1985, pp. 814-823.

[27] T. Kume and T. Iwakane, "High performance vector controlled ac motor drives-applications and new technologies", *Proceedings of IEEE/IAS Meeting*, 1985, pp. 690-697.

[28] P. Pillay and R. Krishnan, "Modeling of permanent magnet motor drives", *Proceedings of IEEE/IAS Meeting*, 1988, pp. 537-541.

[29] P. Pillay and R. Krishnan, "Control characteristics and speed controller design for a high performance permanent magnet synchronous motor design", *Proceedings of PESC*, 1987, pp. 598-606.

[30] B.K. Bose, "A high performance inverter-fed drive system of an interior permanent magnet synchronous machine", *IEEE Trans. on Industry Applications*, Vol. IA-24, No. 6, 1988, pp. 987-997.

[31] P. Pillay, C.R. Allen and R. Budhabhathi, "DSP-based vector and current controllers for a permanent magnet synchronous motor drive", *Proceedings of IEEE/IAS Meeting*, 1990, pp.539-544.

[32] S. Morimoto, K. Hatanaka, Y.Tong, Y. Takeda and T. Hirasa, "High performance servo drive system of salient pole permanent magnet motor", *Proceedings of IEEE/IAS Meeting*, 1991, pp. 463-468.

[33] S. Morimoto, Y. Takeda, and T. Hirasa, "Current phase control methods for permanent magnet synchronous motors", *IEEE Trans. on Power Electronics*, Vol. 5, No. 2, 1990, pp. 133-139.

[34] B.K. Bose and P.M. Szczesny, "A microcomputer-based control and simulation of an advanced IPM synchronous machine drive system for electric vehicle propulsion", *IEEE Trans. on Industrial Electronics*, Vol. IE-35, No. 4, 1988, pp. 560-571.

[35] T.M. Jahns, "Flux-weakening regime operation of an interior permanent magnet synchronous motor drive", *IEEE Trans. on Industry Applications*, Vol. IA-23, No. 4, 1987, pp. 681-689.

[36] S. Morimoto, Y. Takeda and T. Hirasa, "Flux-weakening control method for surface permanent magnet synchronous motors", *Proceedings of IPEC Meeting*, 1990, pp. 942-949.

[37] M. Bilewski, A. Fratta, L. Giordano, A. Vegati and F. Villata, "Control of high performance interior permanent magnet synchronous drives", *Proceedings of IEEE/IAS Meeting*, 1990, pp. 531-538.

[38] S. Morimoto, T. Ueno, M. Sanada and A. Yamagiwa, "Effects and compensation saturation in PMSM drives", *Proceedings of IEEE/IAS Meeting*, 1993, pp. 59-64.

[39] I. Choy, T. Yoon, K. Kim and M. Park, "Microprocessor-based permanent magnet synchronous motor drives using MRAC", *Proceedings of IPEC*, 1990, pp. 481-488.

[40] C. Namuduri and P.C. Sen, "A servo-control system using a self-controlled synchronous motor (SCSM) with sliding mode controller", *Proceedings of IEEE/IAS Annual Meeting*, 1987, pp. 283-295.

[41] A. Consoli. and C. Antonio, "A DSP based sliding mode field oriented control of an interior permanent magnet synchronous motor drive", *Proceedings of IPEC*, 1990, pp. 296-303.

[42] S. Chung, J. Lee, J. Ko and M.J. Youn, "A robust speed control of brushless direct drive motor using integral variable structure with sliding mode observer", *Proceedings of IEEE/IAS Meeting*, 1994, pp. 393-400.

[43] M. Ghribi and H. Le-Huy, "Optimal control and variable structure combination using permanent magnet synchronous motor", *Proceedings of IEEE/IAS Annual Meeting*, 1994, pp. 408-415.

[44] R.B. Sepe and J.H. Lang "Real-time adaptive control of the permanent magnet synchronous motor", *Proceedings of IEEE/IAS Annual Meeting*, 1990, pp. 545-552.

[45] A.M. Farhoud and A.A. Ghandakly, "Real time self-tuning industrial controllers using a digital parameter optimization technique", *Proceedings of the IEEE/IAS Annual Meeting*, 1994, pp. 1758-1763.

[46] T. Fukuda, and T. Shibata, "Theory and applications of neural networks for industrial control systems", *IEEE Trans. on Industrial Electronics*, Vol. 39, No. 6, 1992, pp. 472-489.

[47] D. Psaltis, A. Sideris, A.A. Yamamura, "A Multi-layered neural network controller", *IEEE Control System Magazine*, Vol. 8, No. 3, 1988, pp. 17-21.

[48] H.N. Derrick and B. Widrow, "Neural networks for self-learning control systems", *IEEE Control System Magazine*, Vol. 10, No. 3, 1990, pp. 18-23.

[49] S.W. Piche, "Steepest descent algorithms for neural network controllers and filters", *IEEE Trans. on Neural Networks*, Vol. 5, No. 2, 1994, pp. 198-211.

[50] S. Weerasooriya, and M. El-Sharkawi, "Identification and control of a dc motor using back-propagation neural networks", *IEEE Trans. on Energy Conversion*, Vol. 6, No. 4, 1991, pp. 663-669.

[51] F.M. El Khouly, A.S. Abdel Gaffar, A.A. Mohammed and A.M. Sharaf, "Artificial intelligent speed control strategies for permanent magnet dc motor drives", *Proceedings of IEEE/IAS Meeting*, 1994, pp. 379-385.

[52] M.A. Hoque, M.R. Zaman and M.A. Rahman, "Artificial neural network based controller for permanent magnet motor drives" *Proceedings of IEEE/IAS Meeting*, 1995, pp. 1775-1780.

[53] M.A. Hoque, M.R. Zaman and M.A. Rahman, "Artificial neural network based permanent magnet dc motor drives", *Proceedings of IEEE/IAS Meeting*, 1995, pp. 98-103.

[54] G.S. Buja, "Neural network implementation of a fuzzy logic controller", *Proceedings of IEEE/IECON*, 1993, pp. 414-417.

[55] G.S. Buja and F. Todesco, "Neural network implementation of fuzzy logic controller", *IEEE Trans. on Industrial Electronics*, Vol. 41, No. 6, 1994, pp. 663-667.

[56] M.R. Buhl and R.D. Lorenz, "Design and implementation of neural networks for digital regulations inverter drives", *Proceedings of IEEE/IAS Annual Meeting*, 1991, pp. 415-421.

[57] M.T. Wishart and R.G. Harley, "Identification and control of induction machines using artificial neural networks", *Proceedings of IEEE/IAS Annual Meeting*, 1993, pp. 703-709.

[58] B. Burton, F. Kamran, R.G. Harley, G.T. Habetter, M. Broike and R. Poddar, "Identification and control of induction motor stator currents using fast on-line random training of a neural network" *Proceedings of IEEE/IAS Annual Meeting*, 1995, pp. 1781-1787.

[59] C. Schaffner, D. Schroder, and U. Lenz, "Application of neural networks to motor control", *Proceedings of IPEC*, 1995, pp. 46-51.

[60] L. Ben-Brahmin, K. Shimane, T. Kudor and H. Naitoh, "Implementation of an induction motor estimator using neural networks", *Proceedings of IPEC*, 1995, pp. 52-57.

[61] Y.S. Kung, C.M. Liaw and M.S. Ouyang, "Adaptive speed control for induction motor drives using neural networks", *IEEE Trans. on Industrial Electronics*, Vol. 42, No. 1, 1995, pp. 25-32.

[62] Z. Kovacic, S. Bogdan and P. Crnosija, "Fuzzy rule-based model reference adaptive control of permanent magnet synchronous motor", *Proceedings of IEEE/IECON*, 1993, pp. 207-212.

[63] B.K. Bose, *Power electronics and ac drives*, Englewood Cliffs, NJ: Prentice Hall, 1986.

[64] P. Vas, *Vector control of ac Machines*, Clarendon Press. Oxford, 1990.

[65] P.C. Krause, *Analysis of electrical machinery*, Mc-Graw-Hill Inc., 1986.

[66] T. Sebastian, G.R. Slemon and M.A. Rahman, "Modelling of permanent magnet synchronous motors", *IEEE Trans. on Magentics*, Vol. MAG-22, No. 5, 1986, pp. 129-134.

[67] M.A. Hoque and M.A. Rahman, "A DSP based variable speed PM Motor Drive", *Proceeding of the Newfoundland Electrical and Computer Engineering Conference*, 1996, p. 13-19.

[68] D.M Brod and D.W. Novotny, "Current control of VSI-PWM inverters", *IEEE Trans. on Industry Applications*, Vol. IA-21, No. 4. 1985, pp. 562-570.

[69] T.G. Habetler and D.M. Divan, "Performance characterization of a new discrete pulse modulated current regulator", *Proceedings of IEEE/IAS Annual Meeting*, 1988, pp. 395-405.

[70] *SIMULINK*, The Math Works Inc., Natick, Mass., 1993.

[71] H. Haykin, *Neural networks : A Comprehensive Foundation*, IEEE Press, Macmillan College Publishing Company Inc., 1994.

[72] R.D. Lorenz, "Design methods and implementation issues for neural network and fuzzy controllers", *IEEE/IAS Tutorial Course Notes*, 1995, chapter 1, pp.1-22.

[73] K.S. Narendra and K. Parthasarathy, "Identification and control of dynamical systems using neural networks", *IEEE Trans. on Neural Networks*, Vol. 1, No. 1, 1990, pp. 4-27.

[74] D.J. Burr, "Experiments on neural net recognition of spoken and written text", *IEEE Trans. on Acoustics, Speech, Signal Processing*, Vol. 36, No. 7, 1988, pp. 1162-1168.

[75] B.Widrow, R.G. Winter and R.A. Baxter, "Layered neural nets for pattern recognition", *IEEE Trans. on Acoustics, Speech, Signal Processing*, Vol. 36, No. 7, 1988, pp. 1109-1118.

[76] M.A. Rahman and P. Zhou, "Analysis of brushless permanent magnet synchronous motors", *IEEE Trans. on Industrial Electronics*, Vol. 43, No. 2, 1996, pp. 256-267.

[77] *Model 200 Series Servo Controllers Installation, Operation and Service Manual*, Copley Controls Corp., 1991

[78] H. Demuth and M. Beale, *Neural network tool-box for use with MATLAB*, The Math Works Inc., Natick, Mass, 1993.

[79] M.A. Hoque and M.A. Rahman, "On-line self-tuning artificial neural network based speed control of permanent magnet dc motor", *Paper accepted for the publication in the IEEE/ASME Trans. on Mechatronics*. Manuscript # 96-102.

[80] N. Kuechner and M. Stevenson, "A Preliminary Comparison of FIR-Synapse Neural Network With and Without Local Output Feedback", *Conference Proceedings, Canadian Conference on Electrical and Computer Engineering*, Vol. 1., 1995, pp. 198-201.

[81] M.A. Hoque and M.A. Rahman, "Speed control of a high performance interior-type permanent magnet synchronous motor drive based on self tuning artficial neural network", *Paper accepted for the presentation at the Fourth International Conference on Control, Automation, Robotics and Vision in Singapore*, December 3-6, 1996.

[82] *MATLAB*, The Math Works Inc., version 4.1, Natick, Mass., 1993.

[83] *DSP-CITeco LD31/LD31NET User's Guide*, dSPACE digital signal processing engineering Gmbh, Germany, version 1.0, 1993.

Appendix A

PM Synchronous Motor Data

Type = Interior type PM motor

Rated Power = 1 hp

Input line to line voltage = 208 V

Rated frequency = 60Hz

Number of poles = 4

q-axis inductance $L_q = 0.0795$ H

d-axis inductance $L_d = 0.0424$ H

Stator resistance per phase $R = 1.5\Omega$

Inertia constant $J = 0.003 Kg.m^2$

Damping constant $B = 0.00008$ (N-m)/rad/sec

Magnet flux linkage $\lambda_M = 0.314$ volts/rad/sec.

Appendix B

PM DC Motor Data

Rated Voltage, V = 35 volt

No-load Speed, N = 6 krpm

Armature inductance L_a = 1.17 mH

Armature resistance R_a = 2.8 Ohm

Rotor inertia $J_m = 0.02288 \times 10^{-3}$ Kg.m^2

Viscous constant B_m = 0.0020 N-m/krpm.

Frictional constant T_f=0.0212 N-m.

Torque constant, K_t = 0.0438 N-m/A

Voltage constant, K_e = 0.0439 volt-sec/rad.

Load torque constant, υ = 0.00018 N-m-sec^2

Appendix C

Analog Interface Circuit

C.1 Description

The main function of the analog interface circuit is to generate six sets of drive pulses for the six transistors of the inverter by using the four channels of the D/A of the DSP controller board DS-1102. The first three channels of the D/A are used to obtain the PWM signals from the hysteresis current controller for the three phases of the inverter. The analog interface circuit splits each phase's PWM signals into two parts corresponding to the positive and negative cycles of the reference currents. The fourth channel of the D/A is used to obtain the rotor position angle θ from the DSP to the interface circuit. With this angle information, three-phase reference currents of fixed magnitude are generated. Since only the zero-crossings are the necessities in this analog circuit, therefore any suitable magnitude of the reference currents can be used. The following relationships are used to generate the three-phase currents.

$$i_a = 10sin\theta \tag{C.1}$$

$$i_c = 10sin(\theta + 120^\circ) = -5sin\theta + 8.66cos\theta \tag{C.2}$$

$$i_b = -(i_a + i_c) \tag{C.3}$$

The function $sin\theta$ and $\cos\theta$ used in the generation of the three-phase reference currents are produced using the Analog Device's IC AD639 as shown in Fig. C.1. Therefore, the reference current of phase 'a' is the sine function obtained from the AD 639. The circuit layout for generating the three-phase reference currents is shown in Fig. C.2. The generated three-phase reference currents are used in the zero crossing de-

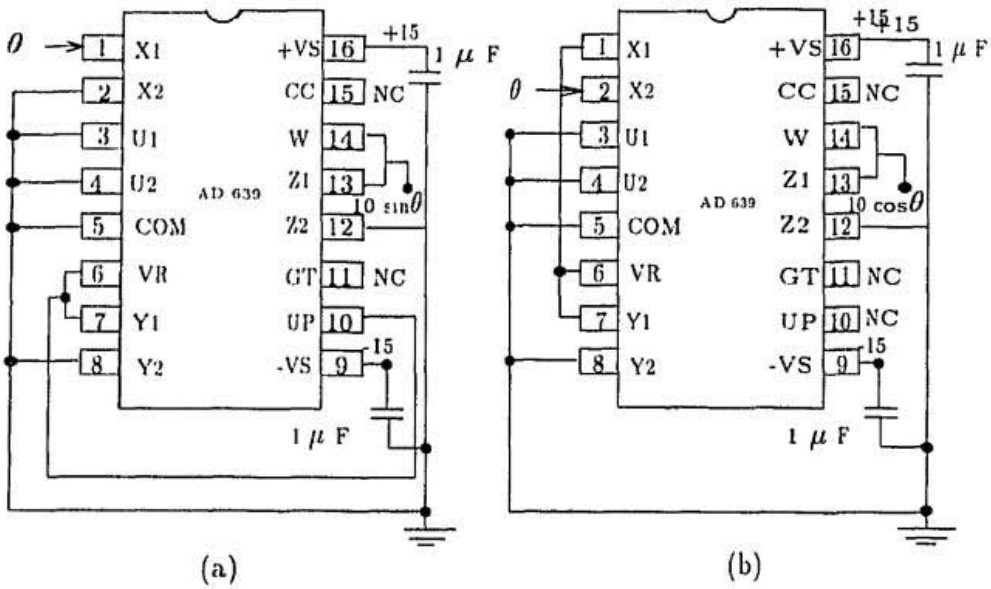

Figure C.1: Sine and cosine function generators

tector circuits in order to generate symmetrical rectangular waves. These rectangular signals are rectified and passed through the logical NOT gates. Therefore two sets of pulses are available (V_T before NOT operation and $\bar{V_T}$ after NOT operation) for upper and lower transistors of the inverter. After that, logical AND operations are performed between the PWM signals coming from the first three D/A channels of the DSP board and the rectangular pulses with dead zone. These operations separate

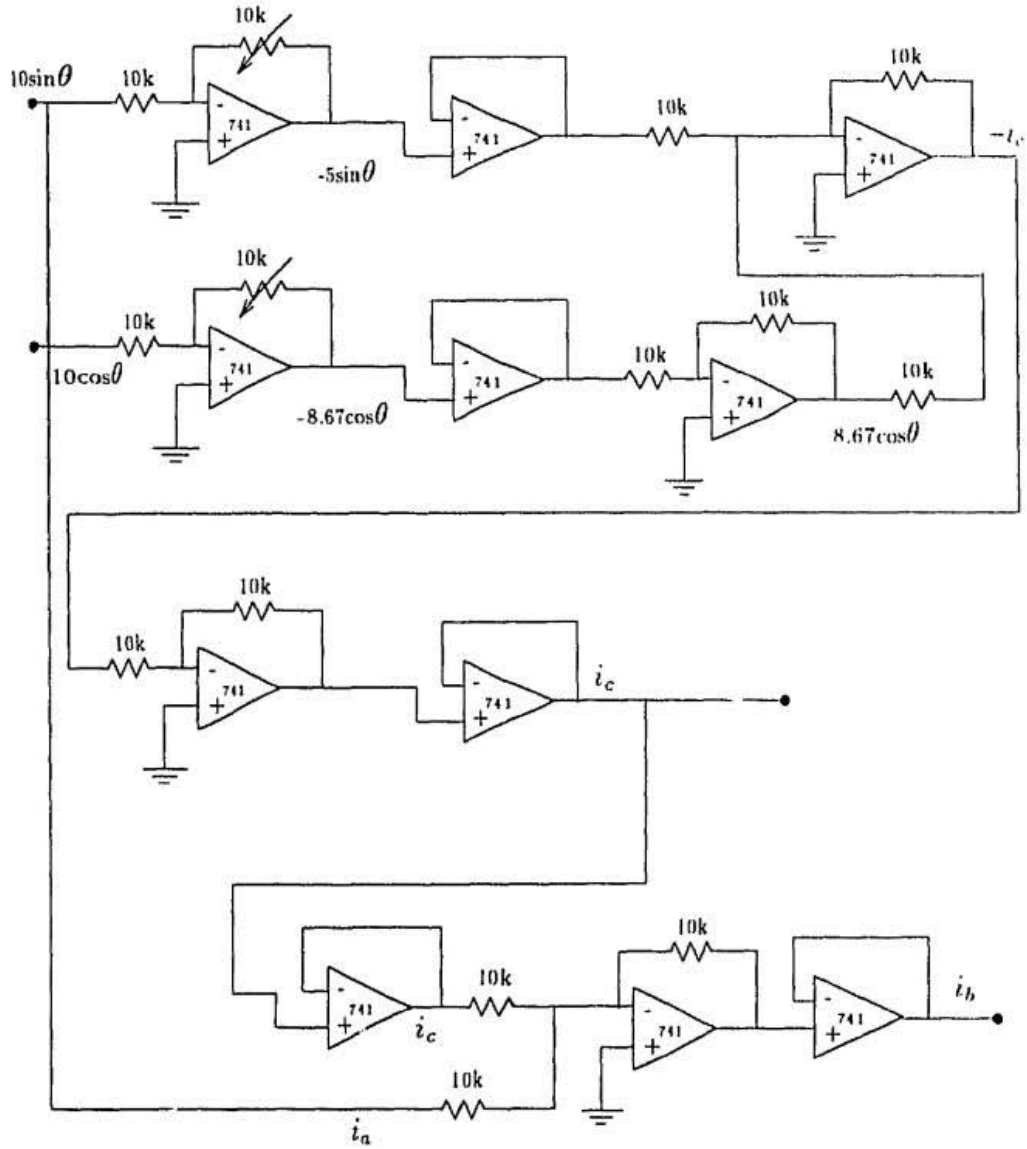

Figure C.2: Analog circuit for the three-phase reference currents generation

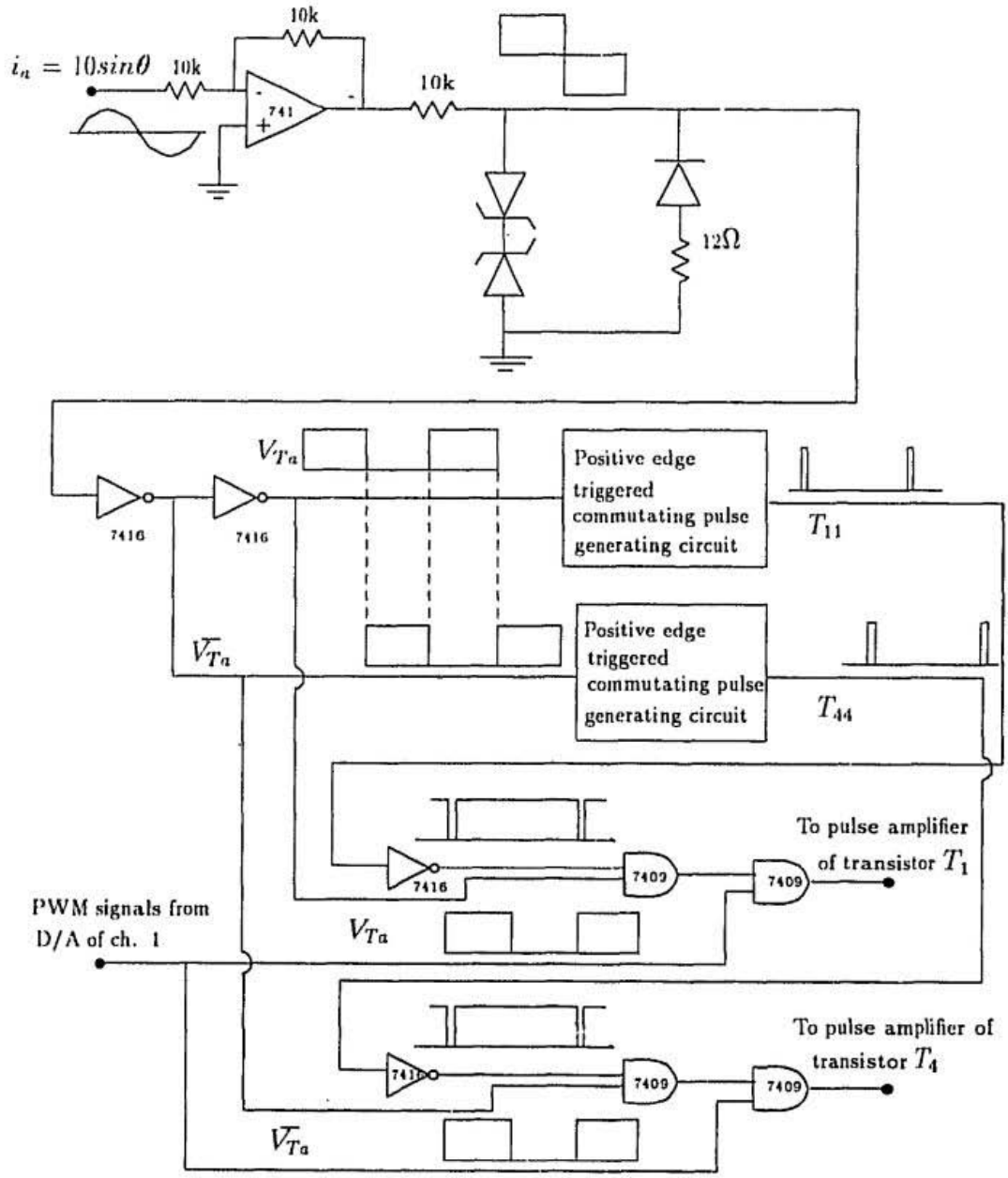

Figure C.3: Circuit layout for the splitting PWM signals between upper and lower transistors of Phase a

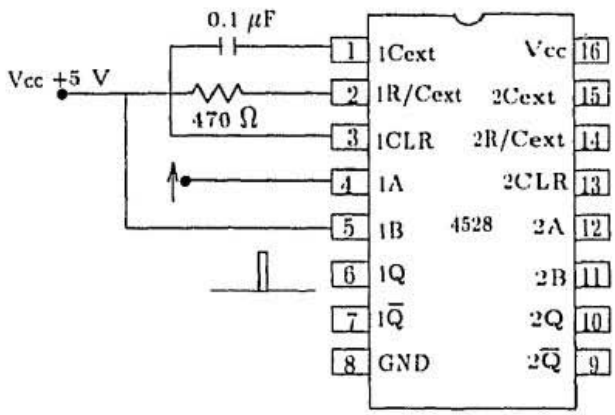

Figure C.4: Commutating pulse generating circuit

the PWM signals of each channel into two parts for the lower and upper transistors of each phase corresponding to the positive and negative half cycles of the reference currents. The details of the circuit diagram for generating PWM pulses for upper and lower transistors of the VSI from the reference current of one phase (phase a) are shown in Fig. C.3. The circuit diagrams for splitting PWM signals between upper and lower transistors of the other two phases are the same as Fig. C.3. Fig. C.4 shows the details of the circuit layout for the positive edge triggered commutating pulse generator circuits which provide a dead zone for the safe commutation of upper and lower transistors of each phase.

Appendix D

SIMULINK Subsystems

D.1 Subsystems of SIMULINK hysteresis current controller

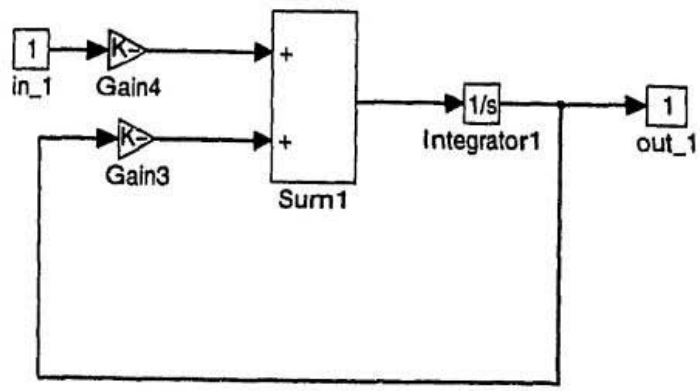

Subsystem

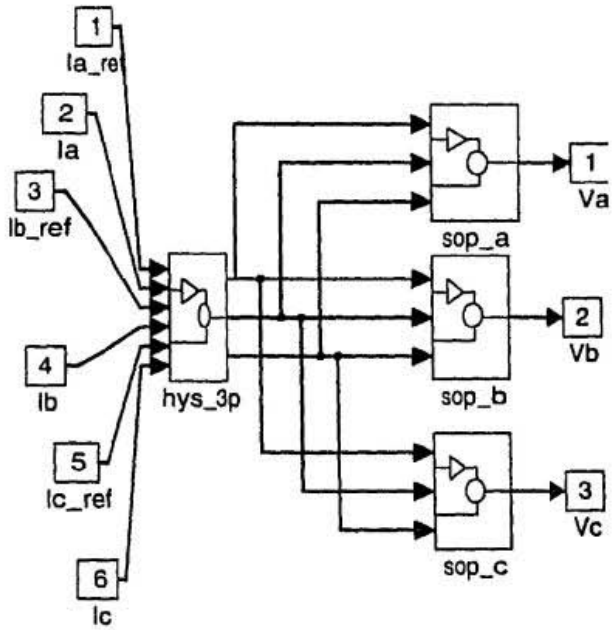
1
Ia_ref
2
Ia
3
Ib_ref
4
Ib
5
Ic_ref
6
Ic
hys_3p
sop_a
sop_b
sop_c
1
Va
2
Vb
3
Vc

Hys_3p

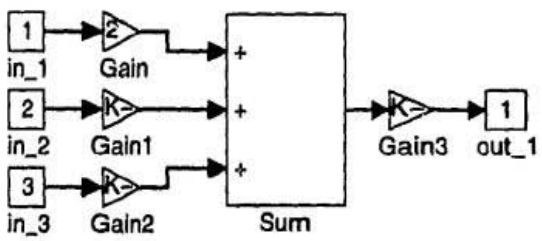
1
in_1
2
Gain
2
in_2
Gain1
3
in_3
Gain2
Sum
Gain3
1
out_1

sop_a

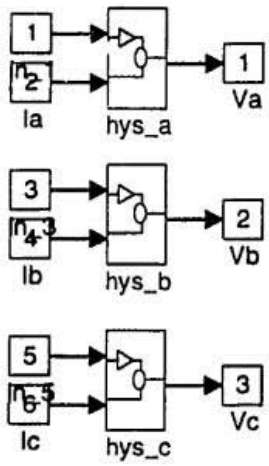
1
2
Ia
hys_a
1
Va
3
4
Ib
hys_b
2
Vb
5
6
Ic
hys_c
3
Vc

hys_3p

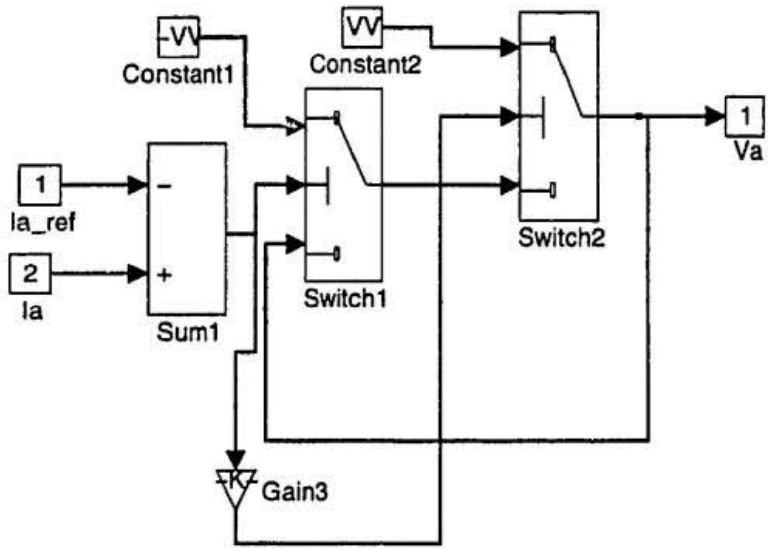
-VV
Constant1
VV
Constant2
1
Va
1
Ia_ref
2
Ia
Sum1
Switch1
Switch2
K
Gain3

hys_a

D.2 Subsystems of the SIMULINK brushless PM synchronous motor drive with the PDF speed controller

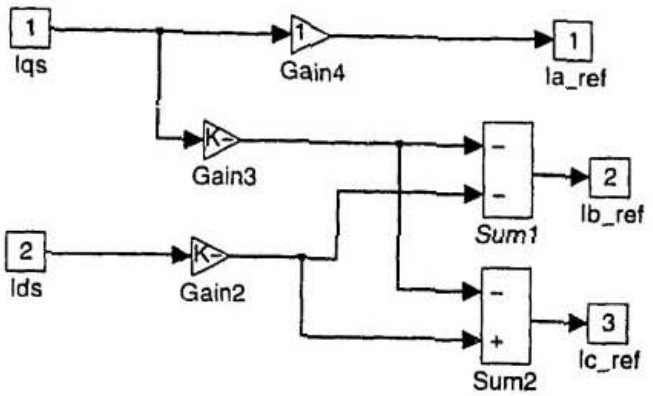

Iabc_ref

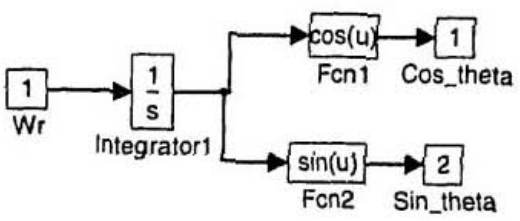

unt_vec

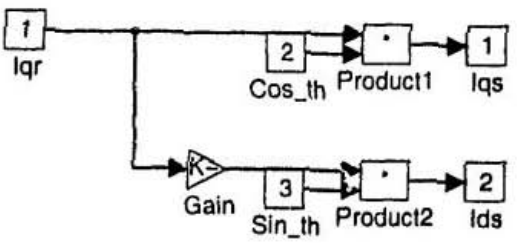

Iqds_ref

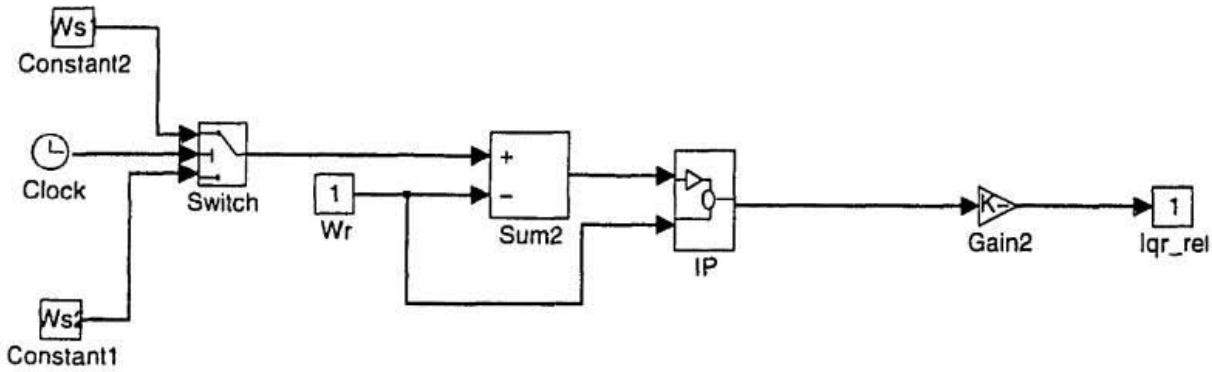

Iqr_ref1

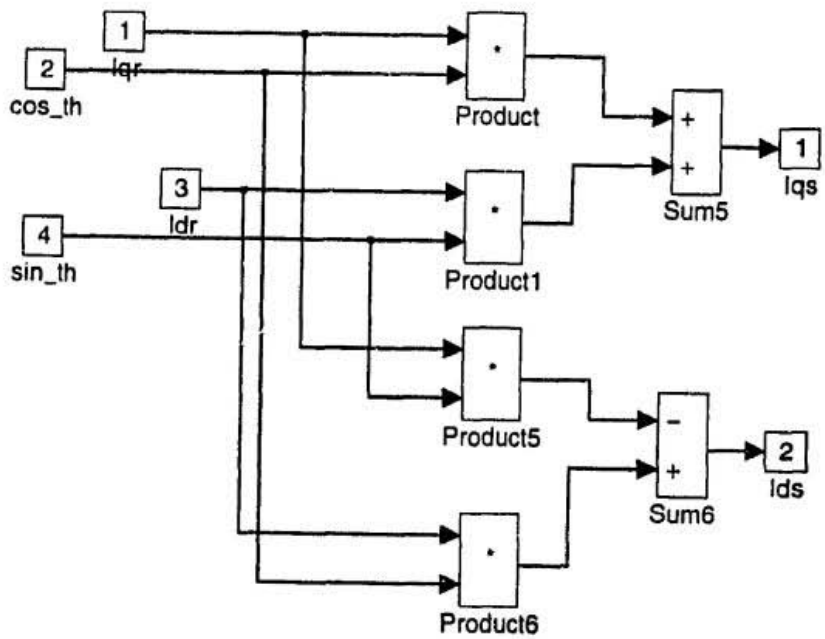

Iqds

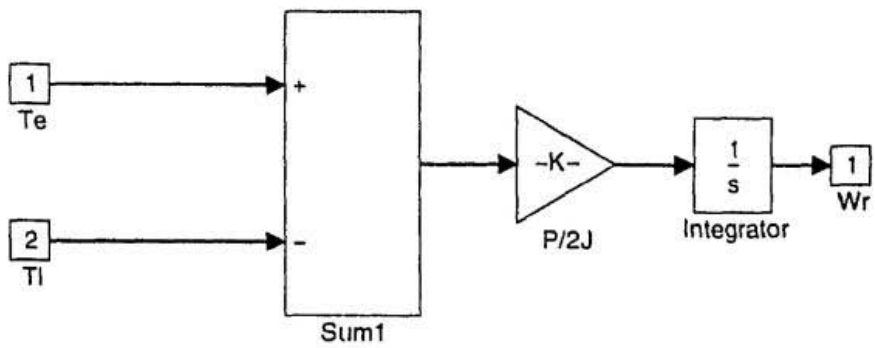

Speed

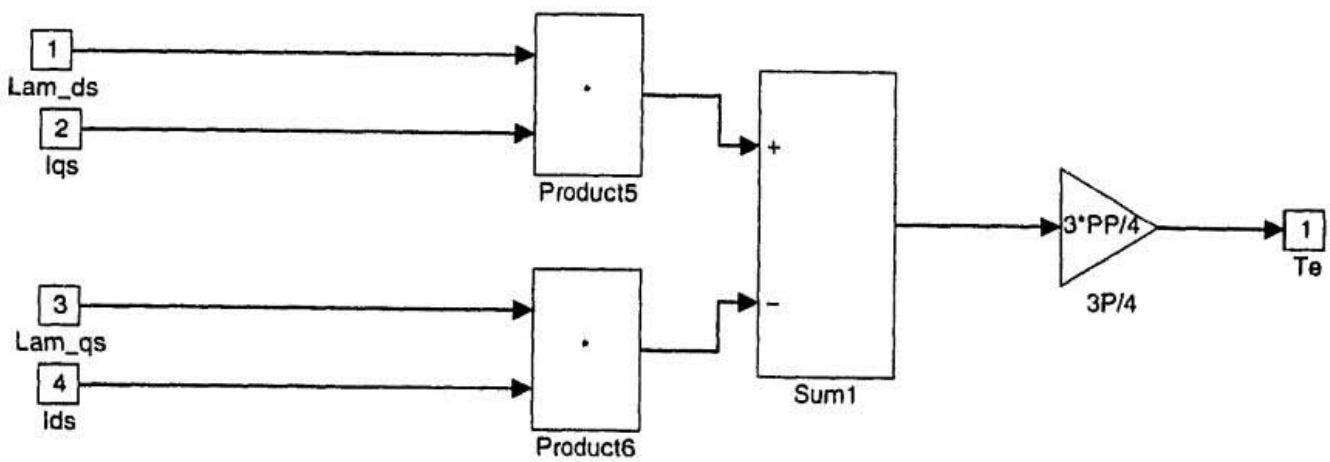

Torque

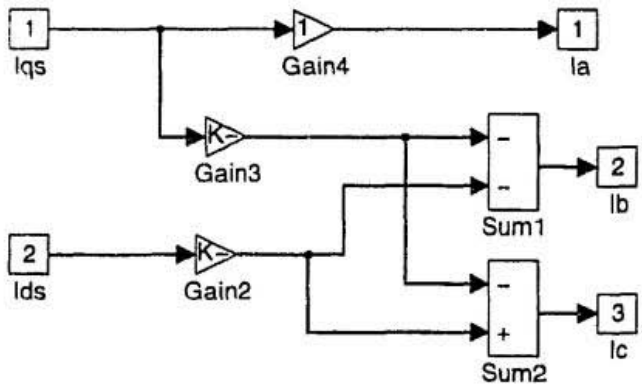

Iabc

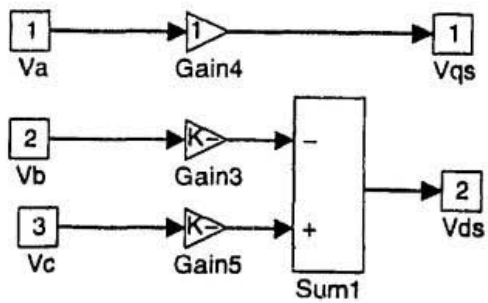

Vqds

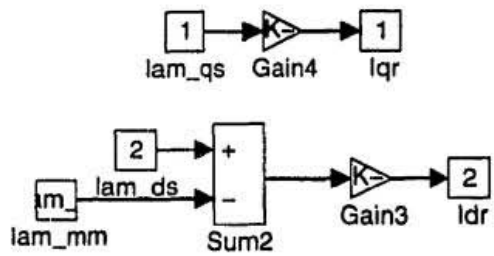

Iqdr

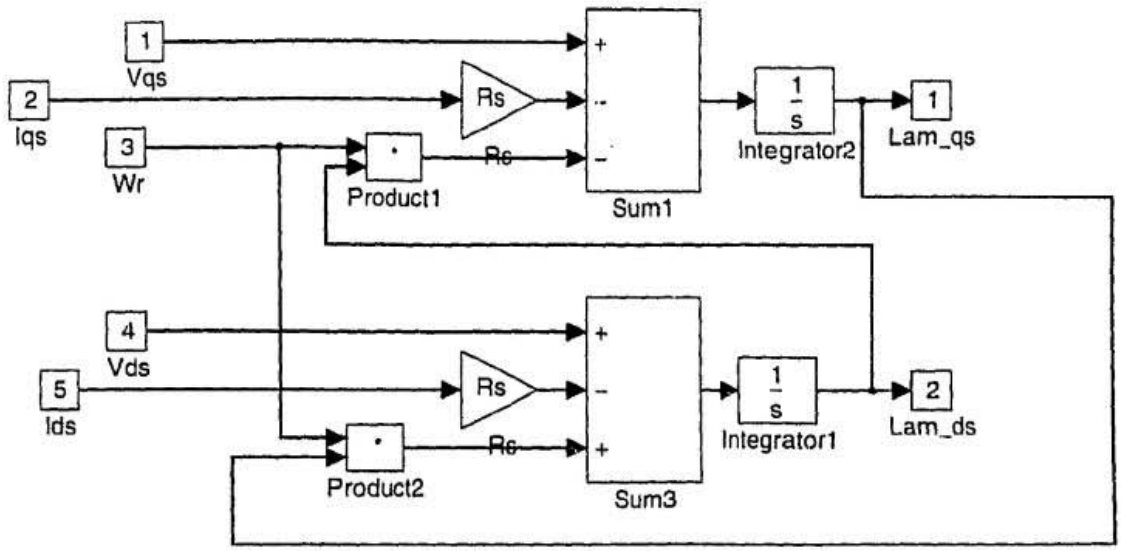
1
Vqs
2
Iqs
3
Wr
Rs
Rs
Product1
Sum1
1/s
Integrator2
1
Lam_qs
4
Vds
5
Ids
Rs
Rs
Product2
Sum3
1/s
Integrator1
2
Lam_ds

Lambda

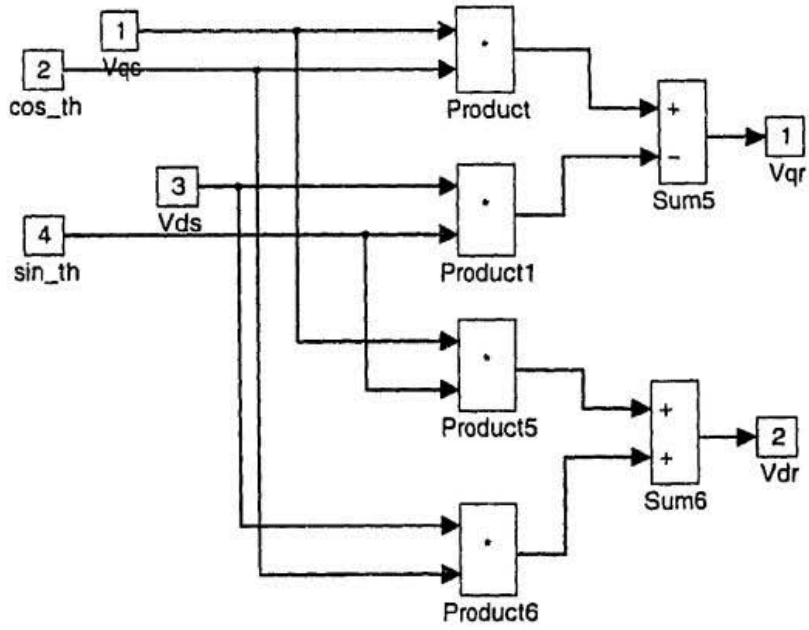
1
Vqc
2
cos_th
3
Vds
4
sin_th
Product
Product1
Product5
Product6
Sum5
Sum6
1
Vqr
2
Vdr

Vqdr